Effects of Channel Estimation and Implementation on the Performance of MIMO Wireless Systems

Mikel Mendicute Errasti

Supervisors:

Jon Altuna Iraola

and

Vicente Atxa Uribe

MONDRAGON
UNIBERTSITATEA

A thesis submitted for the degree of

Doctor por Mondragon Unibertsitatea

Department of Electronics and Computer Science

Mondragon Goi Eskola Politeknikoa

Mondragon Unibertsitatea

September 2008

Effects of Channel Estimation and Implementation on the Performance of MIMO Wireless Systems

Mikel Mendicute Errasti

Supervisors:

Jon Altuna Iraola

and

Vicente Atxa Uribe

MONDRAGON
UNIBERTSITATEA

A thesis submitted for the degree of

Doctor por Mondragon Unibertsitatea

Department of Electronics and Computer Science

Mondragon Goi Eskola Politeknikoa

Mondragon Unibertsitatea

September 2008

Autorización del Director del Departamento

Dr. D. **Josu Galarza Ibarrondo**, en calidad de Director del Departamento de Electrónica e Informática de la Escuela Politécnica Superior de Mondragon Unibertsitatea, **autoriza el depósito y la tramitación de la presente tesis doctoral**, titulada *"Effects of Channel Estimation and Implementation on the Performance of MIMO Wireless System"*, realizada por el Doctorando **D. Mikel Mendicute Errasti**.

En Arrasate-Mondragón, a 12 de Setiembre de 2008.

El Director del Departamento

Fdo:

Autorización de los Directores de Tesis

Dr. D. **Jon Altuna Iraola** y Dr. D. **Vicente Atxa Uribe**, en calidad de Director y Codirector respectivamente de la tesis doctoral *"Effects of Channel Estimation and Implementation on the Performance of MIMO Wireless System"* realizada por el Doctorando **D. Mikel Mendicute Errasti**, autorizan su depósito y tramitación.

En Arrasate-Mondragón, a 12 de Setiembre de 2008.

El Director de la Tesis

Fdo:

El Codirector de la Tesis

Fdo:

Abstract

Bit-rate and quality of service demands of new wireless communication standards are pushing signal theory and algorithm implementation to their limits. One of the main strategies which are being used to achieve the demanded rates is the multiple input-multiple output (MIMO) technique, which employs multiple antennas, both at transmission and reception.

This PhD dissertation concentrates on the analysis of the effects of channel estimation, specially complex due to the number of parameters to estimate, on the performance of MIMO detectors, focusing on both practical and theoretical aspects.

The practical analysis has been addressed by designing and developing a real-time wireless MIMO communication platform. A whole 2×2 system has been implemented which has allowed to evaluate the effects of a real hardware implementation on the performance of the MIMO receiver. A zero-forcing (ZF) detector and a sphere decoder (SD) have been implemented in order to evaluate their degradation in bit error rate (BER) performance in a realistic environment including synchronization, channel estimation or quantization effects.

On the other hand, a simulation-based analysis has been carried out to evaluate the effects of channel estimation on the comparative performance of the main detectors in fundamental MIMO systems, including narrowband, orthogonal frequency-division multiplexing (OFDM) and single-carrier with frequency-domain equalization (SCFDE) schemes. The effects of channel estimation on iterative Turbo-MIMO systems have also been analyzed, proposing a performance prediction tool based on analytical extrinsic information transfer (EXIT) functions.

Finally, a parallel decision-directed semi-iterative channel estimation architecture has been proposed which is specially designed to fit in field-programmable gate array (FPGA) devices and solves some of the problems of other iterative approaches with a moderate complexity.

Resumen

Las expectativas, tanto de calidad de servicio como de tasa de bits, de los nuevos estándares de comunicaciones inalámbricas están llevando la teoría de la señal y la implementación hardware de algoritmos a sus límites. Una de las técnicas que se están empleando para conseguir las tasas demandadas es la denominada MIMO (*multiple input-multiple output*), la cual consiste en la utilización de múltiples antenas, tanto en transmisión como en recepción.

Esta tesis se centra en el análisis del efecto de la estimación de canal MIMO, especialmente compleja debido al número de parámetros a estimar, sobre el rendimiento de los detectores multiantena, centrándose tanto en aspectos prácticos como teóricos.

El análisis práctico ha consistido en el desarrollo de una plataforma de prototipado de tiempo real para comunicaciones MIMO, así como en la implementación de un sistema completo 2×2, el cual ha servido para evaluar el efecto de la implementación hardware sobre el rendimiento del receptor MIMO. Se han incluido el detector ZF (*zero-forcing*) y el decodificador esférico dentro de un sistema hardware completo, permitiendo la evaluación de la degradación de las tasas BER (*bit error rate*) en entornos realistas donde se aprecian los efectos de los errores de sincronización, estimación de canal, cuantificación, etc.

Por otro lado, se ha desarrollado un estudio del efecto de la estimación de canal sobre el rendimiento comparativo de las principales técnicas de detección MIMO. Este análisis ha sido realizado tanto para sistemas de comunicaciones de banda estrecha como para sistemas de banda ancha basados en OFDM (*orthogonal frequency-division multiplexing*) y SCFDE (*single carrier with frequency-domain equalization*). Del mismo modo, se ha estudiado el efecto del error de estimación de canal en sistemas iterativos Turbo-MIMO básicos, proponiéndose una herramienta de predicción de tasas BER basada en funciones EXIT (*extrinsic information transfer*) analíticas.

Por último, partiendo de las conclusiones obtenidas en los puntos anteriores, se ha propuesto una arquitectura paralela para estimación de canal iterativa, especialmente apropiada para ser implementada en dispositivos lógicos FPGA (*field-programmable gate array*). Dicha arquitectura soluciona varios de los problemas de otros esquemas iterativos introduciendo un aumento moderado de complejidad.

Laburpena

Haririk gabeko komunikazio estandar berrien zerbitzu-kalitate eta abiadura eskaerek seinalearen teoria eta algoritmoen hardware inplementazioa euren mugetaraino daramatzate. Aipatutako abiadurak lortzeko erabiltzen ari diren tekniketako bat, garrantzitsuena agian, MIMO (*multiple input-multiple output*) delako sistema da, non antena anitz erabiltzen diren, bai igorlean baita hartzailean ere.

Doktoretza-tesi honen gai nagusia MIMO kanalaren estimazioan datza eta honek MIMO hartzailean duen efektua ikertzea du helburu, bereziki garrantzitsua suerta baitaiteke estimatu beharreko parametro kopuru handia dela eta. Bi bide ezberdin jarraitu dira ikerketa jorratzeko: bata praktikan oinarritua eta bestea, aldiz, teorian.

Atal praktikoan denbora errealeko prototipaia plataforma bat diseinatu eta sortu da. Honetaz gain, 2×2 MIMO sistema oso bat ere gauzatu da, benetako inplementazio baten eragina ikertzeko balio izan duelarik. Dekodifikatzaile esferikoa eta ZF (*zero-forcing*) detektoreak gauzatu dira, sistema erreal baten ondorioak (sinkronizazioa, estimazioa, zenbakapena, e.a) kontutan hartu ahal izateko.

Bestalde, simulazioetan oinarritutako ikerketa teorikoa ere jorratu da, kanalaren estimazioak MIMO hartzaile garrantzitsuenetan daukan eragina aztertuz. MIMO sistema mota nagusienak hartu dira kontuan: banda estukoa, OFDM (*orthogonal frequency-divison multiplexing*) eta SCFDE (*single carrier with frequency-domain equalization*). Era berean, kanalaren estimazioaren erroreak Turbo-MIMO direlako sistema iteratiboetan daukan eragina ere aztertu da, EXIT (*extrinsic information transfer*) funtzio analitikoetan oinarritutako ebaluaketa tresna proposatu delarik.

Azkenik, aurreko ataletatik ateratako ondorioetan oinarrituz kanalaren estimazio iteratiborako arkitektura paraleloa proposatu da. Proposaturiko arkitektura hau erraz gauza daiteke FPGA (*field-programmable gate array*) gailu programagarri batean eta beste estimazio tekniken hainbat akats saihes ditzake konplexutasuna neurriz kanpo gehitu gabe.

Declaration of Originality

I hereby declare that the research recorded in this thesis and the thesis itself were developed entirely by myself at the Signal Theory and Communications Area, Department of Electronics and Computer Science, at the University of Mondragon.

The software used to perform the simulations and the different real-time hardware implementations of the algorithms were developed entirely by myself, with the following exception:

- The System Generator implementation of the sphere decoder, which was used during a collaboration project with the University of Edinburgh, has been entirely designed by Luis G. Barbero and John S. Thompson, as has been clearly stated in the thesis.

Mikel Mendicute Errasti
Department of Electronics and Computer Science
Mondragon Goi Eskola Politeknikoa
Mondragon Unibertsitatea
September, 2008

Eskerrak

Bost urte igaro dira tesi honi ekin nionetik. Bide luzea izan da, seinalearen tratamenduaren eta haririk gabeko komunikazioen mundu bitxian zehar. Jende ugari ezagutzeko aukera izan dut eta denek lagundu didate honaino iristen, bakoitzak bere erara. Nire esker ona erakutsi nahi diet bereziki:

- Nire tesi zuzendari izan diren **Jon Altuna** eta **Vicente Atxa** doktore jaunei, tesia egiteko aukera, baliabideak eta aholkuak emateaz gain, beti nigan erakutsitako konfidantza eta fedeagatik.

- **Eusko Jaurlaritza**ko **Hezkuntza, Unibertsitate eta Ikerketa** sailari, *Ikertzaileen Prestaketarako Programa*ko bekaren bitartez emandako laguntzagatik.

- **Mondragon Unibertsitateko Mondragon Goi Eskola Politeknikoa**ri, bertan tesia egiteko aukera eta dirulaguntza ematearren.

- **Edinburgoko Unibersitateko *Institute for Digital Communications***-eko taldeari, bertako **John S. Thompson**-i eta gaur egun Belfasteko **Queens University** delakoan dagoen **Luis G. Barbero**-ri, Edinburgon egindako egonaldian emandako laguntzagatik eta dekodifikagailu esferikoaren inguruan egindako elkarlanagatik.

- Nire lankide diren edo izan diren **Ane Antia**, **Imanol Bilbao**, **Amaia Bizkarguenaga**, **Javi Del Ser**, **Unai Garro** eta **Miguel San Miguel**-i, tesiak eragin dituen *marroiak* eta nire desagerpenak jasatearren, eta bereziki **Egoitz Arruti**, **Javier Oyarzun** eta **Jose Mari Zabalegi**-ri, tesia amaitzeko behar nuen denbora emateagatik.

- Tesian zehar nire lankide izandako **Wilfredo Falcón**, **Fidel Hernández**, **Aitzol Iturrospe**, **Imanol Martínez**, **Iker Sobrón** eta bereziki hardware kontuetan lagun izan dudan **Gorka Landaburu**-ri.

- Jasan behar izan nauten Arrasateko pisukide eta lagunei: **Borja**, **Cristina**, **Iker** eta **Javi**-ri.

- Asteburuetan nere falta sumatu duten **Eibarko koadrila**ko astokiloei. Hau irakurriko ez dutenez, ez dut uste izenak jartzea merezi duenik ;-).
- Eta azkenengoak garrantzitsuenak, honaino iritsi ahal izateko aukera, hezkuntza eta indarra eman didan sendiari: **aita**, **ama** eta **anaia**ri, tesia oso garrantzitsua dela (eta batez ere, ez dela) gogoratzeagatik. Eta nola ez, tesi hau birritan irakurri behar izan duen nire **neskalagun *kotxauari***, bihotz-bihotzez.

ESKERRIK ASKO!

Acknowledgments

It is five years since I began to work on this PhD thesis. It has been a long journey through the bizarre world of signal processing and wireless communications. I have had the chance to meet many interesting people and all of them have helped me in many different ways. I would like to express my deepest gratitude to:

- My supervisors **Dr. Jon Altuna** and **Dr. Vicente Atxa** for giving me the support and all the means to do this PhD, as well as for the confidence and faith they have shown on me.
- The **Department of Education, Universities and Research** of the **Basque Government**, for the funding received through a *Researcher Training* grant.
- The **High Polytechnical School** of the **University of Mondragon**, for the chance and funding to develop the PhD.
- The ***Institute for Digital Communications*** of the **University of Edinburgh**, specially to **Dr. John S. Thompson** and **Dr. Luis G. Barbero**, currently at Queens University Belfast, for their help during my internship in Ediburgh and for the collaboration project on the sphere decoder.
- To my current and past colleagues **Ane Antia**, **Imanol Bilbao**, **Amaia Bizkarguenaga**, **Javi Del Ser**, **Unai Garro** and **Miguel San Miguel**, for standing the *browns* derived from my PhD and all my disappearances. Very specially to **Egoitz Arruti**, **Javier Oyarzun** and **Jose Mari Zabalegi**, for giving me the time I needed to finish this work.
- To my former PhD officemates **Wilfredo Falcón**, **Fidel Hernández**, **Aitzol Iturrospe**, **Imanol Martínez**, **Iker Sobrón** and specially **Gorka Landaburu**, who has fought beside me against hardware implementation.
- My flatmates and friends in Arrasate: **Borja**, **Cristina**, **Iker** and **Javier**.

- **My friends from Eibar**, who have missed me all the weekends I have dedicated to the PhD. They will never read this, so I will not enumerate all of them. ;-)
- And last, the most important ones, those who have given me all the opportunities, education, support and strength to be what I am: **my father, mother and brother**, for reminding me how important this thesis is (and is not). And how not, very specially to my ***poor*** **girlfriend**, who has had to read this PhD dissertation several times.

THANKS!

Aita, ama eta Xabirentzat.

Ta Marletarentzat.

...
What might have been is an abstraction
Remaining a perpetual possibility
Only in a world of speculation
What might have been and what has been
Point to one end, which is always present.
Footfalls echo in the memory
Down the passage which we did not take
Towards the door we never opened
...

T. S. Eliot,
Burnt Norton

Contents

Abstract . . . iii
Declaration of Originality . . . vi
Acknowledgments . . . vii
Contents . . . xii
List of Figures . . . xv
List of Tables . . . xix
List of Symbols . . . xxv

1 Introducción **1**
1.1 Introducción y Estado del Arte . . . 1
1.1.1 Sistemas Inalámbricos MIMO . . . 2
1.1.2 Estimación de Canal . . . 3
1.1.3 Demostradores y Sistemas de Prototipado MIMO . . . 4
1.2 Motivación . . . 5
1.3 Objetivos y Metodología . . . 5
1.3.1 Objetivos del Estudio Teórico . . . 6
1.3.2 Objetivos de la Implementación Práctica . . . 7
1.3.3 Metodología . . . 7
1.3.3.1 Teoría y Simulaciones . . . 7
1.3.3.2 Implementación Práctica . . . 8
1.4 Contribuciones de la Tesis . . . 8
1.5 Estructura de la Tesis . . . 10

2 MIMO Systems in Wireless Communications **11**
2.1 Introduction . . . 11
2.2 Narrowband MIMO Wireless Systems . . . 12
2.2.1 System Model . . . 12
2.2.2 Capacity of MIMO Channels . . . 13
2.2.2.1 Deterministic MIMO Channel . . . 13

2.2.2.2 Random MIMO Channel . . . 15
2.2.3 Space-Time Coding Techniques . . . 15
2.2.3.1 Spatial Multiplexing . . . 16
2.2.3.2 Space-Time Block Codes . . . 17
2.2.3.3 Space-Time Trellis Codes . . . 19
2.2.4 Summary of MIMO Detection Algorithms . . . 20
2.2.4.1 The Sphere Decoder . . . 22
2.2.5 Performance Comparison of MIMO Detection Schemes . . . 24
2.3 MIMO-OFDM Systems . . . 25
2.3.1 OFDM . . . 25
2.3.2 MIMO-OFDM . . . 27
2.3.3 MIMO-Based WLAN Standard: IEEE 802.11n . . . 28
2.3.4 Performance Results . . . 29
2.4 MIMO-SCFDE Systems . . . 29
2.4.1 SCFDE Modulation . . . 30
2.4.2 MIMO-SCFDE . . . 31
2.4.3 Performance Comparison of MIMO-SCFDE and MIMO-OFDM . . . 32
2.5 Iterative MIMO Receivers . . . 32
2.5.1 Fundamental System Model . . . 33
2.5.2 Performance Evaluation . . . 35
2.5.3 EXIT Charts . . . 35
2.5.4 EXIT Function-Based Performance Prediction . . . 37
2.6 Chapter Summary . . . 37

3 MIMO Prototyping Platform and Implementations 39
3.1 Introduction . . . 39
3.2 Algorithm Prototyping Methodology and Tools . . . 40
3.2.1 Xilinx Design, Synthesis and Implementation Tools . . . 41
3.2.2 Simulink-Based Design of Real-Time Algorithms . . . 42
3.3 Off-line Transmission Platform . . . 44
3.4 Real-time Algorithm Prototyping Platform . . . 47
3.4.1 Rapid Prototyping Boards . . . 47
3.4.2 RF Transceivers . . . 48
3.5 "Hardware in the Loop" Approach . . . 48
3.5.1 Synchronization between Matlab/Simulink and Real-Time Hardware 49
3.5.2 Application Examples . . . 50
3.6 Implementation of a Basic 2x2 MIMO System . . . 51
3.6.1 Transmitter Algorithms . . . 52

3.6.2 Receiver Algorithms . . . 53
3.6.3 Design Partitioning . . . 54
3.6.3.1 RF Chain Partitioning . . . 55
3.6.4 Complexity and Resources . . . 55
3.7 Implementation of a Sphere Decoder-Based MIMO System . . . 56
3.7.1 Integration of the SD Model into the MIMO Implementation . . . 56
3.7.2 Complexity and Resources . . . 58
3.8 Chapter Summary . . . 59

4 MIMO Channel Estimation **60**
4.1 Introduction . . . 60
4.2 Narrowband MIMO channels . . . 61
4.2.1 Training-Based Channel Estimation . . . 62
4.2.1.1 Least-Squares Channel Estimation . . . 62
4.2.1.2 Linear Minimum Mean Squared Error Channel Estimation . 64
4.2.1.3 Other Training-Based Techniques . . . 65
4.2.2 Semi-Blind Techniques . . . 66
4.2.2.1 Iterative Channel Estimation . . . 66
4.2.2.2 Second and Higher-Order Statistics-Based Approaches . . . 67
4.3 MIMO-OFDM and MIMO-SCFDE . . . 72
4.3.1 Time-Domain LS-ML Channel Estimation . . . 72
4.3.2 Frequency-Domain LS Channel Estimation . . . 76
4.3.3 Optimal Training Structures for MIMO-OFDM . . . 77
4.4 Channel Estimation in Iterative MIMO Systems . . . 79
4.4.1 EM Channel Estimation in Turbo-MIMO Systems . . . 79
4.4.2 Analytical EXIT Functions with Channel Estimation Errors . . . 81
4.4.2.1 Adaptation of the Performance Evaluation Algorithm . . . 83
4.4.3 Channel Estimation Error Models . . . 83
4.4.3.1 Training-Based least-squares (LS) Channel Estimation . . . 84
4.4.3.2 Iterative EM Channel Estimation . . . 84
4.4.4 Simulation Results . . . 84
4.5 Chapter Summary . . . 85

5 Impact of Channel Estimation on the Performance of MIMO Detectors **87**
5.1 Introduction . . . 87
5.2 Scenarios for the Analysis of Channel Estimation Implementation . . . 87
5.2.1 LS Estimator in Fully Implemented MIMO Scenario . . . 88
5.2.2 Flexible Matlab-Based Channel Estimator Implementation Evaluation 91
5.3 Narrowband MIMO Channels . . . 92

5.3.1 Evaluation of Channel Estimation on the Real-Time MIMO Platform 92
5.3.1.1 Zero-Forcing Receiver . . . 93
5.3.1.2 Optimal Sphere Decoder-Based MIMO System . . . 93
5.3.2 Simulation-Based Evaluation . . . 95
5.3.2.1 Uncoded 4 x 4 System . . . 96
5.3.2.2 Coded 4 x 4 System . . . 99
5.3.2.3 4 x 6 Setup . . . 99
5.3.2.4 Summary of Main Results . . . 101
5.4 MIMO-OFDM and MIMO-SCFDE Systems . . . 101
5.4.1 MIMO-OFDM . . . 101
5.4.1.1 Uncoded 4x4 System . . . 102
5.4.1.2 Coded 4x4 System . . . 103
5.4.2 MIMO-SCFDE . . . 104
5.4.2.1 Uncoded 4x4 System . . . 104
5.4.2.2 Coded 4x4 System . . . 105
5.4.3 Comparative Performance and Considerations . . . 105
5.5 Design of a Parallel Decision-Directed Channel Estimation Architecture . . . 107
5.5.1 Narrowband Systems . . . 108
5.5.2 Extension to MIMO-OFDM and MIMO-SCFDE Systems . . . 110
5.6 Chapter Summary . . . 113

6 Conclusion and Further Research **115**
6.1 Summary . . . 115
6.2 Thesis Contribution . . . 116
6.3 Suggestions for Further Research . . . 117

A Publications **119**

References **156**

List of Figures

1.1 Bloques principales y parámetros del sistema evaluado. 6

2.1 Basic diagram of a wireless MIMO system. 12
2.2 10%-outage capacity of random MIMO channels with $M = N$. 16
2.3 Diagram of an uncoded $N \times M$ spatial multiplexing MIMO system. 17
2.4 Diagrams of horizontally (a) and vertically (b) encoded spatial multiplexing transmitters. 17
2.5 Trellis diagram for a 4-QAM, 4-state STTC code with $M = 2$. 20
2.6 Structure of a generic detector with successive interference cancellation. . . . 22
2.7 Schematic of the sphere decoder search principle for the 2-dimensional case. . 22
2.8 BER performance of basic MIMO detectors for uncoded 4×4 (a) and 2×3 (b) QPSK transmission. 24
2.9 Diagram of OFDM transmission and reception chains for a SISO channel. . . 26
2.10 Orthogonal subcarriers of an OFDM wireless system. 27
2.11 Diagram of a general MIMO-OFDM system. 28
2.12 Diagram of a generic 4×4 IEEE 802.11n MIMO-OFDM transmitter [EWC05]. 29
2.13 BER performance curves of basic MIMO detectors for uncoded (a) and rate-1/2 coded (b) 4×4 QPSK OFDM transmission. 30
2.14 Diagram of transmission and reception chains for a SISO-SCFDE system. . . 30
2.15 Schematic of a MIMO-SCFDE spatial multiplexing transmission and reception system. 31
2.16 BER performance comparison of basic MIMO detectors for uncoded (a) and rate-1/2 coded (b) 4×4 SCFDE (solid line) and OFDM (dashed line) transmissions. 32
2.17 Diagram of a MIMO transmitter with coding and interleaving. 33
2.18 Diagram of a generic interference cancellation-based iterative Turbo-MIMO receiver. 34

2.19 BER performance curves for an iterative MIMO receiver in a 4×4 system with fixed (a) and Rayleigh fading (b) wireless channels with 0, 1 and 2 iterations. 35
2.20 EXIT trajectory for a MMSE-PIC receiver with $E_b/N_0 = 3$ dB. 36

3.1 Main stages of the simulation and implementation flow. 40
3.2 Real-time MIMO algorithm design and validation flow with real transmission. 41
3.3 Combined use of Matlab, Simulink and System Generator models. 43
3.4 Block diagram of the off-line MIMO transmission platform (2×2 setup). . . 44
3.5 Main hardware elements of the off-line transmission platform. 46
3.6 Main elements of the real-time MIMO algorithm prototyping platform: antenna sets (1), Heron board (2) and RF transceivers (3). 48
3.7 Scheme of a 2x2 real-time HaLo MIMO system controlled from Simulink. . . 50
3.8 Matlab-emulated channel in a real-time running rapid prototyping platform. 51
3.9 Diagram of the implemented 2x2 MIMO wireless system. 52
3.10 System Generator implementation of the 2x2 MIMO transmitter. 53
3.11 Schematic of the partitioned design which comprises 4 FPGA devices. 54
3.12 Structure of the System Generator implementation of the SD decoder, developed at the University of Edinburgh. 57
3.13 BER (a) and throughput (b) performance curves for the FPGA implementation of the SD algorithm. 58

4.1 Structure of the transmitted symbol matrix $\mathbf{S}$. 62
4.2 NMSE (a) and BER (b) performance curves of LS channel estimation for a 4×4 spatial multiplexing system with MMSE detection. 64
4.3 NMSE (a) and BER (b) performance curves of LS and LMMSE channel estimation for a 4×4 spatial multiplexing system with MMSE detection. 65
4.4 NMSE and BER curves of iterative LS channel estimation for a 4×4 spatial multiplexing system with MMSE detection. 68
4.5 NMSE (a) and BER (b) curves of training-based, iterative LS and WR channel estimation techniques for a 4×4 BPSK transmission of 100 bits per antenna. 69
4.6 cdf of output SINR for different channel estimators and E_b/N_0 values. 70
4.7 BER performance of ACMA-based channel estimation with different training lengths and E_b/N_0 values of 0, 10 and 20 dB. 71
4.8 NMSE (a) and BER (b) performance of ML channel estimation for a 4×4 HIPERLAN/2 A channel model ($L = 11$ taps). 74
4.9 NMSE (a) and BER (b) performance of ML channel estimation for a 4×4 HIPERLAN/2 C channel model ($L = 31$ taps). 74
4.10 Structure of the 802.11a preamble, showing a double-length symbol for channel estimation [IEEE99]. 75

4.11 NMSE (a) and BER (b) performance of LS channel estimation for a 2×2 HIPERLAN/2 B channel model ($L = 21$ taps) using the double-length preamble provided by the IEEE 802.11a standard. 75
4.12 Training structures for frequency-domain MIMO-OFDM channel estimation. 76
4.13 Structure of a $4 \times N$ MIMO-OFDM preamble with training blocks spread across 2 subcarriers and 2 consecutive OFDM symbols. 76
4.14 Examples of two channel estimates using FFT-based and linear interpolation schemes. 77
4.15 Comparison of the NMSE and BER curves of a 4×4 QPSK MIMO-OFDM system with FFT-based (int. 1) and linear (int. 2) interpolation techniques. 78
4.16 Diagram of a generic interference cancellation-based iterative MIMO receiver with channel estimation. 80
4.17 Comparison of EXIT fuction-based and MC simulation results for LS channel estimation with a training length of $L_T = 8$ (a) and $L_T = 16$ (b). 85
4.18 Comparison of EXIT fuction-based and MC simulation with soft decision-directed EM channel estimation and an initial 4×8 training matrix. 86

5.1 First blocks of the MIMO receiver, including frame detection, symbol-time synchronization and channel estimation. 89
5.2 Structure of the implemented LS channel estimator. 90
5.3 Matlab/Simulink-based channel estimation evaluation testbed. 91
5.4 BER degradation of the ZF algorithm due to channel estimation and implementation effects. 94
5.5 Effects of channel estimation and realistic implementation on the BER performance (a) and achievable throughput (b) of a complete SD-based MIMO system. 95
5.6 a) BER performance of a 4×4 spatial multiplexing system with LS channel estimation with $L_T = 4$ (solid line) and $L_T = 12$ (dashed line). b) Performance comparison of ML (SD) and MMSE-V-BLAST with iterative channel estimation for $L_T = 4$. 96
5.7 BER performance of an uncoded 4×4 spatial multiplexing system with LS channel estimation with $L_T = 4$ (solid line) and $L_T = 12$ (dashed line) for 16-QAM (a) and 64-QAM (b) modulations. 98
5.8 Comparison of the SD and an MMSE-V-BLAST detector with enhanced channel estimation for 4×4 16-QAM transmission. 98
5.9 BER performance of an coded 4×4 spatial multiplexing system with LS channel estimation with $L_T = 4$ (solid line) and $L_T = 12$ (dashed line) for QPSK (a) and 16-QAM (b) modulations. 99

5.10 BER performance of uncoded (a) and coded (b) 4×6 spatial multiplexing system with LS channel estimation with $L_T = 4$ (solid line) and $L_T = 12$ (dashed line) for QPSK modulation. 100
5.11 BER performance of an uncoded MIMO-OFDM spatial multiplexing system with LS channel estimation with $L_T = 1$ (solid line) and $L_T = 4$ (dashed line) for QPSK (a) and 16-QAM (b) modulation. 102
5.12 BER performance of an coded MIMO-OFDM spatial multiplexing system with LS channel estimation with $L_T = 1$ (solid line) and $L_T = 4$ (dashed line) for QPSK (a) and 16-QAM (b) modulation. 103
5.13 BER performance of an uncoded MIMO-SCFDE spatial multiplexing system with LS channel estimation with $L_T = 1$ (solid line) and $L_T = 4$ (dashed line) for QPSK (a) and 16-QAM (b) modulation. 104
5.14 BER performance of a coded MIMO-SCFDE spatial multiplexing system with LS channel estimation with $L_T = 1$ (solid line) and $L_T = 4$ (dashed line) for QPSK (a) and 16-QAM (b) modulation. 105
5.15 Effects of channel estimation on the performance of a coded 16-QAM spatial multiplexing system. 106
5.16 Architecture of PDD receiver with P=4. 108
5.17 Mean NMSE for every received symbol in a frame for MMSE-V-BLAST detection with $L_T = 4$ QPSK (a) and $L_T = 8$ 16QAM (b) systems. 110
5.18 BER performance curves of different iterative channel estimators and the PDD architecture for QPSK MMSE (a) and 16QAM ZF (b) scenarios. 110
5.19 BER of a 4×4 QPSK ZF system with different channel estimators including the PDD. 111
5.20 Evolution of channel estimate of a sample $\mathbf{H}_{nm}$ subchannel for E_b/N_0 values of 12 dB (a) and 4 dB (b). 111
5.21 BER comparison of PDD channel estimation architecture and the decision-directed (DD) approach for a 4×4 MIMO-OFDM system with MMSE (a) and MMSE-V-BLAST (b) detection algorithms. 112
5.22 BER comparison of PDD channel estimation architecture and the decision-directed (DD) approach for a 4×4 MIMO-SCFDE system with MMSE (a) and MMSE-V-BLAST (b) detection algorithms. 113

List of Tables

2.1 BER performance evaluation algorithm for each channel realization of an iterative MIMO receiver. 38

3.1 FPGA resources used by the ZF-based real-time implementation. 55
3.2 FPGA resources used by the SD-based real-time implementation. 58

4.1 Examples of optimal MIMO-OFDM preambles for $T = 8$ subcarriers, $M = 4$ antennas and a channel length of $L = 2$ taps [Minn06]. 79
4.2 BER performance evaluation algorithm for each channel realization of an iterative MIMO receiver with channel estimation. 83

Acronyms

ADC	analog to digital converter
AM	amplitude modulation
API	application programmer interface
APP	a posteriori probability
AWGN	additive white Gaussian noise
BER	bit error rate
BICM	bit-interleaved coded modulation
BPSK	binary phase shift keying
BSS	blind source separation
cdf	cumulative distribution function
CDM	code divison multiplexing
CDMA	code division multiple access
CP	cyclic prefix
CSI	channel state information
D-BLAST	diagonal Bell-Labs layered space-time
DE	diagonal encoding
DFT	discrete Fourier transform
DSP	digital signal processor

EM	expectation maximization
EWC	Enhanced Wireless Consortium
EXIT	extrinsic information transfer
FDE	frequency-domain equalization
FDM	frequency-divison multiplexing
FE	front-end
FEC	forward error correcting
FER	frame error rate
FIFO	first in-first out
FFT	fast Fourier transform
FPGA	field programmable gate array
GUI	graphical user interface
HaLo	hardware in the loop
HE	horizontal encoding
IF	intermediate frequency
IFFT	inverse fast Fourier transform
i.i.d.	independent and identically distributed
ILS	iterative least squares
ISI	inter-symbol interference
LC	linear combiner
LDPC	low-density parity check
LLR	log-likelihood ratio
LMMSE	linear minimum mean squared error
LS	least-squares
Mbps	megabits per second

MBps	megabytes per second
MC	Monte Carlo
MI	mutual information
MIMO	multiple input-multiple output
ML	maximum likelihood
MMSE	minimum mean squared error
MSE	mean squared error
MSps	mega samples per second
NMSE	normalized mean squared error
OFDM	orthogonal frequency-division multiplexing
OSIC	ordered successive interference cancellation
OSTBC	orthogonal space-time block coding
PAPR	peak-to-average power ratio
PCI	parallel carrier interface
PDD	parallel decision-directed
pdf	probability density function
PIC	parallel interference cancellation
PSK	phase shift keying
QAM	quadrature amplitude modulation
QPSK	quaternary phase shift keying
RC	raised cosine
RF	radio-frequency
rms	root mean square
SC	sphere constraint
SCFDE	single carrier with frequency-domain equalization

SD	sphere decoder
SE	Schnorr-Euchner
SINR	signal to interference and noise ratio
SIP	superimposed pilot
SISO	single input-single output
SISO*	soft input-soft output
SM	spatial multiplexing
SNR	signal to noise ratio
ST	space-time
STBC	space-time block coding
STC	space-time coding
STTC	space-time trellis codes
V-BLAST	vertical Bell-Labs layered space-time
VE	vertical encoding
VHDL	very high-level design language
WLAN	wireless local area network
WMAN	wireless metropolitan area network
WR	whitening-rotation
ZF	zero-forcing
ZMCSCG	zero mean circularly symmetric complex Gaussian

List of Symbols

Γ_m	SINR value at the m-th output branch of the soft MIMO detector
Λ_c^a	A priori log-likelihood ratio of bit c
Λ_c^e	Extrinsic log-likelihood ratio of bit c
ρ	Signal to noise ratio
b	Uncoded data bit
$\mathbf{b}$	Vector of uncoded data bits
B	Number of points of a constellation
B_w	Bandwidth of the communication channel
C	Capacity of a wireless channel
$\det(A)$	Determinant of matrix A
$\mathbf{D}$	$T \times T$ discrete Fourier transform matrix
E_b	Average energy per bit
E_s	Average energy per symbol
$\mathrm{E}(x)$	Expectation of x
$f(x)$	Probabilty density function of x
$F_m(\cdot)$	Transfer function for the m-th output branch of the soft MIMO detector
$\mathbf{h}_j$	j-th column of the channel matrix $\mathbf{H}$
h_{nm}	Channel gain between transmit antenna m and receive antenna n

$h[\tau]$	Channel impulse response at delay τ
$\mathbf{H}$	$N \times M$ channel matrix
$\mathbf{H}^{+}$	Pseudoinverse of matrix $\mathbf{H}$
$\mathbf{H}^{H}$	Hermitian of matrix $\mathbf{H}$
I_{in}^{D}	Input mutual information at the decoder
I_{in}^{R}	Input mutual information at the MIMO detector
$\mathbf{I}_{M}$	$M \times M$ identity matrix
I_{out}^{D}	Output mutual information from the decoder
I_{out}^{R}	Output mutual information from the MIMO detector
$I(\mathbf{x};\mathbf{y})$	Mutual information of vectors $\mathbf{x}$ and $\mathbf{y}$
j	Iteration number at the iterative MIMO receiver
k	Sampled symbol period index
K	Number of symbols in a frame
l	Uncoded bit index
l_b	coded bit index
l_d	coded and demultiplexed bit index
L	Maximum delay of the channel impulse response
L_b	Number of uncoded transmitted bits
L_c	Number of coded transmitted bits
L_{CP}	Length of the cyclic prefix
M	Number of transmit antennas
$\mathbf{n}$	N-vector of noise samples at the receiver antennas
N	Number of receive antennas
N_0	Noise power spectral density at reception
$P(a)$	Probability of event a

$\mathbf{r}$	N-vector of received symbols
r_s	Spatial code rate
r_t	Temporal code rate
$\mathbf{R}$	$N \times K$ matrix of received symbols
$\mathbf{R_{ss}}$	$M \times M$ covariance matrix of $\mathbf{s}$
$\mathbf{s}$	M-vector of transmitted symbols
$\tilde{s}$	Soft estimate of symbol s
$\hat{s}$	Hard estimate of symbol s
$\mathbf{S}$	$M \times K$ matrix of transmitted symbols
T	Number of frequency bins or subcarriers
$Tr(\mathbf{A})$	Trace of matrix $\mathbf{A}$

Capítulo 1
Introducción

1.1 Introducción y Estado del Arte

Gracias a la evolución de la electrónica y de la teoría de la señal, los sistemas de comunicación inalámbricos se han vuelto omnipresentes, destacándose servicios como la telefonía móvil, la difusión de televisión y radio, las redes metropolitanas WMAN (*wireless metropolitan area network*) o las redes inalámbricas locales WLAN (*wireless local area network*). A modo de ejemplo, las tasas de bits de estas últimas han pasado en 8 años de los 11 megabits por segundo (Mbps) de la norma IEEE 802.11b a los cerca de 300 Mbps propuestos para el nuevo estándar IEEE 802.11n [EWC05, IEEE07].

Las necesidades del mercado, tanto de tasa de bits como de fiabilidad, así como las limitaciones de ancho de banda, han obligado a la comunidad científica a exprimir la teoría de la información y comunicación llevando hasta sus límites aspectos como la modulación, la codificación y, en especial, la materialización hardware (en chip) de los algoritmos de procesado de la señal [Rupp03, Burg06]. La mayoría de las aplicaciones de las comunicaciones inalámbricas exigen un tamaño reducido y un consumo mínimo de potencia, junto a elevadas prestaciones.

Son varios los caminos adoptados para maximizar las tasas de bits de los sistemas de comunicaciones inalámbricas: aumento del tamaño de las constelaciones, códigos más eficientes, optimización de los algoritmos de recepción, etc. Sin embargo, hay una técnica que destaca por encima del resto: la utilización de varias antenas, tanto en transmisión como en recepción. Esta técnica, denominada MIMO (*multiple input-multiple output*) permite multiplicar el límite de la capacidad de canal establecida por Shannon [Foschini98, Telatar99]. Debido a este incremento de capacidad, esta técnica ha sido incluida prácticamente en todos los nuevos estándares de comunicaciones inalámbricas, incluyendo el borrador del IEEE 802.11n para redes WLAN [EWC05, IEEE07].

La detección de una señal MIMO exige el conocimiento de los parámetros que definen el canal multiantena, los cuales se multiplican debido al número de antenas de transmisión y recepción. La estimación de estos parámetros de canal resulta una tarea com-

pleja y primordial para el rendimiento y la eficiencia espectral del sistema de comunicación [Hassibi00, Biguesh06].

Esta tesis doctoral analiza el efecto de la estimación de canal sobre el rendimiento de los detectores MIMO básicos, centrándose en su estudio mediante simulación y a través de una implementación hardware de tiempo real. Como se demostrará más adelante, esta implementación ha permitido cotejar los resultados de simulación con datos reales obtenidos en la plataforma hardware, así como conocer en detalle los aspectos relacionados con la materialización de los algoritmos.

Los siguientes apartados resumen de forma introductoria los tres ejes sobre los que se ha desarrollado esta tesis: los sistemas MIMO, la estimación de canal y la implementación hardware de algoritmos de tiempo real.

1.1.1 Sistemas Inalámbricos MIMO

Los sistemas MIMO representan uno de los mayores avances en el campo de las comunicaciones inalámbricas [Foschini98, Telatar99]. La principal característica de estos sistemas es la utilización de varias antenas tanto en recepción como en transmisión, donde se transmiten varios símbolos independientes de forma simultánea, más allá del concepto tradicional del conformado de haz y las antenas inteligentes. Los símbolos transmitidos por las diferentes antenas pueden corresponder a información independiente (multiplexado espacial) o a una codificación espacio-temporal de los símbolos de información. En función de la estrategia empleada, la utilización de múltiples antenas puede proporcionar un incremento en la tasa de bits, mayor fiabilidad de la comunicación o una combinación de ambas ventajas [Paulraj03].

La utilización de múltiples antenas permite multiplicar la capacidad de canal establecida por Shannon para canales de antena única [Foschini98, Telatar99], gracias al concepto de diversidad espacial, el cual consiste en asumir independencia o decorrelación entre los subcanales que se forman entre las diferentes antenas de transmisión y recepción. Sin embargo, la inclusión de múltiples antenas no es ninguna panacea: por un lado, se multiplica el número de cadenas de transmisión y recepción requeridas, incluyendo moduladores, conversores de frecuencia intermedia a radiofrecuencia, antenas, etc. Por otro lado, el coste computacional se dispara, sobre todo en recepción, debido al aumento de la complejidad de los algoritmos de sincronización, estimación de canal y, especialmente, la detección multiantena [Burg06]. Por lo tanto, la implementación de los algoritmos asociados a MIMO es vital de cara al desarrollo de sistemas realistas cuyo objetivo consiste en un equilibrio entre el rendimiento y el coste.

1.1.2 Estimación de Canal

La recepción y detección de una señal MIMO requiere el conocimiento del canal de comunicación, el cual adquiere una estructura matricial debido a la multiplicidad de antenas en transmisión y en recepción. A modo de ejemplo, si se supone un canal con una respuesta impulsional de 11 instantes de muestreo o *taps*, el número de parámetros complejos (amplitud y fase) a estimar puede pasar de 11 (esquema 1×1) a 176 (configuración 4×4). Este incremento del número de parámetros implica el rediseño de las secuencias de aprendizaje, así como una optimización de los algoritmos de estimación de canal [Hassibi00, Li03, Lang04].

La estimación de canal MIMO puede realizarse siguiendo tres estrategias diferentes:

1. **Estimación supervisada**: El transmisor transmite una secuencia de símbolos conocida por el receptor, permitiendo que este último pueda identificar el canal de una forma sencilla [Hassibi00, Biguesh06].

2. **Técnicas ciegas**: Los parámetros de canal son calculados (hasta cierto grado de ambigüedad) empleando únicamente los símbolos de información [Tong94, Tong98, Bölckskei02, Larsson03]. Por lo tanto, no se transmite ningún preámbulo que pueda facilitar la tarea del receptor.

3. **Estimación semi-ciega**: Se transmite un preámbulo que permite obtener una estimación inicial que es posteriormente mejorada empleando los símbolos de información [Muquet99, Míguez02, Wang03, Jagannatham06]. Es decir, estos métodos son una combinación de las técnicas supervisadas y ciegas.

Diversos estudios teóricos han evaluado la medida en que la información de canal puede limitar la capacidad teórica de un sistema MIMO [Hassibi00, Yong04, Cosovic07], así como las propiedades óptimas de los algoritmos de estimación para las configuraciones más habituales [Marzetta99a, Barhumi03, Biguesh06]. Sin embargo, resulta prácticamente imposible relacionar estos resultados teóricos (capacidades máximas, límites superiores, etc.) con el rendimiento de sistemas reales.

Se han publicado numerosos trabajos que han analizado el efecto de la estimación de canal sobre las tasas de errores de bit (BER, *bit error rate*) de varios tipos de sistemas: multiplexación espacial con DFE (*decission feedback equalizer*) [Zhu03b], sistemas iterativos Turbo-MIMO [Mysore05], sistemas MIMO multiportadora en canales espacialmente correlados [Chung06], sistemas de precodificación MIMO [Edward08], etc. Estos trabajos se centran en el análisis del efecto de un conjunto de estimadores de canal sobre un sistema MIMO en concreto. Sin embargo, no se han publicado resultados que muestren el rendimiento comparativo de los detectores MIMO empleando diferentes estimadores de canal, el cual es el objetivo principal de esta tesis doctoral. Asimismo, no se ha presentado ninguna metodología

sencilla que permita escoger la mejor combinación estimador-detector para un determinado sistema.

1.1.3 Demostradores y Sistemas de Prototipado MIMO

Uno de los objetivos principales de esta tesis ha sido el análisis del efecto de la implementación de algoritmos, especialmente la estimación de canal, sobre el rendimiento de un sistema MIMO completo. A tal efecto se ha diseñado y desarrollado un sistema MIMO 2×2 de tiempo real para el cual se han tenido que implementar todos los algoritmos de transmisión y recepción.

La implementación de algoritmos de tiempo real de procesado de señal se desarrolla habitualmente sobre dos clases de dispositivos: los dispositivos lógicos programables FPGA (*field-programmable gate array*) y los microprocesadores con prestaciones de tratamiento de la señal DSP (*digital signal processor*) [Rupp03, Kaiser04]. Generalmente, un sistema complejo consta de uno o varios de estos elementos. Los dispositivos FPGA, cuya principal virtud es el paralelismo de los recursos y la velocidad de operación que pueden alcanzar, suelen emplearse para la implementación de algoritmos no secuenciales y con cierta estructura, tales como filtros digitales, moduladores, ecualizadores, etc. Los microprocesadores DSP, en cambio, gracias a sus capacidades de procesado matemático y a su carácter secuencial, se destinan normalmente a operaciones complejas y de frecuencias de repetición reducidas, tales como cálculos de transformadas, inversas de matrices, etc.

Debido a la velocidad de procesado requerida, se han empleado dispositivos FPGA para la implementación de todos los algoritmos que conforman el sistema MIMO descrito en esta memoria. Dada la complejidad del diseño y la dificultad que conlleva la validación de los sistemas de comunicaciones, la implementación hardware de estos sistemas suele realizarse empleando herramientas de alto nivel, que combinan las prestaciones de lenguajes como Matlab[1] o C con la capacidad de definición de hardware de lenguajes de diseño tales como VHDL o Verilog, destacándose las dos siguientes:

- ***System Generator for DSP*** de Xilinx [Xilinx08]: Permite generar código VHDL sintetizable desde un entorno basado en Matlab/Simulink, ampliamente extendido en el campo del procesado de la señal. Existen muchas otras herramientas orientadas a las FPGA desarrolladas por otras compañías, tales como Altera o Sinplify, cuyas prestaciones son similares [Sinplicity].

- ***System C*** [SystemC]: Estándar de reciente creación basado en una versión sintentizable del lenguaje C++, el cual permite flexibilizar el diseño de algoritmos hardware así como facilitar su proceso de validación. Existen otras variantes, no tan estandarizadas

[1] Matlab y Simulink son marcas registradas de The Mathworks, Inc. [Mathworks].

pero probablemente más sofisticadas, basadas en lenguajes derivados de C/C++, entre los que destaca Handel C.

La herramienta System Generator for DSP ha sido considerada la mejor opción debido a su interfaz basada en Matlab y el amplio mercado abarcado por la casa Xilinx, tanto en el campo industrial como académico.

Existen numerosas plataformas de prototipado para comunicaciones inalámbricas, sobre todo en el ámbito universitario, que combinan varios de los citados dispositivos con entradas y salidas analógicas, posibilitando el desarrollo de aplicaciones complejas. Se han presentado numerosas plataformas con transmisores y receptores MIMO, tanto completamente integrados en hardware de tiempo real [Adjoudani03, Zelst04, Mehlführer05] como controlados *off-line* (transmisión de tiempo real y procesado en PC) desde Matlab [Kaiser04, Stege04, Caban06]. Algunas de estas plataformas MIMO han sido comercializadas por varias empresas, entre las que destaca la casa Signalion [Signalion].

1.2 Motivación

Tal y como se ha comentado anteriormente, la estimación de canal es un proceso especialmente complejo y costoso en los sistemas MIMO, sobre todo en términos de implementación y eficiencia de ancho de banda. El rendimiento de los algoritmos de estimación de canal suele compararse midiendo el error cuadrático medio normalizado (NMSE, *normalized mean squared error*) o, en determinados casos, evaluando las tasas BER de un sistema concreto con diferentes estimadores de canal.

Diversos estudios teóricos han determinado la medida en que la información de canal puede limitar la capacidad de un sistema MIMO [Marzetta99a, Hassibi00, Yong04, Cosovic07]. Sin embargo, no existen estudios teóricos o prácticos que evalúen la importancia de la estimación de canal dentro del diseño de un receptor MIMO completo. Es decir, no se han presentado resultados o análisis que comparen las tasas BER de varios detectores MIMO provistos de algoritmos diferentes de estimación de canal.

Esta tesis doctoral ha evaluado el efecto de la estimación de canal sobre el rendimiento comparativo de las técnicas básicas de detección MIMO, estableciendo la medida en que puede limitar dicha estimación el rendimiento de un receptor, así como evaluando la posibilidad de reducir la complejidad de un detector MIMO mejorando la calidad de la estimación de canal.

1.3 Objetivos y Metodología

Este proyecto de tesis ha analizado el efecto de la estimación de canal sobre los detectores MIMO siguiendo dos vertientes, una teórica y otra práctica. La primera ha tratado de

evaluar el efecto de la estimación de canal sobre las tasas BER de las diferentes técnicas de detección MIMO. La segunda, en cambio, ha desarrollado un sistema MIMO de tiempo real con el objetivo de evaluar su complejidad y su rendimiento en un entorno real donde se aprecian efectos de la implementación tales como fallos de sincronización, errores del estimador de canal, cuantificaciones, etc.

1.3.1 Objetivos del Estudio Teórico

El principal objetivo de esta tesis doctoral ha sido conocer el grado en que afecta la calidad de la estimación de canal al rendimiento comparativo de los esquemas de detección MIMO en sistemas de multiplexación espacial. Se han evaluado varios casos diferentes: con y sin diversidad en recepción, empleando transmisión de banda estrecha y de banda ancha, diferentes órdenes de modulación y ratios de codificación, etc.

Se ha planteado como objetivo el diseño de una metodología que permita comparar las curvas de tasas BER de los detectores MIMO empleando diferentes calidades de estimación de canal. En ocasiones, y en función del modelo de error del estimador, se han comparado los resultados de diferentes estimadores empleando el NMSE, pero se ha establecido la tasa BER como parámetro definitivo.

El diagrama de la figura 1.1 muestra los diferentes parámetros que intervienen en los procesos de detección y estimación de canal MIMO, así como las principales alternativas que se han evaluado.

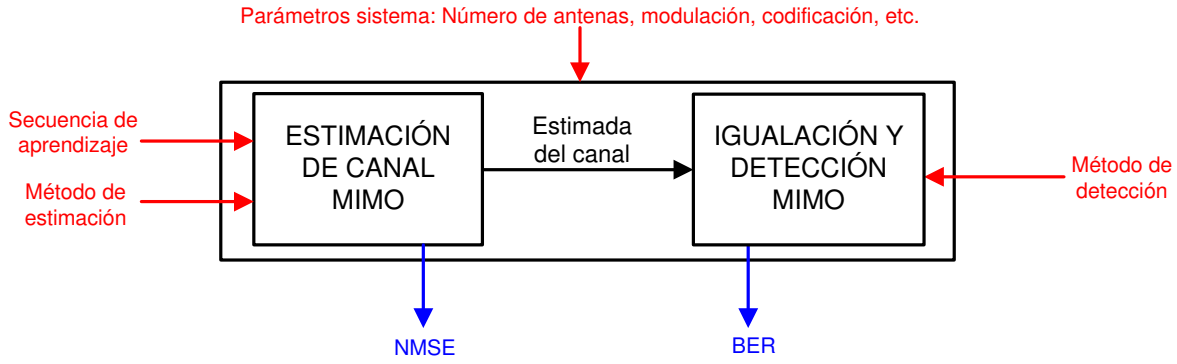

Figura 1.1: Bloques principales y parámetros del sistema evaluado.

El objetivo final ha sido el análisis de la importancia del proceso de estimación de canal en el diseño de un receptor MIMO, de tal forma que se pueda determinar la combinación idónea de métodos de estimación y detección en función de la limitación de recursos y las exigencias de rendimiento. Se han considerado tres sistemas MIMO de referencia: banda estrecha, banda ancha (OFDM y SCFDE) y un sistema iterativo Turbo-MIMO, el cual puede ser combinado con cualquiera de los anteriores para mejorar su rendimiento.

1.3.2 Objetivos de la Implementación Práctica

La parte más práctica de este trabajo ha consistido en la implementación de un sistema MIMO de tiempo real y sus algoritmos más importantes, incluida la estimación de canal, en una plataforma de prototipado rápido diseñada y desarrollada a tal efecto.

El principal objetivo ha consistido en la evaluación del coste de implementación de un sistema MIMO básico, así como en el análisis del impacto de la estimación de canal y otros algoritmos sobre el rendimiento de un receptor real. Los parámetros cuya evaluación se ha planteado son los siguientes:

1. Recursos necesarios para una implementación realista de un sistema MIMO 2×2 completo de tiempo real.

2. Complejidad real del algoritmo de estimación de canal (cantidad de bloques o celdas de la FPGA, número de multiplicadores, etc.)

3. Degradación sufrida por la tasa BER debido a la estimación de canal y a las características de la implementación real, tales como la resolución en la cuantificación, implementaciones de reducida complejidad, etc.

4. Latencias introducidas por los diferentes algoritmos.

1.3.3 Metodología

Este apartado detalla la forma en que se ha desarrollado la tesis doctoral y los pasos que se han seguido para la consecución de los objetivos planteados. Al igual que la definición de objetivos, la descripción de la metodología se dividirá en las partes relativas a la teoría y a la práctica, cuyo desarrollo se ha efectuado en paralelo.

1.3.3.1 Teoría y Simulaciones

A continuación se enumeran los pasos seguidos durante el desarrollo de la tesis para el análisis teórico y de simulación, así como los principales objetivos parciales y condiciones que dichos pasos han tenido como hitos.

1. Definición de las características de los sistemas que se han empleado para las comparaciones entre métodos. Se ha establecido un número determinado de modelos cuya comparación ha permitido reflejar el efecto de parámetros como el número de antenas, la longitud de las secuencias de aprendizaje, la modulación, el grado de diversidad, etc.

2. Establecimiento de un criterio de comparación del rendimiento de los detectores MIMO para varios grados de calidad de estimación de canal.

3. Implementación Matlab de los algoritmos de estimación de canal y su simulación para los diferentes modelos, realizando los siguientes pasos por cada algoritmo nuevo:

   (a) Corroboración de los resultados NMSE y BER obtenidos con los teóricos, en caso de haberlos, indicados en la bibliografía.

   (b) Comparación de los resultados BER con el caso del conocimiento exacto del canal.

   (c) Evaluación de las diferencias de resultados, en caso de haberlas, entre los diferentes sistemas con el objetivo de identificar los parámetros más influyentes de los modelos.

1.3.3.2 Implementación Práctica

De cara a la implementación práctica y su análisis, las pautas seguidas han sido las siguientes:

1. Selección de las herramientas que se han empleado para la implementación de los algoritmos del sistema MIMO. Se ha considerado primordial que dichas herramientas permitan simular los bloques implementados en hardware junto al código Matlab del sistema completo.

2. Validación de las tarjetas de prototipado rápido Heron de la Universidad de Mondragón y asimilación de todas sus herramientas de programación, depuración y control desde PC.

3. Diseño de una herramienta de cosimulación hardware/software para un sistema completo de comunicaciones MIMO.

4. Implementación de los algoritmos más sencillos: mínimos cuadrados (LS, *least-squares*) para la estimación de canal y la anulación o inversa (ZF, *zero-forcing*) para la detección MIMO. Esta primera implementación ha sido utilizada para validar la plataforma de desarrollo y la metodología de diseño de algoritmos de tiempo real.

5. Integración del decodificador óptimo (ML, *maximum likelihood*), implementado como un decodificador esférico (SD, *sphere decoder*), desarrollado en colaboración con la Universidad de Edimburgo. Se han evaluado los efectos de la implementación real y la estimación de canal sobre el rendimiento del decodificador esférico.

1.4 Contribuciones de la Tesis

Esta sección describe las contribuciones principales de cada uno de los capítulos que conforman la tesis, indicando dónde se proponen técnicas y resultados originales, así como su comparación con otras referencias bibliográficas de interés.

- **Capítulo 2:** Se ha realizado una comparación del rendimiento de los esquemas MIMO-OFDM y MIMO-SCFDE en sistemas WLAN basados en una extensión multiantena del estándar IEEE 802.11a, publicado en [Mendicute04a, Mendicute04b]. Estudios similares han sido presentados en [Coon03], aunque con detectores y parámetros muy diferentes.

- **Capítulo 3:** Se ha diseñado y materializado un demostrador MIMO 2×2 16-QAM. Se han implementado todos los algoritmos de tiempo real necesarios para su funcionamiento en un canal de banda estrecha. Como contribuciones especiales, destacan el diseño de un sistema de cosimulación y síntesis presentado en [Mendicute05], el desarrollo de un sistema "Hardware in the Loop" a medida para la plataforma MIMO de la Universidad de Mondragón [Mendicute06b], y la implementación de un sistema completo MIMO basado en el decodificador esférico, junto a la Universidad de Edimburgo, el cual ha permitido evaluar su complejidad de implementación y su rendimiento en un entorno realista con estimación de canal, sincronización, cuantificaciones, etc. [Mendicute06a]. Esta implementación ha sido la primera en integrar un decodificador esférico en un sistema MIMO completo.

- **Capítulo 4:** Dentro de la evaluación de métodos de estimación de canal para sistemas MIMO, se ha propuesto una técnica de predicción de tasas BER para receptores Turbo-MIMO basados en detectores MMSE-PIC con error de estimación de canal. Se ha propuesto una herramienta simple que permite incluir dicho error y sus efectos en las técnicas de evaluación BER basadas en tablas EXIT analíticas [Mendicute07], ampliando las técnicas propuestas en [Hermosilla05] para el caso de conocimiento perfecto del canal.

- **Capítulo 5:** Se han mostrado resultados que permiten evaluar la importancia de la estimación de canal y la implementación hardware sobre sistemas MIMO completos basados en el receptor más simple (ZF) y la implementación más común (SD) del receptor óptimo ML [Mendicute06a]. Asimismo, se han presentado resultados de simulación que analizan el efecto de los errores de estimación de canal sobre los diferentes receptores MIMO, tanto para banda estrecha como para OFDM y SCFDE.

  Finalmente, se ha propuesto una arquitectura paralela, implementable en dispositivos FPGA, de un estimador de canal semi-iterativo basado en realimentación de decisión. Esta estructura de estimación de canal reduce la latencia del sistema y aumenta su rendimiento con un coste computacional moderado. A la fecha de redacción de este documento, los resultados de este capítulo no han sido aún publicados, aunque están en preparación tal y como se indica en el listado del apéndice A.

1.5 Estructura de la Tesis

La estructura de esta memoria de tesis es la siguiente: en el capítulo 2 se describen las principales características de los sistemas MIMO, así como sus extensiones de banda ancha basados en OFDM y SCFDE, realizando una comparación de rendimiento de estos últimos en sistemas MIMO WLAN. Asimismo, se detalla la estructura de un sistema iterativo MIMO basado en un receptor MMSE-PIC, junto a herramientas analíticas de evaluación de convergencia y estimación de tasas BER basadas en funciones EXIT analíticas.

El capítulo 3 se se centra en el desarrollo de la plataforma de prototipado rápido y la implementación MIMO 2x2 de tiempo real. Como aspecto importante, este capítulo incluye la integración de un decodificador esférico dentro del sistema MIMO completo, realizada en colaboración con la Universidad de Edimburgo.

El capítulo 4 describe las principales técnicas de estimación de canal para los sistemas escogidos, centrándose en técnicas aplicables en la realidad, tales como los métodos supervisados o esquemas iterativos sencillos. Se muestran los principales aspectos de la estimación de canal para sistemas MIMO, MIMO-OFDM, MIMO-SCFDE y Turbo-MIMO. En la parte final de este capítulo se propone una extensión de las herramientas de evaluación de rendimiento basadas en funciones EXIT a sistemas iterativos MIMO con estimación de canal.

El capítulo 5 describe los análisis efectuados para evaluar el impacto de la calidad de la estimación de canal sobre las técnicas MIMO fundamentales, enfocándolo desde dos puntos de vista. Por un lado, se analiza su efecto empleando la plataforma MIMO de tiempo real. Por otro lado, se muestra la evaluación del efecto de la estimación de canal sobre sistemas más complejos, la cual se ha llevado a cabo mediante simulaciones de Matlab. Este último capítulo propone en su parte final una arquitectura paralela para la estimación de canal MIMO, mostrando su eficacia en sistemas de banda estrecha, OFDM y SCFDE.

Por último, el capítulo 6 resume el trabajo realizado y las principales conclusiones obtenidas, así como las líneas futuras que pueden servir para completar y ampliar el trabajo presentado en esta memoria de tesis.

Chapter 2

MIMO Systems in Wireless Communications

2.1 Introduction

This chapter shows an introductory analysis and the simulation-based performance evaluation of several fundamental multiple input-multiple output (MIMO) wireless communication systems. First, the main model and capacity bounds are described for a generic narrowband (frequency-flat fading) MIMO wireless system. The performance and complexity issues of different space-time coding (STC) approaches and detection techniques are summarized, focusing on the main MIMO detection algorithms for spatial multiplexing (SM) schemes. Comparative bit error rate (BER) performance results are provided for coded and uncoded SM systems to illustrate the behavior of the MIMO detection algorithms.

If the actual capacity gains of multi-antenna systems are to be reached, these fundamental MIMO schemes must be combined with wideband transmission techniques. Sections 2.3 and 2.4 analyze the extension of basic SM techniques to frequency-selective fading channels, based on orthogonal frequency-division multiplexing (OFDM) and single carrier with frequency-domain equalization (SCFDE), respectively. The BER performance curves of these techniques are compared in a multi-antenna wireless local area network (WLAN) scenario based on an adaptation of the IEEE 802.11a standard.

Finally, the application of MIMO techniques to iterative (Turbo) receivers is analyzed in Section 2.5, where the basic structure is shown for a linear MIMO receiver with parallel interference cancellation (PIC) processing. The convergence and the BER performance of the system are analyzed by means of standard Monte Carlo (MC) simulations and extrinsic information transfer (EXIT) based semi-analytical tools.

2.2 Narrowband MIMO Wireless Systems

Most wideband MIMO communication systems, such as those based on OFDM or code division multiple access (CDMA), can be reduced to multiple parallel narrowband schemes. Hence, the basic analysis of STC coding and MIMO detection algorithms can be carried out for a simple canonical system model, based on single-carrier transmission in a frequency-flat fading channel environment. As will be shown later in this chapter, it is straightforward to extend these fundamental MIMO techniques to wideband modulation schemes, such as OFDM or SCFDE.

2.2.1 System Model

The considered theoretical system model has, as depicted in Figure 2.1, M transmit and N receive antennas. An input sequence of L_b information bits $b(l)$ is space-time coded, providing K M-vectors of transmitted symbols $\mathbf{s}(k)$, which belong to a generic quadrature amplitude modulation (QAM) constellation of B points. Scalars l and k denote the bit and symbol period indexes, respectively. Symbols $\mathbf{s}(k)$ are modulated and transmitted simultaneously by M transmit antennas through the $M \times N$ wireless channel, being received at the N reception antennas, where they are sampled and demodulated simultaneously. The N-vector of received symbols $\mathbf{r}(k)$ is then processed by a MIMO detection block, which outputs the estimates of the transmitted bits, denoted as $\hat{b}(l)$.

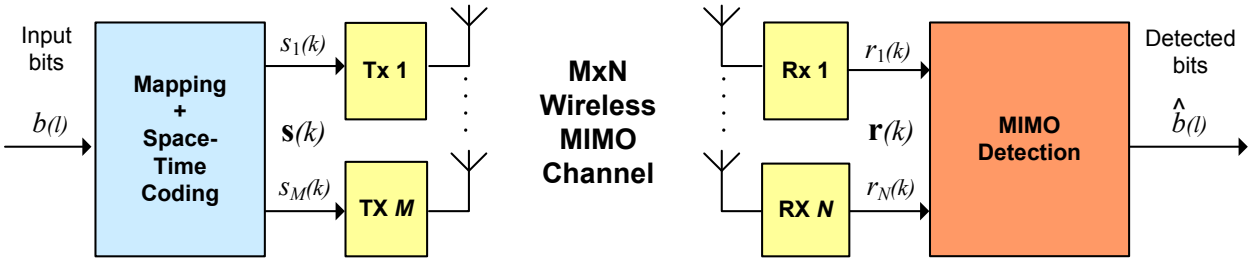

Figure 2.1: Basic diagram of a wireless MIMO system.

Assuming symbol-synchronous receiver sampling and ideal timing, the system of Figure 2.1 can be represented using matrix notation as

$$\mathbf{r}(k) = \sqrt{\frac{E_s}{M}}\mathbf{H}(k)\mathbf{s}(k) + \mathbf{n}(k), \tag{2.1}$$

where $\mathbf{s}(k) = [s_1(k), s_2(k), ..., s_M(k)]^T$ denotes the vector of transmitted symbols with normalized average energy $\mathrm{E}[|s_i|^2] = 1$, E_s is the total transmitted symbol energy, which is independent of the number of transmit antennas, $\mathbf{n}(k) = [n_1(k), n_2(k), ..., n_N(k)]^T$ is the vector of independent and identically distributed (i.i.d.) complex additive white Gaussian

noise (AWGN) samples with variance N_0, and $\mathbf{r}(k) = [r_1(k), r_2(k), ..., r_N(k)]^T$ is the vector of received symbols. The $N \times M$ matrix $\mathbf{H}(k)$ represents the $M \times N$ MIMO channel at symbol index k, being defined as

$$\mathbf{H}(k) = \begin{bmatrix} h_{11}(k) & h_{12}(k) & ... & h_{1M}(k) \\ h_{21}(k) & h_{22}(k) & ... & h_{2M}(k) \\ : & : & : & : \\ h_{N1}(k) & h_{N2}(k) & ... & h_{NM}(k) \end{bmatrix}, \tag{2.2}$$

where h_{nm} represents the complex channel gain between transmit antenna m and receive antenna n. If a quasi-static frame-based transmission scheme is assumed, where the channel $\mathbf{H} = \mathbf{H}(k)$ is assumed constant over a whole burst, vectors $\mathbf{s}(k)$, $\mathbf{r}(k)$ and $\mathbf{n}(k)$ can be stuck into matrices, leading to the following system model:

$$\mathbf{R} = \sqrt{\frac{E_s}{M}}\mathbf{HS} + \mathbf{N}, \tag{2.3}$$

where $\mathbf{R}$ is the $N \times K$ matrix of received symbols, $\mathbf{S}$ is the $M \times K$ transmitted symbol matrix, and $\mathbf{N}$ contains the $N \times K$ noise samples.

2.2.2 Capacity of MIMO Channels

The channel capacity, defined as the maximum achievable error-free data rate, was first derived for AWGN single input-single output (SISO) channels by Claude Shannon in 1948 [Shannon48]. For such a system, the channel capacity is given by:

$$C_{SISO} = \log_2(1 + \rho) \text{ bps/Hz}, \tag{2.4}$$

where $\rho = E_s/N_0$ denotes the signal to noise ratio (SNR) of the wireless system. The derivation of MIMO channel capacity bounds has been and still is a very active research area. Many capacity and performance limits have been published for different STC systems and channel models [Paulraj03]. The results of the two most significative approaches will be summarized in the following sections, based on the deterministic and the random channel assumptions.

2.2.2.1 Deterministic MIMO Channel

The capacity of the MIMO channel is defined by the following equation [Foschini96, Telatar99]:

$$C = \max_{f(\mathbf{s})} I(\mathbf{s}; \mathbf{r}), \tag{2.5}$$

where $f(\mathbf{s})$ is the probability density function (pdf) of $\mathbf{s}$ and $I(\mathbf{s};\mathbf{r})$ is the mutual information between $\mathbf{s}$ and $\mathbf{r}$, which can be expressed as

$$I(\mathbf{s};\mathbf{r}) = H(\mathbf{r}) - H(\mathbf{r}|\mathbf{s}), \tag{2.6}$$

where $H(\mathbf{r})$ is the differential entropy of $\mathbf{r}$ and $H(\mathbf{r}|\mathbf{s})$ is the conditional differential entropy of $\mathbf{r}$ given that $\mathbf{s}$ is known. Since the vectors $\mathbf{s}$ and $\mathbf{n}$ are independent, Equation (2.6) simplifies to

$$I(\mathbf{s};\mathbf{r}) = H(\mathbf{r}) - H(\mathbf{n}). \tag{2.7}$$

Hence, maximizing $I(\mathbf{s};\mathbf{r})$ reduces to maximizing $H(\mathbf{r})$, which occurs when $\mathbf{s}$ is a zero mean circularly symmetric complex Gaussian (ZMCSCG) vector whose distribution is completely characterized by its covariance matrix $\mathbf{R_{ss}}$. The differential entropies $H(\mathbf{r})$ and $H(\mathbf{n})$ are given as [Paulraj03]

$$H(\mathbf{r}) = \log_2 \det\left(\pi e \mathbf{R}_{rr}\right) = \log_2 \det\left(\pi e\left(N_0\mathbf{I}_N + \frac{E_s}{M}\mathbf{H}\mathbf{R}_{ss}\mathbf{H}^H\right)\right) \text{ bps/Hz}, \tag{2.8}$$

and

$$H(\mathbf{n}) = \log_2 \det\left(\pi e N_0 \mathbf{I}_N\right) \text{ bps/Hz}. \tag{2.9}$$

Therefore, the capacity becomes [Telatar99]

$$C = \max_{\mathrm{Tr}(\mathbf{R}_{ss})=M} \log_2 \det\left(\mathbf{I}_N + \frac{\rho}{M}\mathbf{H}\mathbf{R}_{ss}\mathbf{H}^H\right) \text{ bps/Hz}, \tag{2.10}$$

where $\mathrm{Tr}(\mathbf{R_{ss}}) = M$ limits the transmitted symbol energy. The capacity C in (2.10) is often referred to as the error-free spectral efficiency or the data rate per unit bandwidth that can be sustained reliably over the MIMO link.

If no channel knowledge is available at the transmitter, the transmitted signals are independent and equi-powered, i.e., $\mathbf{R}_{ss} = \mathbf{I}_M$, and the capacity is given as

$$C = \log_2 \det\left(\mathbf{I}_N + \frac{\rho}{M}\mathbf{H}\mathbf{H}^H\right) \text{ bps/Hz}. \tag{2.11}$$

If the eigendecomposition of $\mathbf{H}\mathbf{H}^H$ is carried out, the capacity in (2.11) can be expressed as

$$C = \sum_{i=1}^{r_c} \log_2\left(1 + \frac{\rho}{M}\lambda_i\right), \tag{2.12}$$

where r_c is the rank of the channel and λ_i $(i = 1, 2, ..., r_c)$ are the positive eigenvalues of $\mathbf{H}\mathbf{H}^H$. Equation (2.12) expresses the capacity of the MIMO channel as the sum of the capacities of r_c SISO channels, each having a gain λ_i and a transmit energy of E_s/M.

It has been shown that orthogonal channel matrices ($\mathbf{H}\mathbf{H}^H = \alpha\mathbf{I}_M$) maximize the capac-

ity [Paulraj03]. Furthermore, if the elements of $\mathbf{H}$ satisfy $\|\mathbf{H}_{i,j}\|^2 = 1$ and a full-rank MIMO channel with $M = N = r_c$ is considered, the capacity of the MIMO channel becomes:

$$C = M\log_2(1+\rho). \tag{2.13}$$

The MIMO capacity for this particularly illustrative case is therefore M times the scalar SISO channel capacity.

All the aforementioned capacity values can be improved if the channel or some of its statistics are known at the transmitter side [Marzetta99b, Paulraj03], which is not the case for the research described in this document.

2.2.2.2 Random MIMO Channel

If a random channel matrix $\mathbf{H}$ is assumed, each realization of the fading channel has a maximum information rate defined by (2.11) and (2.13). Two capacity values can be calculated: the ergodic and the outage channel capacity. The first assumes an independent channel realization for each channel use and represents the ensemble average of information rate over the distribution of elements of $\mathbf{H}$. The ergodic capacity can therefore be written as

$$C = \mathrm{E}\left[\log_2 \det\left(\mathbf{I}_N + \frac{\rho}{M}\mathbf{H}\mathbf{R}_{\mathbf{ss}}\mathbf{H}^H\right)\right] \quad \text{bps/Hz}. \tag{2.14}$$

On the other hand, the outage capacity quantifies the level of capacity that can be guaranteed with a certain level of reliability [Paulraj03]. The g%-outage capacity $C_{out,g}$ is defined as the information rate that is guaranteed for $(100-g)$% of the channel realizations, i.e., $P(C \leq C_{out,g}) = g\%$ [Biglieri98]. Figure 2.2 shows the 10%-outage capacity values for random MIMO wireless channels with $M = N$ and no channel state information at the transmitter side. As it can be seen, the capacity values increase considerably with the number of transmit antennas.

2.2.3 Space-Time Coding Techniques

STC techniques define how the information bits $b(l)$ are coded into the transmitted symbol vector matrix $\mathbf{S}$. Assume that the $L_c = L_b$ data bits are first mapped onto a QAM constellation of B points leading to the data symbols $d(n)$, where n ranges from 1 to $N_c = L_c/q$ and $q = \log_2 B$ represents the modulation order. These N_c symbols are then processed by a space-time coder that adds additional $MK - N_c$ parity symbols, resulting in the $M \times K$ transmitted symbol matrix $\mathbf{S}$. Hence, the signalling data rate of the channel is $L_b/K = qN_c/K = qr_s$, where $r_s = N_c/K$ is the spatial code rate.

If a common forward error correcting (FEC) code of rate r_t, such as a convolutional code, is used before the symbol mapping, i.e., $L_c = L_b/r_t$ and $N_c = L_b/(qr_t)$, the final signalling

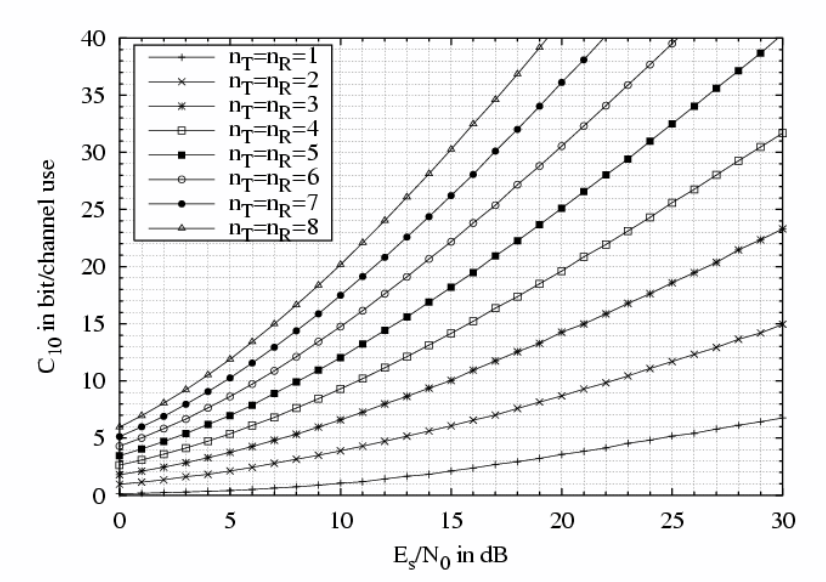

Figure 2.2: 10%-outage capacity of random MIMO channels with $M = N$.

rate can be expressed as:

$$\frac{L_b}{K} = \frac{L_c r_t}{K} = \frac{q N_c r_t}{K} = q r_s r_t. \tag{2.15}$$

Depending on the choice of the STC scheme, the spatial rate r_s varies from 0 (infinite coding diversity) to M (full multiplexing). For certain classes of codes, such as space-time trellis codes (STTC) or bit-interleaved coded modulation (BICM), the functions of the symbol mapper and the space-time (ST) coder can be combined into a single block.

The following subsections show the structures and benefits of the most common STC techniques. The channel is assumed unknown to the transmitter and perfectly known at the receiver side for the rest of this chapter.

2.2.3.1 Spatial Multiplexing

Figure 2.3 shows the basic structure of an uncoded SM system, also known as vertical Bell-Labs layered space-time (V-BLAST). As it is shown, the information bits are mapped onto a QAM constellation and divided into M substreams which are transmitted independently, leading to a spatial rate of $r_s = M$. This approach results in a signalling rate of qM bits per transmission symbol period.

Three main schemes can be distinguished that combine temporal FEC-based coding and SM systems: horizontal encoding (HE), vertical encoding (VE) and diagonal encoding (DE).

- **Horizontal Encoding:** In HE the bit stream is first demultiplexed into M separate streams, as is shown in Figure 2.4a. Each stream undergoes independent temporal coding, interleaving, symbol mapping and modulation, and is transmitted from one antenna.

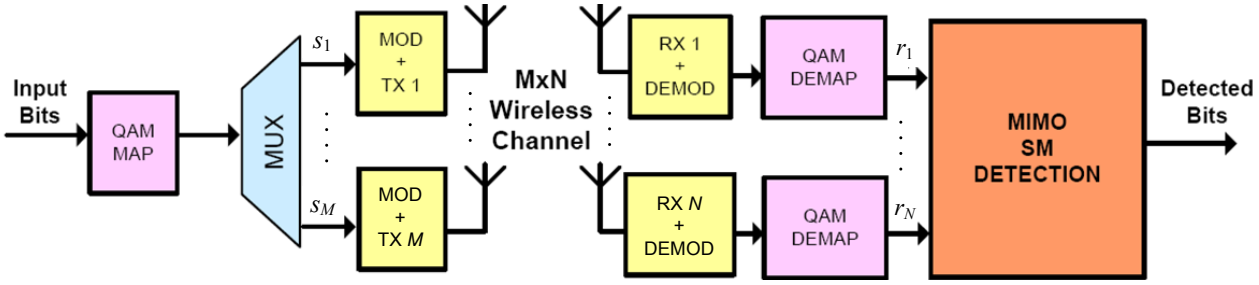

Figure 2.3: Diagram of an uncoded $N \times M$ spatial multiplexing MIMO system.

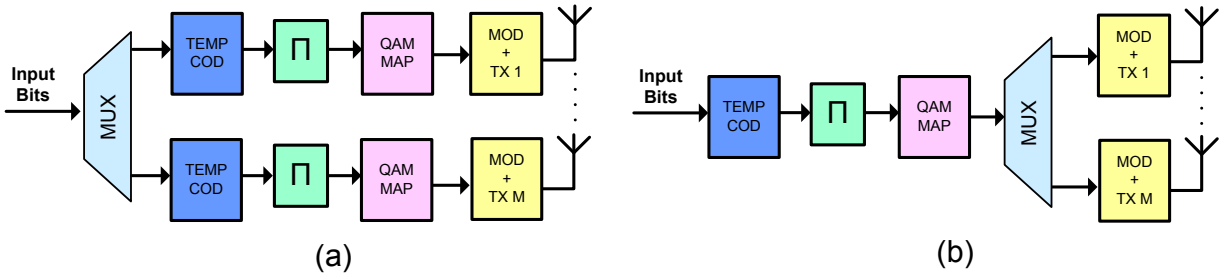

Figure 2.4: Diagrams of horizontally (a) and vertically (b) encoded spatial multiplexing transmitters.

- **Vertical Encoding:** In VE the bit stream first undergoes temporal coding, interleaving and symbol mapping, after which it is demultiplexed into M transmission streams, as is depicted in Figure 2.4b. This encoding scheme achieves better performance results than the previous HE approach, since each information stream is spread across all the antennas. However, it can be very complex since joint decoding of the substreams must be peformed at the receiver.

- **Diagonal Encoding:** In DE, which was introduced as diagonal Bell-Labs layered space-time (D-BLAST) in [Foschini96], the data stream first undergoes HE encoding, after which each symbol stream is split into blocks. These blocks are rotated in a round-robin fashion so that the bit stream-antenna association is periodically shifted, ensuring that the codeword from any stream is sent over all the antennas.

2.2.3.2 Space-Time Block Codes

While SM multiplies the transmission rate by the number of transmit antennas, space-time block coding (STBC) provides higher diversity by coding the information symbols in the spatial domain.

Alamouti Scheme

A pioneering and popular STBC scheme is the Alamouti code, which was originally de-

signed for systems with two transmit and one receive antennas [Alamouti98]. This technique divides the transmitted symbol stream in pairs $\mathbf{s} = [s_1, s_2]$ which are mapped into a 2×2 matrix $\mathbf{S_A}$ which is defined as

$$\mathbf{S_A} = \begin{pmatrix} s_1 & -s_2^* \\ s_2 & s_1^* \end{pmatrix}, \tag{2.16}$$

where the first and second column represent the symbols transmitted at the first and second symbol periods, respectively. Assuming that the channel remains constant over these periods and the fading is frequency-flat, the signal at the reception antenna for symbol time indexes 1 and 2 is given by:

$$r_1 = \sqrt{\frac{Es}{2}} h_1 s_1 + \sqrt{\frac{Es}{2}} h_2 s_2 + n_1 \tag{2.17}$$

$$r_2 = -\sqrt{\frac{Es}{2}} h_1 s_2^* + \sqrt{\frac{Es}{2}} h_2 s_1^* + n_2 \tag{2.18}$$

where h_1 and h_2 are the complex channel gains from transmit antennas 1 and 2 to the receive antenna. If the received signals are rearranged and stuck into a vector $\mathbf{y}$ as follows

$$\mathbf{y} = \begin{bmatrix} r_1 \\ r_2^* \end{bmatrix}, \tag{2.19}$$

the system can be expressed as

$$\mathbf{y} = \sqrt{\frac{E_s}{2}} \begin{bmatrix} h_1 & h_2 \\ h_2^* & -h_1^* \end{bmatrix} \begin{bmatrix} s_1 \\ s_2 \end{bmatrix} + \begin{bmatrix} n_1 \\ n_2^* \end{bmatrix} = \sqrt{\frac{E_s}{2}} \mathbf{H}_{eff} \mathbf{s} + \mathbf{n}, \tag{2.20}$$

where $\mathbf{s} = [s_1\ s_2]^T$, $\mathbf{n} = [n_1\ n_2^*]^T$ and the effective channel $\mathbf{H}_{eff}$ is orthogonal, so that $\mathbf{H}_{eff}^H \mathbf{H}_{eff} = \|\mathbf{h}\|_F^2 \mathbf{I}_2$. If $\mathbf{z} = \mathbf{H}_{eff}^H \mathbf{y}$, then

$$\mathbf{z} = \sqrt{\frac{E_s}{2}} \|\mathbf{h}\|_F^2 \mathbf{I}_2 \mathbf{s} + \tilde{\mathbf{n}}, \tag{2.21}$$

where $\tilde{\mathbf{n}}$ is a vector of zero-mean noise samples with covariance $\mathrm{E}\{\tilde{\mathbf{n}}\tilde{\mathbf{n}}^H\} = \|\mathbf{h}\|_F^2 N_0 \mathbf{I}_2$. Hence, (2.21) can be simplified as

$$z_i = \sqrt{\frac{E_s}{2}} \|\mathbf{h}\|_F^2 s_i + \tilde{n}_i,\ i = 1, 2, \tag{2.22}$$

which can be considered as two individual detection problems. The received SNR value η corresponding to each symbol is given by

$$\eta = \frac{\|\mathbf{h}\|_F^2 \rho}{2}. \tag{2.23}$$

If $\mathrm{E}\left(\|\mathbf{h}\|_F^2\right) = 2$, the SNR at detection becomes $\eta = \rho$, where $\rho = E_s/N_0$ is the SNR of the system, which is also the SNR per transmitted information symbol for the Alamouti scheme. This means that this STC scheme does not allow array gain, thought it achieves a diversity gain of 2 [Alamouti98, Paulraj03].

General STBC Schemes

The Alamouti scheme can be extended to larger systems using orthogonal space-time block coding (OSTBC). These codes can be designed for any number of transmit antennas with a spatial rate of $r_s = 1$, provided that only real constellations are used [Tarokh99]. An example of such coding schemes, which can achieve a diversity gain of MN, is the orthogonal code design for $M = 4$, whose structure is the following:

$$\mathbf{S}_{STBC} = \begin{bmatrix} s_1 & -s_2 & -s_3 & -s_4 \\ s_2 & s_1 & s_4 & -s_3 \\ s_3 & -s_4 & s_1 & s_2 \\ s_4 & s_3 & -s_2 & s_1 \end{bmatrix} \tag{2.24}$$

If linear processing is applied at the receiver, the decoding is decoupled into simpler scalar (SISO) detection problems, resulting in an input-output relation similar to that described in (2.22) for the Alamouti scheme.

In the case of complex constellations, orthogonal designs with spatial rate $r_s = 1$ only exist for systems with $M = 2$ transmit antennas [Tarokh99]. However, orthogonal STBC codes exist for spatial rates of $r_s = 1/2$ with any number of transmit antennas. One of such codes is shown below for $M = 3$ and complex constellations:

$$\mathbf{S}_{STBC} = \begin{bmatrix} s_1 & -s_2 & -s_3 & -s_4 & s_1^* & -s_2^* & -s_3^* & -s_4^* \\ s_2 & s_1 & s_4 & -s_3 & s_2^* & s_1^* & s_4^* & -s_3^* \\ s_3 & -s_4 & s_1 & s_2 & s_3^* & -s_4^* & s_1^* & s_2^* \end{bmatrix}. \tag{2.25}$$

2.2.3.3 Space-Time Trellis Codes

STTC techniques are an extension of conventional trellis codes to multi-antenna systems. These schemes can achieve coding gain and full spatial diversity. Each node or trellis state has A groups of symbols to the left, where A is the constellation size, with each group consisting of M entries. Each group represents the output for a given input symbol and the M entries correspond to the symbols to be transmitted from the M antennas. Figure 2.5 shows a trellis diagram for a 4-QAM, 4-state STTC scheme for $M = 2$ transmit antennas. These codes can be designed to maximize the coding gain, diversity order or ease of decoding for a given rate.

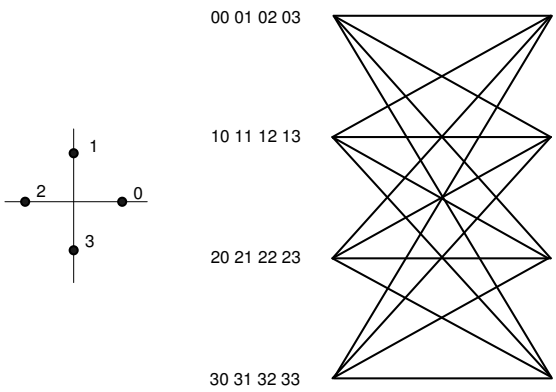

Figure 2.5: Trellis diagram for a 4-QAM, 4-state STTC code with $M = 2$.

The transmitted frames are decoded at the receiver using maximum likelihood (ML) sequence estimation, based on a multi-antenna extension of the Viterbi decoder. The number of states in the trellis and the number of receive antennas define the coding and diversity gains of STTC techniques. Other STC coding approaches, such as delay diversity coding, can be considered as particular cases of STTC techniques.

2.2.4 Summary of MIMO Detection Algorithms

The choice of the MIMO detection algorithm depends on the STC technique used at the transmitter side. For example, when OSTBC codes are used, MIMO detection can be considered a set of parallel SISO detection problems, so it can be simplified [Paulraj03]. On the other hand, if STTC coding is selected for transmission, no general simplifying rule exists and Viterbi-like multi-antenna Trellis-based algorithms are applied.

Spatial multiplexing, where no proper spatial coding exists ($r_s = M$), is the case that best represents the multi-antenna detection problem, so it can be chosen as a reference when evaluating MIMO detection and channel estimation techniques. The most common and interesting detection algorithms are shown in the following list, where the symbol index k of (2.1) has been dropped for simplicity.

1. **Linear techniques**, where the detected symbol vector $\hat{\mathbf{s}}$ is calculated multiplying the received vector $\mathbf{r}$ by a spatial filtering matrix $\mathbf{G}$, as it can be seen in the following equation:

$$\hat{\mathbf{s}} = \mathbf{G}\mathbf{r}. \tag{2.26}$$

   The two most common linear approaches are the following:

   (a) **Zero-forcing (ZF)**: It tries to eliminate the interference between the transmission antennas, being the nulling matrix $\mathbf{G}$ given by

$$\mathbf{G}_{ZF} = \sqrt{\frac{M}{E_s}}\mathbf{H}^{+} = \sqrt{\frac{M}{E_s}}(\mathbf{H}^{H}\mathbf{H})^{-1}\mathbf{H}^{H} \tag{2.27}$$

where $^{+}$ and ^{H} denote the pseudoinverse and Hermitian operations, respectively. This MIMO detection technique, which is the easiest to implement, has a very limited performance due to noise enhancement [Foschini98].

(b) **Minimum mean squared error (MMSE)** [Böhnke03]: It balances the interference nulling and the noise enhancement of the filter matrix by minimizing the total output error. The new filter matrix $\mathbf{G}_{MMSE}$ can be calculated as

$$\mathbf{G}_{MMSE} = \sqrt{\frac{M}{E_s}}(\mathbf{H}^{H}\mathbf{H} + \frac{M}{\rho}\mathbf{I}_M)^{-1}\mathbf{H}^{H} \tag{2.28}$$

2. **Non-linear techniques**

(a) **Maximum likelihood (ML)** [Paulraj97, Larsson03]: Optimal detection technique based on the minimization of an error metric which is evaluated for all the possible transmitted symbols, as is represented in (2.29). Its complexity can be prohibitive for systems with large constellations or many transmission antennas, due to the B^M metrics that must be evaluated.

$$\hat{\mathbf{s}} = \arg\min_{\mathbf{s}} \left\| \mathbf{r} - \sqrt{\frac{E_s}{M}}\mathbf{H}\mathbf{s} \right\|_F^2 \tag{2.29}$$

(b) **ZF-V-BLAST** [Golden99, Böhnke03]: It is based on the so-called ordered successive interference cancellation (OSIC) methods. The symbols transmitted at each antenna are detected successively following a descending signal to interference and noise ratio (SINR) criterion, as is shown in Figure 2.6. Every time a symbol is detected, its effects are removed from the received signal, decreasing the error probability of the remaining symbols. If a horizontal encoding scheme is used, the decoder can be included in the feedback chain, as is represented in Figure 2.6, where $\mathbf{b}_m$ represents the sequence of detected bits for transmit antenna m.

(c) **MMSE-V-BLAST** [Golden99, Böhnke03]: It is an extension of ZF-V-BLAST that uses the MMSE spatial nulling technique. Its performance and complexity are clearly higher than those of linear MMSE and ZF-V-BLAST algorithms, as will be shown in the BER performance comparisons of Section 2.2.5.

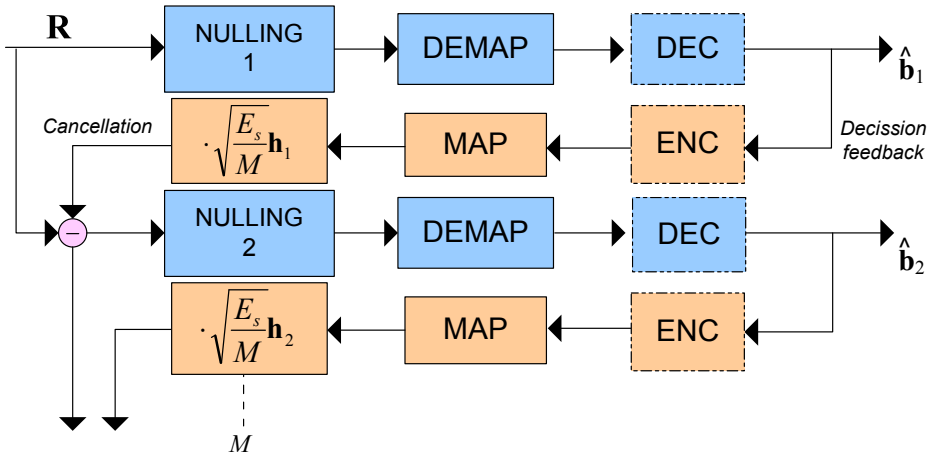

Figure 2.6: Structure of a generic detector with successive interference cancellation.

2.2.4.1 The Sphere Decoder

The sphere decoder (SD) is a specially relevant detection algorithm because it achieves the optimal ML solution with a considerable reduction in the number of calculated metrics, which depends on the SNR value and the channel realization [Damen00, Hassibi01]. This algorithm reduces the computational complexity of the maximum likelihood (ML) detector by searching over only those noiseless received points, defined as $\frac{\sqrt{E_s}}{M}\mathbf{Hs}$, that lie within a hypersphere of radius R around the received signal $\mathbf{r}$, as is shown in Figure 2.7 for a simplified 2-dimensional case, where the dots represent the noiseless received constellation and the cross represents the actual received point contaminated with noise.

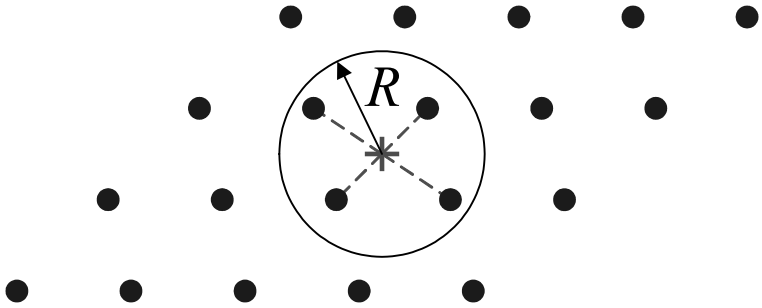

Figure 2.7: Schematic of the sphere decoder search principle for the 2-dimensional case.

The complex version of the SD is considered here, which is applied directly to the complex lattice $\Lambda(\mathbf{H}) = \{\sqrt{\frac{\mathbf{E_s}}{\mathbf{M}}}\mathbf{Hs}\}$ [Hochwald03]. The process can be represented by

$$\hat{\mathbf{s}}_{ml} = \arg\{\min_{\mathbf{s}} \|\mathbf{r} - \sqrt{\frac{\mathbf{E_s}}{\mathbf{M}}}\mathbf{Hs}\|^2 \leq R^2\}\,. \tag{2.30}$$

The sphere constraint in (2.30) can also be written, after matrix decomposition and removal

of constant terms, as

$$\|\mathbf{U}(\mathbf{s}-\hat{\mathbf{s}})\|^2 \leq R^2 \tag{2.31}$$

where $\mathbf{U}$ is an $M \times M$ upper triangular matrix, with entries denoted as u_{ij}, obtained through Cholesky decomposition of the Gram matrix $\mathbf{G}_G = \frac{E_s}{M}\mathbf{H}^H\mathbf{H}$ and $\hat{\mathbf{s}} = \sqrt{\frac{M}{E_s}}(\mathbf{H}^H\mathbf{H})^{-1}\mathbf{H}^H\mathbf{r}$ is the unconstrained ML estimate of $\mathbf{s}$ [Hochwald03].

The solution of the sphere constraint (SC) in (2.31) can be obtained recursively using a tree search algorithm, starting from $i = M$ and working backwards until $i = 1$. For each level, the constellation points s_i that satisfy

$$|s_i - z_i|^2 \leq \frac{T_i}{u_{ii}^2} \tag{2.32}$$

are selected as partial ML candidates, where

$$z_i = \hat{s}_i - \sum_{j=i+1}^{M} \frac{u_{ij}}{u_{ii}}(s_j - \hat{s}_j) \tag{2.33}$$

and

$$T_i = R^2 - \sum_{j=i+1}^{M} u_{jj}^2 |s_j - z_j|^2 . \tag{2.34}$$

When a new point is found inside the hypersphere (at $i = 1$) the radius is updated with the new minimum Euclidean distance and the algorithm continues the search with the new SC. This process can be seen as a tree search through M levels where each node on each level contains P branches. If $T_i \leq 0$, at any level i, the squared Euclidean distance from the root to that node has exceeded the SC and the entire branch plus all its descendants can be discarded, yielding a speed increase compared to an exhaustive search. The search finishes when the radius has been reduced so that no more points are found that satisfy the SC: the last point found satisfying the SC is the ML solution $\hat{\mathbf{s}}_{ml}$.

In order to further reduce the complexity of the SD, the points that satisfy (2.32) are searched according to increasing distance to z_i, following the Schnorr-Euchner (SE) enumeration [Schnorr94]. The use of this enumeration has two effects:

- On a particular node, The SE enumeration follows the branches with lowest distance increment $|s_i - z_i|^2$ first in any level i. Thus, the first points searched are more likely to be the ML solution, reducing the overall complexity of the search.

- Although the initial radius R is normally set according to the noise variance N_0, the use of the SE enumeration reduces the effect that the initial radius has on the complexity of the SD. From a simulation point of view, the initial radius still has a marginal effect on the complexity of the SD [Damen03]. However, in a parallel implementation of the

algorithm, the initial value can be set to the end of the scale so that no estimate of the noise level is required at the receiver [Burg05].

2.2.5 Performance Comparison of MIMO Detection Schemes

This section provides BER performance comparison results for flat-fading spatial multiplexing systems with different MIMO detection schemes. The optimal ML, MMSE, ZF and their respective V-BLAST extensions are compared in a baseband scenario simulated in Matlab[1]. Perfect synchronization and channel estimation are assumed at the receiver, while no channel state information is available at the transmitter side. Quaternary phase shift keying (QPSK) transmission has been simulated through a flat-fading Rayleigh channel with no antenna correlation. The E_b/N_0 ratio has been chosen for the BER plots in order to allow fair and realistic comparisons of different modulation and coding schemes. Figure 2.8 shows the BER performance curves for antenna setups of 4×4 (a) and 2×3 (b).

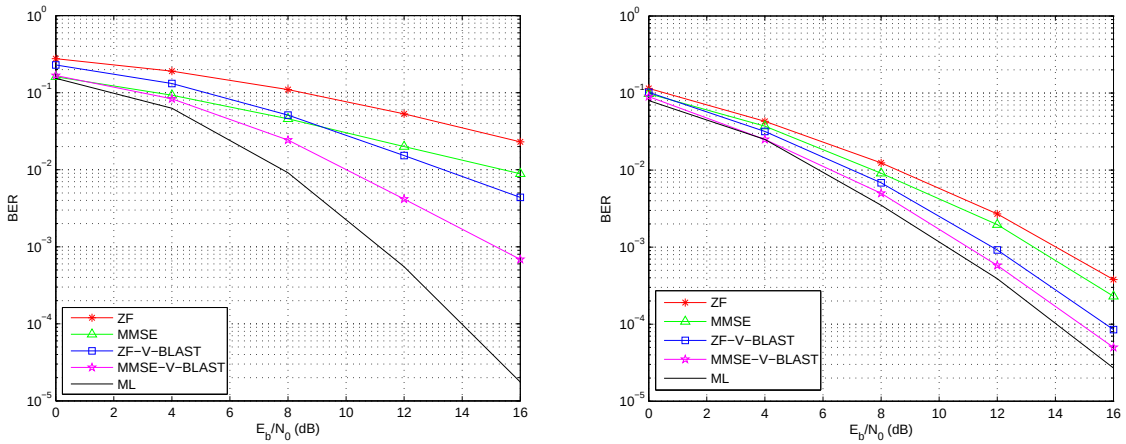

Figure 2.8: BER performance of basic MIMO detectors for uncoded 4×4 (a) and 2×3 (b) QPSK transmission.

As it is shown in Figure 2.8a, the SD clearly outperforms the rest of the detectors. If the final slope of the curves is analyzed, which is closely related to the diversity order, it can be noticed that the V-BLAST schemes achieve a slightly higher diversity than ZF and MMSE, while SD shows the greatest diversity. Figure 2.8b shows the same performance comparison for a 2×3 setup, with increased reception diversity. It can be seen that the conclusions from the 4×4 case hold. Nevertheless, the differences between detectors are reduced and the performance curves of V-BLAST schemes, which depend of the feedback of detected symbols, get closer to the optimal detector SD.

[1]Matlab is a trademark of The Mathworks, Inc. [Mathworks].

2.3 MIMO-OFDM Systems

If the actual capacity of MIMO wireless systems is to be reached, the multi-antenna transmission and reception schemes of Section 2.2 must be combined with efficient wideband modulation techniques such as OFDM, which has become the main solution to overcome the complexity limitations of time-domain equalization in multi-path frequency-selective fading channels [Bingham90]. This multi-carrier modulation technique, which is summarized in the following subsection, is present in nearly all new wireless standards, such as WLAN IEEE 802.11 and wireless metropolitan area network (WMAN) IEEE 802.16.

2.3.1 OFDM

The complexity of optimal ML and even suboptimal equalization of wideband modulation systems grows exponentially with the length of the channel impulse response L. OFDM avoids the complexity of time-domain equalization techniques by transmitting information symbols in frequency-orthogonal narrowband subcarriers which can be equalized independently with a relatively low computational cost.

Consider the transmission of a block of T information symbols, represented by vector $\mathbf{s}$, through a wideband or frequency-selective wireless link of bandwidth B_w. The $1/B_w$-interval sampled baseband channel impulse response, which includes all the transmit and receive filter effects, is represented by $h[\tau]$, where $\tau = 0, 1, ..., L-1$.

Figure 2.9 shows the structure of a SISO-OFDM wireless system that transmits the information symbol block $\mathbf{s}$. As it can be seen, the transmitter first performs a T-point inverse fast Fourier transform (IFFT) operation on $\mathbf{s}$, locating each information symbol at a different frequency bin or subcarrier, yielding the vector $\tilde{\mathbf{s}}$. The IFFT operation can be represented using matrix notation as

$$\tilde{\mathbf{s}} = \mathbf{D}^H \mathbf{s}, \tag{2.35}$$

where $\mathbf{D}$ is a $T \times T$ discrete Fourier transform (DFT) matrix whose element at position m, n is given by:

$$[\mathbf{D}]_{m,n} = \frac{1}{\sqrt{T}} e^{-\frac{j2\pi(m-1)(n-1)}{T}}. \tag{2.36}$$

The transmitted symbol vector $\mathbf{s}'$ is constructed by appending a cyclic prefix (CP) of length L_{CP} to the vector $\tilde{\mathbf{s}}$. The CP consists of the last L_{CP} symbols of $\tilde{\mathbf{s}}$. The vector $\mathbf{s}'$ is known as the OFDM symbol and its elements are transmitted serially. Hence, an OFDM symbol has $T + L_{CP}$ samples. The condition $L_{CP} \geq L - 1$ must be satisfied to avoid inter-symbol interference (ISI) between successive OFDM symbols.

A vector $\mathbf{r}'$ of length $T + L_{CP} + L - 1$ is received, which comprises the OFDM symbol

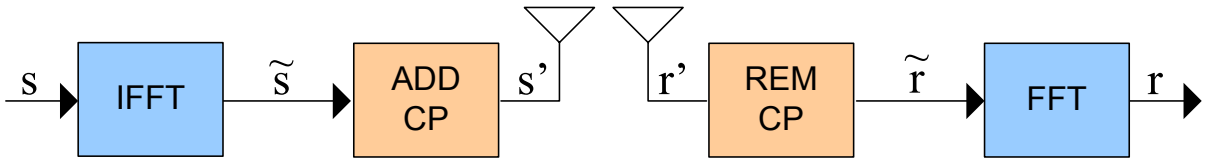

Figure 2.9: Diagram of OFDM transmission and reception chains for a SISO channel.

convolved with the channel of length L. The receiver removes the CP and gathers T samples of the received signal $\tilde{\mathbf{r}}$ that satisfy

$$\tilde{\mathbf{r}} = \sqrt{Es}\mathbf{H}_c\tilde{\mathbf{s}} + \mathbf{n}, \tag{2.37}$$

where $\mathbf{H}_c$ is a $T \times (T + L - 1)$ Toeplitz matrix given by

$$\mathbf{H}_c = \begin{bmatrix} h[0] & 0 & \cdots & 0 & 0 & h[L-1] & \cdots & h[1] \\ h[1] & h[0] & 0 & \cdots & 0 & 0 & \ddots & \vdots \\ \vdots & h[1] & h[0] & 0 & 0 & \ddots & 0 & h[L-1] \\ h[L-1] & \vdots & h[1] & \ddots & 0 & \ddots & 0 & 0 \\ 0 & h[L-1] & \vdots & \ddots & h[0] & \ddots & \ddots & 0 \\ \vdots & 0 & h[L-1] & \ddots & h[1] & h[0] & 0 & 0 \\ \vdots & \vdots & 0 & \ddots & \vdots & \ddots & \ddots & 0 \\ 0 & 0 & \cdots & 0 & h[L-1] & \cdots & h[1] & h[0] \end{bmatrix}. \tag{2.38}$$

The CP renders the matrix $\mathbf{H}_c$ circulant and its eigendecomposition can be expressed as

$$\mathbf{H}_c = \mathbf{D}^H\mathbf{\Omega}\mathbf{D}, \tag{2.39}$$

where $\mathbf{\Omega} = \text{diag}\{w[0], w[1], ..., w[T-1]\}$ and $w[k]$ is the sampled frequency response of the channel at the subcarrier index k. Hence, if a fast Fourier transform (FFT) is performed on $\tilde{\mathbf{r}}$, the received signal $\mathbf{r}$ is given by

$$\mathbf{r} = \mathbf{D}\tilde{\mathbf{r}} = \sqrt{E_s}\mathbf{\Omega}\mathbf{s} + \tilde{\mathbf{n}}, \tag{2.40}$$

where $\tilde{n}$ is a T-vector with the noise samples at the T subcarriers. Equation (2.40) represents how OFDM decouples the frequency-selective channel into T parallel flat-fading channels, which can be represented for each individual subcarrier f as

$$r(f) = \sqrt{E_s}w[f]s[k] + \tilde{n}[f], \;\; f = 0, 1, ..., T-1. \tag{2.41}$$

Therefore, T information symbols are transmitted in parallel during one OFDM symbol period. Each information symbol is allocated at a different orthogonal subcarrier and occupies a bandwidth of B_w/T, as is shown in Figure 2.10. The main benefit of OFDM is that it simplifies the equalization task because the channel convolution becomes a multiplication per subcarrier or tone. OFDM can profit from diversity if the information is interleaved and coded across different tones, leading to a modulation technique called coded OFDM (COFDM). The main drawback of OFDM is the high peak-to-average power ratio (PAPR) of the signal, which makes amplifiers more expensive [Dardari00].

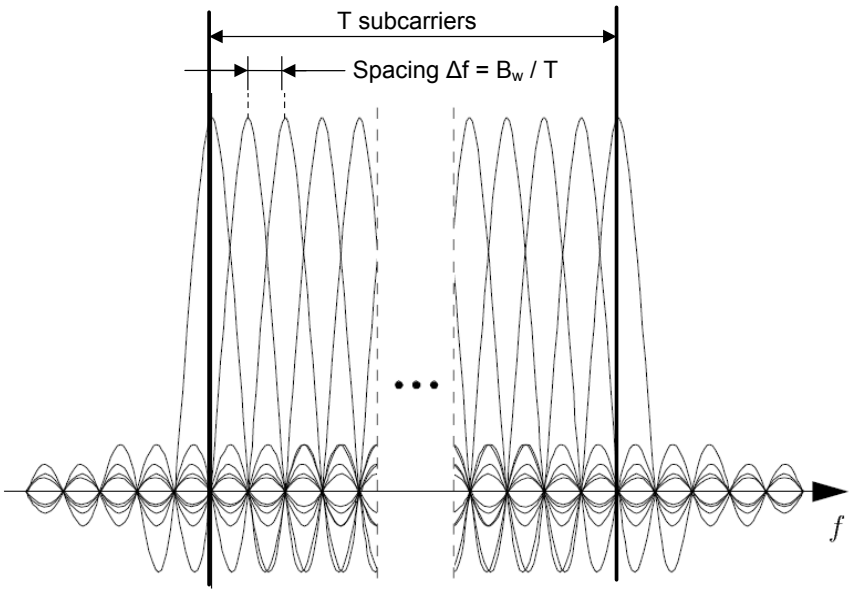

Figure 2.10: Orthogonal subcarriers of an OFDM wireless system.

2.3.2 MIMO-OFDM

The combination of MIMO and OFDM techniques is the main way to reduce the equalization complexity in frequency-selective fading MIMO channels. Figure 2.11 shows the general diagram of a MIMO-OFDM system, where the transmission bits are mapped and coded in space (M antennas), frequency (T subcarriers or tones) and time (different OFDM symbols). As it is shown, an IFFT is applied at each transmission chain after the spatial, frequency and time-domain coding process.

If the simplest MIMO-OFDM system is assumed, the generic coding block of Figure 2.11 can be replaced by a spatial multiplexer that assigns one information symbol to each subcarrier and transmit antenna, leading to the maximum spatial rate of ($r_s = M$). The detection algorithms of 2.2.5 can then be applied to each subcarrier, leading to T parallel narrowband MIMO detectors.

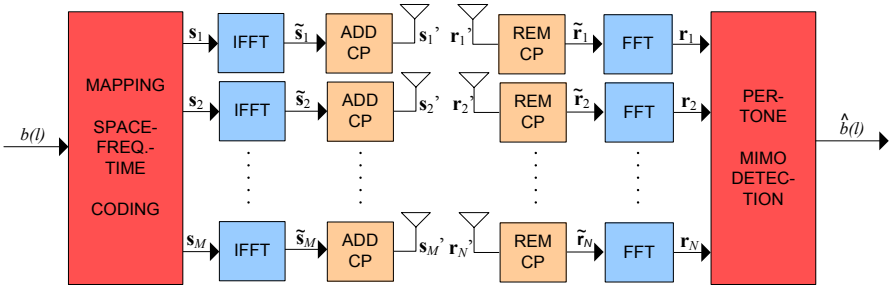

Figure 2.11: Diagram of a general MIMO-OFDM system.

2.3.3 MIMO-Based WLAN Standard: IEEE 802.11n

OFDM has been chosen as the main modulation scheme for the physical layer of many recent and future wireless communication standards, such as IEEE 802.16 (WMAN) and IEEE 802.11 (WLAN). The latter has been chosen for the simulations and analysis carried out in this thesis. Two are the current WLAN standards that include single-antenna OFDM transmission: 802.11a and 802.11g, at 5.2 and 2.4 GHz, respectively [IEEE99, IEEE03a].

These standards, which were published in 1999 and 2003, reach bit-rates of up to 54 megabits per second (Mbps). Further efforts are being developed by the task group 802.11n for the standardization of a MIMO-OFDM based WLAN standard able to transmit data at several hundreds of Mbps. Drafts 1 and 2 of this standard have already been approved and several final products can be found that comply with 'pre-802.11n' and '802.11n draft 2' specifications. Both drafts are based on the work developed by the Enhanced Wireless Consortium (EWC) [EWC05, IEEE07].

Three are the most relevant differences that can be noticed if the EWC proposal is compared with 802.11a. First, the use of up to 4 transmit chains and antennas is supported. New concepts, such as space-time stream and spatial stream, are included in order to define the spatial multiplexing, mapping and space-time coding features of the transmitter, which are summarized in the diagram of Figure 2.12. Second, the transmission bandwidth can be doubled, i.e., two frequency bands or channels can be allocated in order to increase the transmission rate. Last, the convolutional code of 802.11a has been replaced by more efficient low-density parity check (LDPC) and Turbo coding schemes.

Regarding the use of multiple antennas, the EWC specification and the pre-802.11n drafts lie on the most basic MIMO transmission techniques: SM and STBC. The transmitter must be able to select the most efficient configuration for each link depending on the channel conditions. For instance, SM can be used to multiply the data bit-rate in high SNR scenarios, whereas STBC or diversity techniques can be more suitable in noisy environments. Hence, the transmitter must be able to adapt the STC scheme, as is done in 802.11a with the constellation size or the coding rate.

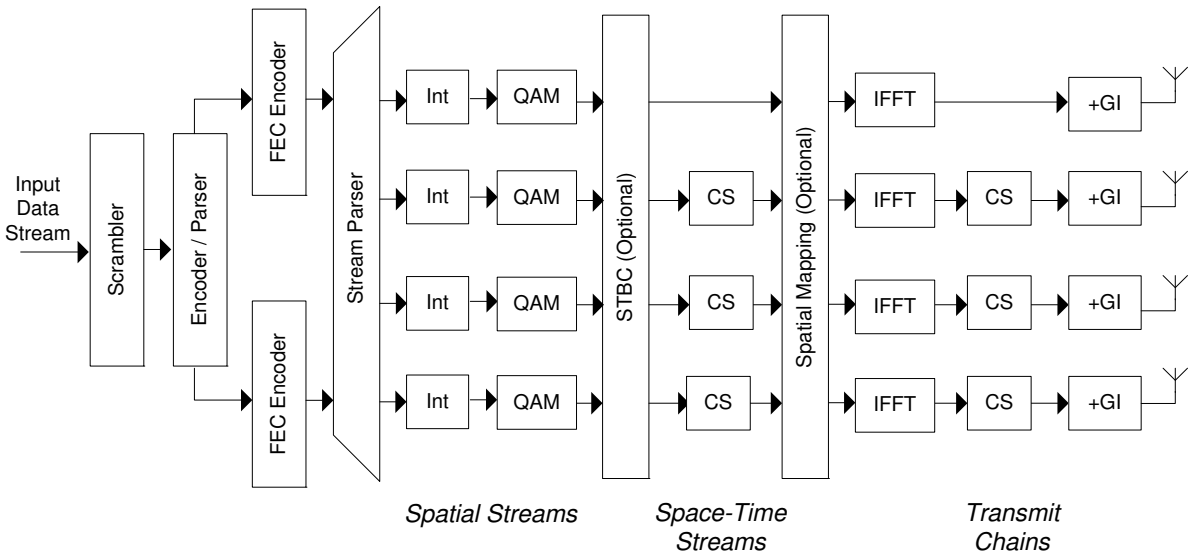

Figure 2.12: Diagram of a generic 4×4 IEEE 802.11n MIMO-OFDM transmitter [EWC05].

2.3.4 Performance Results

Figure 2.13a shows the BER performance of an uncoded 4×4 MIMO-OFDM system with the linear and V-BLAST detectors. The IEEE 802.11a standard has been taken as a reference, which is the basis of the IEEE 802.11n. 64 subcarriers are allocated in a bandwidth of 20 MHz. According to the standard, only 48 of the 64 subcarriers have been used for data transmission, being the rest reserved for pilot allocation and spectrum shaping purposes. Once again, QPSK modulation has been selected. The wireless channel has been simulated following the parameters defined by the HIPERLAN/2 channel model A, which is defined by an root mean square (rms) delay of 50 ns (11 taps) [Medbo98].

As it can be deduced from its structure, OFDM needs codification and interleaving to profit from frequency diversity and avoid the effects of fading. The BER performance of a rate-1/2 coded MIMO-OFDM system is shown in Figure 2.13b, where the benefits of coding are shown. As it can be seen, the MMSE-V-BLAST receiver outperforms the ML due to the HE approach, where all the bits from an antenna can be decoded together, so that the correction capability of the decoder is used to improve the performance of the MIMO detector.

2.4 MIMO-SCFDE Systems

As has been stated in Section 2.3, OFDM has become the main modulation scheme for high data rate transmission in frequency-selective channels. Nevertheless, other very interesting single-carrier modulation techniques have been proposed which can profit from the simplicity

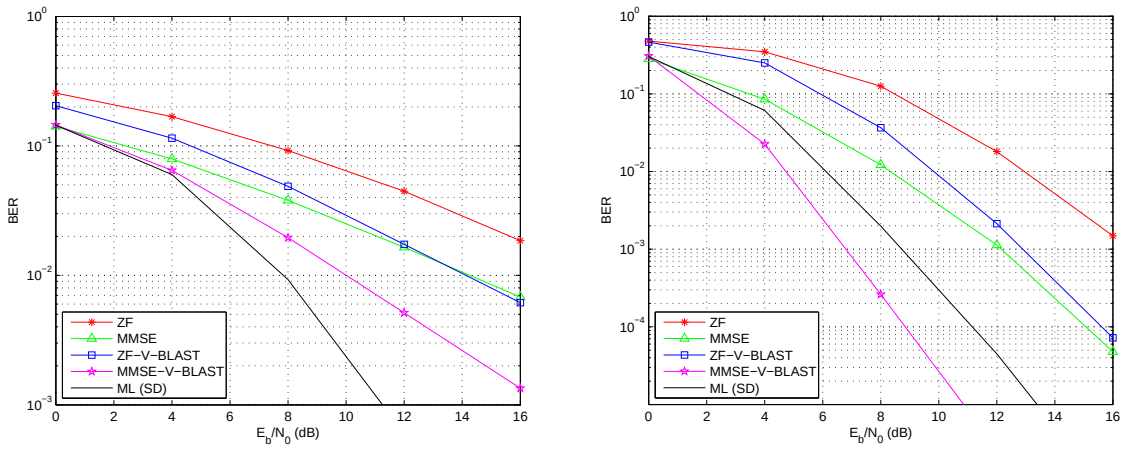

Figure 2.13: BER performance curves of basic MIMO detectors for uncoded (a) and rate-1/2 coded (b) 4×4 QPSK OFDM transmission.

of frequency-domain equalization (FDE) without the known drawbacks of OFDM, such as the high PAPR and the lack of frequency diversity in uncoded scenarios. This kind of single-carrier transmission techniques have been considered when designing many recent wireless standards, though they have been included partially in standards such as the IEEE 802.16a [IEEE03b].

This section will first summarize the structure and benefits of SCFDE modulation for SISO systems, after which the model will be briefly extended to a MIMO scenario. Last, a comparison of SCFDE and OFDM modulation schemes will be provided for MIMO transmission in WLAN scenarios.

2.4.1 SCFDE Modulation

Figure 2.14 shows the structure of a cyclic-prefixed SCFDE (CP-SCFDE) transmission scheme [Falconer02]. As it can be seen, the transmitter is mostly identical to an usual single-carrier system. Nevertheless, the data symbols are processed block-wise and a CP is added to each block in order to achieve the circulant matrix property described in Section 2.3.1, thus making the frequency-domain equalization possible.

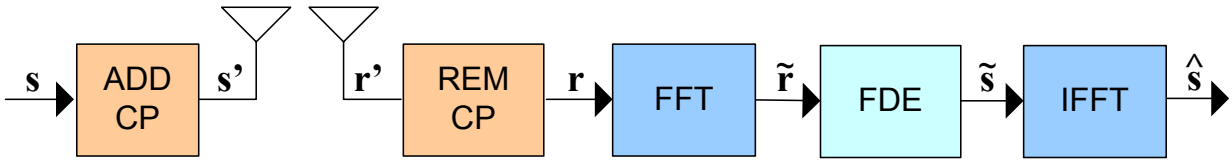

Figure 2.14: Diagram of transmission and reception chains for a SISO-SCFDE system.

As it can be noticed, the receiver side is rather different from the narrowband single-

carrier case. The equalization of the frequency-selective fading channel is not carried out in the time domain, but in the frequency domain. Thus, an FFT must be applied after the CP removal to process the symbols in the frequency domain. The equalization is identical to the OFDM case, i.e., it is a subcarrier-based multiplication. The main difference is that the equalization is not performed on the information symbols, but on their frequency-domain transforms.

Once the symbols are equalized, they must be converted back to the time-domain, where the detection and the following steps are carried out. Hence, the number of operations (one FFT and one IFFT) are the same as in OFDM, but their location changes.

This transmission technique avoids the high PAPR problem of OFDM [Dardari00] and profits from a natural frequency-domain diversity, since each information symbol is spread across all the frequency bins. Its main drawback consists on the separation of the equalization and detection steps, which are done in frequency and time domain, respectively. This is specially important in decision-directed iterative systems, where an FFT must be included in the feedback chains. As will be shown later, SCFDE outperforms OFDM in BER performance when high coding rate is selected and performs slightly worse with low coding rates.

2.4.2 MIMO-SCFDE

The extension of SCFDE techniques to MIMO is straightforward. Figure 2.15 shows a spatial multiplexing SCFDE system. As it is shown, the MIMO spatial cancellation and the symbol detection are now in different domains. This can complicate the MIMO detection process for feedback-based techniques (V-BLAST), since FFT blocks must be included in the feedback chains. On the other hand, the implementation of the optimal ML detector becomes prohibitively complex because the decisions are not made in the frequency-domain, where the simple narrowband MIMO model can be applied.

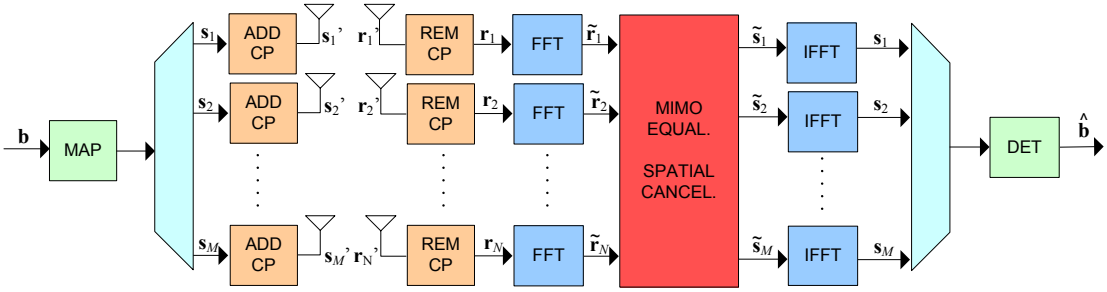

Figure 2.15: Schematic of a MIMO-SCFDE spatial multiplexing transmission and reception system.

2.4.3 Performance Comparison of MIMO-SCFDE and MIMO-OFDM

This section shows comparative BER performance results for MIMO-SCFDE (solid lines) and MIMO-OFDM (dashed lines) schemes in a WLAN scenario. A 4×4 QPSK transmission has been simulated over a HIPERLAN/2 A channel [Medbo98] using the maximum and minimum code rates of the IEEE 802.11a standard ($r_t = 1$ and $r_t = 0.5$) [IEEE99].

As it can be seen in Figure 2.16, the BER performance of ZF-based SCFDE schemes is very poor due to the noise enhancement and the associated lack of stability of some frequency bins, which affects all the information symbols.

As it is shown in Figure 2.16a, SCFDE outperforms OFDM for uncoded and high coding rate systems. If the rate-1/2 coded case which is shown in Figure 2.16b is analyzed, it can be stated that SCFDE can perform close to OFDM in low coding rate systems. More results on this performance comparison for WLAN-like systems can be found in [Coon03, Mendicute04a, Mendicute04b].

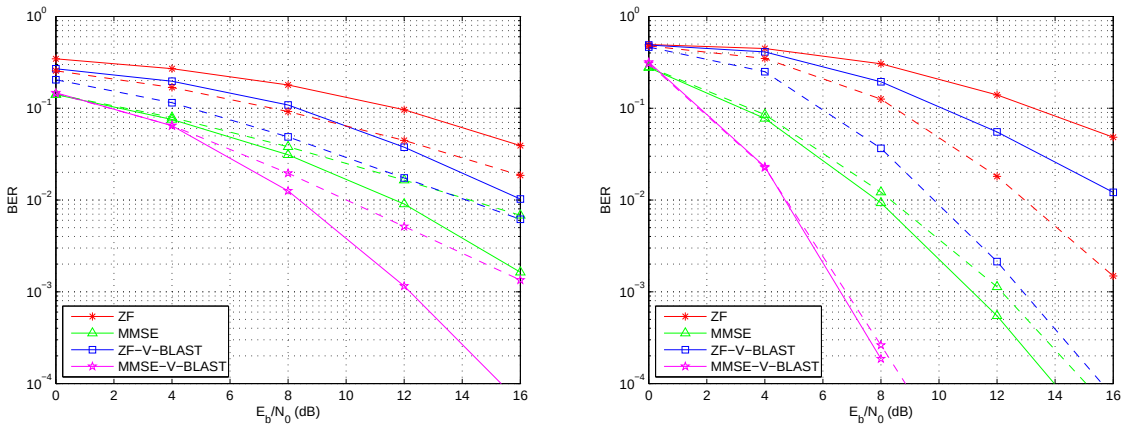

Figure 2.16: BER performance comparison of basic MIMO detectors for uncoded (a) and rate-1/2 coded (b) 4×4 SCFDE (solid line) and OFDM (dashed line) transmissions.

2.5 Iterative MIMO Receivers

The MIMO systems shown in previous sections must be combined with efficient coding schemes in order to get close to their theoretical capacity limits [Foschini98, Telatar99]. Iterative receivers, based on the "Turbo" principle [Berrou93], can approach the optimal performance limits of coded MIMO systems with reduced complexity [Sellathurai02, Biglieri04].

This section analyzes the structure of a specific iterative MIMO receiver. Although a simple flat-fading iterative MIMO receiver is going to be analyzed in this dissertation, the

same technique can be applied to wideband OFDM or SCFDE systems [Horseman03].

The turbo receiver analyzed in this section consists of an inner soft input-soft output (SISO*) MIMO detector and an outer SISO* decoder, which iteratively transfer soft information to each other in order to improve the accuracy of the soft bit estimates. This section shows the main block diagram of this Turbo-MIMO system, its benefits and the main analysis methods used to predict its performance.

First, the model of an iterative MMSE-PIC receiver will be shown, after which performance improvement results will be provided for several iterations. Last, the main convergence and performance analysis methods, EXIT charts and analytic functions, will be briefly introduced in Sections 2.5.3 and 2.5.4, respectively.

2.5.1 Fundamental System Model

Figure 2.17 shows the structure of the transmitter of the Turbo-MIMO system under consideration. The information bits $b(l)$ are encoded, interleaved by a block random interleaver and demultiplexed into M parallel streams. The resulting bits $c_m(l_d)$, where m and l_d denote the transmission antenna and the demultiplexed coded bit index, respectively, are mapped onto a generic QAM constellation of B points. The mapped symbols $s_m(k)$, which can be stuck into the vector $\mathbf{s}(k)$, are then modulated and transmitted simultaneously by M antennas.

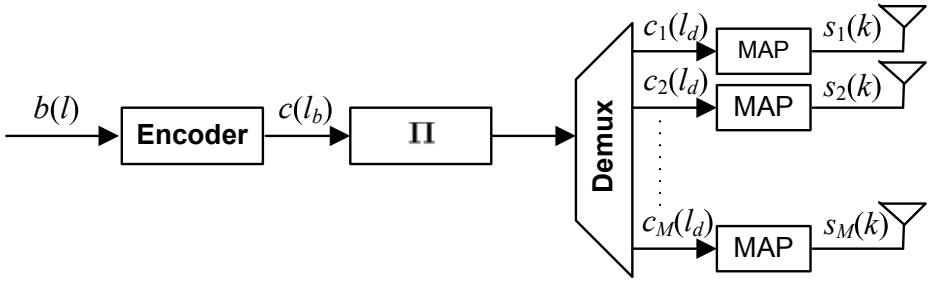

Figure 2.17: Diagram of a MIMO transmitter with coding and interleaving.

Figure 2.18 shows the structure of the iterative receiver. The received symbols $\mathbf{r}(k)$ are processed by the SISO* MIMO detector, whose outputs are the soft symbol estimates $\mathbf{y}(k) = [y_1(k), y_2(k), ..., y_M(k)]^T$. This soft MIMO detector receives two kind of inputs: the received signal vector $\mathbf{r}(k)$ and the extrinsic soft bit information fed back by the outer decoder as the log-likelihood ratio (LLR) values $\Lambda_c^{ex,D}(l_c)$, which become $\Lambda_{c_m}^{a}(l_d)$ after interleaving and demultiplexing.

A MIMO detector that carries out PIC and MMSE combining has been implemented, whose operation can be summarized as:

$$\mathbf{r}'_m(k) = \mathbf{r}(k) - \sqrt{\frac{E_s}{M}} \sum_{\substack{p=1 \\ p \neq m}}^{M} \mathbf{h}_p \tilde{s}_p = \mathbf{r}(k) - \sqrt{\frac{E_s}{M}} [\mathbf{H}\tilde{\mathbf{s}}(k) - \mathbf{h}_m \tilde{s}_m(k)] \tag{2.42}$$

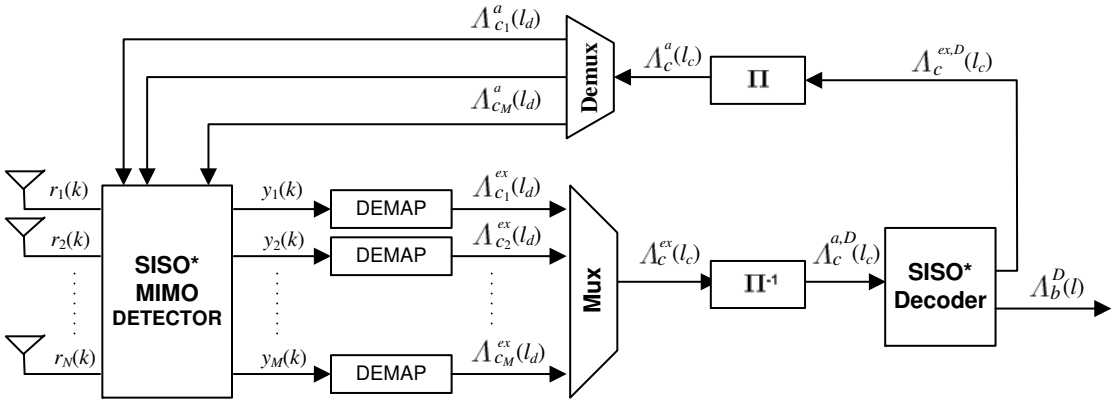

Figure 2.18: Diagram of a generic interference cancellation-based iterative Turbo-MIMO receiver.

and

$$y_m(k) = \mathbf{w}_m^H \mathbf{r}'_m(k), \tag{2.43}$$

where m denotes the detected branch, $\mathbf{h}_m$ is the m-th column of the channel matrix $\mathbf{H}$ and $\tilde{\mathbf{s}}(k)$ is an $M \times 1$ vector of soft symbol estimates $\tilde{s}_m(k)$, which are derived from the a priori LLR metrics $\Lambda^a_{c_m}(l_d)$ fed back from the decoder [Tüchler02].

The spatial combining matrix $\mathbf{w}_m$ is calculated from the channel matrix $\mathbf{H}$ as follows:

$$\mathbf{w}_m = \sqrt{\frac{M}{E_s}} \left(\mathbf{H}\bar{\mathbf{V}}\mathbf{H}^{\mathbf{H}} + (1-\bar{v}_m)\mathbf{h}_m\mathbf{h}_m^H + \frac{N_0 M}{E_S}\mathbf{I}_N \right)^{-1} \mathbf{h}_m, \tag{2.44}$$

where matrix $\bar{\mathbf{V}} = diag(\bar{v}_1, ..., \bar{v}_M)$ represents the mean of symbol estimation error variance matrices $\mathbf{V}(k) = diag(v_1(k), ..., v_M(k))$ with [Biglieri04, Hermosilla05]:

$$v_m(k) = E\{|s_m(k) - \tilde{s}_m(k)|^2\} = E\{|s_m(k)|^2\} - |\tilde{s}_m(k)|^2.$$

The symbol estimates $\mathbf{y}(k)$ are soft-demapped [Tüchler02], providing the extrinsic LLRs of the coded bits $\Lambda^{ex}_{c_m}(l_d)$, which become the input of the SISO* decoder after multiplexing and deinterleaving operations. The outer soft decoder, which has been implemented using the log-MAP version of the BCJR algorithm [Bahl74], delivers the following metrics:

- A posteriori probability (APP) LLRs of the uncoded bits $\Lambda^D_b(l)$, whose signs define the finally detected bit values.
- Extrinsic LLRs of coded bits $\Lambda_c^{ex,D}(l_c)$, which are fed back to the MMSE-PIC for interference cancellation.

2.5.2 Performance Evaluation

Figure 2.19 shows the BER performance of an iterative MMSE-PIC MIMO receiver. Results are shown for 0, 1 and 2 iterations. As it can be seen, the iterative processing and the exchange of soft extrinsic information improves the performance at moderate and high SNR regimes. A fixed 4×4 MIMO channel, as defined in [Hermosilla03], has been used for the results shown in Figure 2.19a, while a narrowband Rayleigh fading channel has been selected for Figure 2.19b. The fixed channel results are interesting for the following sections, where analytical and semi-analytical BER performance tools are described.

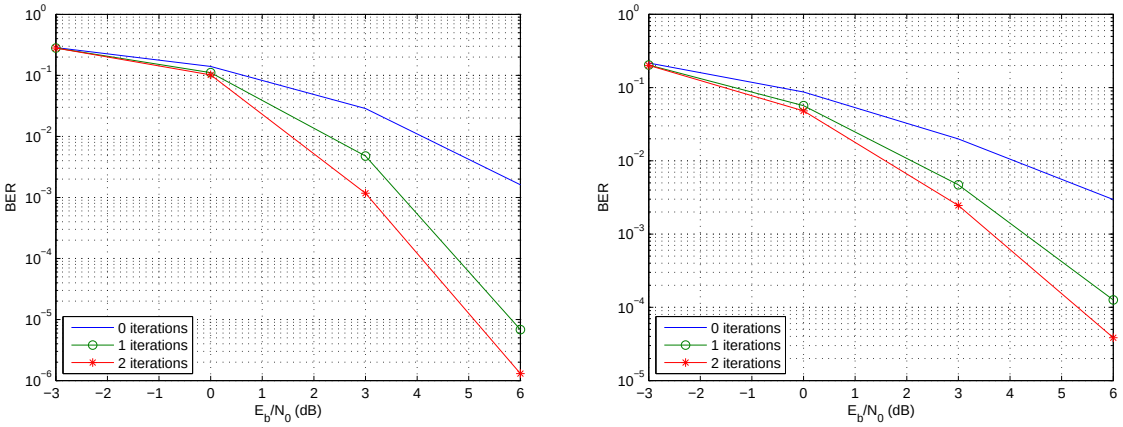

Figure 2.19: BER performance curves for an iterative MIMO receiver in a 4×4 system with fixed (a) and Rayleigh fading (b) wireless channels with 0, 1 and 2 iterations.

2.5.3 EXIT Charts

Extensive MC simulations are commonly used for the performance evaluation of communication systems. Nevertheless, computationally simpler analytical and semi-analytical tools exist which are useful to reduce the simulation time or to evaluate the convergence behavior of iterative receivers. EXIT charts, which are the most popular of these convergence analysis methods, have been extensively applied in iterative or Turbo processing for the evaluation and design of decoders and receivers [Brink01, Tüchler02, Zelst01].

The main objective of EXIT charts is to reduce the analysis of the whole iterative process to the evaluation of the exchange of one parameter, usually the mutual information (MI), between the inputs and outputs of the SISO* processors (detectors or decoders) that conform a receiver. Figure 2.20 shows the EXIT chart for the iterative receiver of Section 2.5.1. As it can be seen, a MI transfer curve is calculated for each signal processing block. For the case analyzed here, two curves are generated: one for the soft MMSE-PIC detector and one for the SISO* decoder.

A system with $M = 4$, $N = 4$ and $E_b/N_0 = 3$ dB has been selected for the example shown in Figure 2.20. Three curves are depicted: the thin solid line corresponds to the transfer function of the soft decoder, which has been drawn with the input MI I_{in}^{D} in the vertical axis; the dashed curve corresponds to the transfer function of the MMSE-PIC detector, whose input I_{in}^{R} is shown in the horizontal axis; and the thick solid lines represent the EXIT trajectory. The horizontal lines represent the exchange of information from the MMSE-PIC detector to the decoder, while the horizontal lines correspond to the information exchange from the decoder to the MIMO detector. The final BER at each iteration step can be estimated from tables, which are calculated and stored when generating the transfer function curves [Hermosilla03, Biglieri04].

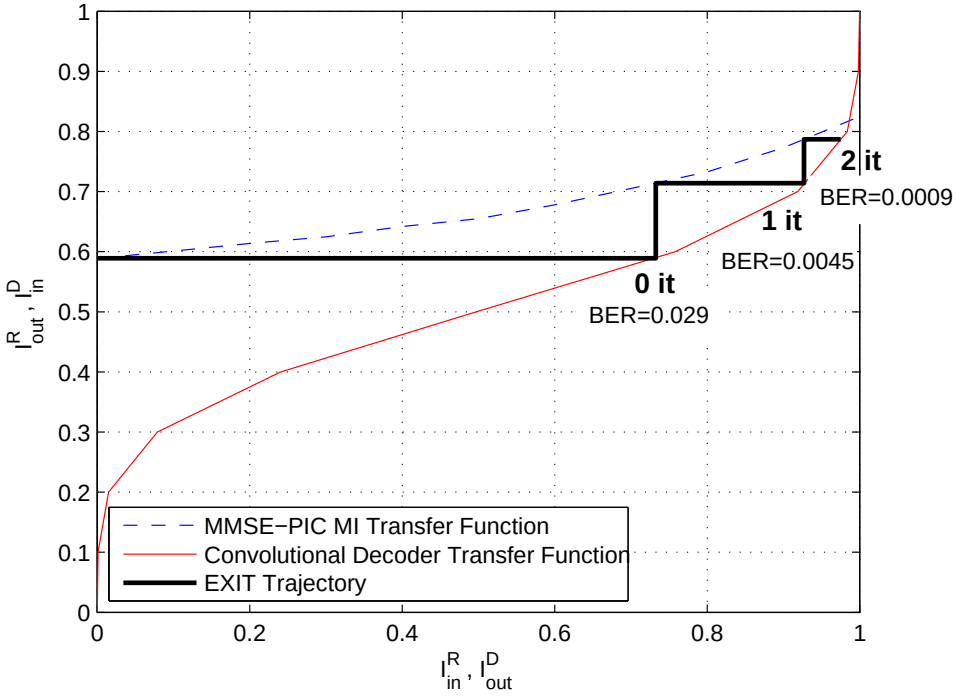

Figure 2.20: EXIT trajectory for a MMSE-PIC receiver with $E_b/N_0 = 3$ dB.

The results of Figure 2.20 can be used to design convergent decoder/detector pairs in an efficient way, to analyze the convergence of specific iterative receivers or to obtain BER results without the computational cost of MC simulations. The BER performance curves predicted by the EXIT charts for the fixed channel match the results of Figure 2.19a, which have been obtained through MC simulation.

When a Rayleigh-fading channel is assumed, the EXIT charts do not match the actual trajectories exactly, since the mean of output mutual information values is used to calculate an unique EXIT chart for each E_b/N_0 value [Hermosilla03, Biglieri04]. This limitation can be overcome if analytical tools are used for the calculation of the EXIT trajectories, as will be shown in the next section.

2.5.4 EXIT Function-Based Performance Prediction

The lack of accuracy of the EXIT chart-based performance evaluation methods can be solved if analytical functions are used. The EXIT transfer function-based performance evaluation method of [Hermosilla05] divides a generic front-end (FE) into two elementary blocks, a so-called linear combiner (LC) and a non-linear demapper. Here the FE is the MIMO detector, which can be decomposed into two elementary devices: the MMSE-PIC linear combiner and the non-linear demapper. In [Hermosilla05], where the channel is perfectly known at the receiver, the FE is represented by the following parametric transfer functions:

$$\Gamma_m = F_m(I_{in}^R; \mathbf{H}, \rho), \tag{2.45}$$

$$I_{out,m}^R = G_d(\Gamma_m, I_{in}^R) \tag{2.46}$$

and

$$I_{out}^R = \frac{1}{M} \sum_{m=1}^{M} I_{out,m}^R \ . \tag{2.47}$$

Function F_m describes the LC behavior for a certain channel state and ρ value, giving an output SINR value Γ_m for the m-th branch depending on the input MI I_{in}^R. Function G_d characterizes the soft demapper and its output is the MI at each demapped branch $I_{out,m}^R$. Parting from these analytical functions and the EXIT transfer function of the SISO* decoder, which does not depend on any system parameter, the authors in [Hermosilla05] introduced a performance evaluation algorithm that reduces drastically the simulation time and shows good accuracy in quasi-static Rayleigh-fading MIMO channels. The performance evaluation algorithm is shown in Table 2.1. As it is shown, only F_m must be calculated online for each channel realization, while the rest of the functions are generated off-line. Functions f^D and f_{BER} represent the EXIT transfer function and the BER estimation function of the decoder, respectively [Biglieri04, Hermosilla05].

Following this reduced-complexity semi-analytical method, the BER performance and convergence properties of an iterative MIMO system can be accurately predicted, as is shown in [Hermosilla05] for an MMSE-PIC-based receiver.

2.6 Chapter Summary

This chapter has shown an introductory analysis of the main MIMO transmission schemes that are commonly used in wireless communication systems. It has briefly described the scenarios that will be used in forecoming chapters for the evaluation of the impact of channel estimation and implementation on the performance of MIMO receivers.

Performance Evaluation Algorithm
(0) Generate $\mathbf{H}$.
(1) Initialization: iteration $j = 1$; $I_{out}^{D,(0)} = 0$.
(2) Get FE input MI. $I_{in}^{R,(j)} = I_{out}^{D,(j-1)}$.
(3) Compute $\bar{\mathbf{V}}$ from $I_{in}^{R,(j)}$, as in [Hermosilla05].
(4) Calculate $\mathbf{w}_m$ vectors from (2.44) and Γ_m values from (2.45).
(5) Compute $I_{out,m}^{R,(j)}$ and $I_{out}^{R,(j)}$ via (2.46) and (2.47).
(6) Obtain the decoder's output $I_{out}^{D,(j)} = f^D(I_{out}^{R,(j)})$.
(7) Calculate $BER^{(j)} = f_{BER}(I_{out}^{D,(j)})$.
(8) Return to step (2) with $j = j + 1$.

Table 2.1: BER performance evaluation algorithm for each channel realization of an iterative MIMO receiver.

First, the narrowband multi-antenna model has been introduced and the fundamental MIMO capacity limits have been shown, as well as the main transmission and detection schemes that can be used to profit from the capacity enhancement provided by the MIMO channel.

In order to use MIMO in more realistic frequency-selective systems, two main approaches have been selected: OFDM, which is present in nearly all the new wireless standards, and SCFDE, which profits from the main advantages of OFDM avoiding many of its drawbacks. Results have been provided for several MIMO detectors in SM systems with the aforementioned two modulation schemes, which show the validity of SCFDE as a substitute of OFDM in high coding rate wireless systems.

Last, the model of an iterative or turbo-MIMO receiver has been shown, based on an MMSE-PIC receiver followed by a conventional soft convolutional decoder, based on the well-known BCJR algorithm. The benefits of iterative processing have been shown and tools that allow to design and evaluate the performance of such systems have been introduced.

Chapter 3

MIMO Prototyping Platform and Implementations

3.1 Introduction

One of the main objectives of this thesis is to compare the performance of MIMO channel estimation and detection algorithms by simulation. Nevertheless, the actual real-time implementation issues and performance results must be considered in order to allow a fair and realistic analysis. Many algorithms exist in the bibliography that achieve good performance results, but some of them may be too complex, expensive or just unfeasible.

This chapter summarizes the work developed to set up and validate a real-time MIMO algorithm design, simulation and prototyping platform. Matlab/Simulink[1], which is extensively used in signal processing, has been chosen as the basis of the whole algorithm development flow [Mathworks]. Xilinx System Generator for DSP[2] has been selected as the algorithm design, validation and hardware co-simulation tool [Xilinx]. The real-time hardware implementation has been carried out on a modular Hunt Heron prototyping board, which can include several field programmable gate array (FPGA) and digital signal processor (DSP) devices [Hunt].

The first section of this chapter describes the MIMO prototyping methodology and the software tools used to implement the real-time algorithms. An off-line MIMO transmission system is then summarized, which has been used to validate the fundamental synchronization and channel estimation algorithms with real signals before before implementation.

Section 3.4 summarizes the main features of the hardware development platform, focusing on the direct relationship between the Matlab simulation and the final implementation. A special section is dedicated to the "Hardware in the Loop" (HaLo) approach, which allows for co-simulation of Matlab and real hardware-implemented algorithms.

The last sections of the chapter focus on the development of a complete real-time 2×2

[1] Simulink is a trademark of The Mathworks, Inc. [Mathworks].

[2] Chipscope Pro, ISE Foundation, System Generator for DSP and AccelDSP are trademarks of Xilinx, Inc. [Xilinx].

wireless system, which has been used to validate the whole platform, and the implementation of a SD-based real-time MIMO system, developed in collaboration with the Institute for Digital Communications of the University of Edinburgh. These two implementations have been used to evaluate the BER performance degradation due to channel estimation error and real-world implementation effects.

3.2 Algorithm Prototyping Methodology and Tools

As it has been stated in the introduction of this chapter, Matlab/Simulink has been chosen as the base of the whole algorithm development flow. This mathematical tool has been extensively used in signal processing and is specially suitable for the matrix operations required for MIMO systems. The main objective of the work described here has been to develop tools that allow for a progressive transition from pure-Matlab models to real-time hardware. Figure 3.1 shows the main implementation stages of the design flow, which must take into account many real-world issues, such as:

- Fixed-point resolution and error.
- Computational complexity.
- Required hardware resources.
- Latency.
- Achievable throughput.

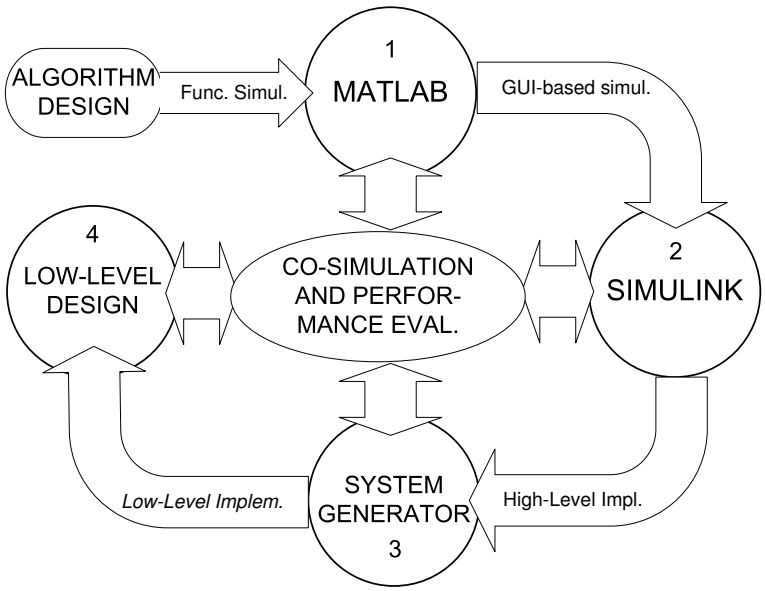

Figure 3.1: Main stages of the simulation and implementation flow.

As it can be seen in Figure 3.1, the design of the algorithms and the first behavioral simulations are carried out in Matlab. Simulink provides a graphical user interface (GUI) which provides a high-level interface for FPGA design and synthesis tools, using special toolboxes like Synplify DSP[3] or Xilinx System Generator for DSP. The latter has been used in this research work because it allows direct very high-level design language (VHDL) code synthesis from Simulink and hardware co-simulation [Xilinx08]. Furthermore, it has been validated in several MIMO testbeds, protoyping platforms and implementations [Kaiser04, Barbero05b, Caban06]. Once the algorithms are validated using System Generator, their performance can be further improved optimizing the final implementation in low-level languages, such as VHDL.

One of the main features of the developed design and validation flow is the ability to simulate at all the different implementation levels, from the highest level of abstraction (Matlab) to the final VHDL hardware design. Furthermore, all these simulation skills can be combined with real-time co-simulation and debugging using the "Hardware in the Loop" approach [Stege04].

The aforementioned design methodology allows a transition from pure Matlab to full FPGA implementation, following the design and validation flow of Figure 3.2. The algorithms are first tested in Matlab with real signals, using the off-line transmission platform that will be described in Section 3.3. Once the algorithms are fully validated, they are progressively translated into synthetizable System Generator blocks, which can be tested through flexible Matlab-based simulations. Depending on the stage of the overall design, the developed logic blocks can be tested with real signals using either the off-line transmission platform of Section 3.3 or the final real-time prototyping board of Section 3.4, where true hardware can be combined with simulation software. As can be seen in Figure 3.2, these flexible flow leads to the final full real-time hardware implementation.

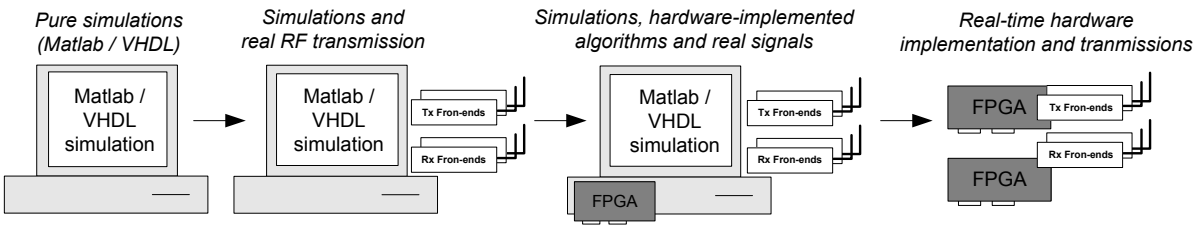

Figure 3.2: Real-time MIMO algorithm design and validation flow with real transmission.

3.2.1 Xilinx Design, Synthesis and Implementation Tools

As will be shown later in this chapter, Xilinx FPGAs have been selected as the main devices for the implementation of the signal processing algorithms required by MIMO communica-

[3]Synplify DSP is a trademark of Sinplicity, Inc. [Sinplicity].

tions. Xilinx provides several tools for the design, synthesis and validation of programmable logic for DSP applications, which can be summarized as:

- **Modelsim XE**[4]**:** A simulation tool that allows to validate VHDL designs and post-synthesis logic. It can also be used to simulate VHDL cose in Matlab/Simulink using a plug-in called "Link for Modelsim".
- **Chipscope Pro:** It allows to evaluate the behavior of a VHDL design in-circuit, analyzing real-time signals stored when a trigger condition occurs. It consists of two main modules: Chipscope Analyzer, which is a logic analyzer that shows the evolution of signals inside the FPGA, and Chipscope Core Inserter, which creates the logic structure that is necessary to generate the trigger conditions and to store the captured signals.
- **ISE Foundation:** It is an integrated graphical environment that provides a design, synthesis, implementation and programming interface for logic designs. Most of the tools used in Xilinx devices, such as Modelsim or Chipscope Pro, can be automatically executed from Xilinx ISE.
- **System Generator for DSP:** A toolbox of graphical simulation blocks for generating VHDL designs directly from Matlab/Simulink. Its main benefit is the ability to simulate a true programmable logic implementation in Matlab. For example, a specific algorithm implementation can be simulated inside a complete transmitter/receiver system modelled in Matlab. The behavior of a System Generator-based design can even be compared with its equivalent Matlab algorithm. The use of Matlab/Simulink can make validation of FPGA algorithms more flexible and simple, avoiding the generation of traditional testbenches and extensive Modelsim simulations.
- **AccelDSP:** An automatic Matlab to VHDL translator which can also generate System Generator models. It is specially suited for DSP application and matrix-based operations, which are very common in MIMO scenarios. This solution is considered interesting for complex matrix operations, such as QR decomposition or inverse calculation. System Generator for DSP and AccelDSP have recently been merged to create a product called DSPTools.

3.2.2 Simulink-Based Design of Real-Time Algorithms

As has been stated in Chapter 2, all the simulations are based on a flexible Matlab simulator that has been developed and maintained during this PhD thesis. This simulator, which

[4]Modelsim is a trademark of Menthor Graphics Corp. [Mentor].

works mainly in the baseband of wireless systems, has been extended to include more realistic communication algorithms such as modulation, filtering, synchronization and channel estimation. The main features of these algorithms will be detailed in Section 3.6.

Due to the size and complexity of the aforementioned Matlab simulator, the translation to Simulink has not been carried out in a functional block basis. The original MIMO model has been embedded into two s-function blocks, which have been the starting point of the algorithm implementation. This structure has allowed an easy coexistence of the baseband Matlab simulator and the hardware-oriented Simulink model. It has also eased the step-by-step design of algorithms in System Generator, which have been tested one by one.

Figure 3.3 shows the main diagram of the first model. As it can be seen, it consists of two main elements: the Matlab model and the System Generator block, which may contain the implementation of some or all of the real-time algorithms. These two elements are connected in both directions, providing the feedback required for the calculation of the BER performance curves. The model is based on the transmission of symbols in frames or bursts.

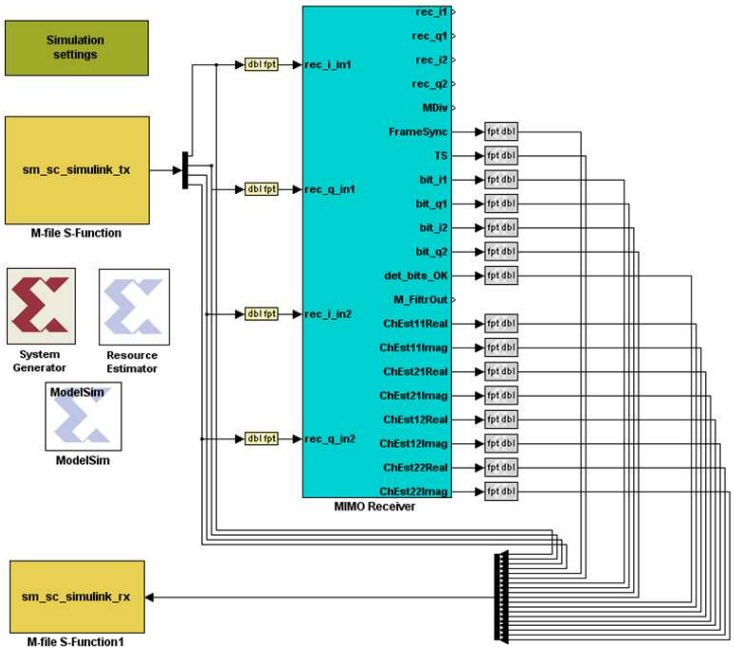

Figure 3.3: Combined use of Matlab, Simulink and System Generator models.

The main configurable parameters of Xilinx blocks, such as the fixed-point resolution, the latency or the use of embedded multipliers, can be defined as common Matlab workspace variables. This means that they can be adjusted any time from an initialization script file. These variables affect the simulation performance of the algorithms, as well as their actual VHDL design and hardware implementation.

The use of Matlab/Simulink and System Generator has allowed to validate every step in the implementation process. For example, the ideal Matlab performance of a symbol-time synchronization algorithm has been compared with several fixed-point implementations.

System Generator can even estimate the resources demanded by each block, the highest delay of the circuit and the achievable maximum clock rate. All this information is only preliminary, but can be used to evaluate the bottlenecks of a design as well as its feasibility on a specific hardware device [Xilinx08].

The output of System Generator is a VHDL entity with all the design created using its Simulink toolbox. The created structure can be included in a larger Xilinx ISE project which may contain more System Generator blocks, as well as other VHDL designs with the logic required to make the FPGA platform work.

Due to the complexity and resources required by the selected algorithms, the System Generator design has been divided and implemented on up to four different FPGA devices. The communications between these devices, which require up to 20 megabytes per second (MBps) of throughput, have been implemented directly in VHDL using specific resources of the Heron platform. Hence, the partitioning of the whole design, which will be explained later in this chapter, has been one of the biggest challenges of the real-time implementation of the MIMO system.

3.3 Off-line Transmission Platform

As it has been stated in the previous section, the basic Matlab algorithms have been validated through MC simulations. Since these algorithms are the base for later real-time implementations, their behavior must be evaluated with real signals, i.e., with the radio-frequency (RF) hardware that is going to be used in the final designs. A simple off-line transmission platform has been set up to allow the combination of Matlab algorithms and real RF transmissions. Figure 3.4 shows the the block diagram of the developed off-line system which consists of the following hardware and software elements:

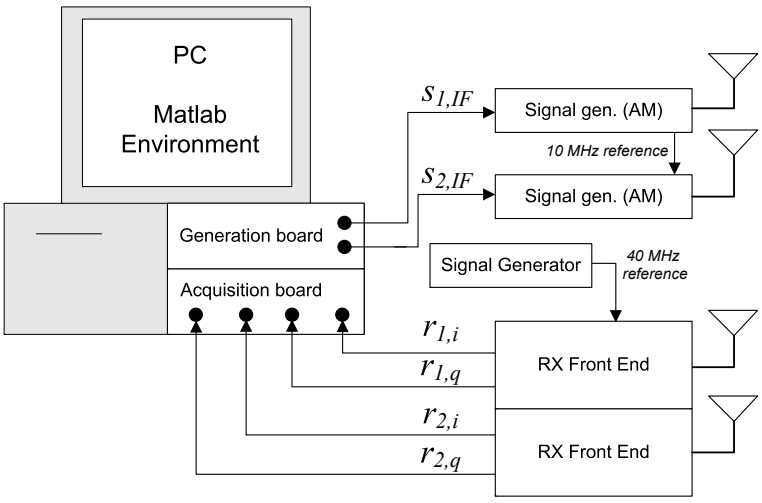

Figure 3.4: Block diagram of the off-line MIMO transmission platform (2×2 setup).

1. Dual-band (2.4 and 5 GHz) RF tranceivers.
2. Parallel carrier interface (PCI) based analog signal acquisition and generation boards:
3. Rohde & Schwarz SMV03 signal generators.
4. Agilent E4440 spectrum analyzer.
5. Personal computer with 2 GB RAM and Intel Dual-Core processor working at 1.9 GHz.
6. Matlab application for signal transmission and reception, PCI board control and RF front-end configuration.

As can be seen in Figure 3.4, all the system is controlled by a Matlab application that generates the digital samples to be transmitted to the PCI signal generation board. Each transmitted signal may have two different formats:

- Two baseband components (I and Q), which will be modulated by the front-end. Note that these signals require two analog outputs per transmitted stream.
- One intermediate frequency (IF) signal, which will be upconverted to the final RF frequency using the amplitude modulation (AM) functions of the signal generators. This solution, which has been used for the block diagram shown in Figure 3.4, allows to generate two transmission streams with the signal generation board.

Figure 3.5 shows a picture of the Matlab-based MIMO off-line transmission platform developed at the University of Mondragon with the 2×2 configuration depicted in the block diagram of Figure 3.4.

RF transceivers and signal generators

The platform is equipped with Maxim MAX2827EVKit boards, which can transmit or receive RF signals in the 2.4 and 5 GHz bands [Maxim]. These boards are able to modulate and demodulate baseband IQ signals of up to 20 MHz using an external 40 MHz reference which has been provided by a common signal generator. This solution avoids the need of implementing modulation and demodulation algorithms, but requires two analog signals to be generated or acquired for each transceiver.

The number of analog ports can be halved when needed if modulated IF signals are generated and upconverted employing equipment such as signal generators, which is the case for the block diagram shown in Figure 3.4. For example, the combination of signal generators and the aforementioned transceivers allows the implementation of a 2x3 system

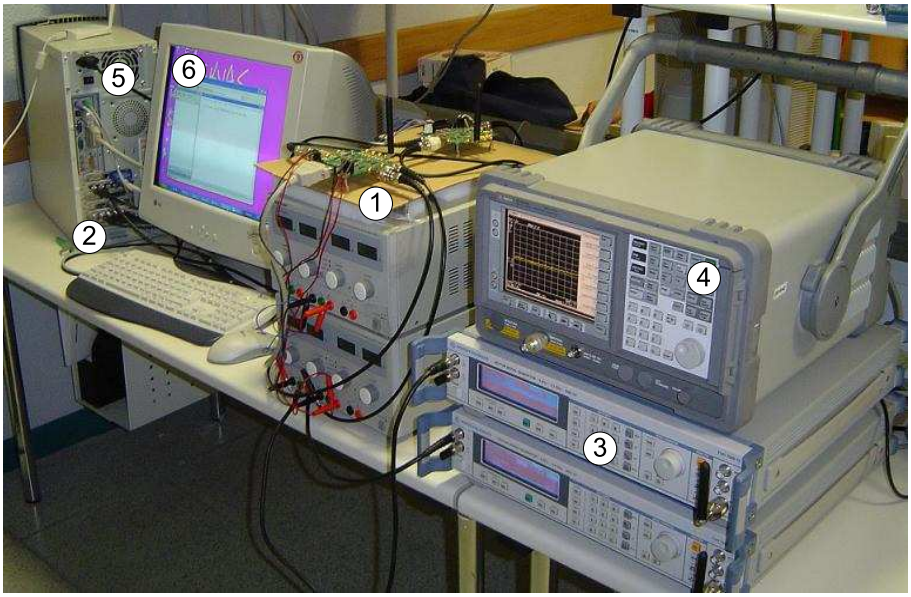

Figure 3.5: Main hardware elements of the off-line transmission platform.

employing two analog outputs and six analog inputs, all managed from a computer running Matlab.

Analog signal acquisition and generation boards

The platform is equipped with an Acquitek CH-3150 PCI board, which allows to generate two analog signals with 12-bits of resolution and can work at up to 20 mega samples per second (MSps) [Acquitek]. The main features of the board include two analog inputs with a bandwidth of 70 MHz, 16 MB of memory and several programming interfaces. One of these interfaces allows to access the board directly from Matlab.

A PCI-based Adlink 9812A analog acquisition board has also been included, which allows to acquire up to 4 analog signals with 12 bits of resolution at up to 20 MSps and 20 MHz of bandwidth [Adlink]. The synchronized combination of this board and the aforementioned generation card provides a Matlab-based off-line transmission system with 2 outputs and 6 inputs, which can be used in combination with the RF boards to implement a 2×3 MIMO system.

Off-line transmission and reception control

The mentioned hardware elements are controlled from Matlab through a PCI-based application programmer interface (API). A frame-based transmission system has been developed that allows the validation of all the algorithms required for a real transmission.

The maximum length of transmitted frames (L_{max}) is limited by the minimum of the memory sizes of the generation and acquisition boards (M_{min}), as stated in the following equation:

$$L_{max} = \frac{M_{min}}{O_f N R_s}, \tag{3.1}$$

where O_f is the oversampling factor, N is the number of receive antennas and R_s is the number of bits per sample. For instance, if 2 antennas, QPSK modulation, 12-bit resolution (which requires 16 bits of memory) and an oversampling factor of 8 are selected, the maximum length of the frame is limited to 4096 symbols.

3.4 Real-time Algorithm Prototyping Platform

The MIMO system and algorithms described in this paper have been implemented on a rapid prototyping platform developed at the University of Mondragon. As it can be seen in Figure 3.6, this platform consists mainly of the following three elements: antenna sets, Hunt Heron rapid prototyping boards and RF transceivers.

3.4.1 Rapid Prototyping Boards

The platform is based on modular rapid prototyping HERON HEPC9 boards from Hunt Engineering [Hunt]. The main advantage of these PCI-based carrier cards is their very flexible architecture, based on the internal HEART bus which allows communications of up to 400 MBps between the modules. The following modules have been mounted on the carrier board for the implementations described here:

- Two HERON-IO2V2 modules with 2 analog inputs and 2 analog outputs of up to 125 MSps with 12 and 14 bits of resolution, respectively. These modules include a 1-million (M)-gate Xilinx VirtexII FPGA and provide a JTAG interface that allows real-time in-system debugging with Xilinx Chipscope and hardware co-simulation with System Generator.
- One HERON-IO5 module with 2 analog inputs and 2 analog outputs of up to 210 MSps with 12 and 16 bits of resolution, respectively. This module includes a 3M-gate VirtexII FPGA, which also contains a JTAG debugging interface.
- One HERON-FPGA3 module with a 1M-gate VirtexII FPGA. This module has been replaced by a Virtex-IV module during the last stage of this work.

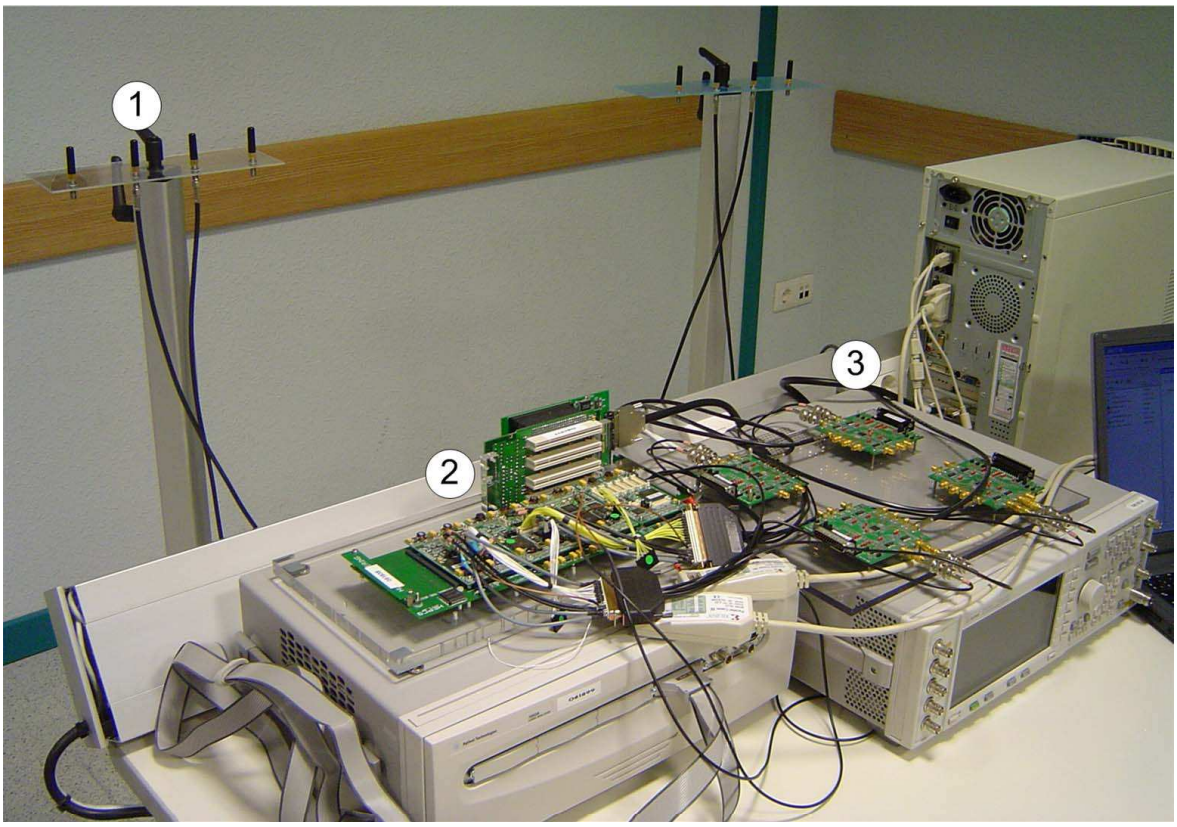

Figure 3.6: Main elements of the real-time MIMO algorithm prototyping platform: antenna sets (1), Heron board (2) and RF transceivers (3).

3.4.2 RF Transceivers

The platform is equipped with Maxim's MAX2827EVKit boards [Maxim], which have been detailed in Section 3.3. The combination of the analog ports of the aforementioned prototyping boards and these transceivers allows the implementation of systems with up to three transmit and receive antennas. Figure 3.6 shows four of these RF transceivers with the HEPC9-based rapid prototyping platform. As can be seen, two of the transceivers are configured as transmitters and two as receivers to set up a 2×2 MIMO system.

3.5 "Hardware in the Loop" Approach

FPGA designs developed using System Generator blocks or any other high-level design language can be tested in two ways:

- **Hardware co-simulation**: The algorithm runs on real hardware, but not in real-time [Rupp03, Mehlführer05]. This means that some real-time issues, such as clock offsets or synchronization problems, can not be included in the simulations. If the algorithms do not run in real time, the FPGA implementation of the transmitter and receiver algorithms can not be properly tested with real signals.

- **Hardware in the loop (HaLo)**: The algorithm runs on real hardware and in real-time for a transmission burst. Real-time execution is configured, triggered and stopped from Simulink. The whole system implementation can be validated in real-time or combined with off-line matlab simulations [Stege04].

This section describes the HaLo structure that has been developed for the MIMO prototyping platform of the University of Mondragon. Thanks to this HaLo approach, any algorithm implemented at any design level can be tested with real signals, executed in real-time or can even be embedded in a real transmission system, thus facing real conditions from the first design stages.

3.5.1 Synchronization between Matlab/Simulink and Real-Time Hardware

The hardware co-simulation block of System Generator provides two different modes that allow the synchronization between Simulink and design running on an FPGA:

- ***Single stepped*** mode: The FPGA device is clocked from Simulink, being therefore limited by the performance of the computer.
- ***Free running*** mode: The FPGA runs off an internal clock and is sampled asynchronously when Simulink wakes up the hardware co-simulation block. As the hardware must run in real-time, the "free running" mode is selected for the implementation of HaLo, establishing two clock domains: Simulink simulation clock domain and the FPGA free-running clock domain.

Fig. 3.7 shows a basic 2x2 MIMO HaLo application which allows to send and receive Matlab generated data by means of real-time running signal processing algorithms over real MIMO channels. The interfacing between both clock domains is carried out by asynchronous read and write memories located inside the FPGA and connected to Simulink by the JTAG port. Simulink clock domain is presented in the left-hand side of the figure, while the right-hand side shows the real-time running hardware scheme. The interfacing memory blocks can be implemented using first in-first out (FIFO) buffers or dual-port RAMs, extensively used in multi-clock applications, providing a reliable and safe way to transfer data between the host PC and the FPGA.

As it can be seen in Fig. 3.7, the first module is selected as the main link between Simulink and the whole board. In this example, memory interfacing control signals are directly generated through a Matlab s-function block. Data read and write operations through the JTAG port are asynchronous, as the hardware is running in "free-running" mode, i.e. real-time

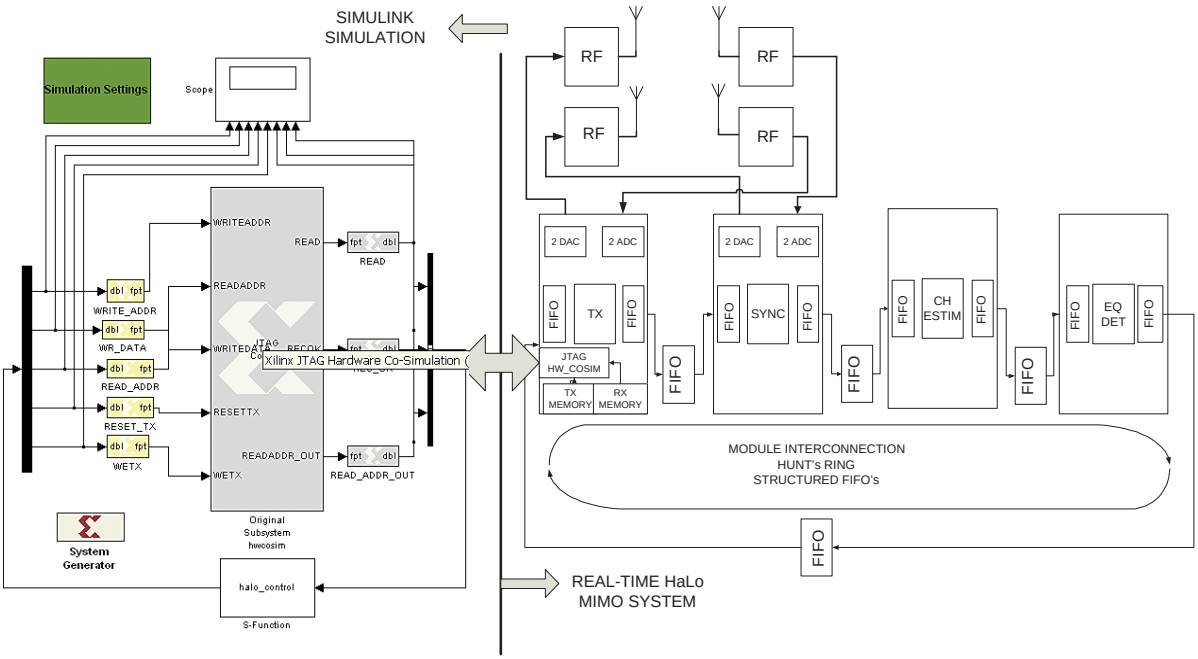

Figure 3.7: Scheme of a 2x2 real-time HaLo MIMO system controlled from Simulink.

clocked. Once all the data has been loaded into the transmission memory, the first module is triggered and real-time data processing starts. The signal is modulated, transmitted, received, demodulated and processed in real time.

When all the received information bits are detected, the Matlab control algorithm receives a notification and reads the information bits from the reception memory. BER and frame error rate (FER) measurements are carried out in Matlab and any other analysis, such as normalized mean squared error (NMSE) of the channel estimator, can be performed.

3.5.2 Application Examples

This section describes some of the applications of the developed "Hardware in the loop" approach. Most of these applications have been necessary for the implementations described in this chapter.

Validation of a complete 2x2 MIMO system

The HaLo features of the platform have been employed to implement the 2x2 spatial multiplexing system that will be detailed in the following section. The MIMO signal processing algorithms have been progressively translated from Matlab/Simulink and tested with real transmissions. The implemented algorithms include frame detection, symbol time synchronization, frequency offset correction, LS channel estimation and MIMO detection based on a zero-forcer or a sphere decoder.

Real-time execution with Matlab-simulated channels

A more complex channel model, developed in Matlab or Simulink, can also be used if the HaLo approach is selected. Fig. 3.8 shows the diagram of a real-time MIMO system where the real transmissions have been replaced by an off-line Matlab-based channel. The inclusion of known channels allows repeatability and eases the debugging of real-time algorithms before their final validation with real transmissions.

Hardware/software co-simulation with real signals

The system can act as a basic testbed that combines Matlab code, hardware implementation and real signals. Thanks to the flexibility of the system, any of the algorithms of the system can be implemented in hardware or simulated in Simulink [Stege04].

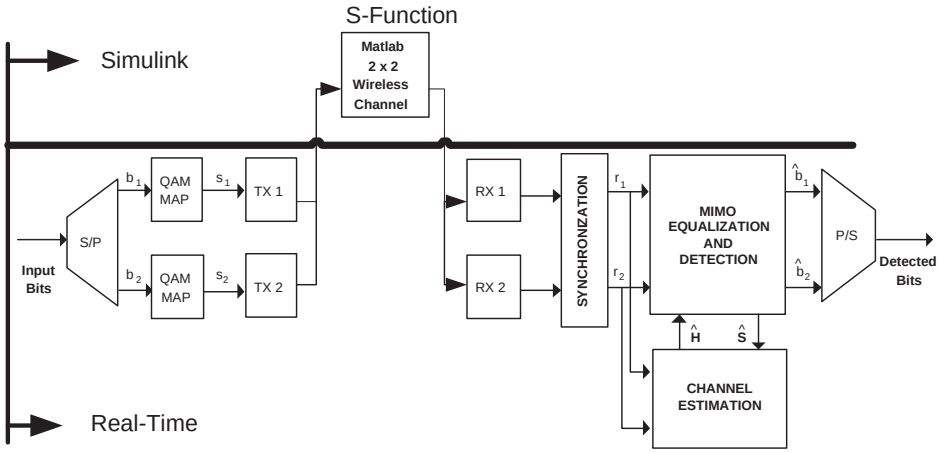

Figure 3.8: Matlab-emulated channel in a real-time running rapid prototyping platform.

Hardware acceleration of computationally intensive simulations

The HaLo approach proposed in this section can also be used to accelerate the simulation time of complex systems, such as decoding algorithms. For instance, the simulation of the System Generator design of the whole MIMO system can run more than 20 times faster on the FPGAs than in Simulink.

3.6 Implementation of a Basic 2x2 MIMO System

This section describes the implementation of a basic narrowband 2x2 MIMO system based on a ZF receiver, which has allowed to test the elements of the platform and the validity of

the design methodology. As has been detailed in Section 3.4, the RF transceivers operate with baseband IQ signals. Therefore, the modulation does not need to be implemented in the FPGA. Figure 3.9 shows the main blocks of the hardware implementation.

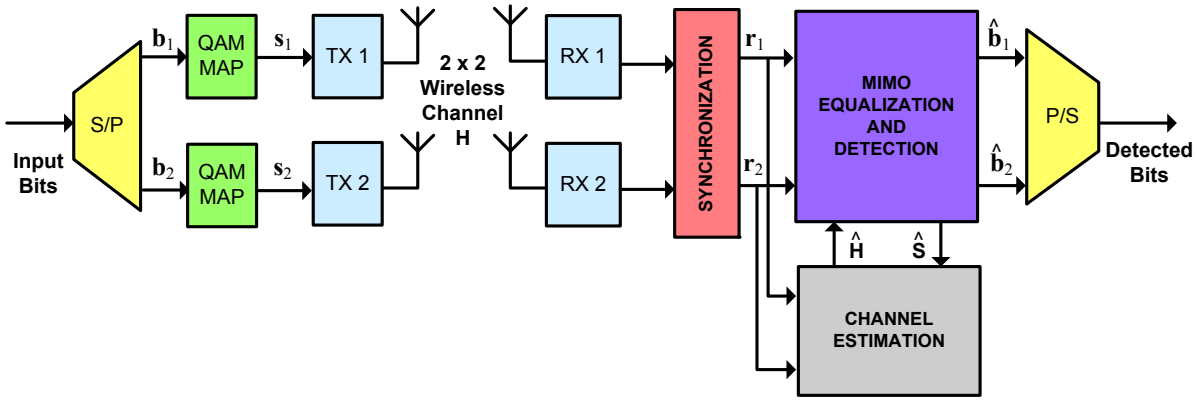

Figure 3.9: Diagram of the implemented 2x2 MIMO wireless system.

3.6.1 Transmitter Algorithms

The main signal processing algorithms implemented at the transmitter are:

1. **Preamble generation**: A preamble is added at the transmitter to allow synchronization and channel estimation at the receiver. Orthogonal binary phase shift keying (BPSK) modulated Walsh codes have been selected.

2. **Multiplexing**: The information bits are divided into two separate streams which are mapped, modulated and transmitted simultaneous and independently.

3. **Symbol Mapping**: The information bits are mapped onto a QAM constellation, which can correspond to BPSK, QPSK or 16-QAM modulation.

4. **Oversampling**: The symbol stream is oversampled by a factor of 8.

5. **Pulse Shaping**: A raised cosine (RC) pulse-shaping filter is applied to each symbol stream with a roll-off factor of $\beta = 0.5$.

6. **Inline MIMO channel emulator**: A flat-fading Rayleigh channel emulator has been created to allow hardware co-simulation of the whole system. This channel emulator is based on Gaussian noise generators and channel coefficients stored in a large RAM block. This allows to test the hardware implementation at its maximum rates without breaking the flat-fading channel assumption.

Figure 3.10 shows a sample System Generator design including all the algorithms implemented at the transmitter side.

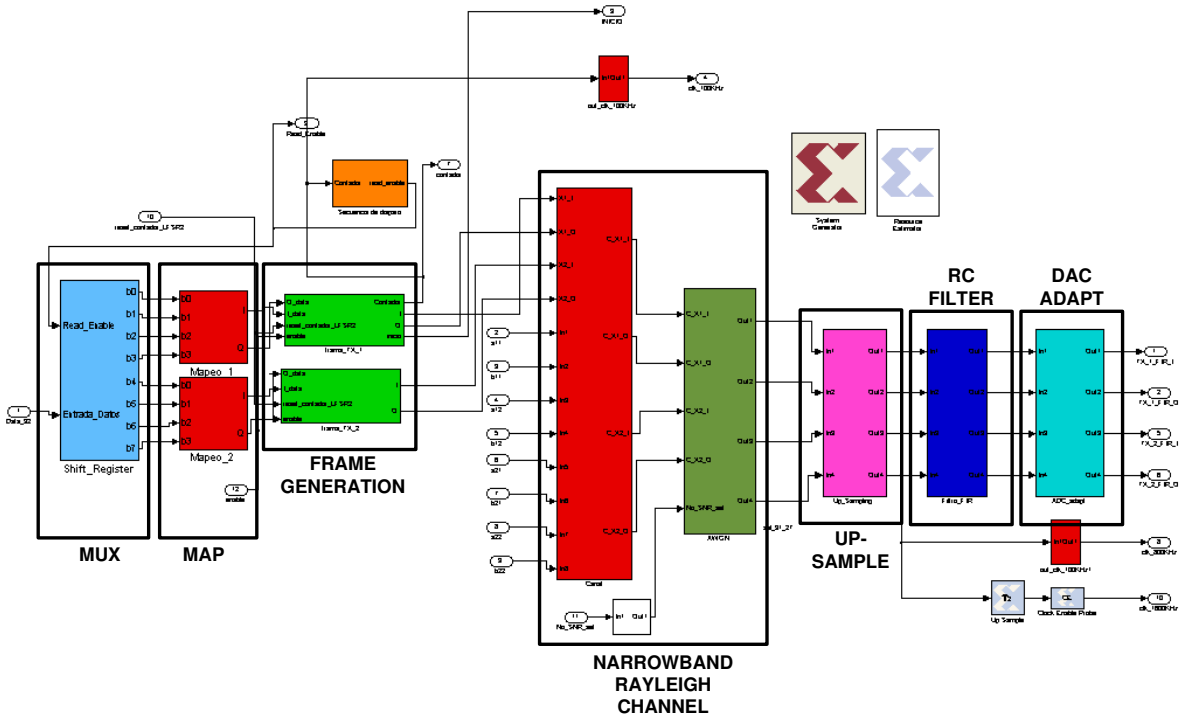

Figure 3.10: System Generator implementation of the 2x2 MIMO transmitter.

3.6.2 Receiver Algorithms

The following algorithms have been implemented at the receiver side, where most of the complexity and resource demands arise:

1. **Frame synchronization**: a multi-antenna extension of the double-sliding window technique has been applied [Heiskala02].
2. **Sample-time synchronization**: the ML approach of [Naguib98] has been chosen.
3. **Frequency Offset Estimation**: a reduced complexity iterative offset estimation technique has been used as in [Simoens04].
4. **Channel Estimation**: a basic training-based LS (Least-Squares) MIMO channel estimator has been implemented [Marzetta99a].
5. **Inverse calculation**: A direct implementation of a 2×2 matrix inversion has been developed, which is required by the ZF detector [Burg06].
6. **MIMO equalization and detection**: The ZF algorithm described in Section 2.2.4 has been implemented as a direct product of two complex 2×2 matrices.

3.6.3 Design Partitioning

Design partitioning, or the separation of a system across several DSP and FPGA devices, is a major issue in the prototyping of complex systems, such as MIMO transceivers [Rupp03, Kaiser04, Huang08]. Three are the main concerns in this field: the efficient separation of algorithms, the communication of data among all the elements and the generation of all the code (DSP) and hardware designs (FPGA) required for all the devices.

As it has been shown in Section 3.4, the Heron rapid prototyping board consists of four FPGA modules, which must be interconnected to be able to work with large designs. System Generator provides its own interfacing libraries for some commercial boards. Unfortunately, the Heron HEPC9 board is not directly supported. Even if System Generator provides ways to set up new systems, the specific structure of the hardware and inter-modular link protocols must be taken into account in order to achieve a successful multi-FPGA implementation.

Specific System Generator-based libraries have been created for inter-module communication and control of board resources. The design synthesis flow has also been adapted to the modular Heron platform, enabling the semi-automatic generation of bitstreams for all the FPGAs.

The algorithms shown in the previous section have been implemented in four different Virtex-II FPGA devices, three of which have 1M gates and 3M the other. The final implemented structure is shown in Figure 3.11. As it can be seen, the transmitter has been located into one device, while the receiver has employed the rest of the available resources. The four analog outputs are controlled by two different devices, which must be synchronized to allow MIMO transmissions, as will be shown in the next section. The same problem arises with the four analog inputs.

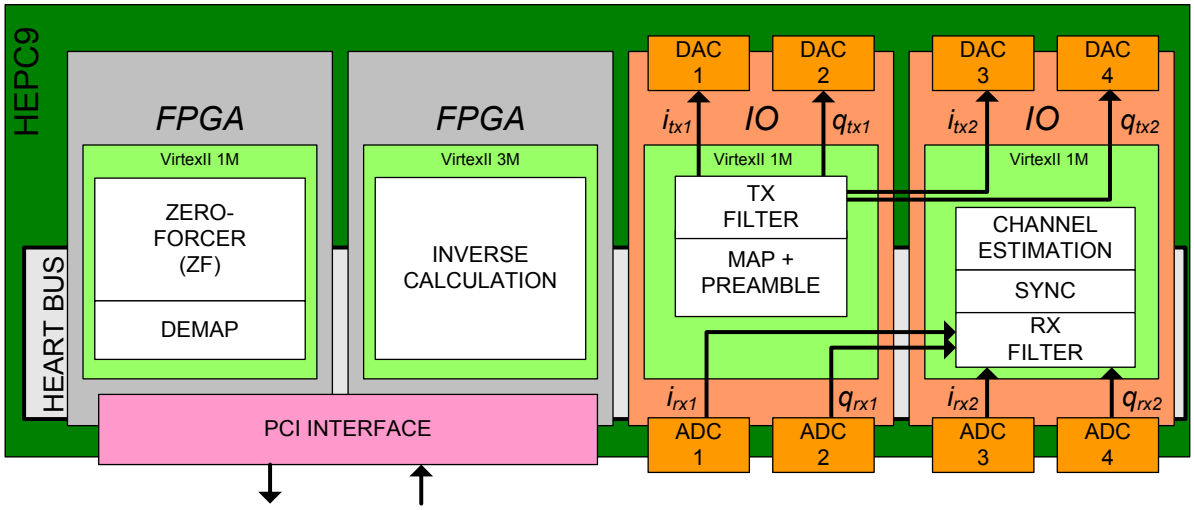

Figure 3.11: Schematic of the partitioned design which comprises 4 FPGA devices.

3.6.3.1 RF Chain Partitioning

As many MIMO algorithms rely on the reasonable assumption of fully synchronized transmission and reception, a timing or frequency offset on one board cannot be tolerated. As the number of antennas grows, each module may not have enough analog inputs or outputs. Therefore, it becomes necessary to distribute transmission and reception signals through different modules, requiring inter-module links with predictable delays.

As it is shown in Fig. 3.11, each IO module has 2 analog outputs and 2 inputs. Therefore, each module can only support one receive and one transmit antenna. The synchronization of the reception or transmission chains is implemented using a completely configurable delay library. Depending on the applied inter-module communication configuration, delay parameters are defined and automatically generated. In the 2x2 case of Fig. 3.11, data symbols are transmitted synchronously by the RF transceivers, delaying one chain in the first module until the other one arrives to the second module through the intermodule connection. The same operation is repeated for received RF chain synchronization.

3.6.4 Complexity and Resources

Table 3.1 shows the FPGA resources of the complete MIMO system using 16-QAM modulation. Only the numbers of embedded multipliers and FPGA slices are shown. They are compared with the total number of resources available on the HEPC9-based rapid prototyping platform.

Algorithm	**Mults**	**Slices**	**% Slices**
Transmitter	0	1,320	5.34%
Receiver	38	8,413	34.07%
Sync & Ch. Est.	*18*	*2,693*	*10.9%*
Inverse	*16*	*3,881*	*15.72%*
ZF	*4*	*1,839*	*7.4%*
Ch. Emulator	20	1,771	7.17%
Comm. & Control	0	1,542	6.24%
Total Used	58	13,046	52.83%
Total Available	216	24,696	

Table 3.1: FPGA resources used by the ZF-based real-time implementation.

The three main blocks of the receiver are also shown to indicate the distribution of the resources. The calculation of the inverse is the most computationally intensive task, followed by the joint synchronization and channel estimation process. It should be noted that the matrix inversion has not been optimized from a resource-consuming point of view,

since it has been implemented using the direct adjoint matrix method, whose application is straightforward, but is computationally inefficient [Burg06].

The algorithm named "Comm. & Control" corresponds to the logic required for the inter-module data communication and the PCI-based control of the real-time execution flow.

3.7 Implementation of a Sphere Decoder-Based MIMO System

As part of the work developed during this thesis, a full SD-based 2×2 MIMO system has been developed, in collaboration with the *Institute for Digital Communications* of the University of Edinburgh. This is the first real-time implementation of a whole SD-based real-time MIMO system. The analysis of the integration of the SD in a realistic whole MIMO prototype is specially interesting to evaluate its feasibility, complexity and performance degradation under implementation constraints.

As will be shown in Chapter 5, this implementation has been used to analyze the effects of channel estimation and implementation errors on the theoretical performance and throughput of an SD-based MIMO system. A 16-QAM constellation has been chosen to have a moderately large set of $B^M = 16^2 = 256$ candidates.

3.7.1 Integration of the SD Model into the MIMO Implementation

The SD algorithm described in Section 2.2.4.1 has been integrated into the whole MIMO implementation described in the previous section. The SD hardware implementation that has been ported to the platform has been designed and validated at the University of Edinburgh using System Generator for DSP [Barbero05a]. Figure 3.12 shows a diagram of the architecture which implements the exact algorithm described in Section 2.2.4.1. Therefore, this detector has a variable throughput and obtains the same solution as the optimal ML detector.

The aforementioned SD module has been ported to the MIMO prototyping platform located at the University of Mondragon. The SD algorithm requires two important pre-processing steps which were executed off-line in the SD implementation of [Barbero05a]. These operations, which have been implemented to make the SD work in a real system, are the following:

- An inverse (or pseudoinverse) calculation for ZF pre-processing.
- A Cholesky decomposition of the Gram matrix $\mathbf{H}\mathbf{H}^H$.

Therefore, these two blocks have been implemented in order to make the SD implementation work in a full real-time MIMO transmission system. The implementation has been

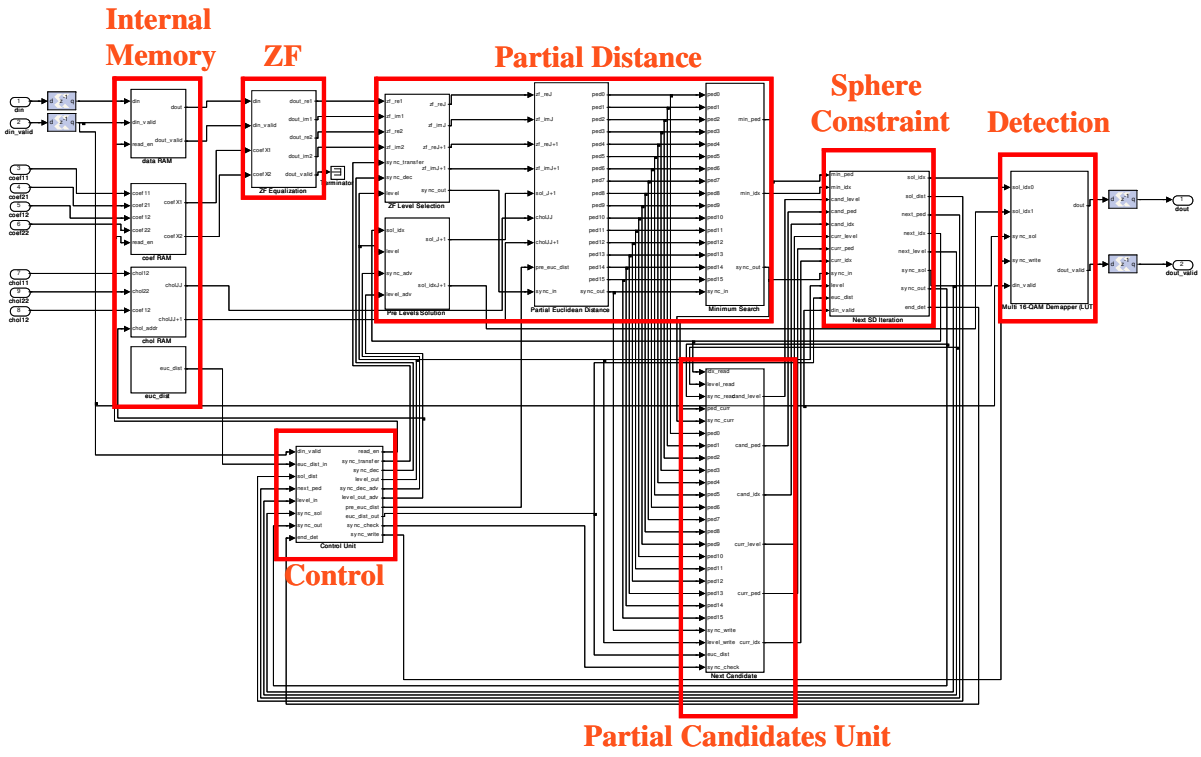

Figure 3.12: Structure of the System Generator implementation of the SD decoder, developed at the University of Edinburgh.

tested running in real time and using the inline channel emulator described in Section 3.4. The use of an inline channel allows to switch between ideal and hardware values for synchronization times, channel estimates or pre-processing matrices. Hence, the partial effect of the implementation of each module or algorithm can be evaluated.

Two are the magnitudes that have been evaluated for different E_b/N_0 values: BER performance and the achievable throughput. Figure 3.13a shows the BER curves of the implemented SD-based MIMO system with perfect synchronization, pre-processing and channel estimation. The BER performance is shown for the FPGA implementation with 16 and 12 bits of resolution at the input. Since the analog to digital converter (ADC) devices of the MIMO platform have a maximum of 12 bits of resolution, this has been the value selected for the final implementation. The results for non-ideal synchronization, pre-processing and channel estimation will be shown in Chapter 5.

Figure 3.13b shows the maximum achievable throughput of the implemented SD-based MIMO system with perfect synchronization, pre-processing and channel estimation for 16-bit and 12-bit FPGA implementations. As it is shown, the throughput of the SD does not depend only on the channel conditions, but also on the effective SINR which depends on quantization and implementation errors.

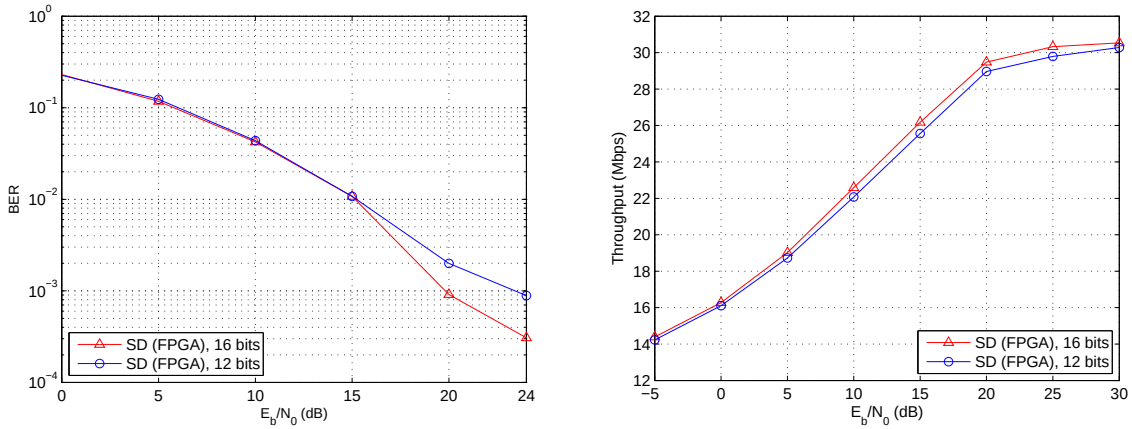

(a) (b)

Figure 3.13: BER (a) and throughput (b) performance curves for the FPGA implementation of the SD algorithm.

3.7.2 Complexity and Resources

Table 3.2 shows the FPGA resources of the complete SD-based MIMO system using 16-QAM modulation. In this case, the calculation of the inverse of the channel matrix and the Cholesky decomposition of the Gram matrix are the most computationally intensive tasks. It should be noted that these two operations have not been optimized from an implementation point of view given that the focus of this work was on the integration of the SD in a MIMO system. As it can be seen in Table 3.2, the implementation of the SD requires a relatively small FPGA area, indicating that several SDs could be implemented in parallel on the same prototyping platform.

Algorithm	**Mults**	**Slices**	**% Slices**
Transmitter	0	1,320	5.3%
Receiver	74	11,923	48.3%
Sync & Ch. Est.	*18*	*2,693*	*10.9%*
Inv. & Chol.	*33*	*4,608*	*18.6%*
SD	*23*	*3,370*	*13.7%*
Ch. Emulator	20	1,771	7.2%
Comm. & Control	0	1,542	6.2%
Total Used	96	16,556	67.0%
Total Available	216	24,696	

Table 3.2: FPGA resources used by the SD-based real-time implementation.

3.8 Chapter Summary

This chapter has described the development of a hardware prototyping platform for the design and validation of real-time signal processing algorithms for MIMO communications. A Matlab/Simulink-based methodology has been developed and a flexible platform has been built which has allowed to port a whole basic MIMO system from Matlab to a multi-FPGA implementation. Xilinx System Generator for DSP has been chosen as the main tool to directly generate VHDL designs and co-simulate from Simulink.

The platform located at the University of Mondragon allows to validate Matlab, VHDL or System Generator algorithms with real signals and with real-time hardware, depending on the needs for every designing stage. The platform is mainly based on modular Hunt Engineering Heron rapid prototyping boards and Virtex-II FPGA devices.

Two fundamental detectors have been implemented at the MIMO receiver: ZF and SD. The latter has been developed in collaboration with the University of Edinburgh, leading to the first SD-based real-time MIMO prototype. Both implementations have been the basis for the analysis of realistic channel estimation and implementation impairments in Chapter 5.

The main contributions and results of these chapter are the development of a flexible MIMO prototyping platform, the design and validation of a real-time algorithm development methodology, and the full real-time implementation of a MIMO wireless system, which can be based on the ZF or the SD detector.

Chapter 4

MIMO Channel Estimation

4.1 Introduction

All the MIMO detection algorithms described in Section 2.2.4 require the knowledge of the channel matrix $\mathbf{H}$ to detect the transmitted symbols. The estimation of the channel is specially complex for MIMO systems, due to the multiplication of the number of channel parameters to estimate. For example, if a system with $M = 4$, $N = 4$ and a channel impulse response length of $L = 16$ is considered, $MNL = 256$ complex values must be estimated. Therefore, if the SISO case is established as a reference, the number of parameters to estimate has been multiplied by MN, whereas the number of received symbols is only N times larger.

The efficiency of channel estimation can affect the performance of the system in two different ways: introducing a channel estimation error that reduces the channel capacity and dedicating a fraction of its bandwidth to the transmission of pilots or training symbols [Hassibi00, Biguesh06].

The capacity bounds of MIMO systems with channel estimation error have been theoretically evaluated for a set of reference systems [Marzetta99a, Hassibi00, Yong04, Cosovic07], though these theoretical analysis can not be linked to practical performance results.

Three are the main strategies for the design of MIMO channel estimation algorithms:

1. **Supervised or training-based methods**: A set of known information symbols are sent so that the receiver can estimate the channel [Hassibi00, Biguesh06].

2. **Blind techniques**: The channel values are recovered from the statistical properties of the received information symbols up to some kind of ambiguity [Tong94, Tong98, Bölckskei02, Larsson03]. A reduced number of training symbols is usually still needed to obtain an estimate.

3. **Semi-Blind channel estimation**: A training matrix is used to allow a first estimate, which is improved using statistical properties of the received signal or information from already detected symbols [Muquet99, Míguez02, Wang03, Jagannatham06].

This chapter analyzes the most common channel estimation algorithms used in MIMO wireless communications. Following the structure of Chapter 2, the main estimation techniques are summarized for each fundamental MIMO system, focusing on practical and feasible algorithms. The objective of this chapter is to classify and evaluate by simulations the algorithms whose effects will be analyzed in the following chapter.

As it has been stated in Chapter 2, many wideband MIMO communication systems, such as MIMO-OFDM, can be modelled as multiple narrowband transmissions. Although this is not strictly true for channel estimation issues, frequency-flat fading MIMO channel estimation, which is detailed in Section 4.2, has been considered the basis for the analysis of more complex systems. Since most of the wireless standards transmit pilots or known information symbols, only trained and semi-blind channel estimation algorithms have been considered as practical cases.

Section 4.3 analyzes the estimation of frequency-selective channels in MIMO-OFDM and MIMO-SCFDE systems. The main time-domain and frequency-domain algorithms are analyzed and compared by simulations for burst transmissions in a WLAN scenario. Iterative channel estimation for Turbo-MIMO systems is then analyzed in Section 4.4, focusing on a decision-directed expectation maximization (EM) channel estimation algorithm. Simulation-based performance results are shown for an MMSE-PIC receiver with channel estimation error. Last, a BER evaluation tool is proposed which allows to predict the BER performance of iterative MMSE-PIC systems with channel estimation, extending the semi-analytical EXIT functions described in Section 2.5.

4.2 Narrowband MIMO channels

In common frame or burst based wireless systems, such as the WLAN scenarios defined by the IEEE 802.11a standard, known symbols are transmitted with the information symbols to allow channel estimation at the receiver [IEEE99]. These training symbols are usually inserted either at the beginning of the frame (preamble) to allow the first channel estimate or spread among all the information symbols for channel tracking in fast-fading channels [Sun02, Lang04].

A quasi-static fading model is assumed for the work described in this chapter, i.e., the channel can be considered constant for a burst or frame. Therefore, the training symbols can be inserted at the beginning of each frame as a preamble of length L_T. The transmitted symbol matrix $\mathbf{S}$ can be then represented as the concatenation of a known training matrix $\mathbf{S}_T$ and the data symbol matrix $\mathbf{S}_D$ of dimensions $M \times L_T$ and $M \times L_D$, respectively, as depicted in Figure 4.1. The received symbol matrix $\mathbf{R}$ can be equally split into a training-related part $\mathbf{R}_T$ and a data matrix $\mathbf{R}_D$ of dimensions $N \times L_T$ and $N \times L_D$, respectively.

Since a frame-based wireless system is assumed, and with implementation in mind, only

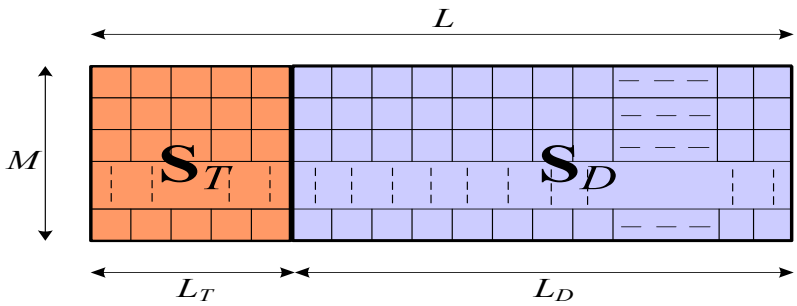

Figure 4.1: Structure of the transmitted symbol matrix $\mathbf{S}$.

simple supervised and semi-blind schemes are considered in this section. First, basic LS and linear minimum mean squared error (LMMSE) channel estimation techniques are considered. Two simple semi-blind techniques are then analyzed, based on hard decision-directed iterative estimation and statistical processing of the received data symbols.

4.2.1 Training-Based Channel Estimation

Training-based estimation of frequency-flat fading MIMO channels is extensively studied in the literature. The capacity limits for these systems have been theoretically analyzed from several points of view [Marzetta99a, Hassibi00, Furrer07]. The optimal values for the training parameters have been calculated from capacity-maximization criteria, concluding that training-based channel estimation is clearly suboptimal, specially for low SNR scenarios [Hassibi00]. Another very important drawback of training-based channel estimation is that the training length must be at least equal to the number of transmitted antennas, which can reduce the efficiency of MIMO systems with a large number of transmission antennas. These are the main arguments that justify the use of semi-blind estimation techniques.

Although there are more approaches to training-based channel estimation of MIMO channels, two are the fundamental schemes which can be used as references for the rest of the systems that will be analyzed later. These are the LS and the LMMSE channel estimation methods. The following sections show the structure of these estimators, as well as some results regarding their performance for different training lengths.

4.2.1.1 Least-Squares Channel Estimation

The LS solution to the training-based channel estimation problem, which is equivalent to ML, can be expressed as

$$\hat{\mathbf{H}}_{LS} = \sqrt{\frac{M}{E_s}}\mathbf{R}_T(\mathbf{S}_T\mathbf{S}_T^H)^{-1}\mathbf{S}_T^H. \tag{4.1}$$

The LS channel estimation involves the inversion of a $M \times M$ matrix, whose rank can

be sufficient only if the length L_T of the training matrix is not smaller than M and the training sequences contained in $\mathbf{S}_T$ are orthogonal. In other words, as many measurements as unknowns are needed in order to obtain the LS solution. Since $\mathbf{S}_T$ is known at reception, $(\mathbf{S}_T\mathbf{S}_T^H)^{-1}\mathbf{S}_T$, which involves a matrix inversion, can be computed off-line. Hence, only a matrix product is required to obtain the channel estimate.

It has been shown in [Hassibi00, Marzetta99a] that the training matrix $\mathbf{S}_T$ is optimal if it is the multiple of a matrix with orthonormal rows, i.e., $tr\left(\mathbf{S}_T\mathbf{S}_T^H\right) = E_T\mathbf{I}_M$, where E_T is the total training energy. It has been proposed in [Biguesh04] that this optimal structure can be obtained using a DFT-like matrix, though BPSK-modulated binary codes, such as Walsh codes, can also be used. The latter have been chosen to obtain the results shown in this chapter. If this kind of BPSK-modulated signals are used, the aforementioned matrix product can be further simplified to addition and substraction operations.

The NMSE of the LS estimation, denoted as γ, is a widely used parameter when evaluating channel estimation algorithms and is calculated as

$$\gamma = \frac{\mathrm{E}(\|\mathbf{H} - \hat{\mathbf{H}}\|^2)}{\mathrm{E}(\|\mathbf{H}\|^2)}, \tag{4.2}$$

where $\hat{\mathbf{H}}$ stands for the estimate of the channel matrix $\mathbf{H}$. The NMSE for LS channel estimation can be expressed as [Biguesh06]

$$\gamma_{LS} = \frac{N_0 M}{E_T}, \tag{4.3}$$

where E_T represents all the training energy. If a fixed training power is assumed, which will be the case for this research work, the energy of the training matrix can only be increased augmenting its length L_T. If the energy per symbol is assumed equal for training and data symbols ($E_T = \|\mathbf{S}_T\|^2 = E_s L_T$), the result in (4.3) becomes

$$\gamma_{LS} = \frac{M}{\rho L_T}. \tag{4.4}$$

Figures 4.2a and 4.2b show the NMSE and BER performances of a 4×4 QPSK transmission system with LS channel estimation and MMSE detection for different training lengths.

Figure 4.2a shows the NMSE curves for 4 different training lengths, from the minimum ($L_T = 4$) to $L_T = 12$. The NMSE decreases linearly with both the SNR value ρ and the training length L_T, as defined in (4.3). As can be seen in Figure 4.2b, the BER performance improves if the training length L_T increases, but this improvement gets smaller for low SNR values and long training blocks. For instance, the BER improvement is remarkable when the training length increases from $L_T = 4$ to $L_T = 6$, but it is negligible when it changes from $L_T = 8$ to $L_T = 12$. Hence, there is not a direct relationship between the NMSE value and the BER, which is the main reference for system performance. Therefore, the NMSE value

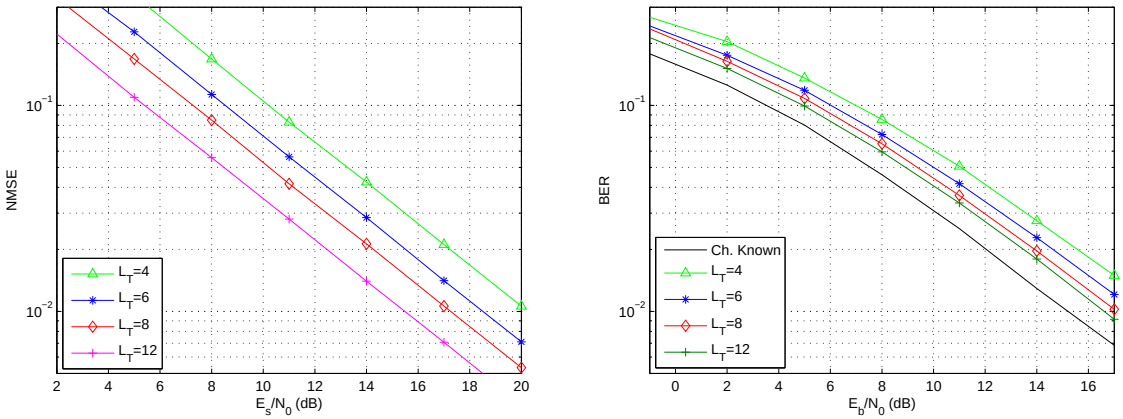

(a) (b)

Figure 4.2: NMSE (a) and BER (b) performance curves of LS channel estimation for a 4×4 spatial multiplexing system with MMSE detection.

can be considered when comparing channel estimation schemes, but the BER measurement must be the reference in order to evaluate the final effect of channel estimation algorithms. As will be shown later, this lack of relationship between NMSE and BER measurements can be more severe when different channel estimators are compared.

4.2.1.2 Linear Minimum Mean Squared Error Channel Estimation

The NMSE curves of LS MIMO channel estimation can be enhanced for low SNR ranges if the SNR value ρ and the channel correlation metrics are employed [Biguesh06]. This is the case of the LMMSE estimator, whose solution can be expressed as

$$\hat{\mathbf{H}}_{LMMSE} = \sqrt{\frac{M}{E_s}}\mathbf{R}_T \left(\mathbf{S}_T \mathbf{R}_H \mathbf{S}_T^H + \frac{M}{\rho}\mathbf{I}_{MxM} \right)^{-1} \mathbf{S}_T^H \mathbf{R}_H, \tag{4.5}$$

where $\mathbf{R}_H = \mathrm{E}(\mathbf{H}\mathbf{H}^H)$ is the expectation of the channel autocovariance matrix, which is directly related to channel path correlation [Schumacher04]. Figure 4.3a shows the NMSE performance comparison for LS and LMMSE channel estimators for a 4x4 spatial multiplexing system with antenna correlation factors of $\sigma_H = 0$ and $\sigma_H = 0.35$ [Schumacher04]. As it can be easily seen, the LMMSE estimator tends to the LS solution at high SNR in uncorrelated fading channels.

These results show that the channel estimation NMSE is clearly improved by the LMMSE estimator for low SNR cases. On the other hand, the estimation NMSE improves slightly when a larger correlation factor is added to the simulations. Furthermore, this NMSE improvement gives rise to a very small decrease in the BER ratio. For instance, Figure 4.3b shows the BER performance of both estimation techniques.

Therefore, despite the large NMSE difference at low SNR regimes, the BER improvement

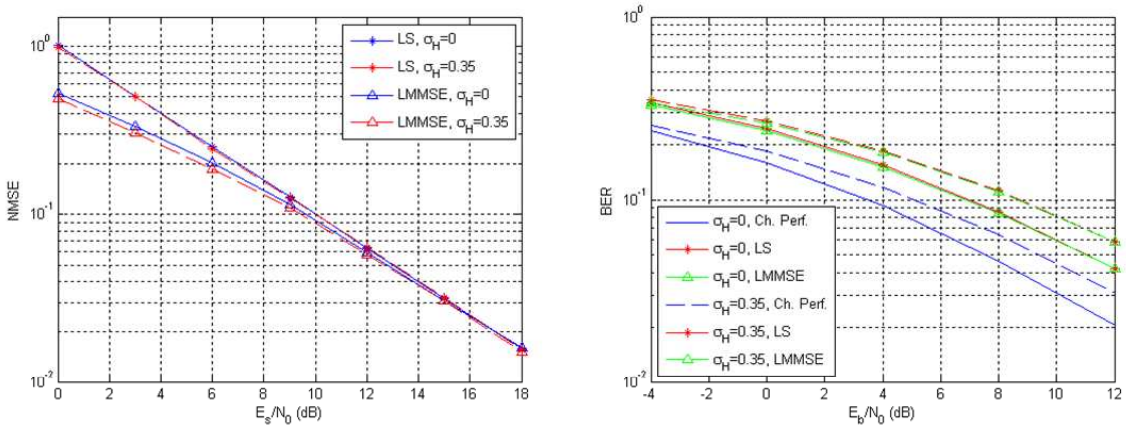

Figure 4.3: NMSE (a) and BER (b) performance curves of LS and LMMSE channel estimation for a 4×4 spatial multiplexing system with MMSE detection.

of LMMSE with respect to LS is negligible. Therefore, the NMSE of the channel estimate can not be considered as an absolute reference. From the results shown in this section, it can be stated that LMMSE does not clearly outperform LS in terms of final BER in systems with a low antenna correlation factor σ_H, despite its greater complexity.

If the implementation cost of both algorithms is analyzed, it can be stated that the LMMSE channel estimator requires an extra addition and a matrix product. Nevertheless, it can be much more complex than the LS implementation since no value can be precomputed, due to the variability of $\mathbf{R}_H$ and ρ. From the results shown by BER simulations and this simplistic complexity analysis, it is concluded that the LS estimator may be a more efficient solution from an implementation point of view.

4.2.1.3 Other Training-Based Techniques

Many other channel estimation techniques exist for training-based systems [Biguesh06]. One of the most interesting approaches, at least from a communication theory point of view, is the superimposed pilot (SIP) scheme, which was first applied to channel estimation in [Farhang-Boroujeny95]. It has been used for MIMO channel estimation and its performance has been analyzed from several points of view, including but not limited to effective maximum throughput, estimation NMSE, final BER, etc. [Zhu03a, Coldrey07].

These SIP structures avoid training overhead by simultaneously transmitting pilots and information symbols, achieving a better throughput. Their main drawback is the channel estimation error induced by the interference of information symbols. The SIP-based channel estimation has been deeply analyzed in [Coldrey07], where its optimal configuration and further iterative performance improvements have been shown. The SIP techniques have

been proven to perform better than conventional pilot schemes only in low SNR and very fast fading scenarios [Coldrey07].

4.2.2 Semi-Blind Techniques

After analyzing the limitations of the main training-based channel estimation techniques (loss of spectral efficiency and suboptimality), this chapter describes several semi-blind algorithms that have been chosen with one or both of the following objectives:

1. Reduction of the length L_T of the training matrix, which can lead to a higher spectral efficiency.

2. Improvement of the results obtained using the training-based schemes.

These semi-blind algorithms employ the whole received symbol matrix $\mathbf{R}$, including the unknown data symbol matrix $\mathbf{R}_D$, to estimate the channel from known properties of the transmitted data symbol matrix $\mathbf{S}_D$, such as independence of the sources, the finite alphabet of the symbols or the constant modulus of phase shift keying (PSK) signals.

Two main algorithm families have been considered:

1. Decision-directed iterative techniques, which iterate between channel estimation and data detection in order to get lower symbol error rates [Talwar96, Grant00b, Deng03, Khalighi05].

2. Second and higher-order statistics-based methods [Veen96, Medles03, Jagannatham06].

The main features of these estimation techniques and basic performance results will be shown in this subsection.

4.2.2.1 Iterative Channel Estimation

Although iterative channel estimation in coded Turbo-MIMO systems will be analyzed later in this chapter, other simpler decision-directed approaches are summarized here for uncoded hard-detection systems. These schemes lie on the finite alphabet property of the source signals to improve the channel estimation accuracy or to reduce the length of the training sequences. Several iterative least squares (ILS) systems have been introduced in [Talwar96, Ranheim05] for blind or semi-blind estimation of different synchronous co-channel signals. These approaches employ the already detected signals as training symbols, consequently improving the channel estimate until a convergence threshold is met. Very similar block-iterative estimation techniques have been derived for iterative coded MIMO system using an EM formulation, although soft symbol estimates are used instead of hard decisions for channel re-estimation [Khalighi05], as will be shown in Section 4.4.

The main features of these algorithms can be summarized as:

1. The channel estimation improvement depends directly on the error probability of the MIMO detector. Therefore, the improvement only appears when a minimum SNR level is achieved. Obviously, this estimation approach depends on the symbol constellation.

2. An initialization is required for the first iteration. This can be done assigning zero, random or received symbol-based values to the channel and data symbols. Nevertheless, it has been shown in [Li00] that these approaches can lead to wrong solutions or need several run trials to converge. The use of blind source separation techniques (see next subsection) or training-based LS is suggested in [Li00] to obtain the initial channel estimate required for the first iteration.

3. Even for uncoded and high symbol error rate systems, these algorithms can offer a remarkable BER improvement from the first iteration with a relatively low complexity [Buzzi04].

Similar iterative channel estimation techniques have been presented in [Grant00a, Buzzi04, Ranheim05]. The simplest algorithms have been selected for the results shown in this section, extending the training matrix $\mathbf{S}_T$ with detected symbols using the aforementioned ILS algorithm. As a first approach, this iteration process has been implemented block-wise and only for uncoded bit streams. However, it will be extended to iterative coded systems in 4.4.

Figures 4.4a and 4.4b show the NMSE and BER performance improvements achieved for a 4×4 QPSK system reusing the detected symbols as an extension to the training sequences through an iterative approach. As it can be seen, the iterative algorithm with the minimum training length ($L_T = M = 4$) and 2 iterations outperforms the basic LS algorithm with $L_T = 6$. It is shown that a great improvement can be achieved for the second estimation, though it seems to get smaller as the number of iterations grows. For example, if the minimum training length of $L_T = M$ is considered, the 3 dB gap of the LS channel estimator can be reduced to nearly 1 dB if two iterations are carried out.

4.2.2.2 Second and Higher-Order Statistics-Based Approaches

Although there are a deal of semi-blind estimation algorithms based on second and higher order statistical properties of the signal [Veen96, Via07, Sabri08], two special techniques have been considered here, specially suited for spatial multiplexing systems: a simple algorithm based on second-order statistics, which achieves quite good results in a very simple manner, and a blind source separation-based approach, which can reduce the length of the preamble with a relatively low computational complexity.

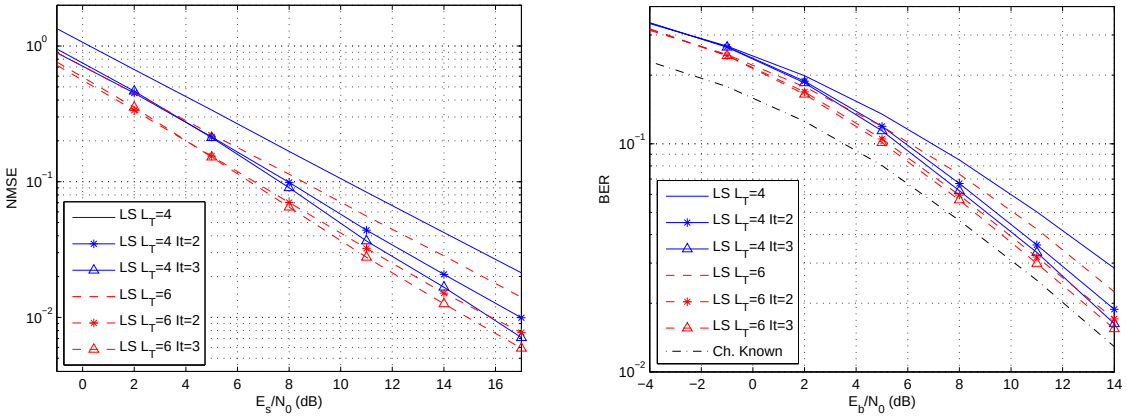

(a) (b)

Figure 4.4: NMSE and BER curves of iterative LS channel estimation for a 4×4 spatial multiplexing system with MMSE detection.

Whitening-Rotation or Gaussian Semi-Blind estimation

A very interesting semi-blind algorithm was introduced in [Medles03] and [Jagannatham06] for MIMO systems, named Gaussian semi-blind or whitening-rotation (WR), respectively. Parting from independent component analysis (ICA) concepts, this estimation algorithm decomposes the channel matrix as the following product:

$$\mathbf{H} = \mathbf{WQ} \tag{4.6}$$

where $\mathbf{W}$ is a whitening matrix with the same dimensions as the channel ($N \times M$) and $\mathbf{Q}$ is a square unitary (rotation) matrix of dimensions $M \times M$.

This technique proposes to estimate the $\mathbf{W}$ matrix from the correlation of the received symbols, i. e., employing second-order statistics, whereas the $\mathbf{Q}$ matrix must be estimated from the training sequence. The main advantages of estimating $\mathbf{Q}$ instead of $\mathbf{H}$ are the following:

1. The matrix to be estimated is of dimensions M x M, instead of N x M.

2. The $\mathbf{Q}$ matrix, being unitary, implies M^2 real parameters, instead of the $2M^2$ of an ordinary complex matrix [Jagannatham06]. This property of the $\mathbf{Q}$ matrix increases the relationship between measurements and unknowns, leading to a better channel estimate.

For example, assuming that $\mathbf{W}$ is perfectly known at the receiver, estimating $\mathbf{Q}$ instead of $\mathbf{H}$ can offer an improvement of up to 3 dB in NMSE [Jagannatham06]. From a complexity point of view, this technique requires the estimation of the correlation matrix from

the outputs and several singular value decomposition operations. Despite its benefits, this technique still requires the use of a training sequence of a length equal or larger than the number of transmitting antennas.

Figure 4.5b shows the BER comparison for 4×4 BPSK spatial multiplexing systems with trained LS, ILS and the WR algorithm. As it is shown, the iterative algorithm outperforms the WR for small constellations. Although it has not been included in this document, the WR algorithm achieves a better performance than the one-iteration ILS for larger constellations, such as 16-QAM.

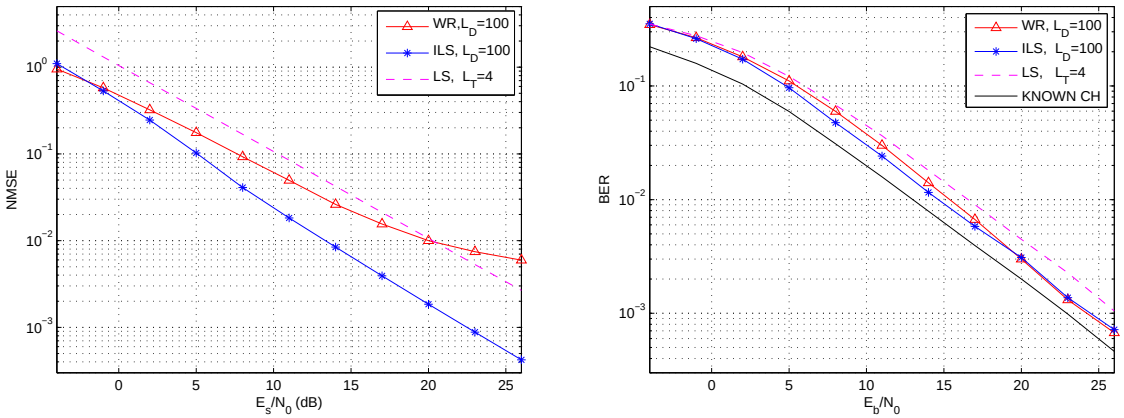

(a) (b)

Figure 4.5: NMSE (a) and BER (b) curves of training-based, iterative LS and WR channel estimation techniques for a 4×4 BPSK transmission of 100 bits per antenna.

If the NMSE curves of Figure 4.5a are analyzed, the estimation performance seems to be much worse than what it actually is. At high SNRs, the WR algorithm seems to perform even worse than the LS, but these results do not fit with the BER performance curves of Figure 4.5b. This case can be considered a good example of the lack of reliability of the NMSE for channel estimator comparison, specially when estimators with different output distributions are used, as will be shown later in this section.

The differences between BER and NMSE results can be easily explained if the cumulative distribution function (cdf) of the output SINR is plotted and compared for the different estimation methods. Figure 4.6 shows the cdf of the output SINR per detected symbol for E_b/N_0 values of 11, 14, 17 and 20 dB. Note that the final BER is determined by the cdf value at which a specific SINR level is met, which depends on the selected constellation.

As it is shown in Figure 4.6, the mean value of the SINR is smaller for the WR method at the mentioned high SNR values, but if the low SINR region of interest is analyzed, it can be seen that the cdf of the SINR gets smaller for the WR method, involving a lower bit error probability. This can be due to the fact that the WR algorithm gets a "spatially" more accurate estimate of the MIMO channel matrix, despite its worse NMSE value.

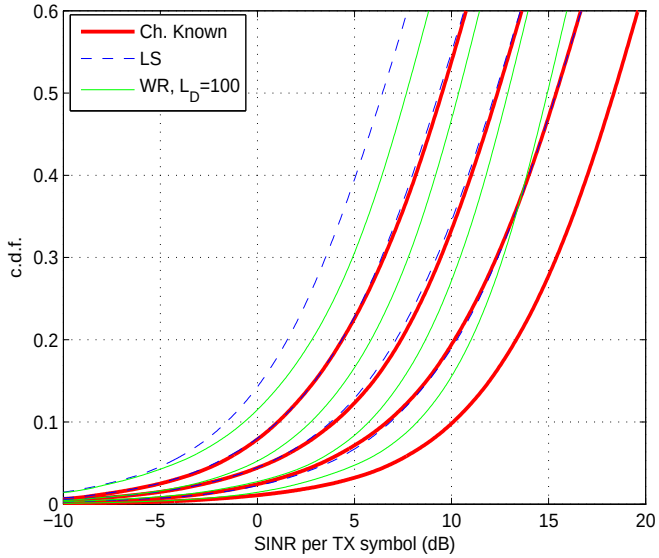

Figure 4.6: cdf of output SINR for different channel estimators and E_b/N_0 values.

Blind Source Separation Based Approaches

Since independent information streams are transmitted in an SM system, another interesting approach can be based on the principles of blind source separation (BSS). These methods allow to recover the MIMO channel blindly up to a permutation and phase rotation of the sources. Equation (4.7) shows the relationship between the blindly recovered symbols $\bar{\mathbf{S}}$, the transmitted symbols $\mathbf{S}$ and the separation matrix $\mathbf{G}$. Matrix $\mathbf{P}$ represents a permutation of the sources and $\bar{\mathbf{D}}$ is a diagonal matrix containing a phase shift at each transmission antenna.

$$\bar{\mathbf{S}} = \mathbf{GR} = \mathbf{P}\bar{\mathbf{D}}\mathbf{S} + \bar{\mathbf{N}} \tag{4.7}$$

The channel matrix can be calculated from $\mathbf{G}$, $\mathbf{P}$ and $\bar{\mathbf{D}}$ [Veen96]:

$$\hat{\mathbf{H}} = \mathbf{G}^{+}\mathbf{P}\bar{\mathbf{D}} \tag{4.8}$$

The $\mathbf{P}$ and $\bar{\mathbf{D}}$ ambiguity matrices can be estimated employing training sequences which can be much shorter than those required for training-only based channel estimation. The main drawbacks of this kind of algorithms are their slow convergence and relatively high complexity. Since a limited frame length has been assumed, algorithms which can lead to short training sequences and fast convergence have been specially considered.

Two special BSS algorithms have been analyzed:

1. *ACMA (Analytical Constant Modulus Algorithm)* [Veen96]: Based on the CM (Constant Modulus) property of some constellations, such as PSK. For systems without

noise, this non-iterative solution needs M^2 information symbols to get a solution. For AWGN channels, this estimation method offers very good results for short frame sizes. It has been proposed in [Lang04] as a possible complement to trained estimation and in [Li00] as a blind initialization technique for ILS algorithms. It has also been combined with space-time codes in [Swindlehurst02]. As many other CM-based algorithms, it can get acceptable results for non-constant modulus constellations like 16-QAM if a larger number of samples is employed.

2. *JADE (Joint Approximate Diagonalization of Eigenmatrices)* [Cardoso93]. This solution, based on 4th order statistics, offers relatively fast convergence and has been proposed in [Wang03] for spatial multiplexing systems with V-BLAST detection. It requires a larger number of samples than the ACMA algorithm, but it does not depend on the CM property.

These two methods employ, direct or indirectly, 4th order statistics and need to solve a joint matrix diagonalization problem. Figure 4.7 shows the comparison of BER rates for a 6×6 MIMO system with ZF detection, ACMA-based channel estimation, considering different training lengths and E_b/N_0 values of 0, 10 and 20 dB. The results for an LS scheme with the minimum training length have been included for comparison purposes. Though simplified, the results show that the ACMA BSS algorithm outperforms LS with only half of the training symbols. Even with just two training periods, the obtained results, though worse than LS, can be valid for the initialization of iterative algorithms, as has been proposed in [Li00, Lang04].

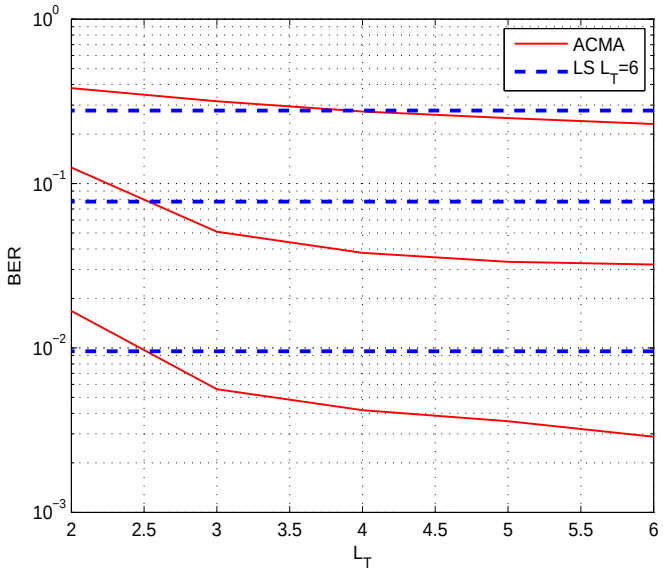

Figure 4.7: BER performance of ACMA-based channel estimation with different training lengths and E_b/N_0 values of 0, 10 and 20 dB.

4.3 MIMO-OFDM and MIMO-SCFDE

This section describes the main MIMO-OFDM and MIMO-SCFDE channel estimation methods. Two cases are analyzed: first, an optimal time-domain channel estimation algorithm is evaluated where the channel impulse response is calculated using an LS approach. The second one, which is simpler and easier to implement, calculates the frequency-domain channel responses at certain frequencies, interpolating the value for the rest of the subcarriers. Several different optimal pilot allocation schemes are then analyzed, focusing on implementation considerations. Although only OFDM is considered in this section, the same techniques can be used for MIMO-SCFDE, as will be shown in the performance results of Chapter 5.

4.3.1 Time-Domain LS-ML Channel Estimation

A MIMO-OFDM system model was shown in Section 2.3, where the CP-induced circulant channel convolution was represented by a Toeplitz matrix $\mathbf{H}_c$, which contained cyclic shifts of the channel impulse response. Since the objective of this section is the estimation of these channel coefficients, another representation is more suitable. Many different models have been published [Li99, Barhumi03, Minn06], where the latter is of special interest because of its general formulation of the problem.

As has been stated for narrowband MIMO systems, the estimation of a generic $M \times N$ system with uncorrelated path gains can be analyzed as N different $M \times 1$ estimation problems. Therefore, the basic $M \times 1$ model will be analyzed here, as defined in [Barhumi03, Minn06]. As a first approach, Q training OFDM symbols of T tones or subcarriers will be sent through M transmission antennas. The frequency-domain training symbol for transmission antenna m and OFDM symbol q can be then expressed as

$$\mathbf{c}_{m,q} = [c_{m,q}[0], c_{m,q}[1], ..., c_{m,q}[T-1]]^T, \tag{4.9}$$

and the respective CP-added time-domain signal of length $T + L_{CP}$ can be represented as

$$\mathbf{s}_{m,q} = [c_{m,q}[-L_{CP}], c_{m,q}[-L_{CP}+1], ..., c_{m,q}[0], c_{m,q}[1], ..., c_{m,q}[T-1]]^T, \tag{4.10}$$

where $L_{CP} > L$ is the length of the CP and L is the maximum length of the channel impulse response.

Assume $\mathbf{S}_m[q]$ is the $T \times L$ training symbol matrix for the m-th transmit antenna and the q-th OFDM symbol, whose elements are given by $[\mathbf{S}_m[q]]_{t,l} = s_{m,q}[t-l]$ for $t \in \{0, ..., T-1\}$ and $l \in \{0, ..., L-1\}$. If all the training matrices $\mathbf{S}_m[q]$ are stuck into an $\mathbf{S}_T$ matrix of dimensions $QT \times LM$ and the M channel path gain vectors of length L are stuck into an

$LM \times 1$ column vector $\mathbf{h}$, the whole system can be represented as

$$\mathbf{r} = \mathbf{S}_T \mathbf{h} + \mathbf{n}, \tag{4.11}$$

where $\mathbf{r}$ is the $QT \times 1$ vector of received symbols after CP removal and $\mathbf{n}$ is the $QT \times 1$ vector of uncorrelated Gaussian noise samples with variance N_0.

Using this representation, the channel coefficients appear only once in the equation, while the time-domain training symbol matrix $\mathbf{S}_T$ includes the Toeplitz structure required by the channel convolution. Once the system model is represented in this way, the LS channel estimate $\hat{\mathbf{h}}$, which is the same as the ML, can be calculated as [Minn06]

$$\hat{\mathbf{h}}_{LS} = \sqrt{\frac{M}{E_s}} \left(\mathbf{S}_T^H \mathbf{S}_T\right)^{-1} \mathbf{S}_T^H \mathbf{r}. \tag{4.12}$$

Note that the inversion of an $ML \times ML$ complex-valued matrix is required, among many other operations. If $\mathbf{S}_T$ is known, which is the case for preamble-based channel estimation, the matrix $\left(\mathbf{S}_T^H \mathbf{S}_T\right)^{-1} \mathbf{S}_T^H$ can be computed off-line so that the channel estimation process becomes a matrix product. The latter can be further simplified depending on the pilot structure, as will be shown in the next section.

The mean squared error (MSE) of the channel estimate is given by $N_0 tr\{\left(\mathbf{S}_T^H \mathbf{S}_T\right)^{-1}\}$ [Minn06] and the NMSE can be represented as:

$$\gamma_{LS} = \gamma_{ML} = \frac{ML}{\rho QT}. \tag{4.13}$$

The conditions for the optimal channel estimation are analyzed in [Minn06] and are fulfilled when

$$\mathbf{S}_T^H \mathbf{S}_T = E_T \mathbf{I}, \tag{4.14}$$

where E_T is the mean training energy per each transmission antenna [Minn06].

Figure 4.8 shows the NMSE and BER performance curves for a 4×4 MIMO-OFDM system with ML channel estimation for uncoded and rate-1/2 coded transmission. A HIPERLAN/2 A Model of 11 taps has been used for the simulation [Medbo98], allowing $ML < T$. As can be seen, the channel estimation error NMSE decreases linearly with the SNR.

The estimation algorithm of (4.12) has two limitations. On one hand, if the number of estimated parameters (ML) is larger than the number of FFT points (T), several symbols must be used for channel estimation. Different groups of transmission antennas can be located in different OFDM symbols, as has been shown in [Minn06], where the design of optimal MIMO-OFDM preamble structures is deeply analyzed. On the other hand, an interesting situation arises when the length of the channel impulse response L is larger than the guard interval L_{CP}. If the structure of the training symbols is the same as the data

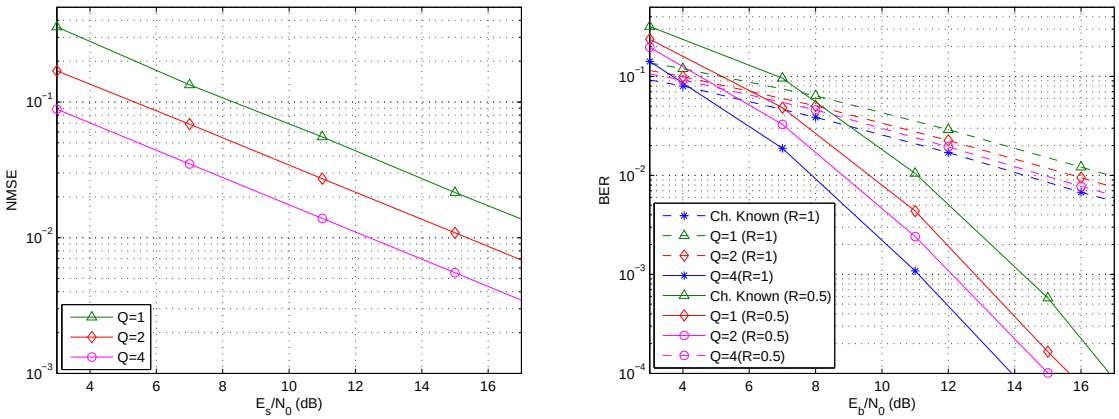

(a) (b)

Figure 4.8: NMSE (a) and BER (b) performance of ML channel estimation for a 4×4 HIPERLAN/2 A channel model ($L = 11$ taps).

symbols, the full channel impulse response cannot be estimated due to ISI. For instance, if the HIPERLAN/2 C channel model of $L = 31$ taps is used in a WLAN 802.11a-based MIMO system with a guard interval of $L_{CP} = 16$ [Medbo98], the number of estimated taps must be limited to 16. Figure 4.9 shows the simulation results for this situation. As can be seen, an error floor appears on the channel estimation NMSE curves, since the last taps of the impulse response are not taken into account. This NMSE error floor translates into a BER floor at high SNR, which can be mitigated with coding, as is shown in Figure 4.9b.

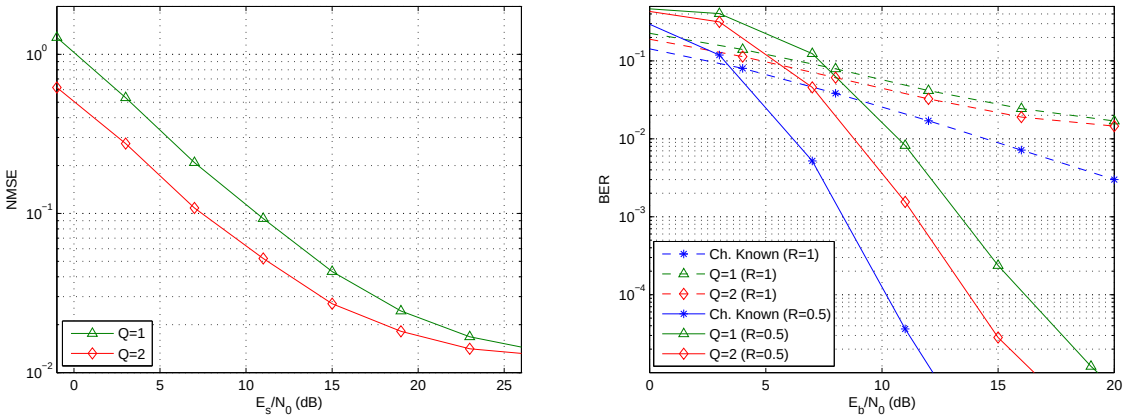

(a) (b)

Figure 4.9: NMSE (a) and BER (b) performance of ML channel estimation for a 4×4 HIPERLAN/2 C channel model ($L = 31$ taps).

The WLAN IEEE 802.11a and IEEE 802.11n standards provide a preamble structure that allows to improve the channel estimation [IEEE99, IEEE07]. As can be seen in Figure

4.10, a double-length symbol is included in the preamble, with a double cyclic prefix. This can simplify the task of estimating channel impulse responses of up to $2L_{CP}$ taps. For instance, Figure 4.11 shows the channel estimation performance when a double-length OFDM preamble is used in a HIPERLAN/2 C channel model of 31 taps. This structure allows to estimate up to 32 taps of the channel impulse response with one double symbol and 2 transmit antennas.

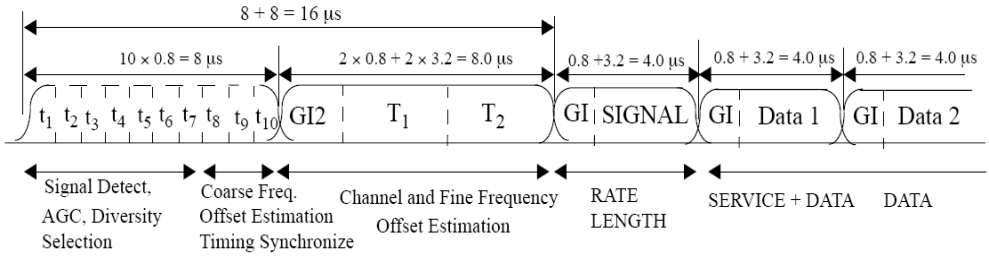

Figure 4.10: Structure of the 802.11a preamble, showing a double-length symbol for channel estimation [IEEE99].

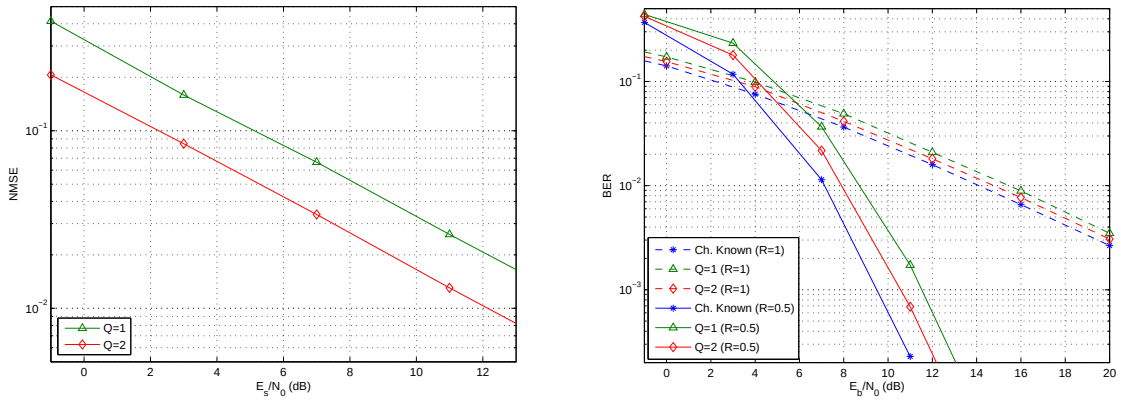

(a) (b)

Figure 4.11: NMSE (a) and BER (b) performance of LS channel estimation for a 2×2 HIPERLAN/2 B channel model ($L = 21$ taps) using the double-length preamble provided by the IEEE 802.11a standard.

The same time-domain channel estimation is shown in [Li99] for a 2×2 STC scheme, though a very different notation is used. A complexity reduction method is proposed based on the estimation of only the most significant taps, which affects directly to the size of the matrix inversion operation [Li99].

4.3.2 Frequency-Domain LS Channel Estimation

The aforementioned channel estimation process can be simplified if it is carried out directly in the frequency-domain. Parting from the narrowband estimation algorithms and preambles, simpler channel estimation schemes can be developed. For example, assuming a 4×4 MIMO-OFDM system, the channel estimation requires 4 subcarriers for each channel estimate. These training symbols can be allocated in subsequent subcarriers and/or OFDM symbols, depending on the frequency and time selectiveness of the channel.

Figure 4.12 shows the structure of two different training sequences which can be used for frequency-domain channel estimation. The first one (a) dedicates each subcarrier to one transmit antenna using frequency-divison multiplexing (FDM), whereas the second one (b) uses 4 subcarriers for 4 channels, applying a frequency-domain code divison multiplexing (CDM) approach. For example, the $\mathbf{S}_T$ blocks shown in Figure 4.12b can be orthogonal Walsh codes, which allow the orthogonality of the transmitted symbol streams. On the other hand, Figure 4.13 shows the structure of a frequency-domain training matrix where the basic training blocks are divided across two consecutive antennas.

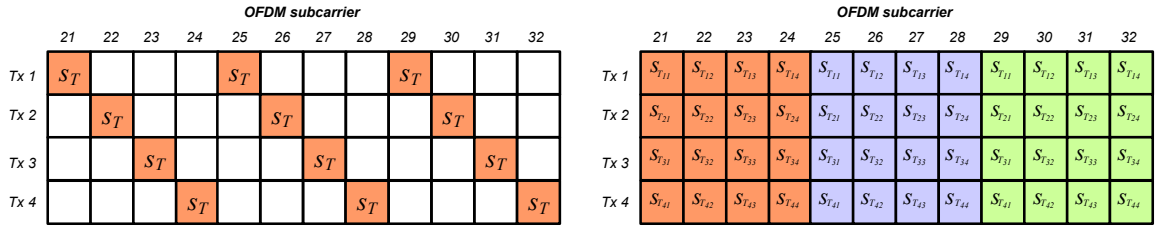

Figure 4.12: Training structures for frequency-domain MIMO-OFDM channel estimation.

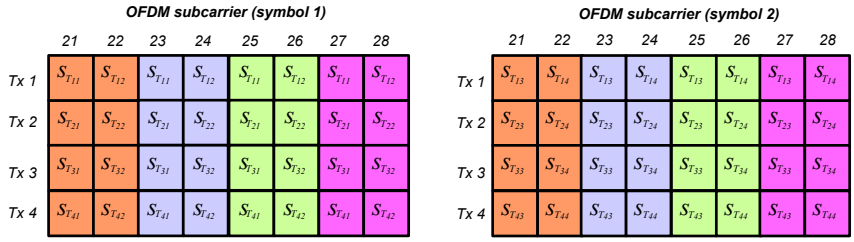

Figure 4.13: Structure of a $4\times N$ MIMO-OFDM preamble with training blocks spread across 2 subcarriers and 2 consecutive OFDM symbols.

Once the channel gain values are estimated for a subset of the subcarriers, they must be interpolated for the rest of subcarriers. This can be done using simple polynomial interpolation techniques [Kim05] or calculating the length-limited temporal channel response through IFFT and FFT operations. A complexity evaluation, based on the number of

required real operations, has been presented in [Krondorf06]. Linear interpolation-based frequency-domain channel estimation is the less resource-demanding technique, while the optimal LS estimation of Section 4.3.1 seems to be the most complex one. On the other hand, the FFT-based interpolation method gives the same NMSE results as the time-domain LS estimation.

Figure 4.14 shows two examples of estimated channel impulse responses using different interpolation methods: FFT-based and linear interpolation. As can be seen, only some of the frequency subcarriers have been used for the estimation of the channel impulse response. Figure 4.14 shows the accuracy of the FFT-based interpolation method, whereas the error of the linear interpolator is remarkable.

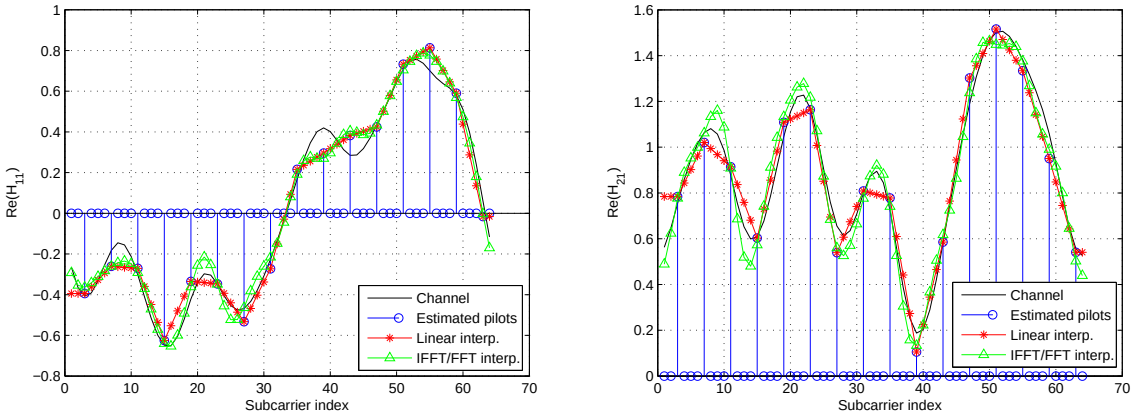

(a) (b)

Figure 4.14: Examples of two channel estimates using FFT-based and linear interpolation schemes.

Figures 4.15a and 4.15b show the NMSE and BER performance curves for the two different interpolation approaches: the FFT-based one (int. 1) and the linear technique (int. 2). As can be seen, the interpolation error, which can be high for the linear interpolation scheme, produces an NMSE error floor and degrades the BER performance. That is the reason why other more sophisticated interpolation methods are commonly used, such as polynomial or spline techniques [Colieri02].

4.3.3 Optimal Training Structures for MIMO-OFDM

As it has been advanced in subsection 4.3.1, an optimal training sequence must fulfill the condition in (4.14) in order to achieve the best NMSE value. The different preamble and pilot structures that can satisfy this optimality condition in LS estimation schemes are summarized in [Barhumi03, Minn06]. The latter divides the optimal training structures into several different categories, depending on the number of symbols transmitted simultaneously

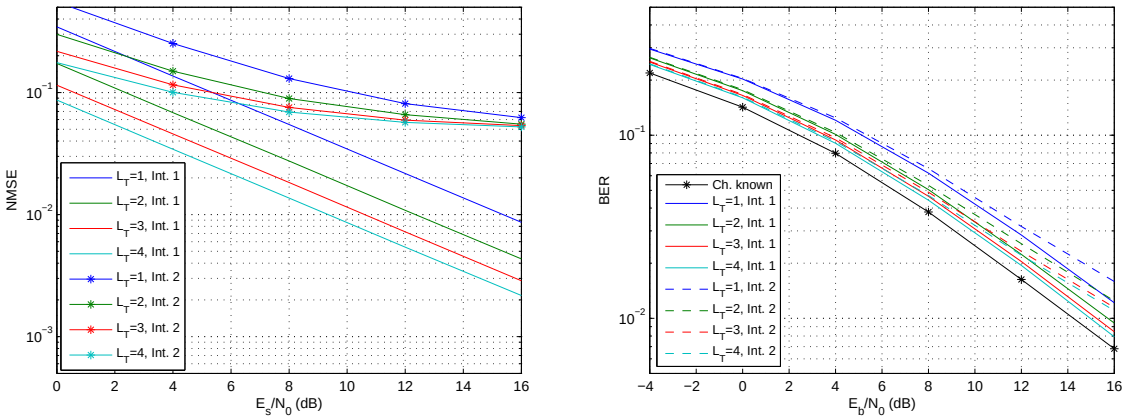

(a) (b)

Figure 4.15: Comparison of the NMSE and BER curves of a 4×4 QPSK MIMO-OFDM system with FFT-based (int. 1) and linear (int. 2) interpolation techniques.

and the number of OFDM symbols:

- **CDM: Code Division Multiplexing**. Orthogonal training sequences are sent across different antennas and subcarriers.
- **FDM: Frequency Division Multiplexing**. Transmission antennas (or blocks of antennas) transmit the pilots at different subcarriers and not simultaneously.
- **F-FDM + C-CDM: Frequency Division Multiplexing**. F Groups of C antennas are transmitted at F different blocks of subcarriers, while code-based orthogonality is used at each group.

Table 4.1 shows examples of optimal training matrices for a system with $T = 8$ subcarriers, $M = 4$ antennas, a channel length of $L = 2$ taps and $Q = 1$ OFDM symbol. As can be seen, a DFT-like matrix has been used in this case to achieve orthogonality between transmission antennas.

Although these training matrices are optimal from an information theoretical point of view, there are two other factors that need to be analyzed for a real implementation:

- PAPR value of the training symbol sequence: For example, if the time-domain sequence associated to the frequency-domain training matrix of Figure 4.12a is analyzed, it can be noticed that most of the symbols have a value of 0. Thus, the PAPR of the signal can be very large, which may degrade the performance of the transmitter [Dardari00, Struhsaker01].
- Transmitted symbols: As has been advanced in the narrowband channel estimation section, once the required matrix is precomputed, a matrix product must be carried

Pilot Allocation	Sub-carrier Index	Ant. 0	Ant. 1	Ant. 2	Ant. 3
CDM(F)	0	α_1	$\alpha_1 e^{j\phi_1}$	$\alpha_1 e^{j\phi_2}$	$\alpha_1 e^{j\phi_3}$
	1	α_2	$\alpha_2 e^{-j\pi/2} e^{j\phi_1}$	$\alpha_2 e^{-j2\pi/2} e^{j\phi_2}$	$\alpha_2 e^{-j3\pi/2} e^{j\phi_3}$
	2	α_3	$\alpha_3 e^{-j2\pi/2} e^{j\phi_1}$	$\alpha_3 e^{-j4\pi/2} e^{j\phi_2}$	$\alpha_3 e^{-j6\pi/2} e^{j\phi_3}$
	3	α_4	$\alpha_4 e^{-j3\pi/2} e^{j\phi_1}$	$\alpha_4 e^{-j6\pi/2} e^{j\phi_2}$	$\alpha_4 e^{-j9\pi/2} e^{j\phi_3}$
	4	α_5	$\alpha_5 e^{-j4\pi/2} e^{j\phi_1}$	$\alpha_5 e^{-j8\pi/2} e^{j\phi_2}$	$\alpha_5 e^{-j12\pi/2} e^{j\phi_3}$
	5	α_6	$\alpha_6 e^{-j5\pi/2} e^{j\phi_1}$	$\alpha_6 e^{-j10\pi/2} e^{j\phi_2}$	$\alpha_6 e^{-j15\pi/2} e^{j\phi_3}$
	6	α_7	$\alpha_7 e^{-j6\pi/2} e^{j\phi_1}$	$\alpha_7 e^{-j12\pi/2} e^{j\phi_2}$	$\alpha_7 e^{-j18\pi/2} e^{j\phi_3}$
	7	α_8	$\alpha_8 e^{-j7\pi/2} e^{j\phi_1}$	$\alpha_8 e^{-j14\pi/2} e^{j\phi_2}$	$\alpha_8 e^{-j21\pi/2} e^{j\phi_3}$
FDM	0	$2\alpha_1$	0	0	0
	1	0	$2\alpha_3$	0	0
	2	0	0	$2\alpha_5$	0
	3	0	0	0	$2\alpha_7$
	4	$2\alpha_2$	0	0	0
	5	0	$2\alpha_4$	0	0
	6	0	0	$2\alpha_6$	0
	7	0	0	0	$2\alpha_8$
2-FDM + 2-CDM(F)	0	$\sqrt{2}\alpha_1$	$\sqrt{2}\alpha_1 e^{j\phi_1}$	0	0
	1	0	0	$\sqrt{2}\alpha_5$	$\sqrt{2}\alpha_5 e^{j\phi_3}$
	2	0	0	$\sqrt{2}\alpha_6$	$-\sqrt{2}\alpha_6 e^{j\phi_3}$
	3	$\sqrt{2}\alpha_2$	$-\sqrt{2}\alpha_2 e^{j\phi_1}$	0	0
	4	$\sqrt{2}\alpha_3$	$\sqrt{2}\alpha_3 e^{j\phi_1}$	0	0
	5	0	0	$\sqrt{2}\alpha_7$	$\sqrt{2}\alpha_7 e^{j\phi_3}$
	6	0	0	$\sqrt{2}\alpha_8$	$-\sqrt{2}\alpha_8 e^{j\phi_3}$
	7	$\sqrt{2}\alpha_4$	$-\sqrt{2}\alpha_4 e^{j\phi_1}$	0	0

Table 4.1: Examples of optimal MIMO-OFDM preambles for $T = 8$ subcarriers, $M = 4$ antennas and a channel length of $L = 2$ taps [Minn06].

out to obtain the channel estimate. This process can be simplified if the symbols in the $\mathbf{S}_T$ matrix are specially designed. For example, if symbols of value ± 1 are only used, all the products required for channel estimation can be eliminated. Obviously, the design of the training symbols must be carefully done to avoid the loss of optimality or a high PAPR.

4.4 Channel Estimation in Iterative MIMO Systems

This section analyzes the most common channel estimation algorithm used in iterative or Turbo-MIMO systems. The iterativo MIMO receiver model of Section 2.5 is extended with a channel estimation block, based on the well-known EM algorithm. The BER performance of this algorithm has been tested by simulations, which are computationally very demanding due to the number of iterations and the complexity of the BCJR algorithm. An extension of the semi-analytical EXIT-based BER prediction tool of [Hermosilla05] has been proposed that allows to predict the BER performance and convergence of iterative MMSE-PIC-based MIMO receivers with channel estimation error.

4.4.1 EM Channel Estimation in Turbo-MIMO Systems

Figure 4.16 shows the structure of the iterative receiver, to which a channel estimation block has been added. As can be seen, the inputs of the channel estimation block are the

training matrix $\mathbf{S}_T$, which is known at the receiver, the received symbol vector $\mathbf{r}(k)$ and soft information from the detected symbols. A basic LS algorithm can be used to get a first channel estimate from the training symbols, which is used at the first iteration. This initial estimate is then updated at every iteration from the soft information fed back from the BCJR decoder. For the sake of simplicity, only the APP LLR metrics of the coded bits $\Lambda_c^D(l_c)$ will be considered for iterative channel estimation, as in [Boutros00, Khalighi05].

Due to the channel estimation error, the MMSE-PIC receiver generates a soft symbol estimate using the channel estimate $\hat{\mathbf{H}}$ instead of the actual value $\mathbf{H}$. Therefore, (2.42) can be rewritten as

$$\mathbf{r}'_m(k) = \mathbf{r}(k) - \sqrt{\frac{E_s}{M}} \sum_{\substack{p=1 \\ p \neq m}}^{M} \hat{\mathbf{h}}_p \tilde{s}_p = \mathbf{r}(k) - \sqrt{\frac{E_s}{M}} [\hat{\mathbf{H}}\tilde{\mathbf{s}}(k) - \hat{\mathbf{h}}_m \tilde{s}_m(k)]. \tag{4.15}$$

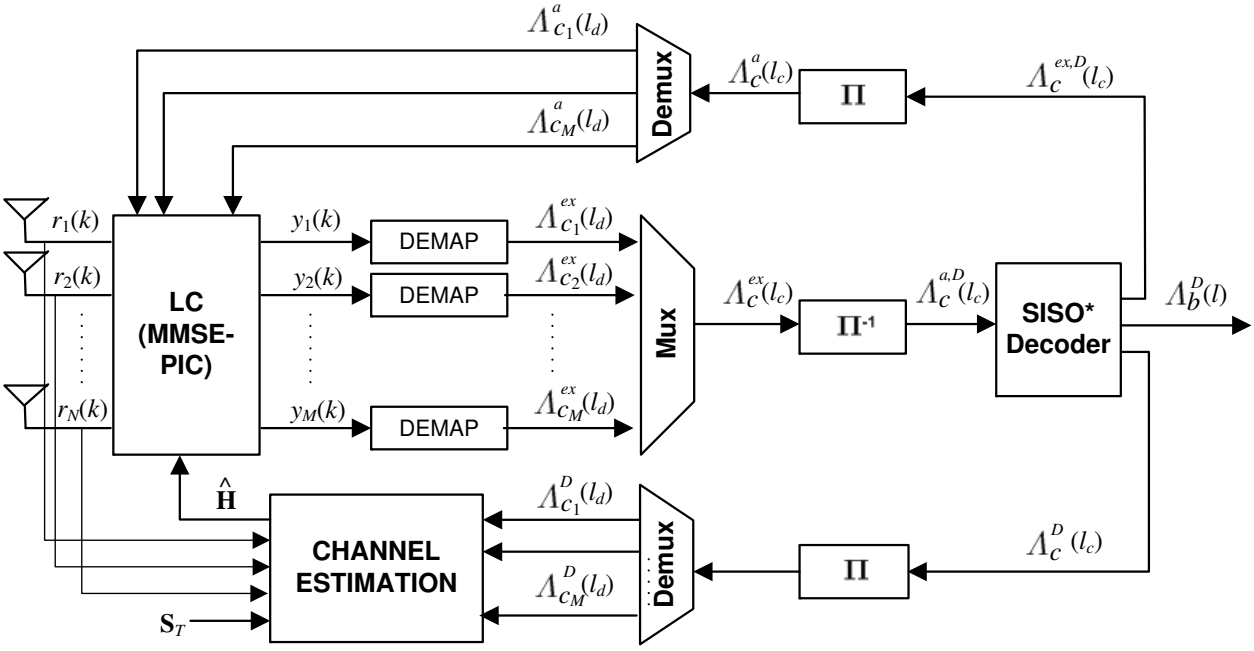

Figure 4.16: Diagram of a generic interference cancellation-based iterative MIMO receiver with channel estimation.

The MMSE combining matrix $\mathbf{w}_m$ in (2.43) is now calculated from the estimated channel matrix $\hat{\mathbf{H}}$ as follows:

$$\mathbf{w}_m = \sqrt{\frac{M}{E_s}} \left(\hat{\mathbf{H}} \bar{\mathbf{V}} \hat{\mathbf{H}}^H + (1 - \bar{v}_m) \hat{\mathbf{h}}_m \hat{\mathbf{h}}_m^H + \frac{N_0 M}{E_s} \mathbf{I}_N \right)^{-1} \hat{\mathbf{h}}_m, \tag{4.16}$$

Training-only based channel estimation techniques do not profit from the iterative nature of turbo receivers. Many algorithms have been developed to re-estimate the channel from hard and soft decision statistics fed back from the SISO* decoder. The classical EM chan-

nel estimation technique [Boutros00, Khalighi05] has been chosen here, where the channel estimate for the $(j+1)$-th iteration is obtained as

$$\hat{\mathbf{H}}^{(j+1)} = \sqrt{\frac{M}{E_s}} \bar{\mathbf{R}}_{rs}^{(j)} \left[\bar{\mathbf{R}}_s^{(j)}\right]^{-1}.$$

If the iteration index j is omitted, the correlation matrices $\bar{\mathbf{R}}_{rs}^{(j)}$ and $\bar{\mathbf{R}}_s^{(j)}$ can be expressed as

$$\bar{\mathbf{R}}_{rs} = \sum_{k=1}^{K} \mathbf{r}(k)\bar{\mathbf{s}}^H(k) = \sqrt{\frac{E_s}{M}}\mathbf{H}\mathbf{R}'_s + \theta,$$

$$\bar{\mathbf{R}}_s(i,j) = \begin{cases} K & ;\ i = j \\ \sum_{k=1}^{K} \bar{\mathbf{s}}_i(k)\bar{\mathbf{s}}_j^*(k) & ;\ i \neq j \end{cases} \tag{4.17}$$

and

$$\mathbf{R}'_s = \sum_{k=1}^{K} \mathbf{s}(k)\bar{\mathbf{s}}^H(k)\ ,\ \theta = \sum_{k=1}^{K} \mathbf{n}(k)\bar{\mathbf{s}}^H(k), \tag{4.18}$$

where vector $\bar{\mathbf{s}}(k)$ contains the soft symbol estimates obtained from the APP LLRs fed back to the channel estimation block [Tüchler02], while θ is the matrix of weighted noise samples with autocovariance $\mathbf{R}_\theta = \rho M \mathbf{R}''_s$, where

$$\mathbf{R}''_s = \sum_{k=1}^{K} \bar{\mathbf{s}}(k)\bar{\mathbf{s}}^H(k). \tag{4.19}$$

The estimated channel $\hat{\mathbf{H}}$ is a biased estimate of $\mathbf{H}$ and can be written as [Khalighi05]:

$$\hat{\mathbf{H}} = \mathbf{H}\mathbf{R}'_s\bar{\mathbf{R}}_s^{-1} + \theta\bar{\mathbf{R}}_s^{-1}. \tag{4.20}$$

4.4.2 Analytical EXIT Functions with Channel Estimation Errors

The EXIT transfer function-based performance evaluation of Section 2.5.4 has been adapted to a more realistic system where the channel must be estimated using pilots and iterative approaches. The approach introduced in [Hermosilla05] divides a generic receiver into two elementary blocks, an LC and a non-linear demapper. Since channel estimation has been included, the FE (the MIMO detector) must be now decomposed into three elementary devices: the MMSE-PIC linear combiner, the non-linear demapper and the channel estimation block.

Only one of the EXIT transfer functions of Section 2.5.4, F_m, needs to be changed if channel estimation error is included in the analysis method. Function F_m, which establishes the relationship between the input mutual information and the output SINR value Γ_m at

the output of the MMSE-PIC receiver, can be now expressed as

$$\Gamma_m = F_m(I_{in}^R; \mathbf{H}, \rho, \tilde{\mathbf{H}}), \tag{4.21}$$

where $\tilde{\mathbf{H}} = \mathbf{H} - \hat{\mathbf{H}}$ is the channel estimation error matrix. These variables will be generated for each channel realization by the channel estimation block, whose generation function H_{est} can be represented for the j-th iteration as:

$$\hat{\mathbf{H}}^{(j)} = H_{est}(\mathbf{H}, \rho, \mathbf{S}_T, I_{in}^{R,(j)}), \tag{4.22}$$

where $I_{in}^{R,(j)}$ is the input MI at the jth iteration. Hence, the randomly generated channel estimate depends on the channel state, the noise, the transmitted training sequence and the mutual information statistics fed back from the decoder, if iterative channel estimation is used.

Therefore, the transfer function F_m has been recalculated for a deterministic channel $\mathbf{H}$ with an also deterministic channel estimation error $\tilde{\mathbf{H}}$. The output SINR Γ_m at the mth branch of a generic MMSE receiver can be defined as [Paulraj03]:

$$\Gamma_m = \frac{E\{s_m s_m^H\}}{tr(E\{e_m e_m^H\})} - 1 = \frac{1}{E\{e_m e_m^H\}} - 1, \tag{4.23}$$

where $e_m = s_m - y_m$. Parting from (2.42-2.43) and omitting the symbol index k, e_m can be written as:

$$\begin{aligned} e_m &= s_m - \mathbf{w}_m^H \left(\sqrt{\frac{E_s}{M}} \mathbf{h}_m s_m + \sqrt{\frac{E_s}{M}} \sum_{\substack{p=1 \\ p \neq m}}^{M} \mathbf{h}_p s_p - \sqrt{\frac{E_s}{M}} \sum_{\substack{p=1 \\ p \neq m}}^{M} \hat{\mathbf{h}}_p \tilde{s}_p + n \right) \\ &= s_m - \sqrt{\frac{E_s}{M}} \mathbf{w}_m^H \left(\mathbf{h}_m s_m + \sum_{\substack{p=1 \\ p \neq m}}^{M} \mathbf{h}_p (s_p - \tilde{s}_p) + \sum_{\substack{p=1 \\ p \neq m}}^{M} \tilde{\mathbf{h}}_p \tilde{s}_p + \sqrt{\frac{M}{E_s}} n \right), \end{aligned}$$

where $\tilde{\mathbf{h}}_m$ is the mth column of the channel estimation error matrix $\tilde{\mathbf{H}}$. Assuming $E\{s_m s_m^H\} = 1$, $E\{(s_m - \tilde{s}_m)(s_m - \tilde{s}_m)^H\} = v_m$ and $E\{(\tilde{s}_m \tilde{s}_m^H)\} = E\{(s_m \tilde{s}_m^H)\} = 1 - v_m$, the error variance can be expressed as

$$E\{e_m e_m^H\} = 1 - \sqrt{\frac{E_s}{M}} \mathbf{w}_m^H \mathbf{h}_m - \sqrt{\frac{E_s}{M}} \mathbf{h}_m^H \mathbf{w}_m + \frac{E_s}{M} \mathbf{w}_m^H \mathbf{R}_{rr} \mathbf{w}_m,$$

where

$$\mathbf{R}_{rr} = \mathbf{h}_m \mathbf{h}_m^H + \frac{M}{\rho}\mathbf{I}_M + \sum_{\substack{p=1 \\ p\neq m}}^{M} \mathbf{h}_p v_p \mathbf{h}_p^H + \underbrace{\sum_{\substack{p=1 \\ p\neq m}}^{M} \tilde{\mathbf{h}}_p (1-v_p) \tilde{\mathbf{h}}_p^H}_{\mathbf{T}} . \tag{4.24}$$

As can be seen, the effect of the wrong channel estimate is twofold: the combining vector $\mathbf{w}_m^H$ is not matched to the actual channel $\mathbf{H}$ and a new error term $\mathbf{T}$ appears in (4.24) due to the wrong cancellation of detected symbols.

4.4.2.1 Adaptation of the Performance Evaluation Algorithm

The performance evaluation algorithm of [Hermosilla05] can be extended to Rayleigh-fading iterative receivers with channel estimation, independently of the estimation technique, as is shown in Table 4.2. As can be seen, a new step has been included, numbered as (3), where a new channel estimate is generated for each channel realization and turbo iteration. The rest of the algorithm works as detailed in [Hermosilla05], transferring MI values between the MIMO detector and the outer soft decoder.

Performance Evaluation Algorithm
(0) Generate $\mathbf{H}$.
(1) Initialization: iteration $j = 1$; $I_{out}^{D,(0)} = 0$.
(2) Get FE input MI. $I_{in}^{R,(j)} = I_{out}^{D,(j-1)}$.
(3) Generate estimate $\hat{\mathbf{H}}^{(j)} = H_{est}(\mathbf{H}, \rho, \mathbf{S}_T, I_{in}^{R,(j)})$.
(4) Compute $\bar{\mathbf{V}}$ from $I_{in}^{R,(j)}$, as in [Hermosilla05].
(5) Calculate $\mathbf{w}_m$ vectors from (2.44) and Γ_m values from (4.23).
(6) Compute $I_{out,m}^{R,(j)}$ and $I_{out}^{R,(j)}$ via (2.46) and (2.47).
(7) Obtain the decoder's output $I_{out}^{D,(j)} = f^D(I_{out}^{R,(j)})$.
(8) Calculate $BER^{(j)} = f_{BER}(I_{out}^{D,(j)})$.
(9) Return to step (2) with $j = j + 1$.

Table 4.2: BER performance evaluation algorithm for each channel realization of an iterative MIMO receiver with channel estimation.

4.4.3 Channel Estimation Error Models

Function $H_{est}(\mathbf{H}, \rho, \mathbf{S}_T, I_{in}^R)$ calculates a channel estimate for each channel realization based on the information fed back from the decoder as APP LLRs and the statistics of the training process. Two classical channel estimation techniques will be considered in this section for the analysis of this function: training-based LS and soft decision-directed EM.

4.4.3.1 Training-Based LS Channel Estimation

If a training symbol matrix $\mathbf{S}_T$ of dimensions $M \times L_T$ is sent before data transmission and the LS channel estimator of Equation (4.1) is applied, the estimation error is uncorrelated among the N receivers and can be easily modelled as a zero-mean Gaussian variable with variance equal to the NMSE value in (4.4).

The estimate generation function $H_{est}^{(1)}(\mathbf{H}, \rho, \mathbf{S}_T)$, which does not depend on I_{in}^{R} if only training symbols are used, must then create a channel estimate $\hat{\mathbf{H}}$ according to the aforementioned statistics for each channel realization.

4.4.3.2 Iterative EM Channel Estimation

The estimation function $H_{est}(\mathbf{H}, \rho, \mathbf{S}_T, I_{in}^{(j,R)})$ must generate an estimate $H^{(j)}$ for all the iterations $j > 1$ according to (4.20), while the training-based function $H_{est}^{(1)}(\mathbf{H}, \rho, \mathbf{S}_T)$ is used at the first iteration. Thus, the matrices in (4.17-4.19) must be calculated from the output statistics of the decoder in order to model the channel estimation error. A very simple approach has been followed which calculates the aforementioned matrices according to the following approximations:

$$\hat{\bar{\mathbf{R}}}_s(i,k) = \begin{cases} N_s & ;\ i = k \\ N_s(1-\sigma_p)\mathbf{w}_i^H \mathbf{h}_k \mathbf{h}_k^H \mathbf{w}_i & ;\ i \neq k \end{cases} \tag{4.25}$$

$$\hat{\mathbf{R}}'_s(i,k) = \begin{cases} N_s\sigma_p & ;\ i = k \\ N_s(1-\sigma_p)\mathbf{h}_k^H \mathbf{w}_i & ;\ i \neq k \end{cases} \tag{4.26}$$

$$\hat{\mathbf{R}}''_s(i,k) = \begin{cases} N_s\sigma_p & ;\ i = k \\ N_s(1-\sigma_p)\mathbf{w}_i^H \mathbf{h}_k \mathbf{h}_k^H \mathbf{w}_i & ;\ i \neq k\ . \end{cases} \tag{4.27}$$

The value of $\sigma_p = E\{\bar{\mathbf{s}}_m \bar{\mathbf{s}}_m^H\}$ has been calculated off-line for each constellation alphabet when generating the EXIT transfer function of the decoder. The approximations in (4.25-4.27) have been tested for QPSK modulation with several different channel realizations.

4.4.4 Simulation Results

A system with $M = 4$ and $N = 4$ antennas has been chosen to validate the performance evaluation method. Simulations with QPSK modulation have been conducted to compare the classical MC simulations and the EXIT-based analytical performance evaluation method with channel estimation error. Up to 10000 data blocks of 2048 coded bits have been simulated with a quasi-static Rayleigh-fading MIMO channel. Walsh codes of 4×8 and 4×16 symbols have been sent as training symbols and perfect timing and demodulation have been

assumed at the receiver. A non-recursive non-systematic convolutional code with generator polynomials $\{5, 7\}_8$ and the common log-map implementation of the BCJR algorithm have been selected for FEC encoding and decoding, respectively, with a random interleaver.

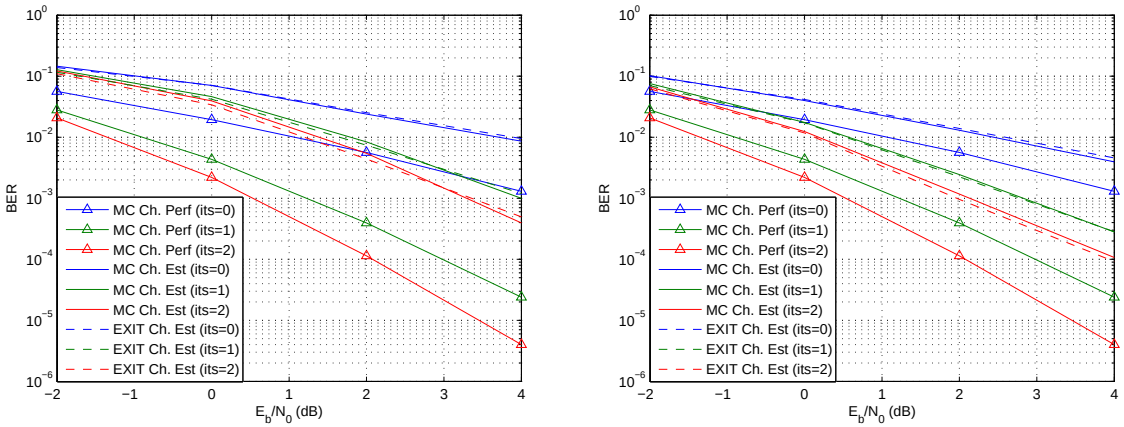

(a) (b)

Figure 4.17: Comparison of EXIT fuction-based and MC simulation results for LS channel estimation with a training length of $L_T = 8$ (a) and $L_T = 16$ (b).

Figure 4.17a shows the BER comparison of EXIT and MC techniques for the iterative MMSE-PIC receiver with LS channel estimation and a 4×8 training matrix. As can be seen, the EXIT-based analysis gives slightly optimistic and quite accurate results for training-based channel estimation. The results of MC simulation with perfect channel estimation have been included in the figures as a reference. Figure 4.17b shows the same comparison for a 4×16 training matrix with similar results.

Figure 4.18 extends the comparison to EM-based channel estimation using the techniques and simplifications of section 4.3. The BER estimation accuracy of the models is shown for a system with iterative channel estimation and an initial training matrix of dimensions 4×8. These results show that this method and the assumed simplifications can be used to estimate or predict the BER performance of iterative receivers with channel estimation. For the case of EM channel estimation, further analysis is required to extend the aforementioned assumptions to other modulations and MIMO detectors.

4.5 Chapter Summary

This chapter has described the most fundamental channel estimation algorithms that can be applied to the MIMO systems described in Chapter 2. Since a feasible MIMO implementation is on the scope of this research, simple and effective narrowband algorithms have been first considered, such as training-based LS and LMMSE, iterative approaches or simple second and higher order statistics-based methods that can be applied to spatial multiplexing scenarios.

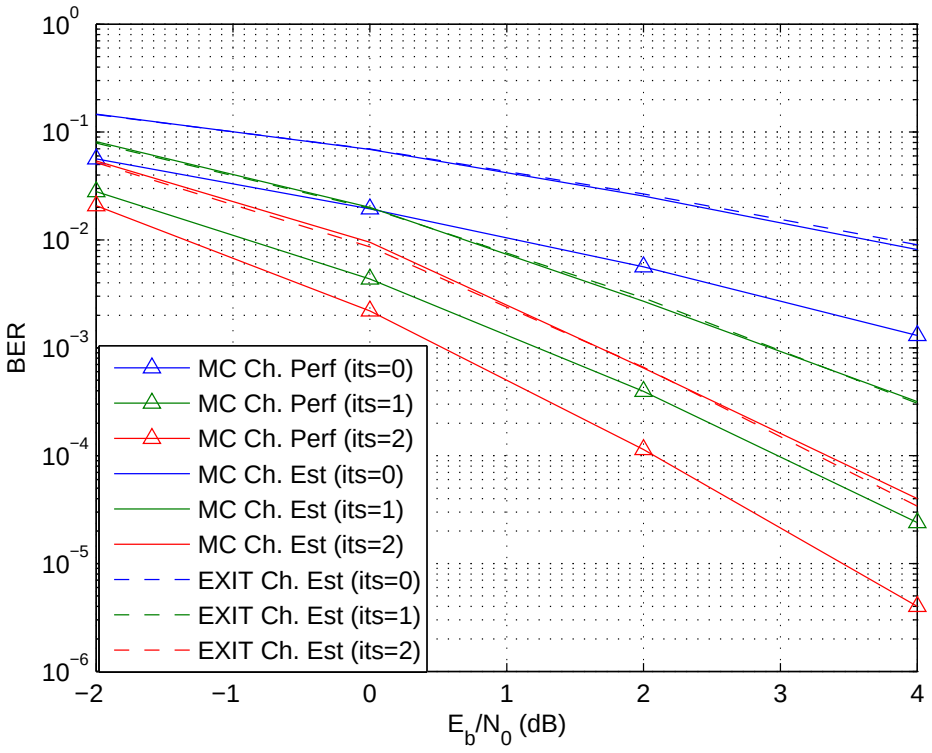

Figure 4.18: Comparison of EXIT fuction-based and MC simulation with soft decision-directed EM channel estimation and an initial 4×8 training matrix.

The narrowband channel estimation techniques have been extended to wideband scenarios based on OFDM and SC-FDE. The optimal time-domain ML-LS has been analyzed, showing its performance in several different scenarios. More simple frequency-domain estimation techniques have also been evaluated, analyzing the effects of different training structures and interpolation schemes.

Finally, iterative channel estimation has been analyzed for turbo-MIMO receivers using a widely-spread EM algorithm. As an interesting contribution of this chapter, the analytical EXIT functions-based performance prediction tools of [Hermosilla05] have been extended to systems with channel estimation errors.

Chapter 5

Impact of Channel Estimation on the Performance of MIMO Detectors

5.1 Introduction

This chapter focuses on the analysis of the impact of channel estimation on the performance of MIMO receivers. The effects of channel estimation error and hardware implementation impairments are analyzed for the MIMO detectors described in previous chapters. Section 5.2 describes the two scenarios that have been considered. First, the real-time 2×2 MIMO system of Sections 3.6 and 3.7 has been used in order to evaluate the BER performance degradation due to practical channel estimation issues. A more flexible testbed has then been designed in Simulink to allow co-simulation of Matlab code and a realistic System Generator-based implementation of some of the algorithms.

Section 5.3 analyzes the impact of channel estimation and implementation on the performance of two fundamental narrowband MIMO receivers based on the optimal (SD) and the most simple (ZF) detectors. Their performance is evaluated under realistic implementation conditions such as limited bits of resolution, imperfect channel estimation, synchronization failure and error propagation through the hardware.

On the other hand, the effects of channel estimation are also analyzed by simulations for more complex MIMO systems such as MIMO-OFDM and MIMO-SCFDE in Section 5.4. Finally, a parallel decision-directed channel estimation architecture is proposed in Section 5.5 which allows a semi-iterative channel estimation with improved BER performance and low latency.

5.2 Scenarios for the Analysis of Channel Estimation Implementation

Two scenarios have been considered to evaluate the effects of channel estimation on the performance of MIMO receivers. First, the full 2×2 MIMO system of Section 3.6 has been

considered, where the impact of channel estimation on the overall performance of a realistic MIMO scheme can be evaluated. This validation scenario has two main drawbacks: it has been designed for 2×2 narrowband transmissions, due to time and resource limitations, and its flexibility is very limited, since the cost of redesigning and validating some of its parts is prohibitive.

Therefore, this platform has only been used for the main narrowband results shown in this chapter. However, a new scenario has also been developed to evaluate channel implementation effects in more complex systems, such as wideband MIMO or systems with a larger number of antennas.

5.2.1 LS Estimator in Fully Implemented MIMO Scenario

As it has been stated in Section 3.6, a full 2×2 MIMO system has been developed and validated using System Generator for DSP. Two receivers have been implemented as reference cases: ZF and SD, the simplest and the most efficient, respectively. Although the MIMO system is composed by many different algorithms, this chapter will focuses on channel estimation and its effects on the performance of the whole receiver or the most critical of its parts, i.e., the MIMO detector.

Figure 5.1 depicts the first blocks of the implemented receiver. The input signals are received at two separate antennas, downconverted to baseband by means of two synchronous front-ends, filtered and processed by the synchronization blocks. Two main synchronization algorithms are carried out: the coarse frame detection, which detects the start of a valid burst using a known sequence of symbols [Heiskala02], and the symbol-time synchronization, which detects the best instant for downsampling [Naguib98]. Once the information symbols are synchronized and downsampled, they are processed by the channel estimation block, which estimates the channel using the received symbol matrix $\mathbf{R}_T$ and the known training matrix $\mathbf{S}_T$.

In the 2×2 scenario described in this section, the symbol-time synchronization and the channel estimation algorithms have been carried out together, thanks to the structure of the synchronization algorithm proposed for narrowband MIMO transmissions in [Naguib98]. The symbol-time sampling instant is chosen in order to maximize the overall received gain for a known transmitted training matrix $\mathbf{S}_T$. For instance, if an oversampling factor of 8 is assumed, the received sequence is sampled at 8 different delays, choosing the one with the highest gain.

In the 2×2 implementation of Section 3.6 this synchronization process, which is closely related to channel estimation, has been implemented calculating up to 24 delayed channel estimates. The output of this process is twofold: On one hand, the best sampling instant is chosen for downsampling. On the other hand, the LS channel estimate is obtained as a subproduct of the synchronization process [Naguib98]. Note that this implementation

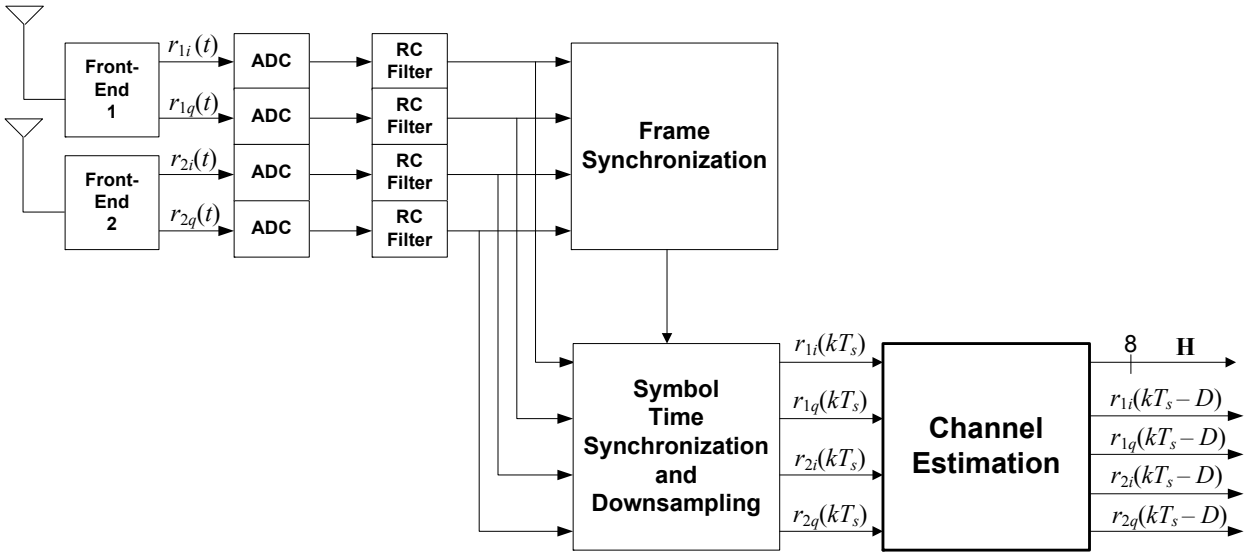

Figure 5.1: First blocks of the MIMO receiver, including frame detection, symbol-time synchronization and channel estimation.

is useful only for narrowband MIMO transmissions and needs to be redesigned for other systems [Heiskala02].

The implemented channel estimator is identical to the LS channel estimation algorithm of Section 4.2.1.1 in terms of NMSE and BER performance. Since the training matrix is known, the inversion (or pseudoinversion) of the matrix can be computed off-line. Furthermore, if the training matrix is chosen to be based on BPSK-modulated Walsh codes, the matrix product can be reduced to a set of simple addition or substraction operations. For instance, if the following training matrix of length $L_T = 8$ is assumed

$$\mathbf{S}_T = \begin{bmatrix} 1 & -1 & 1 & -1 & 1 & -1 & 1 & -1 \\ 1 & 1 & -1 & -1 & 1 & 1 & -1 & -1 \\ 1 & -1 & -1 & 1 & 1 & -1 & -1 & 1 \\ 1 & 1 & 1 & 1 & -1 & -1 & -1 & -1 \end{bmatrix}, \tag{5.1}$$

its pseudoinverse, which is the matrix to be multiplied by the received symbol matrix $\mathbf{R}_T$, becomes

$$\mathbf{S}_T^{\dagger} = \frac{1}{8}\begin{bmatrix} 1 & 1 & 1 & 1 \\ -1 & 1 & -1 & 1 \\ 1 & -1 & 1 & -1 \\ -1 & -1 & 1 & 1 \\ 1 & 1 & 1 & -1 \\ -1 & 1 & -1 & -1 \\ 1 & -1 & -1 & -1 \\ -1 & -1 & 1 & -1 \end{bmatrix}. \tag{5.2}$$

The fact that all the numbers in the $\mathbf{S}_T^{\dagger}$ matrix are +1 or -1 eases the implementation of the channel estimator, reducing the number of operations to $2MNL_T$ additions or subtractions, since the $\mathbf{R}_T$ matrix is a complex matrix. Hence, the Walsh structure also avoids the multiplication of two complex matrices. The implementation of the synchronizer-estimator has been developed so that it generates the estimate $\hat{\mathbf{H}}$ after the last training symbol is received, processing the symbol sequence while it is being received.

Figure 5.2 shows the structure of the implemented narrowband channel estimator, where the two most remarkable elements are the following: the tapped delay line, corresponding to the oversampling of the inputs for the synchronization block, and the matrix multiplication, implemented as a set of addition and subtraction operations.

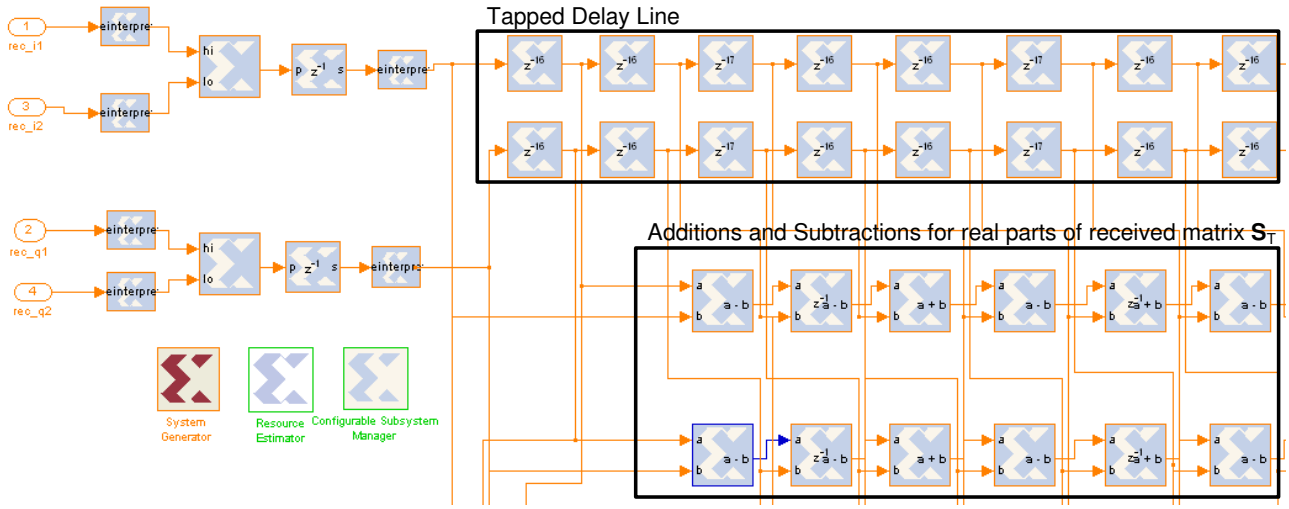

Figure 5.2: Structure of the implemented LS channel estimator.

An oversampling ratio of 8 and a training length of $L_T = 16$ have been chosen for the implementation shown in Figure 5.2. If an addition block is used per each operation, this may require up to $2MNL_T = 128$ adders. If the symbol frequency is not too high, the adder/subtracter sets can be reused for different reception antennas, since the operations to be carried out are the same. In the example of Figure 5.2, two input sequences have

been processed by each of the adder/subtracter sets, thus reducing the number of required adders to 64. From a channel estimation implementation point of view, the accuracy of the estimates can only be degraded by the quantization at the input and the resolution of addition/subtraction operations, which are usually limited to avoid high resource occupation.

5.2.2 Flexible Matlab-Based Channel Estimator Implementation Evaluation

Although the evaluation of realistic estimation algorithms in fully-implemented MIMO systems has been one of the major objectives of this research work, another Simulink-based simulation environment has been designed to extend the results obtained in the 2×2 narrowband hardware platform to other interesting scenarios. The designed testbench, where only some of the algorithms are implemented using System Generator, has helped to develop the full aplication, as well as to evaluate parts of the implementation in a full Matlab scenario.

Figure 5.3 shows the simulation testbed designed to combine a realistic System Generator design of channel estimation algorithms and the flexible Matlab MIMO simulator that has been used for the simulation results shown in all the previous chapters. As it can be observed in Figure 5.3, two are the main elements of the simulator: the Matlab simulation code, which has been transformed into a Simulink s-function block, and the System Generator design that contains the algorithms that have been implemented on the FPGA device.

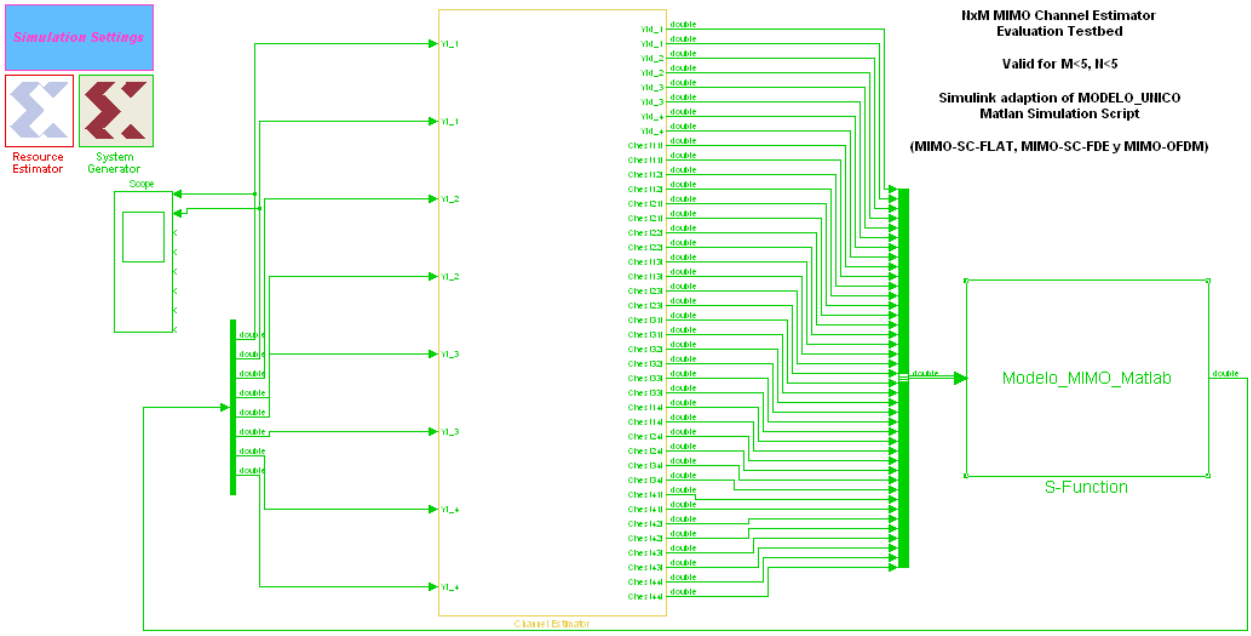

Figure 5.3: Matlab/Simulink-based channel estimation evaluation testbed.

All the system is controlled by the Matlab s-function block, which has the following

functions:

1. Configuration of the system parameters using a flexible table to program the E_b/N_0 range, the number of MC iterations, the QAM constellation, the number of antennas, the coding rate or the MIMO detection scheme.
2. Generation and coding (if required) of information bits.
3. Symbol multiplexing and mapping.
4. Channel convolution and AWGN addition.
5. Generation of the received samples which are transferred to the channel estimation block.
6. Reception of data from the channel estimator block, including the channel estimate and the received symbol stream, which can be quantized and delayed by the channel estimator in order to emulate a real implementation.
7. MIMO detection, demapping, decoding and demultiplexing.
8. BER and NMSE calculation.

This system can be used to analyze partial System Generator implementations in a flexible Matlab model which includes all the fundamental MIMO systems described in the previous chapters, such as MIMO-OFDM, MIMO-SCFDE or turbo-MIMO receivers. This testbed and the aforementioned full 2×2 transmission system have been the scenarios for the results shown in the following sections of this chapter.

5.3 Narrowband MIMO Channels

This section evaluates the performance of real MIMO receivers in a fully implemented scenario for the optimal SD and the low-complexity ZF receiver. These results are then extended to more complex systems, such as 4×4 and 4×6 antenna setups with coded and uncoded transmission, using the Matlab-based simulator of Section 5.2.2.

5.3.1 Evaluation of Channel Estimation on the Real-Time MIMO Platform

This subsection analyzes the effects of a realistic channel estimation algorithm and hardware implementation on the performance of a fundamental real-time 2×2 system with ZF and optimal ML (SD) detection techniques. The LS channel estimator shown in Section 5.2.1

has been used with a training length of $L_T = 16$ and BPSK-modulated Walsh codes. Note that the length of the training sequence is largely greater than the minimum ($L_T = M = 2$), so that a good channel estimation accuracy is expected.

5.3.1.1 Zero-Forcing Receiver

The basic ZF detector in (4.6) requires the multiplication of the received vector by the inverse (or pseudoinverse) of the channel estimate. Therefore, the main operations needed for its implementation are the estimation of the channel matrix, the calculation of its pseudoinverse and a matrix product. All these operations and the quantization of the signals induce an error-floor at high SNR values [Burg06]. For the case of the ZF receiver, whose performance is relatively poor, this error floor arises at very high SNR values.

Figure 5.4 shows the BER performance curves for two different cases. The first one is based on real results from the hardware platform, whereas the second one uses simulation results for comparison purposes. Two curves are shown for each setup: one with the perfect knowledge of the channel and the other one using the LS channel estimator of Section 5.2.1. As it has been stated in Chapter 4, the channel estimation error induces a E_b/N_0 shift for the simulated cases, which is small (1 dB) in this case due to the amount of training symbols ($L_T = 16$). If the hardware-related curves are analyzed, it can be observed that the degradation due to implementation issues is smaller than the error induced by channel estimation, specially for low SNR values. However, the effects of implementation tend to be more important at high SNR due to the aforementioned error floor.

If channel estimation is added to the hardware-implemented ZF receiver, it can be seen that its degradation is slightly smaller than for the simulated case. Therefore, it can be stated that channel estimation plays an important role for low-performance receivers such as the ZF detector. On the other hand, the implementation of the algorithms is less critical, since their effect can only be noticed at very high SNR values. Note that this conclusions have been drawn with a very good channel estimation quality ($L_T = 16$ for $M = 2$), showing the impact of channel estimation on the overall receiver performance.

5.3.1.2 Optimal Sphere Decoder-Based MIMO System

Thanks to a collaboration project with the University of Edinburgh, the effects of imperfect channel estimation and other hardware-related aspects have been evaluated for an optimal ML detector, implemented using the SD algorithm, in the real-time MIMO platform of Section 5.2.1. The implementation has been limited to a 2×2 16-QAM transmission scheme, where the optimal MIMO decoder must choose a solution among $16^2 = 256$ candidates.

As has been already stated, two are the main implementation aspects that degrade the performance of the receiver: on one hand, the quantization of the received samples, which

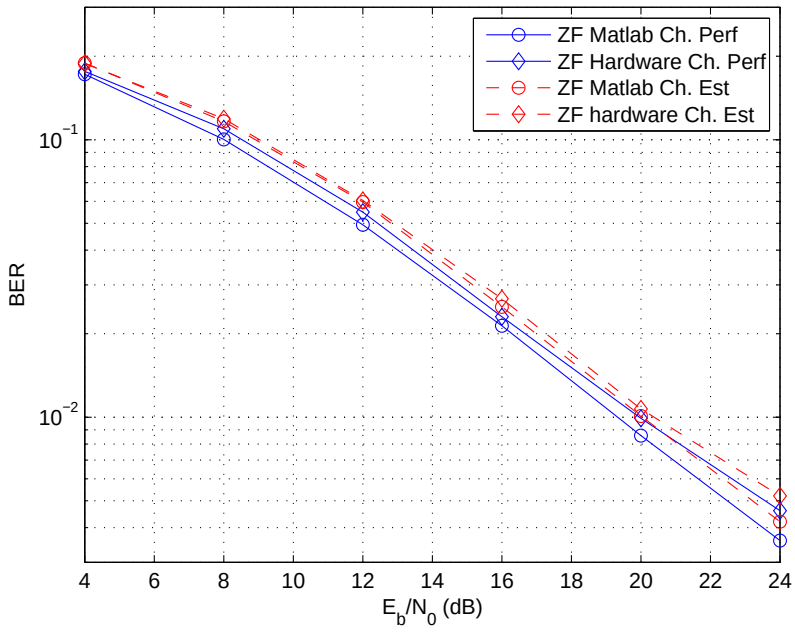

Figure 5.4: BER degradation of the ZF algorithm due to channel estimation and implementation effects.

have been digitalized to 12 bits of resolution; on the other hand, the hardware-limited implementation of the signal processing algorithms, which can generate errors that are propagated through the rest of the system.

Since the SD is an optimal receiver that achieves the same performance as ML, the results for both techniques must be the same with channel estimation and implementation errors, assuming the inputs are the same and the metrics are calculated identically. The main effects of implementation issues are the degradation of detection SINR and a higher deviation at the calculation of the initial search point, which is usually obtained by performing a ZF operation on the received vector [Hochwald03]. As it is well known, ZF enhances the effects of noise and errors, which increase the number of iterations required to obtain the ML solution, hence reducing the maximum achievable throughput of the system.

Figure 5.5 shows the effects of channel estimation and implementation issues on the performance and achievable throughput of the implemented SD receiver. As it is shown, the effects of imperfect channel estimation are one of the main degradation sources of the SD algorithm. This result is quite significative, since a training length of $L_T = 16$ symbols has been used in this implementation, which results on a quite accurate estimate of the channel.

If the BER curve of Figure 5.5a is analyzed, the error floor induced by the implementation-related issues can be noticed. Due to the good performance of the SD algorithm, this error floor is more remarkable, being its importance comparable to that produced by channel estimation for large SNR values. On the other hand, Figure 5.5.b shows the achievable throughput of the SD, whose maximum is degraded from 30 to 28 Mbps. As it can be

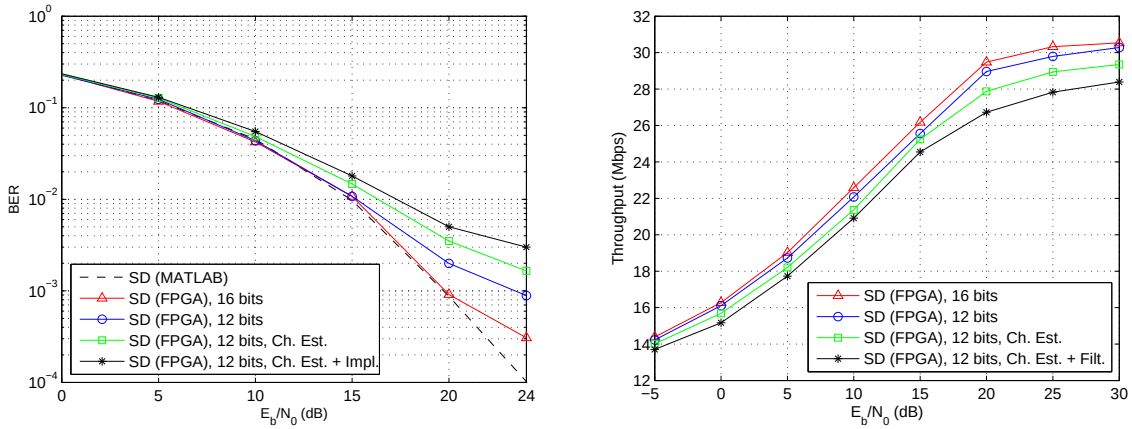

(a) (b)

Figure 5.5: Effects of channel estimation and realistic implementation on the BER performance (a) and achievable throughput (b) of a complete SD-based MIMO system.

observed, the main throughput degradation is due to implementation effects, while the impact of imperfect channel estimation is still remarkable. Therefore, it can be concluded that high-performance algorithms are prone to show error floors at lower SNR values, being more sensitive to implementation aspects, whereas channel estimation plays a more important role in algorithms with lower performance.

5.3.2 Simulation-Based Evaluation

MIMO channel estimation and detection, as well as the implementation aspects of the latter, have been widely analyzed in the literature [Hassibi00, Zelst04, Burg06]. Nevertheless, these studies have been isolated and an overall analysis of their combination is missing. Channel estimators are usually evaluated only using MC simulations, comparing the NMSE of the channel estimates or theoretical Cramer-Rao bounds. On the other hand, the performance of MIMO detectors is compared based on the perfect knowledge of the channel. Therefore, a comparison of MIMO detectors with different channel estimation accuracies may be interesting in order to design an efficient and balanced receiver.

Complex joint estimation and detection schemes exist, but are not prone to be implemented in real systems [Grant00a, Zhu03a]. Assuming that a low-complexity realistic system is composed of separated channel estimation and detection blocks, an in-deep evaluation of their combinations can help to understand the overall complexity and performance issues of the receiver. For instance, the use of a longer preamble or the implementation of a simple iterative channel estimator can make an MMSE-V-BLAST receiver outperform an optimal SD with low-quality channel state information (CSI).

This section shows simulation-based BER performance curves for several fundamental

MIMO receivers with different channel estimation error levels, which can be generated changing the amount of training symbols. In order to simplify the number of simulations and results, the following parameters have been considered:

- Modulation order: QPSK and 16-QAM.
- Antenna setup and MIMO scheme: spatial multiplexing with 4×4 and 4×6 (increased reception diversity) antenna setups.
- Coding: no coding and rate-1/2 convolutional coding with hard Viterbi decoder, as stated in the IEEE 802.11a standard [IEEE99].
- MIMO detectors: ZF, MMSE, ZF-V-BLAST, MMSE-V-BLAST and ML (SD).
- Channel estimation: LS with $L_T = M = 4$ (minimum) and $L_T = 3M = 12$, whose NMSE is related to the SNR value ρ following Equation (4.4).

5.3.2.1 Uncoded 4 x 4 System

Figure 5.6a shows the performance of the previously detailed MIMO detectors for an uncoded 4×4 spatial multiplexing system with QPSK modulation. Two different training lengths of $L_T = 4$ (solid lines) and $L_T = 12$ (dashed lines) have been selected in order to represent two different channel estimation effort levels. The NMSE gap between these two estimation levels can be easily covered using simple semi-blind approaches or extending the training length, which may not be possible in many systems. As it can be observed, all the receivers are affected almost equally (2 dB shift) by the difference in channel estimation quality.

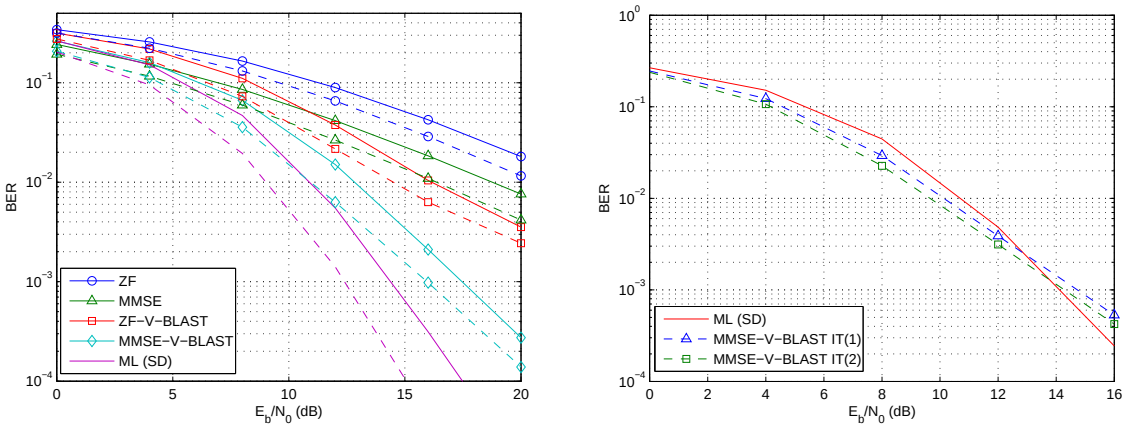

(a) (b)

Figure 5.6: a) BER performance of a 4×4 spatial multiplexing system with LS channel estimation with $L_T = 4$ (solid line) and $L_T = 12$ (dashed line). b) Performance comparison of ML (SD) and MMSE-V-BLAST with iterative channel estimation for $L_T = 4$.

The aim of this kind of simulations is to shed some light on how channel estimation can affect the selection and design of a detector. For instance, it can be seen that an MMSE-V-BLAST detector can perform close to the SD in low and mid SNR values if more resources are dedicated to channel estimation. Therefore, an MMSE-V-BLAST receiver with an improved channel estimator may work better than the SD detector, showing that extra effort in channel estimation may help to reduce the complexity or cost of a receiver.

The channel estimation accuracy may be improved in several ways. Assuming the length of the preamble is fixed by a standard such as the IEEE 802.11a [IEEE99], the estimation can be improved adding simple semi-blind estimation techniques, such as a decision directed channel estimation approach [Grant00b, Buzzi04] or any of the techniques described in Section 4.2.2. Figure 5.6b shows the performance of the optimal detector and an MMSE-V-BLAST receiver with a block-iterative channel estimator with 1 and 2 iterations. Note that the complexity of the MMSE-V-BLAST detector is relatively low in comparison to the SD for large constellations and high number of antennas [Burg06].

The aforementioned iterative approach is just an example of how channel estimation can be taken into account in order to design a whole MIMO receiver. The iterative technique used for the results shown in Figure 5.6b has its drawbacks, such as a high latency due to the block-wise iterative structure or a low efficiency because of the lack of information from the decoder. A parallel architecture is proposed in Section 5.5 which overcomes some of these issues and achieves a good BER performance at a moderate computational cost.

Figure 5.7 shows the same comparisons for 16-QAM and 64-QAM 4×4 spatial multiplexing systems. Following the same strategy as with QPSK modulation, the BER performance is shown using two different channel estimation efforts which correspond to $L_T = 4$ (solid lines) and $L_T = 12$ (dashed lines). If Figure 5.7a (16-QAM) is analyzed, it can be observed that the difference between MMSE and ZF is smaller for both linear and V-BLAST detectors, whereas the SD outperforms clearly the rest.

As interesting cases, it can be observed that ZF and ZF-V-BLAST can perform close to MMSE and MMSE-V-BLAST, respectively, if channel estimation is improved. This case is specially interesting since MMSE requires the knowledge of the SNR level at reception and is slightly more complex. Note that this is not the case for QPSK, where ZF and MMSE curves were further and the latter always outperformed the former. Therefore, it can be stated that the impact of channel estimation on the design of a receiver increases with the modulation order, as is corrobored in Figure 5.7b, where 64-QAM has been used for comparison. The optimal ML (SD) algorithm has not been considered due to its prohibitive complexity for the 4×4 64-QAM system. As interesting cases, it can be seen how the channel estimation improvement is larger than the difference between ZF and MMSE receivers. For instance, ZF can clearly outperform MMSE with a better channel estimation accuracy and MMSE can perform close to MMSE-V-BLAST (much more complex) for low and mid-SNR values

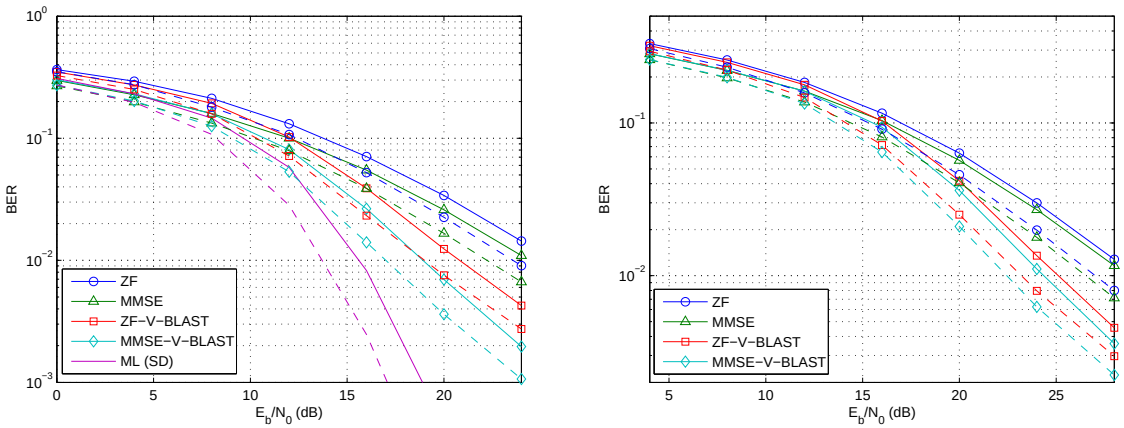

Figure 5.7: BER performance of an uncoded 4×4 spatial multiplexing system with LS channel estimation with $L_T = 4$ (solid line) and $L_T = 12$ (dashed line) for 16-QAM (a) and 64-QAM (b) modulations.

if a better channel estimation is used. These last results confirm the fact that the impact of channel estimation becomes more important when the modulation order increases.

If SD and MMSE-V-BLAST are analyzed for the 16-QAM case, it can be noticed that the latter could perform better if channel estimation was improved. Figure 5.8 shows the performance of the SD and an MMSE-V-BLAST detector with different semi-blind channel estimation approaches, including decision-directed iterative and non-iterative methods. It can be seen that these techniques can perform quite near to ML for low and mid SNR levels, while they suffer from a lack of diversity (slope) at high SNR values. Nevertheless, these approaches can be acceptable if a per-antenna (HE) coding approach is used together with the V-BLAST structure, as it will be shown in the next section.

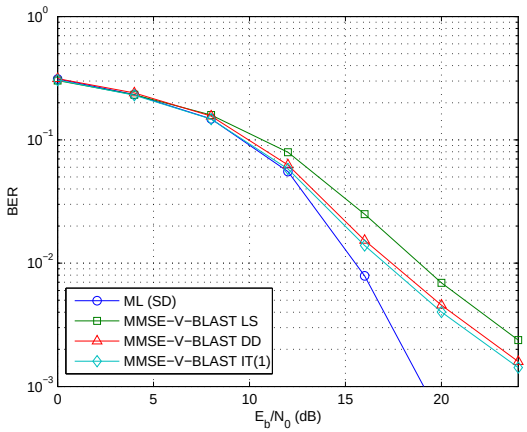

Figure 5.8: Comparison of the SD and an MMSE-V-BLAST detector with enhanced channel estimation for 4×4 16-QAM transmission.

5.3.2.2 Coded 4 x 4 System

Interesting results arise if coded spatial multiplexing systems are analyzed with different channel estimation accuracy levels. Figure 5.9a shows the comparative results for a 4×4 QPSK spatial multiplexing system using a rate-1/2 convolutional code with channel estimation lengths of $L_T = 4$ (solid lines) and $L_T = 12$ (dashed lines). Note that a per-antenna (HE) coding approach has been selected for V-BLAST structures, so a layer profits from the corrected symbols of already decoded streams. Even so, MMSE outperforms ZF and ZF-V-BLAST, while SD is still the best receiver for mid and high SNR values.

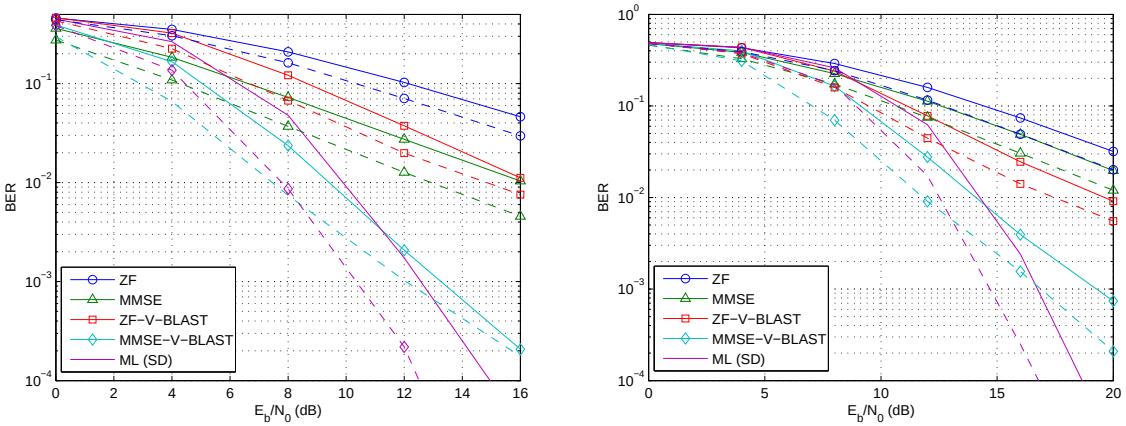

Figure 5.9: BER performance of an coded 4×4 spatial multiplexing system with LS channel estimation with $L_T = 4$ (solid line) and $L_T = 12$ (dashed line) for QPSK (a) and 16-QAM (b) modulations.

If Figure 5.9a is analyzed, it can be observed that the performance of MMSE-V-BLAST and SD are far from the rest. If the effects of channel estimation are evaluated, it can be observed that MMSE-V-BLAST is a very good candidate to avoid the complexity of the SD algorithm. Nearly the same conclusions arise if the 16-QAM scheme is evaluated. As it has already been stated for uncoded systems, the curves of the detectors tend to get closer with larger constellations. As interesting results, MMSE can outperform ZF-V-BLAST if channel estimation is increased. If the best performance is to be reached with a moderate complexity, an MMSE-V-BLAST receiver with iterative channel estimation can be a good candidate for large constellation or number of antennas.

5.3.2.3 4 x 6 Setup

A 4×6 setup is briefly considered in this section in order to analyze the effects of increased diversity on the performance of MIMO systems with channel estimation error. Uncoded and coded QPSK transmission is considered. Figure 5.10a shows the performance of an uncoded

4×6 system with QPSK modulation. As it can be seen, the reception diversity has improved the performance and the slope of the BER curves. It has also reduced the difference between some receivers such as the V-BLAST architectures and the optimal detector. The same happens with the differences between the ZF and MMSE techniques.

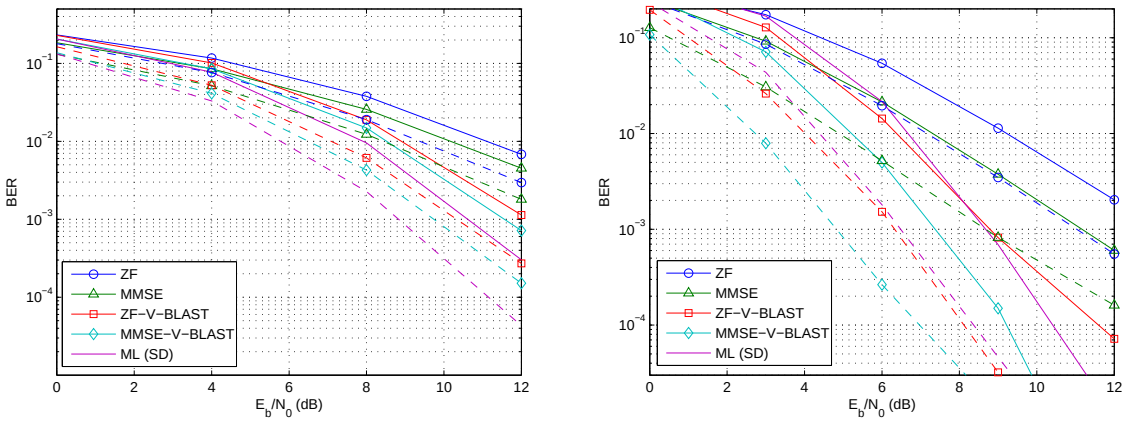

Figure 5.10: BER performance of uncoded (a) and coded (b) 4×6 spatial multiplexing system with LS channel estimation with $L_T = 4$ (solid line) and $L_T = 12$ (dashed line) for QPSK modulation.

Figure 5.10.a represents the effect of two different channel estimation accuracies, corresponding to $L_T = 4$ (solid lines) and $L_T = 12$ (dashed lines) on the performance of the receivers. This is specially interesting since channel estimation introduces nearly the same shifts as in the previous cases, becoming its effect notorious. For instance, all the V-BLAST structures fairly outperform the optimal detector with channel estimation enhancement. This shows that channel estimation becomes specially important in systems with high diversity, where the differences between detection performance curves are smaller.

Figure 5.10b shows the same comparison for a coded 4×6 system. This case becomes quite extreme since the effects of coding and low detection errors reduce the BER in the V-BLAST architectures. It can even be noticed that the ZF-V-BLAST detector can clearly outperform the SD receiver if channel estimation accuracy is improved. These comparisons can be extended to the low-performance receivers, such as ZF and MMSE, where all the differences between detectors are reduced in comparison to the effects of channel estimation. As it can be seen in Figure 5.10b, a ZF-V-BLAST structure can be sufficient to achieve very good results in a system with coding and high diversity if good channel estimation is provided.

5.3.2.4 Summary of Main Results

The simulation results shown in this section have proven the importance of channel estimation on the performance of MIMO detectors. It has been concluded that a proper selection of algorithms and a good channel estimation quality can help to reduce the complexity of a whole MIMO receiver. For instance, it has been shown how simpler structures, such as MMSE-V-BLAST, can outperform the optimal SD if the channel estimation is improved.

It has also been shown that the effects of channel estimation become more important when the modulation order (constellation size) grows or when high diversity is provided. In these cases, where the differences between detectors become smaller for the evaluated SNR range, channel estimation can play an important role in the design of a MIMO receiver. For example a ZF-V-BLAST scheme with increased channel estimation accuracy can perform better than the SD in a per-antenna (HE) coded 4×6 QPSK system, thus reducing the complexity of the receiver. On the other hand, it has been shown that the effects of channel estimation are slightly smaller in coded MIMO systems.

5.4 MIMO-OFDM and MIMO-SCFDE Systems

This section extends the simulation results of Section 5.3 from narrowband to wideband systems, using OFDM and SCFDE, which have been already defined in Chapter 2. Frequency-domain channel estimation with FFT-based interpolation has been chosen for the evaluation of the impact of the CSI. As in the previous section, two levels of channel estimation accuracy have been modelled using two different training lengths, which are related to the NMSE value of the channel estimate by (4.14).

As has been stated in Chapter 2, the WLAN IEEE 802.11a standard has been taken as a reference, thus using FFT and IFFT blocks of $T = 64$ subcarriers [IEEE99]. In order to allow a fair comparison between OFDM and SCFDE, all the available subcarriers have been used so that both techniques transmit at the same rate and through identical channels.

Following the structure of the previous section, the following subsections analyze the effects of channel estimation on MIMO-OFDM and MIMO-SCFDE systems.

5.4.1 MIMO-OFDM

The following results show the effects of channel estimation on a 4×4 MIMO-OFDM system. The HIPERLAN/2 A channel model has been selected, which is defined by an rms delay of 50 ns ($L = 11$ taps) [Medbo98]. Thus, $ML = 4 \cdot 11 = 44$ parameters are estimated per reception antenna. A training length of $L_T = 1$ (one OFDM symbol) is assumed as the minimum channel estimation accuracy level, while up to $L_T = 4$ will be considered. The following simulations show the effects of channel estimation on uncoded and rate-1/2 coded

4×4 systems with QPSK and 16-QAM modulation. The mentioned two coding approaches ($r_t = 1$ and $r_t = 1/2$) represent the limits of the coding possibilities of the 802.11a standard [IEEE99].

5.4.1.1 Uncoded 4x4 System

Figure 5.15a shows the performance of different detectors in a 4×4 MIMO-OFDM systems with QPSK modulation. As it can be seen, the performance gaps between the detectors are very clear. Two channel estimation error levels are shown, corresponding to $L_T = 1$ (solid lines) and $L_T = 4$ (dashed lines). It can be seen that the gap between the curves is larger than the 2 dB shift introduced by the channel estimation error difference. The main conclusion that can be drawn from this curves is that the effect of channel estimation is not determinant in the design of a QPSK MIMO-OFDM receiver, since the choice of the detector plays a more important role. Nevertheless, its impact on the BER performance is still remarkable.

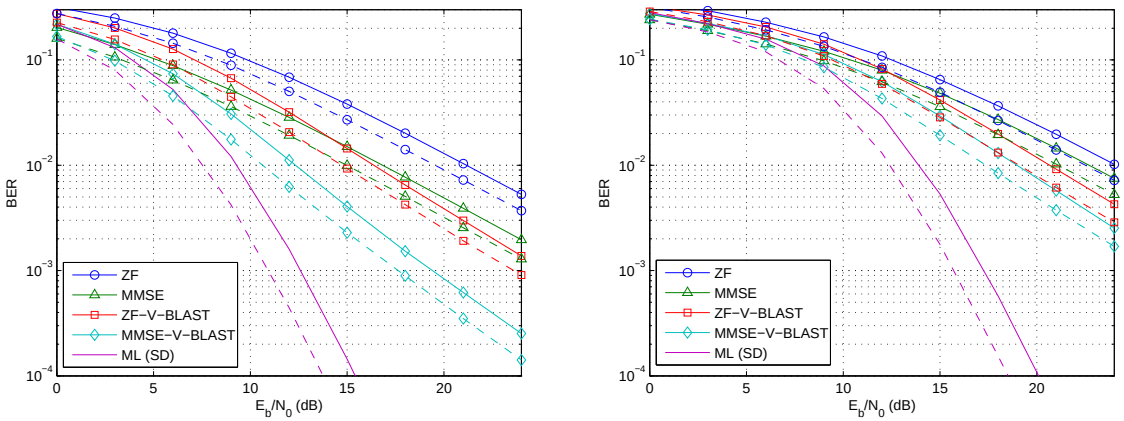

Figure 5.11: BER performance of an uncoded MIMO-OFDM spatial multiplexing system with LS channel estimation with $L_T = 1$ (solid line) and $L_T = 4$ (dashed line) for QPSK (a) and 16-QAM (b) modulation.

The same analysis is shown in Figure 5.15b for 16-QAM modulation. The huge difference between the optimum detector and the others is remarkable, whereas the differences among the rest seem much smaller. If the effects of channel estimation are analyzed, it can be noticed that an increased estimation effort can reduce the complexity of the detector. For example, ZF-V-BLAST with $L_T = 4$ performs similar to MMSE-V-BLAST with $L_T = 1$, while MMSE with $L_T = 4$ can perform close to ZF-V-BLAST with $L_T = 1$, which may be an interesting result for uncoded or high-rate coded system (e.g. $r_t = 5/6$). If these results are compared with the narrowband system of the previous section, it can be noticed that the impact of channel estimation is smaller, though it is still important for large constellations.

5.4.1.2 Coded 4x4 System

OFDM modulation has been conceived to work with channel coding in order to achieve frequency diversity. This section extends the simulation results of the previous section to rate-1/2 coded systems. Two constellations are evaluated: QPSK and 16-QAM. Figure 5.12a shows the performance of the analyzed receivers with QPSK modulation. As has been previously explained for the narrowband case, the V-BLAST structures (where transmitted antenna streams are detected and decoded successively) profit from the correction capability of the channel code. However, ZF-V-BLAST shows a very poor performance, caused by the feedback of the detection errors induced by the noise enhancement of the ZF algorithm, thus reducing its applicability.

Two groups of curves are shown in Figure 5.12a, corresponding to $L_T = 1$ (solid lines) and $L_T = 4$ (dashed lines). As interesting results, it can be noticed that MMSE with a higher channel estimation effort can be a good low-complexity candidate in this kind of systems, whereas MMSE-V-BLAST clearly outperforms SD for the block length used for these simulations.

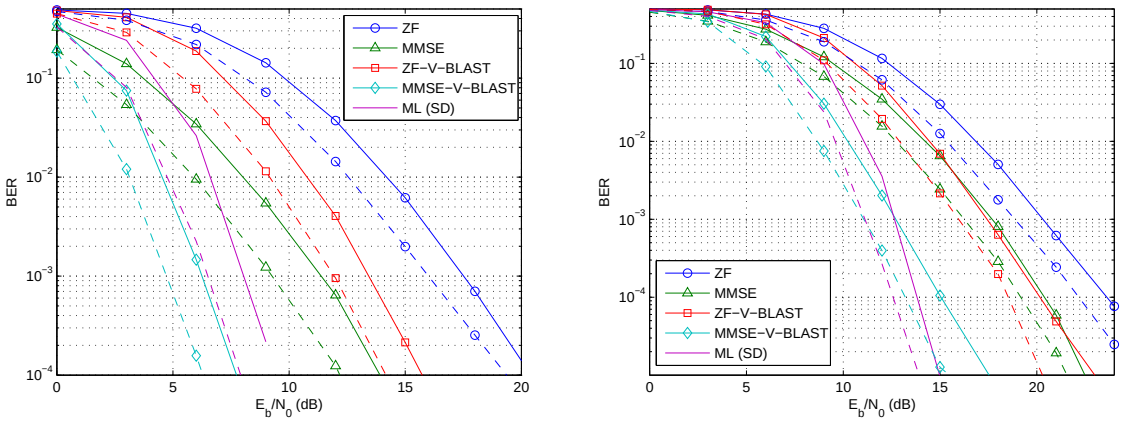

Figure 5.12: BER performance of an coded MIMO-OFDM spatial multiplexing system with LS channel estimation with $L_T = 1$ (solid line) and $L_T = 4$ (dashed line) for QPSK (a) and 16-QAM (b) modulation.

Figure 5.12b shows the same results for a system with 16-QAM modulation. Due to the constellation order, the correcting effects of the V-BLAST architectures are reduced. It can be seen that SD and MMSE detectors can perform similarly to MMSE-V-BLAST and ZF-V-BLAST, respectively, if channel estimation is improved. If the effects of channel estimation errors are analyzed, it can be seen that a worse channel estimate affects more the MMSE-V-BLAST architecture than the SD, but the BER performance curves remain quite similar. The choice between them should be taken evaluating their complexity, which is much larger

for the SD in a 4×4 16-QAM system [Burg06]. If a low complexity detector is required, the MMSE technique seems the unique acceptable candidate, though its performance is 5 dB worse than for the aforementioned techniques.

5.4.2 MIMO-SCFDE

As has been shown in Chapter 2, SCFDE modulation may be an interesting alternative to OFDM for MIMO WLAN scenarios. This section analyzes the effects of channel estimation on the performance of MIMO-SCFDE systems. For simplicity and to allow fair comparisons with OFDM, the same preambles and estimation techniques have been considered. The same structure as for OFDM is followed, although some results are omitted for space limitations. Since the MIMO equalization is done in the frequency-domain, the optimal ML and SD approaches cannot be applied in their original forms, so they have been discarded from the analysis.

5.4.2.1 Uncoded 4x4 System

Figure 5.13a shows the performance of an uncoded 4×4 MIMO-SCFDE system with QPSK modulation with training lengths of $L_T = 1$ (solid lines) and $L_T = 4$ (dashed lines). As can be seen, the performance of the ZF-based approaches (both linear and V-BLAST) are very poor due to the noise enhancement problem at some frequency bins that affects all the information symbols, which are located in the time domain. As has been stated for the OFDM case, the differences between detectors are very large, so channel estimation is not determinant, at least for low-order constellations.

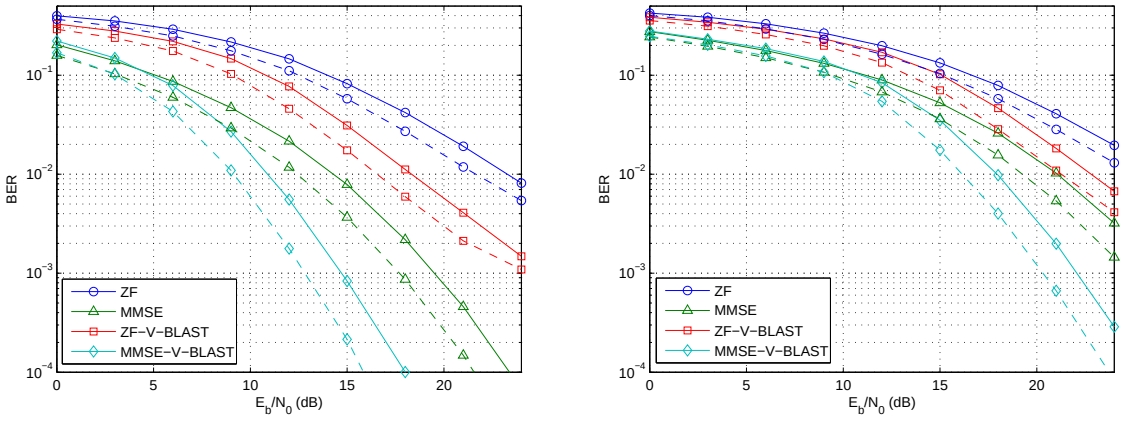

Figure 5.13: BER performance of an uncoded MIMO-SCFDE spatial multiplexing system with LS channel estimation with $L_T = 1$ (solid line) and $L_T = 4$ (dashed line) for QPSK (a) and 16-QAM (b) modulation.

Figure 5.13b shows the same BER performance comparison for 16-QAM. Despite the reduction in the differences between the performances of the detectors, channel estimation is not a determinant factor that can reduce the complexity of the receiver. This conclusion is partial, since some of the selected detection algorithms (ZF and ZF-V-BLAST) can not be used in these scenarios due to their very poor performance, while the ML solution is too complex to be implemented.

5.4.2.2 Coded 4x4 System

Figure 5.14a shows the performance of a coded 4×4 MIMO-SCFDE system, where the same effects of the uncoded case are magnified. The BER performance curves of the detectors show very large differences. Therefore, it can be stated that the impact of channel estimation is not determinant in order to select one detector or another, at least for the detection algorithms evaluated in this analysis. Even so, MMSE detection shows a good complexity-performance trade-off. Therefore, MMSE detection with enhanced channel estimation can be a good low-complexity solution for this kind of systems. Although the gaps between curves seem smaller for the 16-QAM case shown in Figure 5.14b, the same conclusions can be drawn.

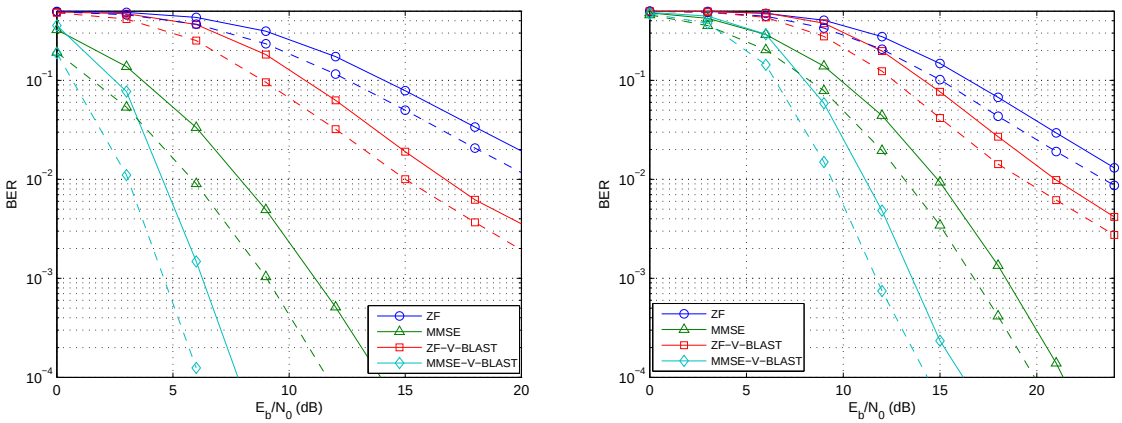

Figure 5.14: BER performance of a coded MIMO-SCFDE spatial multiplexing system with LS channel estimation with $L_T = 1$ (solid line) and $L_T = 4$ (dashed line) for QPSK (a) and 16-QAM (b) modulation.

5.4.3 Comparative Performance and Considerations

Channel estimation error, which can be modelled as a Gaussian variable for the LS channel estimation techniques considered in this section [Biguesh06, Minn06], does not affect the comparative performance of OFDM and SCFDE techniques. Figure 5.15a shows the BER

performance curves for coded MIMO-SCFDE and MIMO-OFDM systems with QPSK modulation. The minimum training length ($L_T = 1$) has been used. The results are as expected, since both systems perform identically for MMSE-based techniques using the lowest coding rate, ($r_t = 1/2$).

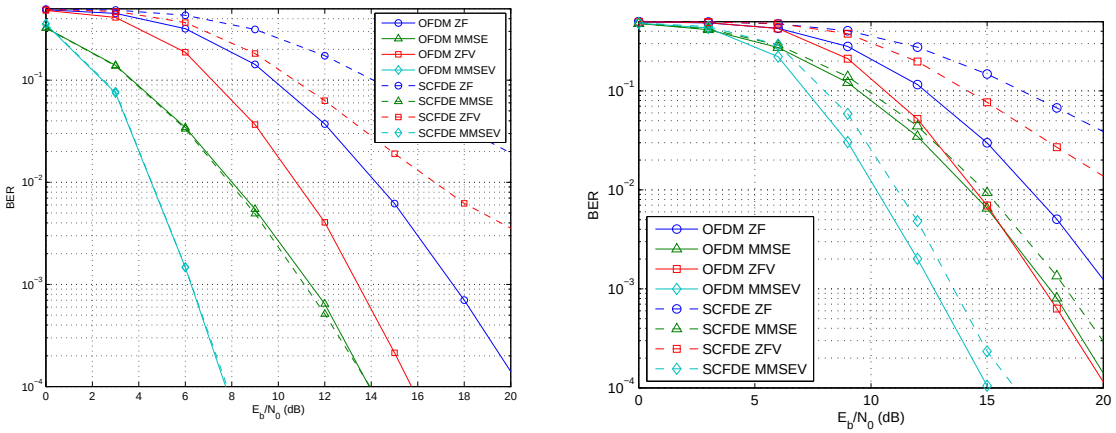

(a) (b)

Figure 5.15: Effects of channel estimation on the performance of a coded 16-QAM spatial multiplexing system.

If the same comparison is carried out with 16-QAM (Figure 5.15b), it can be seen that the performance of SCFDE is degraded in comparison to OFDM, as happens in the perfect CSI case. As a conclusion, channel estimation may be determinant in order to select the detection algorithm and the target performance of the system, but it does not affect the modulation selection (OFDM or SCFDE). Nevertheless, the simplicity of detection in OFDM systems allows more options (ZF, ZF-V-BLAST, ML) in order to jointly design the channel estimator and the MIMO detector.

Therefore, although channel estimation does not affect the comparative behavior of MIMO-SCFDE and MIMO-OFDM, some considerations can be made. For example, if a very low-complexity receiver is to be used, MIMO-OFDM can work with a ZF receiver, whose poor performance can be improved if some resources are dedicated to channel estimation or iterative detection approaches are applied. For both OFDM and SCFDE approaches, MMSE can be an acceptable candidate since it performs relatively well with low complexity, but still far from the MMSE-V-BLAST and SD detectors.

5.5 Design of a Parallel Decision-Directed Channel Estimation Architecture

Results of Section 5.3 show the importance of channel estimation accuracy and how a proper selection of algorithms can reduce the complexity of the overall MIMO receiver. For instance, an MMSE-V-BLAST structure has been shown to outperform the optimal receiver if complexity is added to the channel estimation process. A simple block-iterative algorithm has been used for the reference results shown in the previous sections [Ranheim05]. Nevertheless, the aforementioned algorithm is not efficient from an implementation point of view, since the channel is block-wise re-estimated after the last symbol is received, thus adding a prohibitive latency and requiring large matrix operations.

An interesting channel estimation algorithm was introduced in [Grant00b], where the channel columns (gains of the transmit antennas) are estimated from the detected symbols nulling the effects of the rest of antennas, following a PIC-based approach. For every symbol time k, the channel gain estimate $\hat{\mathbf{g}}_m(k)$ of the m-th transmit antenna can be calculated from the detected symbol vector $\hat{\mathbf{s}}(k)$ as:

$$\hat{\mathbf{g}}_m(k) = \hat{s}(k)^{-1} \left(\sqrt{\frac{M}{E_s}} \mathbf{r}(k) - \sum_{p \neq m} \hat{\mathbf{h}}_p(k) \hat{s}_p(k) \right), \tag{5.3}$$

where $\hat{s}_p(k)$ is the symbol detected at symbol period k for transmit antenna p.

This algorithm can be used to update the MIMO channel every received symbol at a low complexity cost. For example, the channel estimate ($\hat{\mathbf{h}}_m$) can be updated following the next equation:

$$\hat{\mathbf{h}}_m(k) = u \hat{\mathbf{h}}_m(k-1) + (1-u) \hat{\mathbf{g}}_m(k), \tag{5.4}$$

where u is a forgetting factor, whose value ($0 \leq u \leq 1$) depends of the reliability of the detected symbols. This simple decision-directed approach performs slightly worse than the block-iterative techniques [Buzzi04, Ranheim05], but it brings out two benefits: there is no latency added to the system and it may be able to track fading channels, which is not the case for the quasi-static burst-based transmission analyzed in this research. In this context, it must be noticed that the last symbols of the frame are detected using a better channel estimate and that the aforementioned latency properties do not hold if iterations are needed to improve the BER performance [Buzzi04].

Based on this properties and pursuing a simple low-latency decision-directed iterative channel estimation approach that can be easily implemented on an FPGA device, this section proposes a parallel decision-directed (PDD) channel estimation architecture which can be considered semi-iterative and performs better than the block-wise iterative approaches.

Furthermore, this architecture has no latency and can be combined with more complex systems, such as turbo-receivers or hard-decision based convolutional decoders.

The next section shows the main structure of the proposed channel estimation architecture as well as some significant performance results. Once the structure of this channel estimation approach is detailed, it will be extended to wideband MIMO-OFDM and MIMO-SCFDE systems. Results are provided that show the efficiency of the architecture with different detectors and MIMO setups.

5.5.1 Narrowband Systems

This section shows the design of a PDD iterative channel estimation architecture for a reference burst-based narrowband quasi-static fading channel, which will be extended to wideband in the following sections. Figure 5.16 shows the main structure of the PDD architecture with $P = 4$ parallel units, where K stands for the length of the burst in symbol periods. Each of these units consists of a MIMO detector and a decision-directed channel updater, which is described by (5.3) and (5.4).

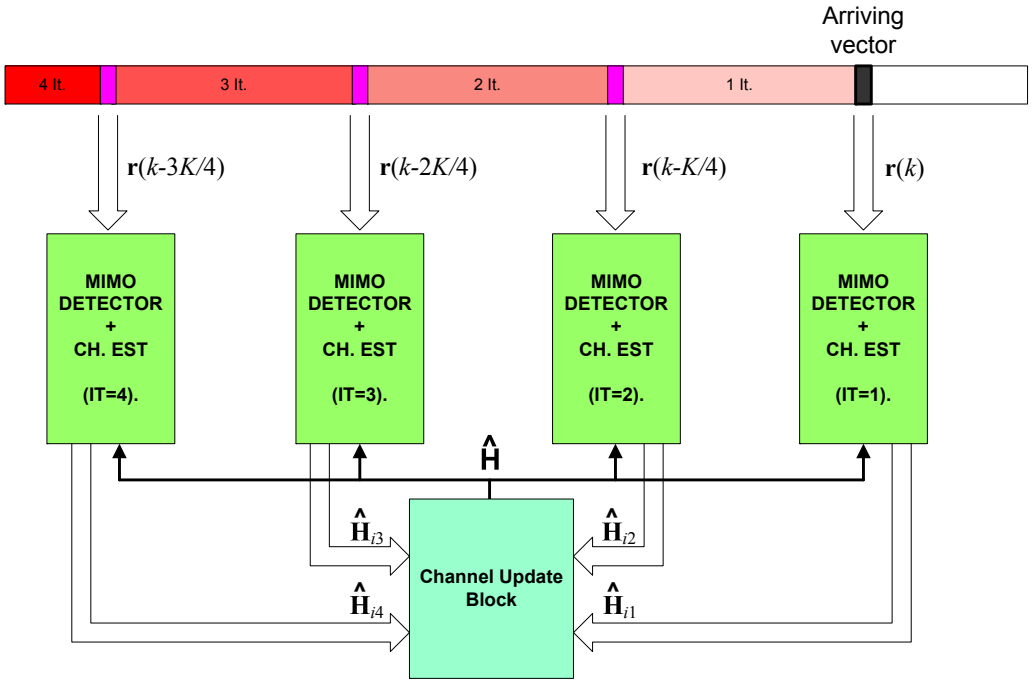

Figure 5.16: Architecture of PDD receiver with P=4.

The structure is based on the decision-directed PIC-based channel estimator of [Grant00b], replicating the MIMO detector and channel estimator blocks (units) so that the first unit is applied to the received symbol vector $\mathbf{r}(k)$, the second one to the vector $\mathbf{r}(k - K/P)$ which

has been received K/P symbols before and so on. In order to reduce the detection latency, the last K/P symbols are detected once, the previous K/P are detected twice, whereas the first K/P symbols are detected P times. Every time a detection is carried out, the channel is re-estimated. Therefore, the information of the reestimated channel symbols is fed back and forward, so that it is used to improve the detection of all the symbols, and not just the last, as it is the case for common non-iterative decision-directed methods.

Figure 5.17 shows the mean NMSE value used to detect every symbol in a received burst or frame for the training-based LS, the PIC decision-directed (DD) approach [Grant00b] and the proposed PDD architecture. The LS channel estimator calculates a channel value which is kept constant for all the symbols in the burst. If the NMSE values of the decision-directed algorithm are analyzed, it can be seen that the channel estimation error is reduced for the last symbols of a frame, thus reducing the number of wrong detections for the last bits. If the PDD architecture shown in this section is applied, the NMSE of the channel estimate can improve for all the symbols of the frame, even improving the last NMSE value of the basic decision-directed architecture due to the up to P iterations performed with some of the previous symbols. One of its main advantages is that it improves the channel estimate used for the detection of all the symbols in a frame, as it can be seen in Figure 5.17.

Figure 5.17a shows the NMSE values for an MMSE-V-BLAST detector with QPSK modulation and an initial LS estimate obtained with a training matrix of length $L_T = 4$. On the other hand, the results of Figure 5.17b have been obtained using the same detector with 16-QAM modulation and a more accurate initial channel estimate ($L_T = 8$). Since the structure lies on the principles of decision-directed channel estimation, the performance results become worse when the constellation size is increased. A block length of 200 symbols (1600 bits) has been selected for these simulations, while a quasi-static flat-fading Rayleigh channel model has been used.

Figure 5.18 shows the BER performance curves of several decision-directed channel estimation algorithms, including the PDD architecture, in two different 4×4 scenarios: QPSK transmission with MMSE detection (Figure 5.18a) and 16-QAM modulation with a ZF detector (Figure 5.18b). As it can be noticed, the PDD structure outperforms the block-iterative approaches in both scenarios without adding any latency to the receiver and with a moderate computational cost.

A very interesting case arises with ZF detection, whose BER performance results are shown in Figure 5.19. It can be observed that both block-iterative and PDD schemes outperform the perfect CSI case. This is due to the noise enhancement problem of the ZF algorithm, which seems to be reduced if iterative channel estimation is employed. This means that these decision-directed channel estimators do not converge to the actual value of the channel matrix, but to a close value whose inverse (which is used for MIMO detection) reduces the noise enhancement problems of the ZF, even with a worse channel estimation

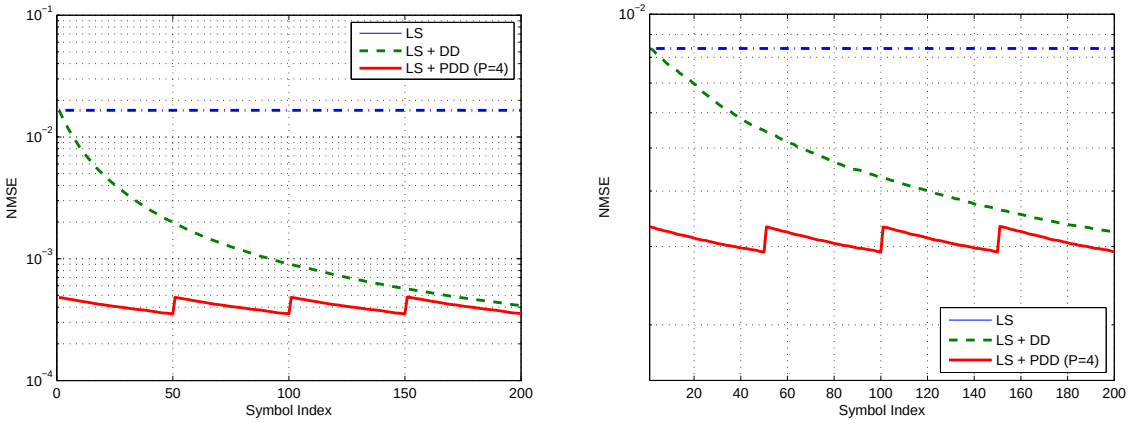

Figure 5.17: Mean NMSE for every received symbol in a frame for MMSE-V-BLAST detection with $L_T = 4$ QPSK (a) and $L_T = 8$ 16QAM (b) systems.

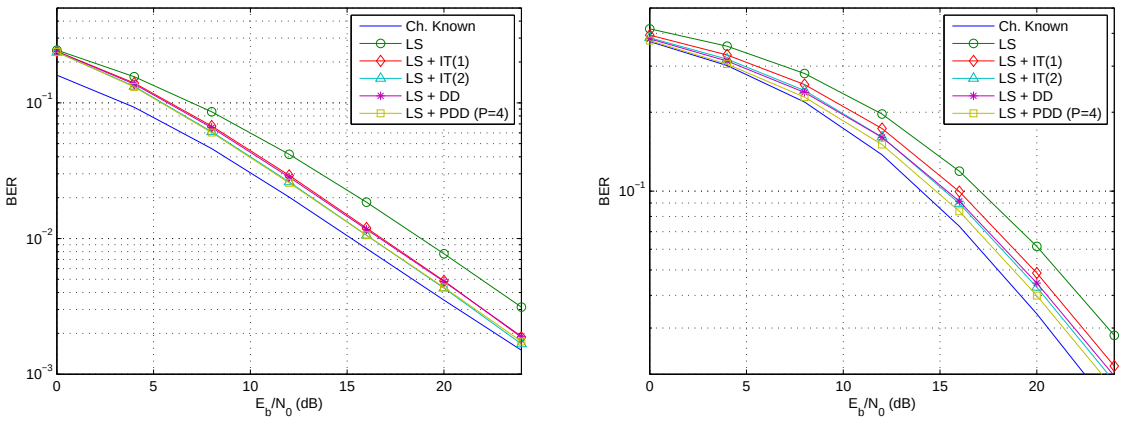

Figure 5.18: BER performance curves of different iterative channel estimators and the PDD architecture for QPSK MMSE (a) and 16QAM ZF (b) scenarios.

quality in terms of NMSE. The results of Figure 5.19 show that the performance of the PDD approach is similar to the block-iterative techniques.

5.5.2 Extension to MIMO-OFDM and MIMO-SCFDE Systems

The PDD architecture introduced in the previous section can be easily extended to OFDM systems, where the iterations are carried out every time a whole symbol is received. The frequency-domain channel estimator, which has been detailed in Section 4.3.2, has been chosen to extend the PDD architecture to MIMO-OFDM systems. Assuming a preamble-based burst transmission as defined in the IEEE 802.11a standard, the first channel estimate

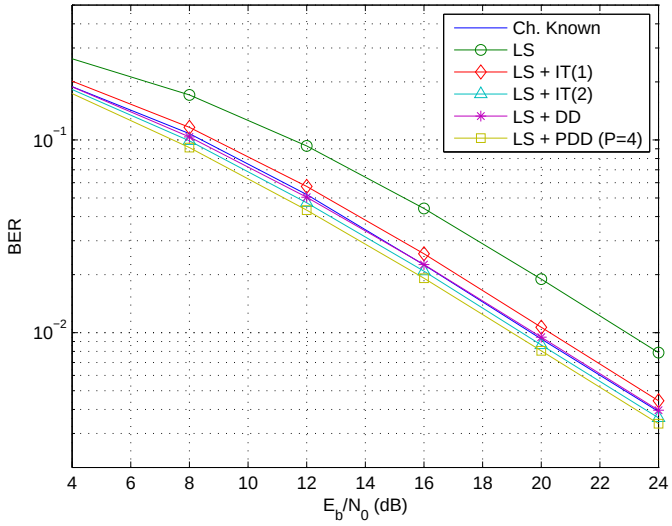

Figure 5.19: BER of a 4×4 QPSK ZF system with different channel estimators including the PDD.

is calculated from the training symbols. When an OFDM symbol is fully received, the channel is updated and the channel estimation is improved while the frame is processed. The same structure of Figure 5.16 is applied so that the P different units are working at different symbol indexes and iteration numbers.

Figure 5.20 shows two examples of the evolution of the frequency response of an $\mathbf{H}_{nm}$ subchannel, from the first trained LS estimate (diamond marker) to the final value (squared marker), while the actual channel is shown in a solid line. Two different E_b/N_0 levels are shown, corresponding to 12 and 4 dB. The selected channel corresponds to the HIPERLAN/2 A channel model (11 taps) [Medbo98].

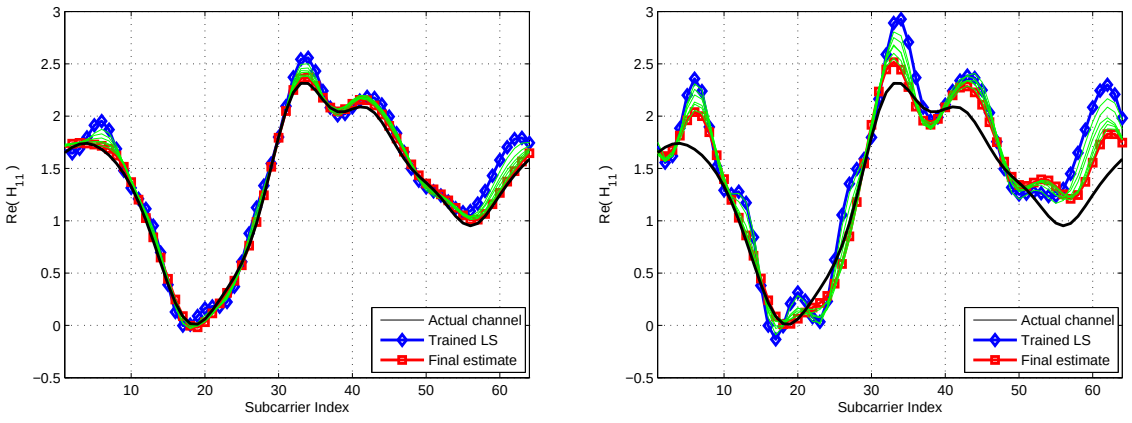

Figure 5.20: Evolution of channel estimate of a sample $\mathbf{H}_{nm}$ subchannel for E_b/N_0 values of 12 dB (a) and 4 dB (b).

Figure 5.21 shows the BER performance of the PDD algorithm in comparison to the basic trained LS and the PIC-based decision-directed algorithm [Grant00b]. It can be observed that the performance improvement is small for low SNR values (incorrect feedback from detected symbols), but the final value gets close to the known channel case for high SNR. The HIPERLAN/2 A channel and blocks of 8 OFDM symbols (4096 bits), which are short enough to guarantee the quasi-static fading assumption, have been used for these simulations.

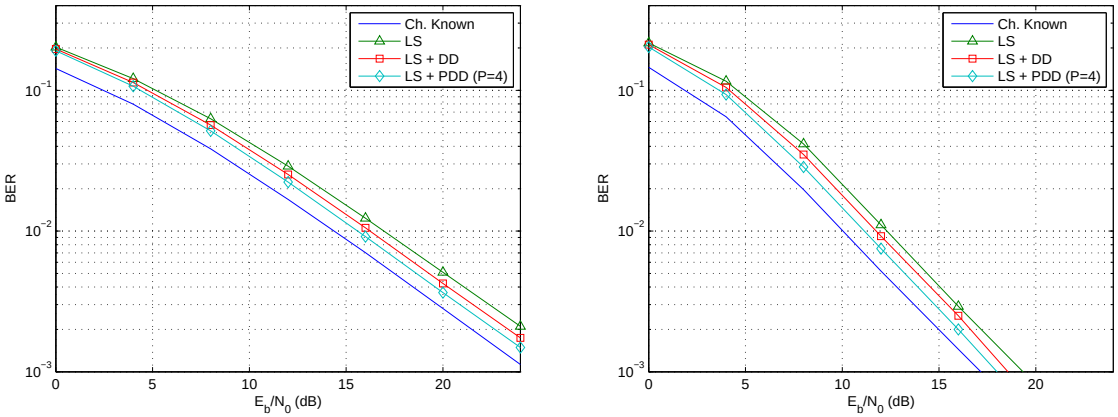

Figure 5.21: BER comparison of PDD channel estimation architecture and the decision-directed (DD) approach for a 4×4 MIMO-OFDM system with MMSE (a) and MMSE-V-BLAST (b) detection algorithms.

The extension of the PDD architecture to MIMO-SCFDE systems is not straightforward. The channel estimation process is carried out in the frequency-domain, where the calculation of the channel gains is relatively simple following (5.3) and (5.4). Nevertheless, SCFDE maps the symbols in the temporal domain. Therefore, IFFT and FFT processes are required to apply the PDD algorithm. Another important difference can be noticed if Equation (5.3) is applied to MIMO-SCFDE systems. It is not the decision on the actual symbol $\mathbf{s}(k)$ which is used for cancellation and estimation, but a frequency bin of the FFT transform of the detected symbol $\mathbf{s}$, which does not fit into any finite alphabet, as it is the case for OFDM. This leads to unstability and noise enhancement in frequency bins with low signal power, degrading the performance for all the symbols.

This problem has been solved assigning a threshold T_h for channel updating. Whenever the power of a frequency bin of the detected symbol is smaller than T_h, the update of the channel value is not carried out. Since all the information symbols tend to follow a uniform distribution, the frequency bins affected by the threshold are not likely to be in the same frequencies in all the SCFDE symbols, so all of them can get updated correctly.

Figure 5.22 shows the BER performance curves for two MIMO-SCFDE systems using the PDD channel estimation architecture. It can be seen that the inclusion of the aforementioned

threshold criterion does not degrade the performance of the architecture, which outperforms the LS estimate and the basic decision-directed estimator. The systems parameters are the same as in the previous OFDM comparisons: QPSK signalling with MMSE and MMSE-V-BLAST detection, 8 OFDM symbols and the HIPERLAN/2 A wireless channel.

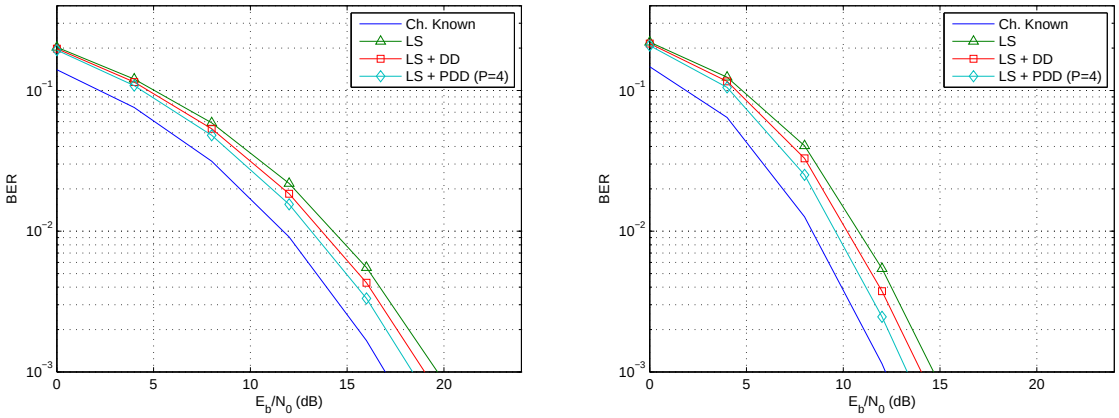

Figure 5.22: BER comparison of PDD channel estimation architecture and the decision-directed (DD) approach for a 4×4 MIMO-SCFDE system with MMSE (a) and MMSE-V-BLAST (b) detection algorithms.

5.6 Chapter Summary

This chapter has focused on the evaluation of the impact of channel estimation on the performance of MIMO detection algorithms using two different strategies. On one hand, the full real-time 2×2 MIMO system of Chapter 3 has been used to analyze the effects of channel estimation and implementation issues on fundamental MIMO receivers. On the other hand, Matlab simulations have been carried out to evaluate the effects of channel estimation accuracy on the performance of the main detectors (ZF, MMSE, ZF-V-BLAST, MMSE-V-BLAST and ML(SD)).

Regarding the implementation-based analysis, it has been shown that the accuracy of the channel estimate is determinant on the final BER performance. For the simplest ZF detector, the channel estimation error has been proven to affect the BER performance curve more than the implementation-based errors. The same analysis has been carried out for the optimal SD detector, where the effects of the implementation have been shown to be more influent, though the effects of channel estimation are still considerable. For all the cases, implementation related issues represent an error floor at high SNR values, while channel estimation induces a horizontal shift of the BER performance curves.

The practical evaluation has been completed with simulations of more complex systems, including wideband MIMO-OFDM and MIMO-SCFDE schemes. It has been observed that the gaps between detection techniques can be covered improving the channel estimation quality, which means that the complexity of the detectors can be reduced if channel estimation is improved. The effects of the channel estimation accuracy are specially remarkable for large constellations in narrowband and MIMO-OFDM scenarios. For example, an MMSE-V-BLAST detector with a simple iterative channel estimation algorithm has been proven to perform similarly or better than the optimal detector (SD), which can be prohibitively complex for large constellations and number of antennas. The impact of channel estimation has been shown to be more determinant in systems with large constellations, high diversity orders and high coding rates.

Finally, a parallel decision-directed (PDD) semi-iterative channel estimation architecture has been proposed which can be used to improve the performance of simple MIMO detectors. This structure enables the benefits of block-iterative channel estimation without adding any latency to the system and can be combined with any of the MIMO setups considered in this dissertation.

Chapter 6

Conclusion and Further Research

This work has focused on the analysis of the effects of channel estimation on the performance of MIMO wireless systems. The performance comparison of channel estimators is usually based on their NMSE values, whereas the evaluation of the receivers focuses on the BER comparison of different detectors with perfect channel knowledge. However, an overall analysis of the different combinations of channel estimation and detection algorithms is missing in the literature. The work detailed in this dissertation aims to shed light on the overall design of a receiver in order to establish the most efficient estimator-detector combination for each MIMO system depending on the target performance and the allowable complexity.

6.1 Summary

The aim of this PhD thesis has been to analyze the effects of channel estimation on MIMO wireless systems under two different scopes. On one hand, the impact of channel estimation on the performance of MIMO detectors has been analyzed theoretically and by means of simulations. On the other hand, this theoretical analysis has been complemented with the implementation and evaluation of a real-time MIMO platform.

The practical analysis of this research has addressed the design and development of a MIMO prototyping platform which has been used to develop a full real-time 2×2 system. This hardware implementation has allowed to understand the implications of the design and validation of real-time MIMO algorithms. Thanks to this MIMO system, which can use a ZF or a SD (ML) detector, the effects of channel estimation error have been evaluated and compared to the impact of the rest of implementation issues. It has been shown that the error induced by channel estimation is critical in low-performance receivers in comparison to other error sources like quantization, channel pre-processing or synchronization failures. However, hardware implementation becomes more influent in more efficient detectors such as the SD, despite the importance of the channel estimation error.

Chapter 4 has shown a brief summary of simple and realistic channel estimation algorithms for MIMO spatial multiplexing systems, including narrowband, OFDM and SCFDE schemes. Channel estimation has also been evaluated for a MMSE-PIC Turbo-MIMO re-

ceiver, proposing analytical EXIT function-based tools which allow to evaluate the BER performance of iterative MIMO systems with channel estimation errors. These analytical EXIT-based tools can help to avoid the computational cost of extensive MC simulations.

A simulation-based analysis has been developed in Chapter 5 which has evaluated the comparative performance of the basic MIMO detectors (ZF, MMSE, ZF-V-BLAST, MMSE-V-BLAST and SD) with different channel estimation accuracy levels. This methodology has allowed to study the trade-off between the complexity of channel estimation and MIMO detection algorithms in narrowband, OFDM and SCFDE systems. It has been shown that channel estimation can play an important role when designing the receiver since the complexity of the detector can be reduced if a proper channel estimator is employed. As an illustrative example, the optimal ML detector can be outperformed by a simpler MMSE-V-BLAST architecture with an iterative channel estimation approach, which can be less complex for large constellation and number of antennas. These simulation-based results have shown the importance of channel estimation for the design of efficient and balanced receivers. It has also been concluded that the impact of channel estimation is more important for narrowband systems, large constellations and systems with higher reception diversity.

Finally, a semi-iterative parallel decision-directed channel estimation architecture has been proposed. This channel estimator can achieve a very good performance, similar to a block iterative technique, without any latency and can be easily implemented on an FPGA device. Results have been provided which show good performance in uncoded narrowband, OFDM and SCFDE MIMO scenarios.

6.2 Thesis Contribution

The main contributions of this research work are the following:

- **Chapter 2:** A comparison between the BER performance curves of MIMO-OFDM and MIMO-SCFDE has been carried out for systems based on the IEEE 802.11a standard [Mendicute04a, Mendicute04b].

- **Chapter 3:** A real-time 16-QAM 2×2 MIMO prototype has been designed and developed, including an inline channel emulator. A Matlab-based hardware and software co-simulation methodology has been developed from scratch for the Heron platform of the University of Mondragon [Mendicute05], including "Hardware in the Loop" simulation tools [Mendicute06b]. An optimal detector, based on the sphere decoder, has been integrated in the whole MIMO system in collaboration with the University of Edinburgh, which has served to evaluate its performance in a full MIMO system [Mendicute06a]. To the author's knowledge, this integration is the first reported implementation of a whole real-time SD-based MIMO system.

- **Chapter 4:** An analytical EXIT function-based BER prediction tool has been proposed for Turbo-MIMO systems with MMSE-PIC receivers with channel estimation errors [Mendicute07]. A simple model has been proposed which includes the effects of channel estimation error for training-based LS and iterative EM channel estimators, extending the methods proposed in [Hermosilla05] for systems with perfect CSI.

- **Chapter 5:** Results have been provided which allow to evaluate the effects of channel estimation and realistic hardware implementation on the BER performance of MIMO detectors, including the simplest detector (ZF) and the optimal ML receiver (implemented as SD) [Mendicute06a]. A simulation-based comparison of several basic detection algorithms has been carried out for different channel estimation error levels in narrowband and wideband MIMO systems (OFDM and SCFDE), which has allowed to evaluate the impact of the selection and design of channel estimation algorithms.

  Finally, a parallel decision-directed semi-iterative channel estimation architecture has been proposed, which achieves good performance with no latency and a moderate complexity. Many of the results of this chapter have not been published yet. See Appendix A for the publications (published or under preparation) derived from this PhD thesis.

6.3 Suggestions for Further Research

The work described in this PhD dissertation can be improved and extended in many ways. These are some of the suggestions for further research:

- The fundamental real-time MIMO implementation and the analysis of Chapter 5 could be extended to more realistic and demanding cases, such as systems with a larger number of antennas or multicarrier modulation.

- The proposed analytical EXIT function-based tools have been applied to a very specific case (MMSE-PIC receiver with LS and EM estimators). Their extension to more generic Turbo-MIMO systems and channel estimation models may be interesting in order to confirm their validity.

- The simple simulation-based methodology that has been used for the analysis of channel estimation effects could be extended to multiuser MIMO scenarios, where CSI is extensively used at both transmitter and receiver sides.

- The proposed PDD architecture could be applied to coded systems, from conventional Viterbi convolutional decoders to BCJR-based SISO* detectors. The applicability and the achievable performance results for this kind of systems should be evaluated.

- The hardware design and implementation of the PDD architecture could be carried out in order to evaluate the real performance and complexity issues of the proposed channel estimator in real scenarios.

Appendix A
Publications

The following papers have been published or are under preparation for publication in refereed journal and conference proceedings. Those marked by † are reproduced in this appendix.

Journal papers:

- M. Mendicute, J. Altuna and, V. Atxa, "A parallel decision-directed MIMO channel estimation architecture", under preparation for its submission to *EURASIP Journal on Wireless Communications and Networking*.

International conference papers:

- M. Mendicute, J. Altuna, V. Atxa and J. M. Zabalegui, "Performance comparison of OFDM and FDE single-carrier modulation for spatial multiplexing MIMO systems", in *Proc. 5th IEEE Signal Processing Workshop on Signal Processing Advances in Wireless Communications (SPAWC '04)*, pp. 532-535, Lisbon, Portugal, Jul. 2004. †

- M. Mendicute, J. Altuna, J. S. Thompson and V. Atxa, "Performance of frequency-domain MIMO equalization for cyclic-prefixed single-carrier spatial multiplexing", in *Proc. 12th EURASIP European Signal Processing Conference (EUSIPCO '04)*, pp. 1849-1952, Vienna, Austria, Sep. 2004. †

- J. Altuna, M. Mendicute, V. Atxa and J. M. Zabalegui, "Blind co-channel interference mitigation in CP-SC-FDE for 2-11 GHz broadband wireless systems", in *Proc. IADAT International Conference on Telecommunications and Computer Networks (TCN '04)*, pp. 88-92, San Sebastian, Spain, Dec. 2004. †

- M. Mendicute, J. Altuna, G. Landaburu and V. Atxa, "Platform for joint evaluation of FPGA-implemented and Matlab algorithms in real MIMO transmissions", in *Proc. 2nd IEE/EURASIP Conference on DSP Enabled Radio (DSPeR '05)*, pp. 3/1-3/4, Southampton, United Kingdom, Sep. 2005. †

- M. Mendicute, L. G. Barbero, G. Landaburu, J. S. Thompson, J. Altuna and V. Atxa, "Real-time implementation of a sphere decoder-based MIMO wireless system", in *Proc. 14th EURASIP European Signal Processing Conference (EUSIPCO '06)*, special session "MIMO: VLSI, testbeds and prototyping", Florence, Italy, Sep. 2006. **Invited paper.** †

- M. Mendicute, J. Altuna and V. Atxa, "Analytical EXIT functions for the performance evaluation of iterative MIMO receivers with channel estimation error", in *Proc. 15th EURASIP European Signal Processing Conference (EUSIPCO '07)*, Poznan, Poland, 2007. †

- M. Mendicute, J. Altuna and V. Atxa, "A parallel decision-directed architecture for wireless MIMO systems", under preparation for its submission to *International Conference on Communications (ICC '09)*, Dresden, Germany, June 2009.

National conference papers:

- M. Mendicute and J. Altuna, "Plataforma para la evaluación de algoritmos Matlab y hardware VHDL en transmisiones reales MIMO", in *Proc. XX Simposium Nacional de la Unión Científica Internacional de Radio (URSI '05)*, Gandía, Spain, Sep. 2005. †

- M. Mendicute, G. Landaburu, J. Altuna, V. Atxa and I. Zuazabeitia, "Sistema 'Hardware in the loop' para el prototipado de algoritmos MIMO de tiempo real", in *Proc. XXI Simposium Nacional de la Unión Científica Internacional de Radio (URSI '06)*, pp. 88-92, Oviedo, Spain, Sep. 2006. †

Other related publications:

- M. Mendicute, I. Sobrón, J. Del Ser, P. Prieto and R. Isasi, "Design, Simulation and implementation of a channel equalizer for DVB-T on-channel repeaters", in *3rd IARIA International Conference on Systems and Networks Communications (ICSNC '08)*, Silema, Malta, Oct. 2008.

- M. Mendicute, P. Prieto, I. Sobrón, J. M. Zabalegui and R. Isasi, "Diseño, simulación e implementación de un ecualizador de canal para gap-fillers de DVB-T", in *Proc. XXI Simposium Nacional de la Unión Científica Internacional de Radio (URSI '08)*, Madrid, Spain, Set. 2008.

Fifth IEEE Workshop on Signal Processing Advances in Wireless Communications, Lisboa, Portugal, July 11-14, 2004

Performance Comparison of OFDM and FDE Single-Carrier Modulation for Spatial Multiplexing MIMO Systems

Mikel Mendicute[1], Jon Altuna, Vicente Atxa and José María Zabalegui
University of Mondragon
Loramendi, 4
20500 Mondragon, Spain
{mmendikute, jaltuna, batxa, jmzabalegui}@eps.mondragon.edu

Abstract — **Multiple-Input Multiple-Output (MIMO) signal processing combined with Orthogonal Frequency Division Multiplexing (OFDM) is a widely accepted solution to achieve the high bit rates that new communication standards require in frequency-selective wireless channels. In recent years, a new Frequency-Domain Equalized (FDE) Cyclic-Prefixed Single-Carrier (CPSC) block transmission system has been proven to achieve similar performance to OFDM for coded systems with the same overall complexity, avoiding its main drawbacks and becoming a candidate for future wireless standards. In this paper, a FDE CPSC spatial multiplexing system is analyzed and compared to OFDM. The implementation of different frequency-domain MIMO equalization and detection schemes is evaluated. Simulation-based performance results prove the efficiency of FDE CPSC based spatial multiplexing systems and highlight that these transmission schemes can outperform OFDM in uncoded and high coding rate MIMO systems, as it has been shown in the literature for the SISO case.**

I. Introduction

As new wireless communication network standards are being defined, the demand for higher throughput is growing enormously. Recent wireless local (WLAN) and metropolitan (WMAN) area network standards such as IEEE 802.11a, 802.11g, 802.16a and ETSI HIPERLAN/2 have chosen Orthogonal Frequency Division Multiplexing (OFDM) to overcome the wireless channel's high frequency selectivity. Newer, not yet defined WLAN standards, such as 802.11n, aim to reach data rates of up to 300 Mbps. In order to achieve these high bit rates, Multiple-Input Multiple-Output (MIMO) signal processing techniques become necessary.

Two basic approaches have been studied to enhance OFDM with MIMO: Space-Time Coding (STC) and Spatial Multiplexing (SM) [1]. STC increases the diversity order of the communication system by coding over the different transmission antennas, which leads to a better performance. On the other hand, SM transmits independent data streams on each antenna simultaneously, thus allowing greater data throughputs for a fixed bandwidth [1, 2].

Although OFDM has been included in many standards due to its simple equalization, alternative cyclic-prefixed or zero-padded single-carrier (SC) block transmission techniques have been proposed and developed in recent years [3, 4]. SC transmission avoids OFDM's three main drawbacks: Large peak-to-average ratio of the signal power, frequency offset sensitivity and no multipath diversity in uncoded systems. The most simple and interesting of these SC techniques is the Frequency-Domain Equalized (FDE) Cyclic-Prefixed Single-Carrier (CPSC) transmission system. As can be seen in Fig. 1, its overall complexity is similar to an OFDM system. As the equalization is done in the frequency-domain, FFT and IFFT blocks are required in reception. This system has been proven to fairly outperform OFDM for uncoded systems and yields similar BER performance in coded transmissions [3]. Its main disadvantages are the loss of subcarrier allocation granularity and the difficulty of coping with fixed narrowband interferers. A very interesting feature of CPSC lies on the fact that the main complexity belongs to the receiver part, so it can be combined with OFDM, allowing asymmetric systems where most of the complexity resides at one side (base station, access point, etc.), as it has been proposed in new 802.16 standards [5]. FDE has been extended to several MIMO systems, such as diversity combining using adaptive LMS and RLS equalization [6] or Space-Time Block Coding with MMSE-FDE detection [7].

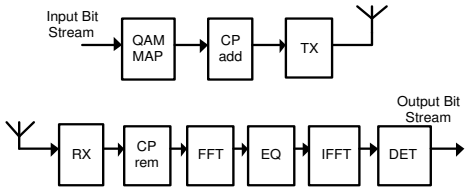

Figure 1: Wireless FDE CPSC transmission and reception systems.

This paper discusses and compares the frequency-domain equalization of CPSC and OFDM spatial multiplexing systems. The main MIMO equalization techniques are analyzed and BER performances of both systems are evaluated with simulations for a HIPERLAN/2 MIMO system. The applicability and performance of known V-BLAST [8] detection algorithms is specially analyzed.

The layout of this paper is as follows: Section II details the evaluated MIMO equalization techniques. In Section III the FDE CPSC-based MIMO transmission and reception systems are introduced. Section IV summarizes the most interesting aspects of MIMO OFDM equalization. Section V shows the simulation results and some conclusions are drawn in Section VI.

[1]Partially sponsored by the Dpt. of Education, Universities and Research of the Basque Government through a Researcher Training Grant.

II. MIMO Equalization and Detection Techniques

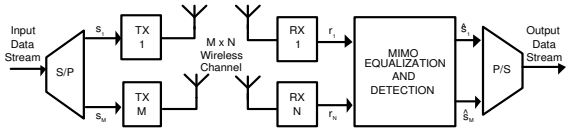

Figure 2: Flat MIMO system

Fig. 2 shows a single-carrier spatial multiplexing system for a frequency-flat fading channel with additive white Gaussian noise (AWGN). This model will be extended to a frequency-selective channel case in Section 4. The system has M transmit and N receive antennas. The path loss from transmit antenna m to receive antenna n is represented as h_{nm}. The sampled baseband system of a flat MIMO channel can be represented in matrix notation as:

$$\mathbf{r} = \sqrt{\frac{E_s}{M}}\tilde{\mathbf{H}}\mathbf{s} + \mathbf{n} \tag{1}$$

where $\mathbf{r}$ is an $Nx1$ vector containing the signals received in each antenna, $\mathbf{s}$ is an $Mx1$ vector with the signals transmitted simultaneously at each transmission branch and $\mathbf{n}$ is an $Nx1$ vector containing channel's AWGN. E_s is the transmitted signal power and $\tilde{\mathbf{H}}$ is a NxM channel matrix, defined as:

$$\tilde{\mathbf{H}} = \begin{pmatrix} h_{11} & h_{12} & ... & h_{1M} \\ h_{21} & h_{22} & ... & h_{2M} \\ : & : & : & : \\ h_{N1} & h_{N2} & ... & h_{NM} \end{pmatrix}$$

Linear non-OSIC MIMO detection

Maximum Likelihood detection using equation (2) should be the optimal detection method for spatial multiplexing. However, it is computationally too complex due to the calculation of the likelihood metrics for S^M possible input vectors, where S is the number of symbols in the constellation.

$$\hat{\mathbf{s}} = \arg\min_{\mathbf{s}} \left\| \mathbf{r} - \sqrt{\frac{E_s}{M}}\tilde{\mathbf{H}}\mathbf{s} \right\|_F^2 \tag{2}$$

MMSE (Minimum Mean Squared Error) and ZF (Zero-Forcing) [9] are simpler solutions, based in the product:

$$\hat{\mathbf{s}} = \mathbf{G}\mathbf{r} \tag{3}$$

where

$$\mathbf{G}_{ZF} = \sqrt{\frac{M}{E_s}}\tilde{\mathbf{H}}^{+} = \sqrt{\frac{M}{E_s}}(\tilde{\mathbf{H}}^{*}\tilde{\mathbf{H}})^{-1}\tilde{\mathbf{H}}^{*} \tag{4}$$

$$\mathbf{G}_{MMSE} = \sqrt{\frac{M}{E_s}}(\tilde{\mathbf{H}}^{*}\tilde{\mathbf{H}} + \alpha\mathbf{I}_{MxM})^{-1}\tilde{\mathbf{H}}^{*} \tag{5}$$

with $\alpha = NoisePower/SignalPower$. The notations * and $^+$ stand for conjugate transpose and pseudoinverser especively. MMSE offers much better results than ZF in AWGN channels, but its performance is still quite far from optimal for $N = M$ [9].

Non-linear V-BLAST (OSIC) detection

An OSIC (Ordered Successive Interference Cancellation) based algorithm has been proposed in [8] to overcome the limitations

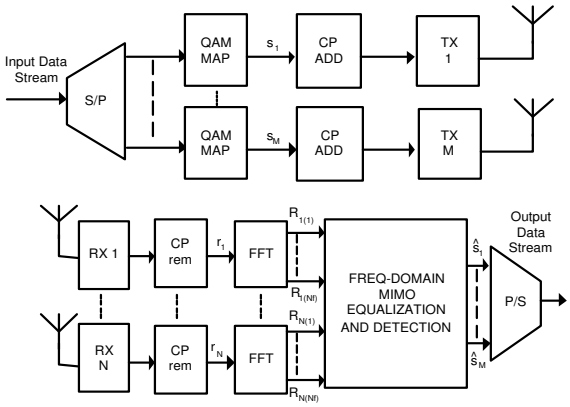

Figure 3: Frequency-Domain Equalized MIMO spatial multiplexing transmission and reception system.

of previous methods with relatively low complexity and has been named ZF-V-BLAST detection. It is based in the iteration of three steps:

1. Ordering: Determine the transmit antenna k with greatest SNR from the estimated channel, selecting the row $(\mathbf{G})_k$ of smallest norm of the nulling matrix $\mathbf{G}$:

$$k = \arg\min_{k} \|(\mathbf{G})_k\|^2 \quad \mathbf{G} = \mathbf{G}_{ZF} \tag{6}$$

2. Nulling and slicing: Detect transmitted symbol at antenna k $\hat{s}_k$:

$$y_k = ((\mathbf{G})_k)^T\mathbf{r} \tag{7}$$

$$\hat{s}_k = \arg\min_{\hat{s}_k} \|\hat{s}_k - y_k\| \tag{8}$$

3. Cancellation: Remove the effect of the detected symbol from received signal vector and its column $\tilde{\mathbf{H}}_k$ in the channel matrix:

$$\mathbf{r} = \mathbf{r} - \sqrt{\frac{E_s}{M}}\tilde{\mathbf{H}}_k\hat{s}_k \tag{9}$$

$$\tilde{\mathbf{H}}_{nm} = 0 \quad \forall m = k \tag{10}$$

Note that the diversity order increases by one in each iteration. Other V-BLAST detection algorithms such as MMSE-VBLAST or SOMLD (Successive Ordered Maximum Likelihood Detection) differ from ZF-V-BLAST in the calculation of the G matrix in (6) and the ordering criterion [2, 9].

III. Frequency-Domain Equalized Cyclic-Prefixed Single-Carrier MIMO system

The baseband flat MIMO channel model in (1) can be easily extended for a L tap frequency-selective channel:

$$\mathbf{r(k)} = \sqrt{\frac{E_s}{M}}\sum_{l=1}^{L}\tilde{\mathbf{H}}(l)\mathbf{s}(k-l) + \mathbf{n}(k) \tag{11}$$

The addition of the cyclic prefix avoids IBI and transforms the linear time convolution of the input signal and the channel response into a circular convolution, thus the model in (11) can be modelled as a product in the frequency domain. This way

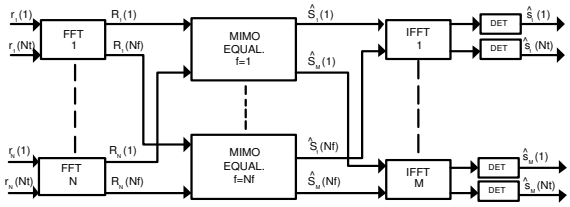

Figure 4: FDE MIMO equalization and detection. A MIMO equalizer is employed at each frequency.

a flat MIMO channel is obtained for each one of the Nf FFT frequency points of Fig. 3:

$$\mathbf{R}(f) = \sqrt{\frac{E_s}{M}}\mathbf{H}(f)\mathbf{S}(f) + \mathbf{N}(f) \tag{12}$$

$\mathbf{R}$, $\mathbf{H}$, $\mathbf{S}$ and $\mathbf{N}$ are the Nf-point FFT transforms of $\mathbf{r}$, $\tilde{\mathbf{H}}$, $\mathbf{s}$ and $\mathbf{n}$, respectively. Note that the MIMO equalization is not done on the information bearing symbols $\mathbf{s}(k)$, but on the frequency-domain FFT points $\mathbf{S}(f)$, so an IFFT is required before the symbol detection. This means that all symbols from an antenna must be equalized before they can be detected. This is particularly important for V-BLAST detection, as it will be shown later.

For the MIMO detection techniques that do not require any decision feedback, such as ZF or MMSE, the Frequency-Domain MIMO detection requires Nf MIMO equalizers, i.e., one for each of the FFT output points, as it can be seen in Fig. 4.

For MIMO equalization techniques requiring detected symbol feedback, such as ZF-V-BLAST or MMSE-V-BLAST, FDE CPSC implies several problematic changes because the IFFT and the FFT operations appear in the feedback chain as it can be seen in Fig. 5. Equations (7) and (8), slicing and cancellation, become:

$$\hat{\mathbf{s}}_k = \arg\min_{\hat{\mathbf{s}}_k} \|\hat{\mathbf{s}}_k - \mathit{ifft}(\hat{\mathbf{S}}_k)\| \tag{13}$$

$$\mathbf{D}_k = \mathit{fft}(\hat{\mathbf{s}}_k)$$

$$\mathbf{R}(f) = \mathbf{R}(f) - \sqrt{\frac{E_s}{M}}\mathbf{H}_k(f)\mathbf{D}_k(f) \tag{14}$$

where $\mathbf{s}_k$ is a whole block transmitted from antenna k in the time domain. $\mathbf{R}$ and $\hat{\mathbf{S}}$ are frequency-domain received and equalized signal and $\mathbf{D}_k$ is the FFT transform of the detected symbol block $\hat{\mathbf{s}}_k$. As it can be deduced from (13) and (14), the equalization and detection must be done per antenna and in a whole block basis due to the IFFT and FFT operations involved in the feedback chain. Thus, the antenna ordering process in (6) will be done for a whole time block, instead of per each FFT point in the frequency domain, like in OFDM, as it would be desirable to reduce the effects of frequency selectivity. This per-block ordering can slightly reduce the performance improvement of the OSIC (V-BLAST) algorithm.

IV. MIMO-OFDM Equalization

In OFDM an Nf-point IFFT operation is done on the information-bearing symbols before the cyclic prefix addition, so each symbol is transmitted on an orthogonal frequency subcarrier. Since a cyclic prefix is also used, equation (12) can also model a MIMO OFDM transmission system, where $\mathbf{S}(f)$ is the

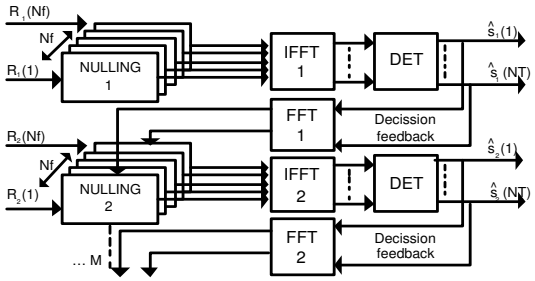

Figure 5: MIMO V-BLAST per-antenna signal detection and decision feedback.

information symbol sent at subcarrier f. Thus, Nf flat MIMO systems are obtained.

Note that the frequency-domain equalization is done directly on the data symbols and not in their FFT transform, as in the FDE CPSC case. This allows symbol based detection and feedback, simplifying the implementation of OSIC algorithms in uncoded systems. For coded transmission, this symbol-by-symbol detection can be improved if a per-antenna coded (PAC) V-BLAST algorithm is applied as described in [2], where coding and soft Viterbi decoding blocks are inserted in the V-BLAST decision feedback chain. If this coded scheme is used, equalization and detection must be done in a whole block basis, like for the FDE-CPSC case.

V. Simulation results

Simulated System Parameters

Two different spatial multiplexing transmission systems are simulated: MIMO FDE CPSC and MIMO OFDM. The main simulation parameters are based on the HIPERLAN/2 standard. For OFDM, this means a 20 MHz bandwith channel with 64 subcarriers, 48 of which are used to carry information symbols. The OFDM symbol duration is 4 us, 0.8 of which are the cyclic prefix. For CPSC, blocks of 64 symbols are sent with a cyclic prefix of 16 symbols at each transmission branch. The symbol duration is 50 ns and a 64-point FFT is employed in equalization. QPSK modulation is analyzed. Both uncoded and coded transmissions are compared. Transmitted symbols are per-antenna coded with an interleaved 1/2 rate convolutional (HIPERLAN/2 standard) code and soft Viterbi decoding is used at reception.

A stochastic MIMO Rayleigh frequency-selective fading channel is used with an rms delay spread of 100ns (channel model B from HIPERLAN/2 specification). The discrete channel impulse responses have exponentially decaying power taps and there is no antenna correlation. Perfect channel knowledge is assumed at reception. Three antenna layouts are compared in order to evaluate how the antenna number and diversity affect BER performance: 1x1 (SISO), 4x4 and 3x4.

Results

The BER performance versus SNR per receive antenna is depicted in Fig. 6 for uncoded QPSK with several antenna setups with no channel correlations and using the MMSE detection technique. MIMO-FDE-CPSC (continuous line) clearly outperforms MIMO-OFDM (dotted line) in uncoded transmissions, as suggested in [3, 4] for SISO systems. When $N = M$ the

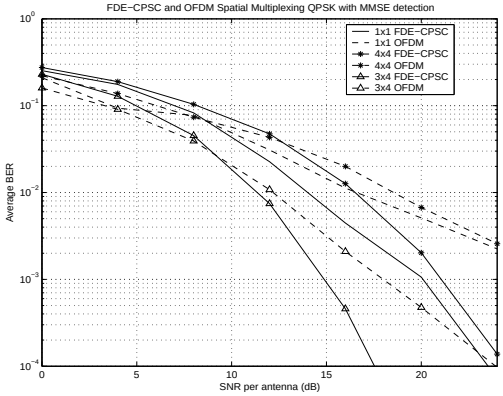

Figure 6: BER performance for uncoded QPSK MIMO FDE CPSC and MIMO OFDM with MMSE equalization.

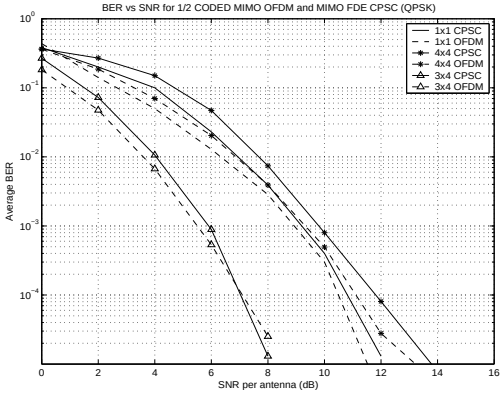

Figure 7: BER performance comparison for coded MIMO FDE CPSC and MIMO OFDM with MMSE equalization.

BER performance degrades slightly with MMSE as the number of transmission and reception antennas grows, but very good BER results can be obtained if reception diversity is increased. For example, the 3x4 antenna setup outperforms the 1x1 BER performance, while transmitting at a three times higher bitrate.

In order to compare OFDM and CPSC, Fig. 7 shows the BER performance results for MIMO coded systems. QPSK modulation and frequency-domain MMSE detection are employed. Coding and interleaving give frequency diversity to OFDM, whose BER performance becomes similar or better to CPSC only for low coding rate frequency-selective systems.

Fig. 8 shows the BER performance results for MIMO coded systems with MMSE-V-BLAST equalization and detection. MMSE-V-BLAST equalization clearly outperforms MMSE, due to the diversity of the OSIC algorithms. The 4x4 antenna setup even outperforms the SISO case at high SNR. OFDM performance (dotted line) is slightly better that FDE CPSC (continuous line). Note that the coding rate used is the lowest of the HIPERLAN/2 standard and that CPSC tends to outperform OFDM as the coding rate grows.

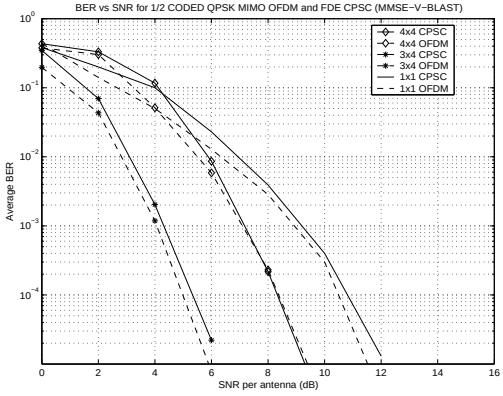

Figure 8: BER performance of MIMO OFDM and FDE CPSC for 3x4, 4x4 and SISO 1/2 coded systems with MMSE-V-BLAST equalization.

VI. Conclusion

We have analyzed the extension and applicability of fundamental MIMO equalization and detection techniques to FDE CPSC systems. ZF, MMSE, ZF-V-BLAST and MMSE-V-BLAST algorithms have been evaluated for FDE CPSC and compared to MIMO-OFDM. BER performance simulations for uncoded and coded QPSK spatial multiplexing systems have been obtained and prove the potential of FDE CPSC MIMO systems. It has been shown that this transmission scheme can equal or outperform MIMO-OFDM in uncoded and high coding rate systems.

References

[1] A. Paulraj, R. Nabar, D. Gore, *Introduction to Space-Time Wireless Communications*, Cambridge University Press, 2003.

[2] A. Van Zelst, T.C.W. Schenk, "Implementation of a MIMO OFDM based Wireless LAN system," *IEEE Transactions on Signal Processing*, vol. 52, no. 2, pp. 483-494, February 2004.

[3] D. Falconer, S. L. Ariyavisitakul, A. Benyamin-Seeyar and B. Eidson, "Frequency Domain Equalization for Single-Carrier Broadband Wireless Systems," *IEEE Communications Magazine*, vol. 40, pp. 58–67, Apr. 2002.

[4] Z. Wang, X. Ma and G.B. Giannakis, "OFDM or Single-Carrier Block Transmissions?," *IEEE transaction on Communications*, vol. 52, no. 3, March 2004.

[5] A. Benjamin-Seeyar, "PHY Layer System Proposal for Sub 11 GHz BWA," *IEEE 802.16 Broadband Wireless Access Working Group,* 2001. http://www.iee802.org/16/.

[6] M. V. Clark, "Adaptive Frequency-Domain Equalization and Diversity Combining for Broadband Wireless Communications," *IEEE Journal on Selected Areas in Communications*, Vol. 16, No. 8, pp. 1385-1395, October 1998.

[7] N. Al-Dhahir, "Single-carrier frequency-domain equalization for space-time block-coded transmissions over frequency-selective fading channels ," *Electronics Letters*, Vol. 5, No. 7, pp. 304-306, July 2001.

[8] G. D. Golden, G. J. Foschini, R. A. Valenzuela, P. W. Wolniansky, "Detection Algorithm and Initial Laboratory Results using the V-BLAST Space-Time Communication Architecture," *Electronic Letters*, Vol. 35, No. 1, pp. 14-15, January 1999.

[9] R. Böhnke, D. Wübben and V. Kühn, "Reduced complexity MMSE detection for BLAST Architectures," *IEEE 2003 Global Communications Conference (Globecom'2003)*, San Francisco, California, USA, December 1-5, 2003.

PERFORMANCE OF FREQUENCY-DOMAIN MIMO EQUALIZATION FOR CYCLIC-PREFIXED SINGLE-CARRIER SPATIAL MULTIPLEXING

Mikel Mendicute, Jon Altuna, John Thompson and Vicente Atxa*

University of Mondragon
Loramendi 4, Mondragon, Spain
phone: +34 943739422, fax: +34 943739410
email: {mmendikute, jaltuna, batxa}@eps.mondragon.edu

*University of Edinburgh
Edinburgh EH93JL, UK
phone: +44 131 650 5585, fax: +44 131 650 6554
email: jst@ee.ed.ac.uk

ABSTRACT

Multiple-Input Multiple-Output (MIMO) signal processing combined with Orthogonal Frequency Division Multiplexing (OFDM) is a widely accepted solution to achieve the high bit rates that new communication standards require in frequency-selective wireless channels. In recent years, a new Frequency-Domain Equalized (FDE) Cyclic-Prefixed Single-Carrier (CPSC) block transmission system has been proven to achieve similar performance to OFDM for coded systems with the same overall complexity, avoiding its main drawbacks and becoming a candidate for future wireless standards. In this paper, a FDE CPSC spatial multiplexing system is analyzed and compared to OFDM. The applicability of different frequency-domain MIMO equalization and detection schemes is evaluated. Simulation-based performance results prove the potential of these techniques and highlight that FDE CPSC can equal or outperform OFDM in uncoded and high coding rate spatial multiplexing systems, as it has been shown in the literature for the SISO case.

1. INTRODUCTION

As new wireless communication network standards are being defined, the demand for higher throughput is growing enormously. Recent wireless local (WLAN) and metropolitan (WMAN) area network standards such as IEEE 802.11a, 802.11g, 802.16a and ETSI HIPERLAN/2 have chosen Orthogonal Frequency Division Multiplexing (OFDM) to overcome the wireless channel's high frequency selectivity. Newer not yet defined WLAN standards, such as 802.11n, aim to reach data rates of up to 300 Mbps. In order to achieve these high bit rates, Multiple-Input Multiple-Output (MIMO) signal processing techniques become necessary.

Two basic approaches have been studied to enhance OFDM with MIMO: Space-Time Coding (STC) and Spatial Multiplexing (SM) [1]. STC increases the diversity order of the communication system by coding over the different transmission antennas, which leads to a better performance. On the other hand, SM transmits independent data streams on each antenna simultaneously, thus allowing greater throughputs [2, 3].

Although OFDM has been included in many standards due to its simple equalization, alternative cyclic-prefixed or zero-padded single-carrier (SC) block transmission techniques have been proposed and developed in recent years [4, 5]. SC transmission avoids OFDM's three main drawbacks: Peak-to-average ratio of the signal power, frequency offset sensitivity and no multipath diversity in uncoded systems. The most simple and interesting of these SC techniques is the Frequency-Domain Equalized (FDE) Cyclic-Prefixed Single-Carrier (CPSC) transmission system. As it can be seen in Fig. 1, its overall complexity is similar to an OFDM system. As the equalization is done in the frequency domain, FFT and IFFT blocks are required in reception. The addition of the cyclic prefix avoids Inter-Block Interference (IBI) and transforms the linear convolution of the signal and the channel into circular, i.e., a product in the frequency domain. This system has been proven to fairly outperform OFDM for uncoded systems and yields similar BER performance in coded transmissions [4]. A very interesting feature of CPSC lies on the fact that the main complexity belongs to the receiver part, so it can be combined with OFDM, allowing asymmetric systems where most of the complexity resides at one side (base station, access point, etc.), as it has been proposed in new 802.16 proposals [6].

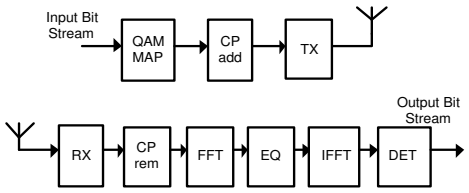

Figure 1: Wireless FDE CPSC transmission and reception systems.

This paper discusses the frequency-domain equalization and detection of CPSC spatial multiplexing systems. The applicability of the main MIMO equalization techniques is analyzed and their implementation is compared to OFDM based MIMO systems. The BER performances of both systems are evaluated with simulations.

The layout of this paper is as follows: Section 2 details the evaluated MIMO equalization techniques. In Section 3 the FDE CPSC-based MIMO transmission and reception systems are introduced. Section 4 shows the most important simulation results and some conclusions are drawn in Section 5.

2. MIMO EQUALIZATION AND DETECTION TECHNIQUES

Fig. 2 shows a single-carrier spatial multiplexing system for a frequency-flat channel with additive white Gaussian noise (AWGN). This model will be extended to a frequency-

Mr. Mendicute's work is partially sponsored by the Dpt. of Education, Universities and Research of the Basque Government through a Researcher Training Grant.

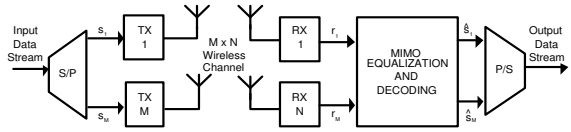

Figure 2: Flat MIMO system

selective channel case in Section 4. The system has M transmit and N receive antennas. The path loss from antenna m to antenna n is represented as h_{nm}. The sampled baseband system of a flat MIMO channel can be represented in matrix notation as:

$$\mathbf{r} = \sqrt{\frac{E_s}{M}}\tilde{\mathbf{H}}\mathbf{s} + \mathbf{n} \tag{1}$$

where $\mathbf{r}$ is an $Nx1$ vector containing the signal received in each antenna, $\mathbf{s}$ is an $Mx1$ vector with the signals transmitted simultaneously at each transmission branch and $\mathbf{n}$ is an $Nx1$ vector containing channel's AWGN. E_s is the transmitted signal power and $\tilde{\mathbf{H}}$ is a NxM channel matrix, defined as:

$$\tilde{\mathbf{H}} = \begin{pmatrix} h_{11} & h_{12} & \dots & h_{1M} \\ h_{21} & h_{22} & \dots & h_{2M} \\ \vdots & \vdots & \vdots & \vdots \\ h_{N1} & h_{N2} & \dots & h_{NM} \end{pmatrix}$$

2.1 Linear non-OSIC MIMO detection

Maximum Likelihood (2) should be the optimal detection method for spatial multiplexing. However, it is computationally too complex due to the calculation of the output of S^M possible input vectors, where S is the number of symbols in the constellation.

$$\hat{\mathbf{s}} = \arg\min_{\mathbf{s}} \left\| \mathbf{r} - \sqrt{\frac{E_s}{M}}\tilde{\mathbf{H}}\mathbf{s} \right\|_F^2 \tag{2}$$

MMSE (Minimum Mean Squared Error) and ZF (Zero-Forcing) [7] are simpler solutions, based in the product:

$$\hat{\mathbf{s}} = \mathbf{G}\mathbf{r} \tag{3}$$

where

$$\mathbf{G}_{ZF} = \sqrt{\frac{M}{E_s}}\tilde{\mathbf{H}}^{+} = \sqrt{\frac{M}{E_s}}(\tilde{\mathbf{H}}^{*}\tilde{\mathbf{H}})^{-1}\tilde{\mathbf{H}}^{*} \tag{4}$$

$$\mathbf{G}_{MMSE} = \sqrt{\frac{M}{E_s}}(\tilde{\mathbf{H}}^{*}\tilde{\mathbf{H}} + \alpha\mathbf{I}_{MxM})^{-1}\tilde{\mathbf{H}}^{*} \tag{5}$$

with $\alpha = NoisePower/SignalPower$. * and $^+$ stand for conjugate transpose and pseudoinverse respectively. MMSE offers much better results than ZF in AWGN channels, but its performance is still quite far from optimal for $N = M$ [7].

2.2 Non-linear V-BLAST (OSIC) detection

An OSIC (Ordered Successive Interference Cancellation) based algorithm has been proposed in [8] to overcome the limitations of previous methods with relatively low complexity and has been named ZF-V-BLAST detection. It is based in the iteration of three steps:

1. Ordering: Determine the transmit antenna k with greatest SNR from the estimated channel, selecting the row $(\mathbf{G})_k$ of smallest norm of the nulling matrix $\mathbf{G}$:

$$k = \arg\min_{k} \|(\mathbf{G})_k\|^2 \quad \mathbf{G} = \mathbf{G}_{ZF} \tag{6}$$

2. Nulling and slicing: Detect transmitted symbol at antenna k $\hat{s}_k$:

$$y_k = ((\mathbf{G})_k)^T\mathbf{r} \tag{7}$$

$$\hat{s}_k = \arg\min_{\hat{s}_k} \|\hat{s}_k - y_k\| \tag{8}$$

3. Cancellation: Remove the effect of the detected symbol from received signal vector and its column $\tilde{\mathbf{H}}_k$ in the channel matrix:

$$\mathbf{r} = \mathbf{r} - \sqrt{\frac{E_s}{M}}\tilde{\mathbf{H}}_k\hat{s}_k \tag{9}$$

$$\tilde{\mathbf{H}}_{nm} = 0 \quad \forall m = k \tag{10}$$

Note that the diversity order increases by one in each iteration. Other V-BLAST detection algorithms such as MMSE-VBLAST or SOMLD (Successive Ordered Maximum Likelihood Detection) differ from ZF-V-BLAST in the calculation of the G matrix in (6) and the ordering criterion [3, 7].

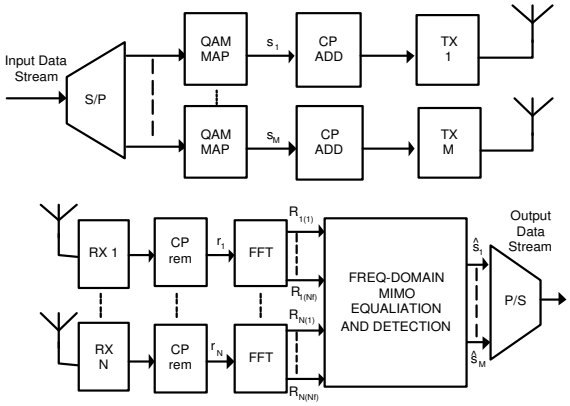

Figure 3: Frequency-Domain Equalized MIMO spatial multiplexing transmission and reception system.

3. FREQUENCY-DOMAIN EQUALIZED CYCLIC-PREFIXED SINGLE-CARRIER MIMO SYSTEM

The baseband flat MIMO channel model in (1) can be easily extended for a L tap frequency-selective channel:

$$\mathbf{r(k)} = \sqrt{\frac{E_s}{M}}\sum_{l=1}^{L}\tilde{\mathbf{H}}(l)\mathbf{s}(k-l) + \mathbf{n}(k) \tag{11}$$

The addition of the cyclic prefix avoids IBI and transforms the linear time convolution of the input signal and the channel response into a circular convolution, thus the model in (11) can be modelled as a product in frequency domain. This way a flat MIMO channel is obtained for each one of the Nf FFT frequency points of Fig. 3:

$$\mathbf{R}(f) = \sqrt{\frac{E_s}{M}}\mathbf{H}(f)\mathbf{S}(f) + \mathbf{N}(f) \tag{12}$$

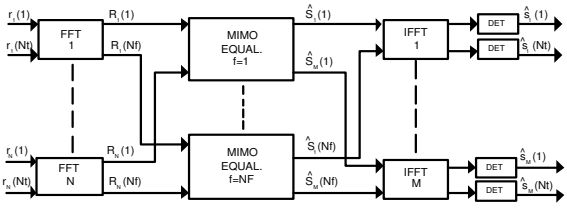

Figure 4: FDE MIMO equalization and detection. A MIMO equalizer is employed at each frequency.

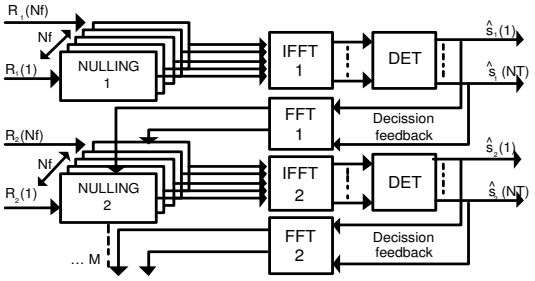

Figure 5: MIMO V-BLAST per-antenna signal detection and decision feedback.

R, **H**, **S** and **N** are the Nf-point FFT transforms of **r**, $\tilde{\mathbf{H}}$, **s** and **n**, respectively. Note that the MIMO equalization is not done on the information bearing symbols $\mathbf{s}(k)$, but on the frequency-domain FFT points $\mathbf{S}(f)$, so an IFFT is required before the symbol detection. This means that all symbols from an antenna must be equalized before they can be detected. This is particularly important for V-BLAST detection, as it will be shown later.

For the MIMO detection techniques that do not require any decision feedback, such as ZF or MMSE, the frequency-domain MIMO detection requires Nf MIMO equalizers, i.e., one for each of the FFT output points, as it can be seen in Fig. 4.

For MIMO equalization techniques requiring detected symbol feedback, such as ZF-V-BLAST or MMSE-V-BLAST, FDE CPSC implies several problematic changes because the IFFT and the FFT operations appear in the feedback chain as it can be seen in Fig. 5. Equations (7) and (8), slicing and cancellation, become:

$$\hat{\mathbf{s}}_k = \arg\min_{\hat{\mathbf{s}}_k} \|\hat{\mathbf{s}}_k - \mathit{ifft}(\hat{\mathbf{S}}_k)\| \tag{13}$$

$$\mathbf{D}_k = \mathit{fft}(\hat{\mathbf{s}}_k)$$

$$\mathbf{R}(f) = \mathbf{R}(f) - \sqrt{\frac{E_s}{M}}\mathbf{H}_k(f)\mathbf{D}_k(f) \tag{14}$$

where $\mathbf{s}_k$ is a whole block transmitted from antenna k in the time domain. **R** and $\hat{\mathbf{S}}$ are frequency-domain received and equalized signal and $\mathbf{D}_k$ is the FFT transform of the detected symbol block $\hat{\mathbf{s}}_k$. As it can be deduced from (13) and (14), the equalization and detection must be done per antenna and in a whole block basis due to the IFFT and FFT operations involved in the feedback chain. Thus, the antenna ordering process in (6) will be done for a whole time block, instead of per each FFT point in the frequency domain, like in OFDM, as it would be desirable to reduce the effects of frequency selectivity. This per-block ordering can slightly reduce the performance improvement of the OSIC (V-BLAST) algorithm.

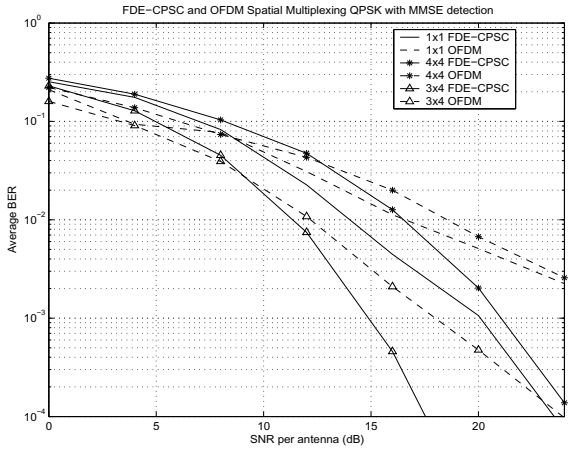

Figure 6: BER performance for uncoded QPSK MIMO FDE CPSC and MIMO OFDM with MMSE equalization.

4. SIMULATION RESULTS

4.1 Simulated System Parameters

Two different spatial multiplexing transmission systems are simulated: MIMO FDE CPSC and MIMO OFDM. The main simulation parameters are based on the Hiperlan/2 standard. For OFDM, this means a 20 MHz bandwith channel with 64 subcarriers, 48 of which are used to carry information symbols and 4 are reserved for pilot tones. The OFDM symbol duration is 4 us, 0.8 of which are the cyclic prefix. For CPSC, blocks of 64 symbols are sent with a cyclic prefix of 16 symbols at each transmission branch. The symbol duration is 50 ns and a 64-point FFT is employed in equalization. QPSK modulation is analyzed. Both uncoded and coded transmissions are compared. Perfect channel knowledge is assumed at reception.

A stochastic MIMO Rayleigh frequency-selective channel [9] is used with an rms delay spread of 100ns (channel model B from Hiperlan/2 specification). The discrete channel impulse responses have exponentially decaying power taps and there is no antenna correlation. Three antenna layouts are compared in order to evaluate how the antenna number and diversity affect BER performance: 1x1 (SISO), 4x4 and 3x4.

4.2 Results

The BER performance versus SNR per receive antenna is depicted in Fig. 6 for uncoded QPSK with several antenna setups with no correlation and MMSE detection technique. MIMO-FDE-CPSC (continuous line) clearly outperforms MIMO-OFDM (dotted line) in uncoded transmissions, as suggested in [4, 5] for SISO systems. When $N = M$ the BER performance degrades slightly with MMSE as the num-

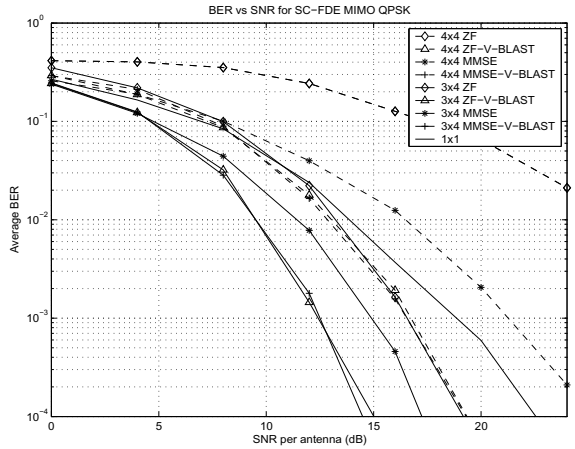

Figure 7: BER performance of the analyzed MIMO detection schemes for 3x4 and 4x4 uncoded FDE-CPSC systems.

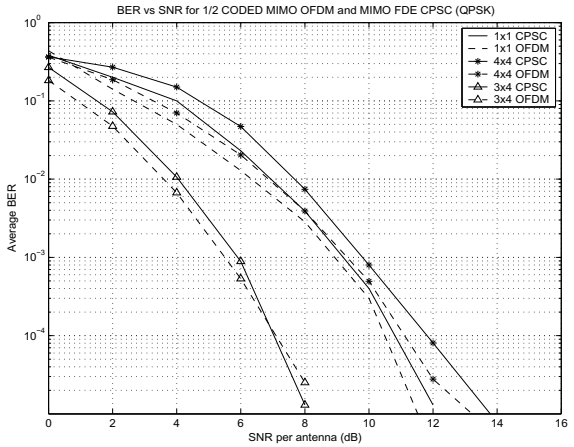

Figure 8: BER performance comparison for coded MIMO FDE CPSC and MIMO OFDM with MMSE equalization.

ber of transmission and reception antennas grows, but very good BER results can be obtained if reception diversity is increased. For example, 3x4 antenna setup outperforms SISO BER transmitting at a three times higher bitrate.

Fig. 7 shows the BER performance of the MIMO equalization schemes analyzed in Section 2 for 4x4 and 3x4 FDE CPSC systems. V-BLAST algorithms are the ones which offer the best performance. The diversity obtained by the OSIC algorithm allows even to outperform the SISO results for high SNR. The effect of including the FFT and IFFT in the decision feedback of V-BLAST detection systems does not degrade their BER performance. MMSE-V-BLAST algorithm performs slightly better than ZF-V-BLAST.

In order to compare OFDM and CPSC, Fig. 8 shows the BER performance results for MIMO coded systems. Transmitted symbols are per-antenna coded (PAC) with an interleaved 1/2 rate convolutional (Hiperlan/2 standard) code. QPSK modulation and frequency-domain MMSE detection are employed. Coding and interleaving give frequency diversity to OFDM, whose BER performance becomes similar or better to CPSC only for low coding rate frequency-selective systems.

5. CONCLUSION

We have analyzed the extension and applicability of fundamental MIMO equalization and detection techniques to FDE CPSC systems. ZF, MMSE, ZF-V-BLAST and MMSE-V-BLAST algorithms have been evaluated for CPSC and compared to MIMO-OFDM. BER performance simulations for uncoded and coded QPSK spatial multiplexing systems have been obtained and compared to OFDM for a frequency-selective Hiperlan/2 standard channel. It has been shown that MIMO equalization can be easily adapted to frequency-domain equalized single-carrier transmission and that this communication scheme can equal or outperform MIMO-OFDM in uncoded and high coding rate systems.

REFERENCES

[1] D. Gesbert, M. Shafi, D. Shiu, P. J. Smith, "From Theory to Practice: An overview of MIMO Space-Time coded Wireless Systems" *IEEE Journal on Selected Areas in Communcations*, vol. 21 no. 3 pp. 281-303, April 2003.

[2] A. Paulraj, R. Nabar, D. Gore, *Introduction to Space-Time Wireless Communications*, Cambridge University Press, 2003.

[3] A. Van Zelst, T.C.W. Schenk, "Implementation of a MIMO OFDM based Wireless LAN system" *to be published in IEEE Transactions on Signal Processing.*

[4] D. Falconer, S. L. Ariyavisitakul, A. Benyamin-Seeyar and B. Eidson, "Frequency Domain Equalization for Single-Carrier Broadband Wireless Systems" *IEEE Communications Magazine*, vol. 40, pp. 58–67, Apr. 2002.

[5] Z. Wang, X. Ma and G.B. Giannakis, "OFDM or Single-Carrier Block Transmissions?" *To appear in IEEE transaction on Communications, 2004.*

[6] A. Benjamin-Seeyar, "PHY Layer System Proposal for Sub 11 GHz BWA" *IEEE 802.16 Broadband Wireless Access Working Group, 2001.* http://www.iee802.org/16/.

[7] R. Böhnke, D. Wübben and V. Kühn, "Reduced complexity MMSE detection for BLAST Architectures", *IEEE 2003 Global Communications Conference (Globecom'2003), San Francisco, California, USA, December 1-5, 2003.*

[8] G. Foschini, "Layered Space-Time architecture for wireless communications in a fading environment when using multi-element antennas" *Bell Labs Technical Journal*, Autumn 1996.

[9] K.I. Pedersen, J.B. Andersen, J.P. Kermoal, P.E. Mogensen, "A stochastic Multiple-Input Multiple-Output radio channel model for evaluation of space-time codes" *Proc IEEE VTC 2000 Fall*, Boston, 2000.

BLIND CO-CHANNEL INTERFERENCE MITIGATION IN CP-SC-FDE FOR 2-11 GHZ BROADBAND WIRELESS SYSTEMS

Jon Altuna, Mikel Mendikute, Vicente Atxa and Jose Mª Zabalegui
University of Mondragón, Department of Electronics
20500 Mondragon, (Spain)
{jaltuna, mmendikute, batxa, jmzabalegui}@eps.mondragon.edu

Abstract

This paper addresses the problem of (semi-) blind channel estimation and equalization for 2-11 GHz Fixed broadband Wireless Access (FBWA) systems in the presence of co-channel interference. In particular, a (semi-) blind technique is proposed which combines a subspace technique for blind channel estimation and cyclostationary statistics. It will be shown that the proposed technique provides consistent estimates of the broadband wireless propagation channel in the presence of interference and is shown to outperform other similar blind subspace-based techniques using conventional second-order statistics or cyclostationary statistics.

Keywords
(Semi-) blind channel estimation, cyclostationary signals, single carrier systems, frequency domain equalization.

1. INTRODUCTION

The increasing demand for high spectral efficiency in broadband wireless communications where multipath delay spread is a major transmission problem has motivated the design of (semi-)blind equalization techniques which require little or no knowledge of the transmitted sequence. A number of blind channel estimation and equalization techniques have been proposed in the literature, which rely on some statistical properties or algebraic structure of the received cyclostationary signal [3]. In particular, several subspace techniques have been proposed for blind and semi-blind channel identification and equalization after the pioneering work by Moulines *et al.* [3] which have been applied for single-carrier systems [6] and multicarrier systems [4]. These techniques are attractive due to their efficiency in terms of the amount of data needed to estimate the propagation channel. Several combinations of subspace techniques and cyclostationary estimation have been proposed in the literature [7][8][9] which exploit the ability of cyclostationary statistics to mitigate the effect of interference from co-channel users on channel estimation.

The technique proposed in this paper combines cyclostationary statistics measured in terms of both the cyclic and conjugate cyclic autocorrelation functions and subspace techniques. It is shown that performance improvements can be obtained when these are combined in comparison with other similar techniques which either rely on the cyclic or the conjugate cyclic autocorrelation functions due to the ability to handle circular and non-circular signals [8]. The proposed blind method is concerned with the ability to mitigate the contribution of jammer signals in the estimation of the propagation channel of the signal of interest, provided that they exhibit different cyclostationary signatures.

In particular, this paper addresses the problem of (semi-)blind channel estimation and equalization for 2-11 GHz broadband wireless systems. The proposed blind channel estimation technique is robust in the presence of co-channel interference and it is suitable for *cyclic-prefixed* (CP) *single-carrier* (SC) *frequency-domain equalization* (FDE) [1]. CP-SCFDE is based on the insertion of a cyclic prefix in each transmitted block of data to remove interblock interference like in OFDM and the main advantage compared to OFDM system is the reduced peak-to-average ratio requirements with similar receiver processing complexity. This technique has recently been proposed as an alternative to uncoded OFDM or low coding rate systems and has been adopted as a PHY standard for Wireless Metropolitan Area Networks (WMAN) IEEE 802.16 (Std 802.16a-2003).

2. SYSTEM ARCHITECTURE

The FBWA systems for Local and Metropolitan Area Networks under study can adopt Point-to-Multipoint (PMP) and Mesh operation modes. In PMP mode, traffic from terminal equipment (TE) is forwarded through

Subscriber Stations (SS) to Base Stations (BS), whereas in Mesh mode, traffic can be routed through other SSs and can occur directly between SSs. The main source of interference comes from the coexistence of BSs from different operators transmitting simultaneously under the coverage of the main beam of the victim BS antenna. Another important source of interference is related to SS-to-BS interference, where one or several SS can be transmitting simultaneously with the desired SS. The problem of interference has been subject to a recommendation and it has been established that an acceptable level would require co-channel interference to be 6 dB below the receiver thermal noise (i.e., I/N$\leq$-6 dB)[5].

Both DL and UL operations require data to be formatted into Bursts as shown in Figure 1. A *Unique Word* (UW) is inserted in the Burst Preamble (BP) for synchronisation and equalizer initialization purposes and it also serves as a cyclic prefix for inter-block interference cancellation [1]. Frank-Zadoff or Chu sequences originally conceived for synchronization of radar systems are used in the UW because they exhibit zero correlation at non-zero correlation lags.

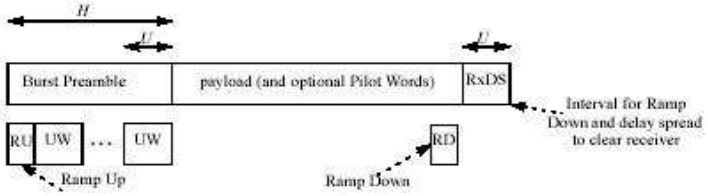

Figure 1. Framed Burst Format.

3. (SEMI-) BLIND CHANNEL ESTIMATION

Figure 2 describes the baseband system model of a CP-SC FDE system [1]. A multichannel model is proposed, where a discrete-time input sequence $x(k)$ is received by K antennas. The received signal at the ith antenna element is converted to the frequency domain (FD) after the cyclic prefix has been removed. Equalization is performed in the FD and proper decoding and detection is carried out in the time-domain. The (semi-) blind channel estimation algorithm samples the received signal at a rate P times faster than the source symbol rate and is formulated as:

$$\underline{y}_k^{(i)} = \mathrm{H}_N^{(i)} \underline{x}_k + \underline{v}_k^{(i)} \tag{1}$$

and

$$\mathrm{H}_N^{(i)} = \begin{pmatrix} h_0^{(i)} & & h_M^{(i)} & 0 & & 0 \\ 0 & h_0^{(i)} & & h_M^{(i)} & 0 & 0 \\ & & & & & \\ 0 & & & 0 & h_0^{(i)} & h_M^{(i)} \end{pmatrix} \tag{2}$$

where $h_k^{(i)} \overset{\text{def}}{=} h^{(i)}(k)$ are the coefficients of the ith subchannel, M+1 is the length of the subchannel impulse response and N is the length of the observation window, both multiples of the oversampling factor P. On the other hand, $\underline{x}_k = [x(k), x(k-1), \quad , x(k-N-M+1)]^{\mathrm{T}}$ is the (N+M)x1 vector which contains the oversampled input sequence $x(k)$, $\underline{y}_k^{(i)} = [y^{(i)}(k), y^{(i)}(k-1), \quad , y^{(i)}(k-N+1)]^{\mathrm{T}}$ represents the Nx1 received signal vector and $\underline{w}_k^{(i)}$ is the noise vector at the ith antenna.

3.1 Channel identification using cyclostationary statistics and subspaces

Let us first define the autocorrelation function of the oversampled input sequence $x(k)$ as:

$$R_x(k,m) = E\{x(k+m)x^*(k)\} = R_x(k+P,m) \tag{3}$$

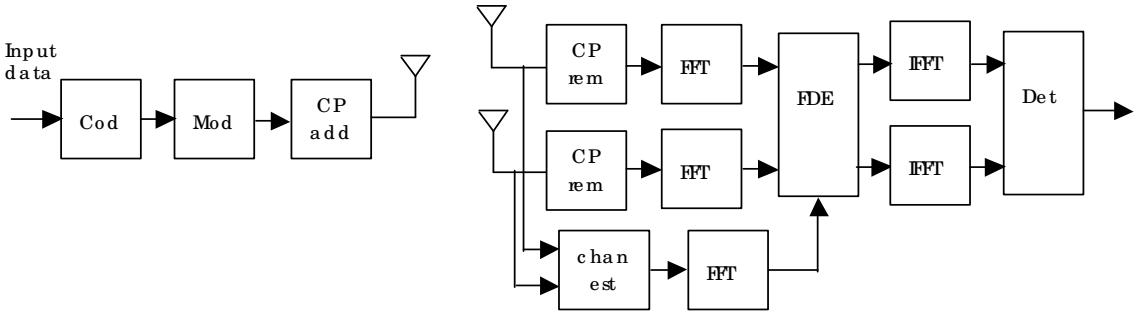

Figure 2. Cyclic Prefixed SC-FDE system block diagram.

which is periodic in k with period P. The cyclic autocorrelation function of the input sequence $x(k)$ can be defined in terms of the Fourier series coefficients of the autocorrelation function

$$R_x(m) = \frac{1}{P}\sum_{k=0}^{P-1} E\{x(k+m)x^*(k)\}e^{-j2\ k} \tag{4}$$

where is a set of frequencies known as the cyclic frequencies [2]. Similarly, the conjugate cyclic autocorrelation can be defined as:

$$R_{xx^*}(m) = \frac{1}{P}\sum_{k=0}^{P-1} E\{x(k+m)x(k)\}e^{-j2\ k} \tag{5}$$

From equation 4, the signal $x(k)$ is said to be wide-sense cyclostationary with period P if there is a non-zero cyclic frequency for which the Fourier coefficients $R_x(m)$ are non-zero. The autocorrelation matrix $\underline{R}_x(k) = E\{\underline{x}_k \underline{x}_k^H\}$ of the zero-padded input sequence $x(k)$ is a diagonal matrix with P-1 zeros interspersed between two non-zero elements defined as:

$$\begin{aligned}
\underline{R}_x(0) &= \mathrm{diag}[\ \sigma_x^2\ \underbrace{0\ \cdots\ 0}_{P-1\,\text{zeros}}\ \sigma_x^2\ 0\ \cdots\ 0\ \sigma_x^2\ 0\ \cdots\ ] \\
\underline{R}_x(1) &= \mathrm{diag}[\ 0\ \sigma_x^2\ 0\ \underbrace{0\ \cdots\ 0}_{P-1\,\text{zeros}}\ \sigma_x^2\ 0\ \underbrace{0\ \cdots\ 0}_{P-1\,\text{zeros}}\ \sigma_x^2\ \cdots\ ] \\
\underline{R}_x(m) &= \mathrm{diag}[\ \underbrace{0\ \cdots\ 0}_{m\,\text{zeros}}\ \sigma_x^2\ 0\ \cdots\ 0\ \sigma_x^2\ 0\ \cdots\ 0\ \sigma_x^2\ 0\ \cdots\ ]
\end{aligned} \tag{6}$$

and thus, following equation 4 we might express

$$\underline{R}_x = \mathrm{diag}[\ 1\ \ e^{-j2\ \ }\ \cdots\ e^{-j2\ \ k}\ \cdots\ e^{-j2\ \ (P-1)}\ ]\ \frac{\sigma_x^2}{P} \tag{7}$$

Since the magnitude of each element on the leading diagonal is nonzero, $\underline{R}_x$ is full rank for all . On the other hand, the output autocorrelation matrix as in [3] can be expressed as:

$$\underline{R}_y(k) = E\{\underline{y}_k \underline{y}_k^H\} = \mathrm{H}_N \underline{R}_x(k)\mathrm{H}_N^H + \underline{R}_w \tag{8}$$

where $\underline{R}_w$ is the autocorrelation matrix of the stationary noise process. By definition, using equations 8 and 4, an expression for the received signal cyclic autocorrelation matrix can be formulated as:

$$\begin{aligned}
\underline{R}_y &= \frac{1}{P}\sum_{k=0}^{P-1} \mathrm{H}_N \underline{R}_x(k)\mathrm{H}_N^H e^{-j2\ \ k} + \frac{1}{P}\sum_{k=0}^{P-1} \underline{R}_w e^{-j2\ \ k} \\
&= \frac{1}{P}\mathrm{H}_N \left\{\sum_{k=0}^{P-1} \underline{R}_x(k) e^{-j2\ \ k}\right\}\mathrm{H}_N^H + \frac{1}{P}\underline{R}_w \sum_{k=0}^{P-1} e^{-j2\ \ k} \\
&= \mathrm{H}_N \underline{R}_x \mathrm{H}_N^H + \frac{1}{P}\underline{R}_w \sum_{k=0}^{P-1} e^{-j2\ \ k}
\end{aligned} \tag{9}$$

From this, for $= 0$

$$\underline{R}_y^0 = \mathrm{H}_N \underline{R}_x^0 \mathrm{H}_N^H + \underline{R}_w \tag{10}$$

is the received signal average autocorrelation matrix but more importantly, for $\neq 0$,

$$\underline{R}_y = \mathrm{H}_N \underline{R}_x \mathrm{H}_N^H \qquad = \frac{l}{P} \quad l \neq nP, \qquad l, n \in Z \tag{11}$$

The *Singular Value Decomposition* (SVD) of the received signal autocorrelation matrix of equation 8 as in [3] or the received signal cyclic or conjugate cyclic of equation 11 as in [7][9], provides subspace information on the signal subspace which can be used for blind channel estimation up to an scalar factor. Similarly to the formulation presented in [8], a cyclic and conjugate cyclic correlation matrix can be expressed as:

$$\underline{R}_{C,y} = \begin{bmatrix} \underline{R}_y & \underline{R}_{yy^*} \\ \underline{R}_{yy^*}^* & \underline{R}_y^* \end{bmatrix} = \begin{bmatrix} \mathrm{H}_N & \underline{0} \\ \underline{0} & \mathrm{H}_N^* \end{bmatrix} \begin{bmatrix} \underline{R}_x(\ ) & \underline{R}_{xx^*}(\ ) \\ \underline{R}_{xx^*}^*(\ ) & \underline{R}_x^*(\ ) \end{bmatrix} \begin{bmatrix} \mathrm{H}_N & \underline{0} \\ \underline{0} & \mathrm{H}_N^* \end{bmatrix}^H = \underline{C}\underline{R}_{C,x}\underline{C}^H \tag{12}$$

The identification of the channel coefficients is based on the SVD of the 2*KN*x2*KN* $\underline{R}_{C,y}$ matrix. Provided that the filtering matrix H_N meets the full column-rank condition [3], the eigenvectors associated with the non-zero eigenvalues span the *signal subspace* and form the signal eigenvectors matrix $\underline{S}$, whereas the eigenvectors associated with the last eigenvalues for $\neq 0$ span the *null-subspace* and collectively form the null-space eigenvector matrix $\underline{G}$. Due to the orthogonality between the columns of matrix $\underline{S}$ and $\underline{G}$ we can conclude that any vector from the null subspace is orthogonal to any column vector in the signal subspace and by extension to any column of the filtering matrix $\underline{C}$

$$\underline{g}_i^H \underline{C} = 0 \qquad 0 \le i < 2.(KN - N - M) - 1 \tag{13}$$

When only sample estimates of the received signal cyclic and conjugate cyclic autocorrelation matrices are available, the set of linear equations of equation 13 can be solved in the least squares sense, as the minimization of the following quadratic form:

$$q = \sum_{i=0}^{2(KN-M-N)-1} |\underline{g}_i^H \underline{C}|^2 \tag{14}$$

Note that for a circular signal, i.e. $E\{x(k+m)x(k)\} = 0$, the conjugate cyclic autocorrelation is null for all *k* and *m*. On the other hand, if the signal is spatially and temporally white, i.e. $E\{x(k+m)x^*(k)\} = {}^2_x\underline{I}\ (m)$, following equation 4 and the derivation to 9, the cyclic autocorrelation of the input signal becomes null for all *k* and *m*. Additive white Gaussian noise is circular and white and will be therefore cancelled from any measurement of the received signal cyclic or conjugate cyclic autocorrelation functions for a sufficiently large observation window.

In this context, it is particularly interesting the fact that some non-circular signals have both non-zero cyclic and conjugate cyclic autocorrelation. In the case of modulation types such as BPSK, where both the cyclic and conjugate cyclic autocorrelation are the same, the rank of the source signal cyclic and conjugate cyclic autocorrelation matrix of equation 12 is essentially the rank of $\underline{R}_x$, i.e. *M*+*N*. However, if the magnitude of the cyclic and conjugate cyclic are different or one of them is zero, the rank of $\underline{R}_{C,x}$ is double. It is apparent that this method only performs better than the method using the received signal conjugate cyclic autocorrelation when the input signal is non-circular and is robust not only in the presence of AWGN but also in the presence of circular interfering signals, which was also observed in [8].

4. SIMULATION RESULTS.

Simulations were conducted to observe the performance of different channel estimation algorithms in a WirelessMAN-SCa scenario. The source signal from the desired user is a 4 Mbps BPSK signal which is received by *K*=4 antennas and the sampling frequency is 12 MHz. The number of data symbols in a burst is 1024 and a Frank-Zadoff sequence of length 64 is used as UW. A SUI-3 channel model was used in the simulations with antenna correlation at the receiver. A training-based LS algorithm, the conventional subspace blind channel estimation method [3], the subspace approach proposed in this paper using both the cyclic and conjugate cyclic autocorrelation functions and only using the conjugate cyclic autocorrelation are compared in terms of the *mean-squared error* (MSE) for a *I/N*≤-6 dB interference scenario. A single 3 Mbps QPSK modulated signal co-channel interferer signal is considered. Both the cyclic and conjugate cyclic autocorrelation functions were evaluated for a cycle frequency $= 4$ MHz, the degree of ISI is $M = 3$ and the width of the temporal window is

$N = 4$. Figure 3 shows a detail of the convergence of the algorithms and it is observed that for the simulated interference scenario, the proposed technique is able to track the channel characteristics correctly and achieves a lower MSE than the rest. It can also be observed that the same blind technique using only the conjugate cyclic autocorrelation function and the conventional blind subspace techniques are unable cannot achieve a desirable channel estimate.

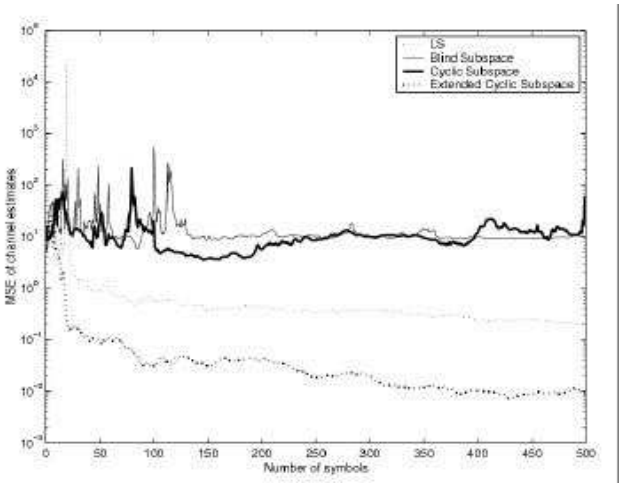

Figure 3. Convergence of channel estimation algorithms in a $I/N \leq$ -6 dB interference scenario.

5. CONCLUSIONS

This paper presents a new approach for blind channel identification in the presence of interfering signals using a different cyclostationary signature from the desired signal. Although conventional multichannel subspace based blind channel estimation techniques are in general more data efficient than purely statistical methods, the combination of cyclostationary statistics measured in terms of both the cyclic and conjugate cyclic autocorrelation and subspace methods can produce consistent estimates of the channel in the presence of jammer signals. It has been shown that the proposed method achieves better performance than the blind subspace methods using only the conjugate cyclic autocorrelation in the presence of signals with nonzero cyclic and conjugate cyclic statistics and are appropriate for CP-SC broadband wireless systems.

References

[1] D. Falconer, S.L. Ariyavisitakul, A. Benyamin-Seeyat and B. Eidson, "Frequency Domain Equalization for Single-Carrier Broadband Wireless Systems", *IEEE Communications Magazine*, pp. 58-66, April 2002.

[2] W.A. Gardner, Cyclostationarity in Communications and Signal Processing, IEEE Press, 1st edition, 1994.

[3] J. Cardoso E. Moulines, P. Duhamel and S. Mayrargue, "Subspace methods for the blind identification of multichannel FIR filters", *IEEE Transactions on Signal Processing*, Vol 43(2),pp 516-525, February 1995.

[4] S. Zhou, B. Muquet and G.B. Giannakis, "Subspace-Based (Semi-) Blind Channel Estimation for Block Precoded Space-Time OFDM", *IEEE Transactions on Signal Processing*, Vol 50(5),pp 1215-1228, May 2002.

[5] IEEE 802.16a, "Air Interface for Fixed Broadband Wireless Access Systems. Part A: Systems between 2-11 GHz".

[6] V. Buchoux, O. Cappe, E. Moulines, A. Gorokhov, "On the performance of semi-blind subspace-based channel estimation", *IEEE Transactions on Signal Processing* , Vol 48(6), pp 1750-1759, June 2000.

[7] L. Deneire and D.T.M. Slock, "Blind channel identification based on cyclic statistics", *IEE Proceedings on Radar, Sonar and Navigation*, Vol: 145, Issue: 1, pp. 58-62, February 1998.

[8] D. Darsena, G. Gelli, L. Paura and F. Verde, "Widely linear subspace-based blind identification of SISO FIR systems with improper random inputs", Proc. of 6th Bayona Workshop on Signal Processing in Communications, pp. 109-114, Bayona (Spain), September 2003.

[9] A. Chevreuil and Ph. Loubaton, "MIMO blind second-order equalization method and conjugate cyclostationarity", *IEEE Transactions on Signal Processing*, Vol 47(2),pp 572-578, February 1999.

PLATFORM FOR JOINT EVALUATION OF FPGA-IMPLEMENTED AND MATLAB ALGORITHMS IN REAL MIMO TRANSMISSIONS

Mikel Mendicute, Jon Altuna, Gorka Landaburu and Vicente Atxa

Communications and Digital Signal Processing Area, Department of Electronics
University of Mondragon
Loramendi 4, Mondragon, Spain
e-mail: {mmendikute, jaltuna, glandaburu, batxa}@eps.mondragon.edu

Keywords: MIMO, FPGA, Implementation, Real-Time.

Abstract

This contribution describes a MIMO simulation and validation platform suitable for a progressive implementation of real-time signal processing algorithms. We describe a platform which allows to share Matlab, simulated VHDL and hardware designs while transmitting through a real MIMO channel. The applicability and first results of this platform are shown for a narrowband 2x2 spatial multiplexing system operating in the 2.4 GHz band.

1 Introduction

MIMO (Multiple-Input Multiple-Output) transmission techniques have become the main solution to achieve the high bit rates required by new communications standards. For example, the emerging 802.11n proposals aim to reach data rates of up to 300 Mbps employing techniques such as spatial multiplexing or space-time coding [4].

The main disadvantages of MIMO techniques lie on the multiplication of the required hardware, due to the number of transmission and reception chains, and on the complexity linked to the multi-antenna signal processing algorithms. The latter has led to many "off-line" MIMO implementations, i.e., systems where real signals are transmitted and processed employing excessive time and resources, such as computers running Matlab. Due to the imminent inclusion of these techniques in new standards and prototypes, the real-time cost-effective implementation of these algorithms is becoming crucial [8][2].

This contribution presents a flexible platform suitable for a progressive transition from Matlab simulated to FPGA-DSP based real-time MIMO algorithms through an intuitive and reliable flow, which is summarized in Fig. 1.

This platform has the following main features:

- It allows a flexible combination of Matlab/Simulink code and simulated or FPGA-running VHDL implementations.
- The simulated FPGA algorithms can run with limited fixed point or full Matlab double resolution.

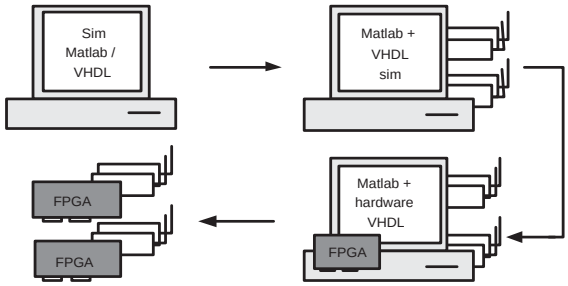

Fig. 1. States of a progressive transition from simulated to hardware-implemented real-time MIMO signal processing algorithms.

- Real transmissions or a simulated MIMO channel can be used.

The layout of this paper is as follows: Section 2 shows the main characteristics of the selected MIMO model and algorithms. Section 3 gives a detailed description of the platform and its main elements. The most interesting application examples are shown in Section 4, while conclusions and future work lines are drawn in Section 5.

2 MIMO model and algorithms

2.1 System model

Fig. 2 shows the basic 2x2 MIMO spatial multiplexing model which has been selected and implemented in order to test the validity of the platform. The transmitted bits are split into two streams which are transmitted independently and received synchronously at two receiver antennas. A low-rate flat channel has been chosen as a first approach. A 50 Ksps (Kilosymbols per second) rate has been used to ensure the flat channel assumption.

A complete Matlab-based model has been created and adapted to Simulink. A MIMO Rayleigh channel has been used and a short frame based burst transmission system has been assumed. The correlation degree of the transmitter and receiver antenna gains has been included in the model, allowing the simulation of different distances between the antennas [6]. A preamble is transmitted to allow simpler synchronization and channel estimation algorithms.

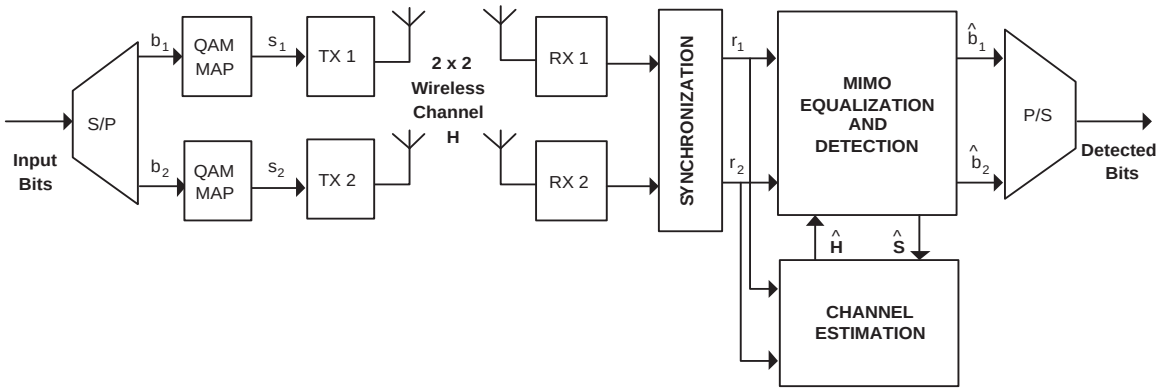

Fig. 2. Structure of a basic 2x2 MIMO spatial multiplexing system.

2.2 Algorithms

The following algorithms have been implemented in Matlab and Simulink in order to apply the aforementioned MIMO model to real signals:

- *Frame synchronization*: a multi-antenna extension of the double-sliding window technique has been applied [3].
- *Sample-time synchronization*: an ML (Maximum Likelihood) approach has been chosen [5].
- *Frequency Offset Estimation*: a reduced complexity iterative offset estimation technique has been used [7].
- *Channel Estimation*: basic training-based MIMO channel estimation techniques, such as LS (Least-Squares) and MMSE (Minimum Mean Squared Error) have been implemented.
- *MIMO Detection*: the following detection techniques have been included in the model: ZF (Zero-Forcing, MMSE (Minimum Mean Squared Error), ML and V-BLAST (Vertical Bell-Labs Layered Space-Time) [1].

3 Description of the platform

The system described in this document is based on a computer with the following elements:

- Vector signal generators and dual-band (2.4 and 5 GHz) RF tranceivers.
- PCI-based analog signal acquisition and generation cards.
- Hunt's DSP and FPGA fast prototyping modular Heron boards.
- Simulation software: Matlab, Simulink and ModelSim.
- FPGA design, synthesis and programming software: Xilinx System Generator, Xilinx ISE and Heron Tools.

3.1 RF transceivers and signal generators

The platform is equipped with Maxim's MAX2827EVKit boards, which can transmit or receive RF signals in the 2.4 GHz and 5 GHz bands. These boards are able to modulate and demodulate baseband IQ signals of up to 20 MHz employing a 40 MHz reference, which must be synchronized for all the transceivers from the same side of the communication. This solution avoids the need of implementing modulation and demodulation algorithms, but requires two analog signals to be generated or acquired from a transceiver.

The number of analog ports can be reduced when needed if a modulated signal is generated and up-converted employing equipment such as signal generators. For example, the combination of signal generators and the aforementioned transceivers allows the implementation of a 2x3 system employing two analog outputs and six analog inputs, all managed from a computer running Matlab.

3.2 Acquisition and generation boards

The platform is equipped with an Acquitek CH-3150 PCI board, which allows to generate two analog signals with 12 bits resolution and 20 MSPS (Mega Samples Per Second). The main features of the board include two analog inputs, 16 MB of memory and many programming interfaces. One of these interfaces allows to access directly to the board from a Matlab simulation.

A PCI-based Adlink 9812A analog acquisition board has also been included, which allows to acquire up to 4 analog signal with 12 bits resolution and 20 MSPS. The synchronized combination of this board and the aforementioned generation card provides a Matlab-based off-line transmission system with 2 outputs and 6 inputs, which can be helpful to test the validity of the Matlab algorithms with real signals.

3.3 Fast prototyping boards

The platform contains two modular fast prototyping Heron HEPC9 boards from Hunt Engineering, which will be used

to develop and test the implementation of real-time signal processing algorithms. These PCI-based boards have an absolutely flexible architecture based on an internal bus that allows communications of 400 MBps between the modules. These carrier boards have been equipped with the following modules:

- Two HERON-IO2V2 modules with 4 analog inputs and 4 analog outputs of up to 125 MSPS with 12 and 14 bits of resolution, respectively. These modules provide many digital ports and a VirtexII FPGA of 1M gates and allow real-time in-system debugging through JTAG interface employing Xilinx Chipscope. This JTAG interface even allows to co-simulate Simulink, System Generator and Xilinx hardware. Apart from the real-time application, these modules can be used off-line as signal generation or acquisition tools if a higher than 20 MSPS sampler rate is required.
- Two HERON-FPGA3 modules with a VirtexII FPGA of 1M gates.
- Two HERON-C6701 modules, which carry a Texas Instruments TMS320C6701 16-bit floating point DSP processor running at 167 MHz.

These HEPC9 boards are controlled through an API that allows to configure the system, program the Xilinx FPGAs and communicate with the board. A C-based application has been developed to send bit streams to and from the board in real-time implementations.

3.4 Design, synthesis and simulation software

Simulink and Xilinx System Generator have been selected as the main design tools to allow co-simulation of Matlab algorithms and simulated VHDL hardware designs. This solution, offers a simple and intuitive GUI-based hardware design and simulation tool for DSP algorithm engineers, achieving a balance between hardware abstraction level and performance.

System Generator environment allows to run a selected part of the algorithms on real hardware through a JTAG interface. Simulation of existing or standard IP cores, such as those provided by Xilinx Core Generator, can also be included in the simulation through System Generator's ModelSim blackbox.

A Simulink MIMO system has been developed including Matlab algorithms through S-function blocks and has been progressively translated to a System Generator architecture, allowing parallel simulation of ideal Matlab algorithms and hardware blocks. Once the algorithms have been tested in Simulink, VHDL netlist designs have been automatically created with System Generator and translated to a Xilinx ISE project, which has been used to manage and synthesize the final design.

4 Application examples

This platform has many modes of operation and can be used in several stages of the implementation of a wireless system. The following subsections show the most representative application examples.

4.1 Matlab/Simulink-based MIMO off-line transmission

Fig. 3 summarizes a 2x2 system transmitting real frames, which are processed off-line in Matlab. The transmitted signals are created and modulated in an intermediate frequency by Matlab and up-converted to the 2.437 band using synchronized signal generators.

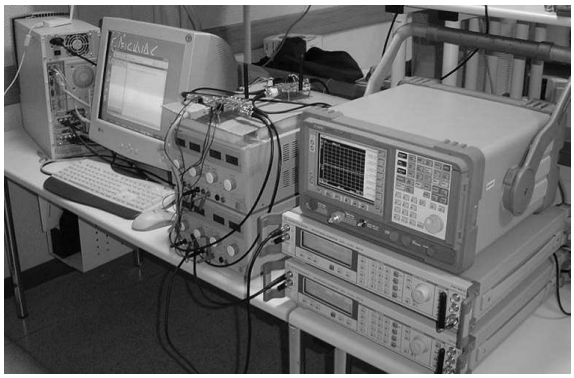

Fig. 3. Platform for off-line evaluation of a frame-based wireless MIMO system.

The transmitted signals are received in two of the Maxim's RF transceivers, which down-convert and demodulate the signal generating 2 baseband IQ stream pairs to be acquired by 4 analog inputs. This system allows to test off-line the selected MIMO algorithms with real transmitted bursts.

4.2 Co-simulation of Matlab/Simulink and VHDL designs

Fig. 4 shows a Simulink model which has been used to evolve from a matlab implementation to a full System Generator implementation of a MIMO receiver for the system described in the previous section. As can be seen in Fig. 4, some of the processes are coded in Matlab and included in Simulink through S-function interface blocks. The whole receiver has been implemented using System Generator Blocks.

This configurations allows to execute the Matlab-coded receiver algorithms in parallel with the System Generator implementation, even running on-chip through the JTAG interface. This makes it possible to compare results such as the channel estimation error or bit error rates for the ideal Matlab algorithms and the implemented solutions. Note that this co-simulation can be combined with the aforementioned real transmissions if necessary.

4.3 Complete real time implementation

As stated before, this platform offers a relatively cost-effective, easy and safe flow towards the FPGA implementation of real-time MIMO algorithms. Once all the algorithms

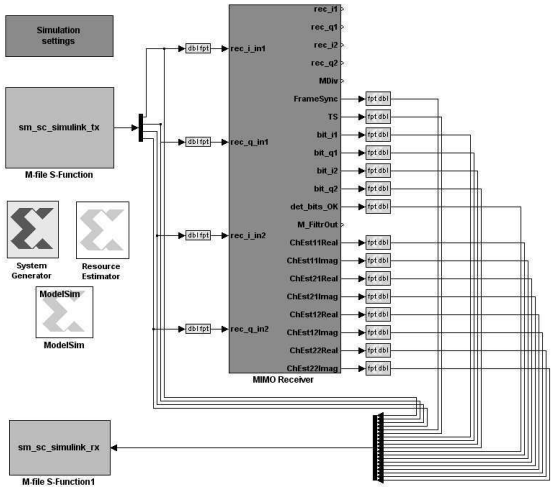

Fig. 4. Simulink/System Generator model which allows test real FPGA implementations in Matlab-based systems.

are tested and co-simulated with the Simulink-based platform, the receiver and transmitter systems can run stand-alone on the Heron HEPC9 boards, which are connected directly to the RF transceivers.

Fig. 5 shows a diagram of the HEPC9 implementation of the 2x2 MIMO transceiver with the distribution of the signal processing algorithms through the Heron modules available. Note that the capacity of this platform has been already shown in [2] for the development of a MIMO-OFDM wireless modem prototype.

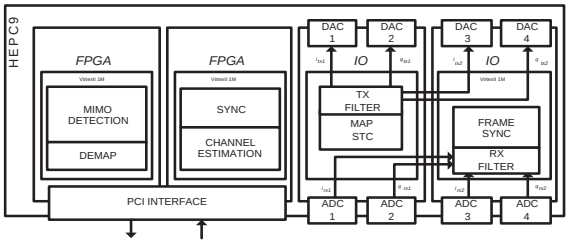

Fig. 5. Structure of a 2x2 real-time MIMO implementation on the Heron modules of the HEP9 board.

5 Conclusion and future work

This contribution describes a simulation and hardware validation platform suitable for a progressive implementation of a real-time MIMO wireless system. A platform has been described which allows to share Matlab, simulated VHDL and real hardware designs while transmitting through a real MIMO channel. A Simulink-based simulation platform has been developed using Xilinx System Generator, which is a relatively simple and effective solution from a DSP designer's point of view.

The applicability and first results of this platform have been shown for a narrowband 2x2 spatial multiplexing system operating in the 2.4 GHz band. A Matlab model has been progressively translated to Xilinx System Generator blocks and validated through simulation. Finally, a real-time implementation of the generated VHDL designs has been implemented on hardware to validate the whole design flow.

This platform is expected to host the real-time implementation of a more realistic wideband MIMO system, based in multicarrier techniques and frequency-domain equalization. This platform will also be the tool to design and validate implementation aspects of specific signal processing and codification algorithms.

Acknowledgments

The first author's work is partially sponsored by the Department of Education, Universities and Research of the Basque Government through a Researcher Training Grant.

References

[1] G. D. Golden, G. J. Foschini, R. A. Valenzuela, P. W. Wolniansky, "Detection Algorithm and Initial Laboratory Results using the V-BLAST Space-Time Communication Architecture " *Electronics Letters, Vol. 35, No. 1, Jan. 7, 1999, pp. 14-15, 1999*

[2] S. Häne, D. Perels et al., "Implementation Aspects of a Real-Time Multi-Terminal MIMO-OFDM Testbed" *IEEE Radio and Wireless Conference (RAWCON)*, Atlanta, GA, Sept. 2004.

[3] J. Heiskala, J. Terry, *OFDM Wireless LANs: A Theoretical and Practical Guide*, Indiana, U.S.A.: Sams Publishing, 2002. ISBN:0-672-32157-2

[4] C. Kose, B. Edwards, et al., IEEE 802.11/05-0149-01-000n, "WiSE group PHY and MAC specification,"

[5] A.F. Naguib, V. Tarokh et al., "A Space-Time Coding Modem for High-Data-Rate Wireless Communications", *IEEE Journal on Selected Areas in Communications*, vol. 16, no. 8, Oct. 1998.

[6] K.I. Pedersen, J.B. Andersen et al., "A Stochastic Multiple-Input Multiple-Output radio channel model for evaluation of space-time codes", *Proc IEEE VTC 2000 Fall*, vol. 2, pp. 893-897, Boston, September 2000.

[7] F. Simoens, M. Moeneclaey, "A Reduced Complexity Frequency Offset Estimation Technique for Flat Fading MIMO Channels", *IEEE CAS Workshop/Symposium on Emerging Technologies, MWC*, Shanghai, China, Jun. 2004.

[8] A. Van Zelst, T.C.W. Schenk, "Implementation of a MIMO OFDM based Wireless LAN system," *IEEE Transactions on Signal Processing*, vol. 52, no. 2, pp. 483-494, Feb. 2004.

REAL-TIME IMPLEMENTATION OF A SPHERE DECODER-BASED MIMO WIRELESS SYSTEM

Mikel Mendicute†*, Luis G. Barbero*∗*, Gorka Landaburu*†*, John S. Thompson*∗*, Jon Altuna*†*, and Vicente Atxa*†

† Communications and Digital Signal Processing Area
Department of Electronics
University of Mondragon
Loramendi, 4, 20500 Mondragon, Spain
e-mail: mmendikute@eps.mondragon.edu

∗ Institute for Digital Communications
School of Engineering and Electronics
University of Edinburgh
EH9 3JL Edinburgh, UK
e-mail: l.barbero@ed.ac.uk

ABSTRACT

This contribution analyzes the integration of the sphere decoder (SD) in a complete field-programmable gate array (FPGA)-based real-time multiple input-multiple output (MIMO) platform. The algorithm achieves the performance of the maximum likelihood detector (MLD) with reduced complexity. However, its non-deterministic complexity, depending on the noise level and the channel conditions, hinders its integration process. This paper evaluates the performance and limitations of the SD in a real-time environment where signal impairments, such as symbol timing, imperfect channel estimation or quantization effects are considered.

1. INTRODUCTION

The use of multiple input-multiple output (MIMO) technology in wireless communication systems enables high-rate data transfers and improved link quality through the use of multiple antennas at both transmitter and receiver [1]. It has become a key technology to achieve the bit rates that will be available in next-generation wireless communication systems, combining spatial multiplexing and space-time coding techniques [2]. In addition, the prototyping of those MIMO systems has become increasingly important in recent years to validate the enhancements advanced by analytical results [3], [4]. For that purpose, field-programmable gate arrays (FPGAs), with their high level of parallelism and embedded multipliers, represent a suitable prototyping platform.

In the case of spatially multiplexed uncoded MIMO systems, the sphere decoder (SD) is widely considered the most promising approach to obtain optimal maximum likelihood (ML) performance with reduced complexity [5], [6]. The SD has been previously implemented in real-time [7], [8], indicating that its variable throughput could potentially represent a problem when integrating it into a complete communication system. However, the problem of the actual integration of the SD into a real-time MIMO system has not been addressed yet.

This paper presents a complete real-time FPGA MIMO system where the SD has been used as the detection algorithm. The SD has been integrated into the MIMO prototyping platform presented in [9]. Thus, the effects of real-time transmission impairments, like imperfect symbol timing and channel estimation or fixed-point precision, have been included in the performance evaluation of the SD.

2. SPHERE DECODER (SD)

2.1 MIMO System Model

The theoretical system model considered has, in the general case, M transmit and N receive antennas, with $N \geq M$, denoted as $M \times N$. The transmitted symbols are taken independently from a quadrature amplitude modulation (QAM) constellation of P points. Assuming symbol-synchronous receiver sampling and ideal timing, the received N-vector, using matrix notation, is given by

$$\mathbf{r} = \mathbf{H}\mathbf{s} + \mathbf{n} \tag{1}$$

where $\mathbf{s} = (s_1, s_2, ..., s_M)^T$ denotes the vector of transmitted symbols with $\mathrm{E}[|s_i|^2] = 1/M$, $\mathbf{n} = (n_1, n_2, ..., n_N)^T$ is the vector of independent and identically distributed (i.i.d.) complex Gaussian noise samples with variance $\sigma^2 = N_0$ and $\mathbf{r} = (r_1, r_2, ..., r_N)^T$ is the vector of received symbols. $\mathbf{H}$ denotes the $N \times M$ channel matrix where h_{ij} is the complex transfer function from transmitter j to receiver i. The entries of $\mathbf{H}$ are modelled as i.i.d. Rayleigh fading with $\mathrm{E}[|h_{ij}|^2] = 1$ and are perfectly estimated at the receiver.

2.2 SD Algorithm

The main idea behind the SD is to reduce the computational complexity of the maximum likelihood detector (MLD) by searching over only those noiseless received points (defined as $\mathbf{H}\mathbf{s}$) that lie within a hypersphere of radius R around the received signal $\mathbf{r}$. In this paper, the complex version of the SD is applied directly to the complex lattice $\Lambda(\mathbf{H}) = \{\mathbf{H}\mathbf{s}\}$ [10]. Avoiding the more common real decomposition of the system results in a more efficient hardware implementation [8].

The process can be represented by

$$\hat{\mathbf{s}}_{\mathbf{ml}} = \arg\{\min_{\mathbf{s}} \|\mathbf{r} - \mathbf{H}\mathbf{s}\|^2 \leq R^2\}. \tag{2}$$

and is shown in Figure 1, where the dots represent the noiseless received constellation and the cross represents the actual received point contaminated with noise. The sphere constraint in (2) can also be written, after matrix decomposition and removal of constant terms, as

$$\|\mathbf{U}(\mathbf{s} - \hat{\mathbf{s}})\|^2 \leq R^2 \tag{3}$$

where $\mathbf{U}$ is an $M \times M$ upper triangular matrix, with entries denoted u_{ij}, obtained through Cholesky decomposition of the Gram matrix $\mathbf{G} = \mathbf{H}^H\mathbf{H}$ (or, equivalently, QR decomposi-

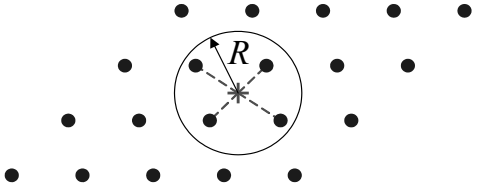

Figure 1: Schematic of the sphere decoder principle for the 2-dimensional case - only the points inside the circle are searched

tion of $\mathbf{H}$) and $\hat{\mathbf{s}} = (\mathbf{H}^H\mathbf{H})^{-1}\mathbf{H}^H\mathbf{r}$ is the unconstrained ML estimate of $\mathbf{s}$ [10].

The solution of the sphere constraint (SC) in (3) can be obtained recursively using a tree search algorithm, starting from $i = M$ and working backwards until $i = 1$. For each level, the constellation points s_i that satisfy

$$|s_i - z_i|^2 \leq \frac{T_i}{u_{ii}^2} \tag{4}$$

are selected as partial ML candidates, where

$$z_i = \hat{s}_i - \sum_{j=i+1}^{M} \frac{u_{ij}}{u_{ii}}(s_j - \hat{s}_j) \tag{5}$$

and

$$T_i = R^2 - \sum_{j=i+1}^{M} u_{jj}^2 |s_j - z_j|^2 . \tag{6}$$

When a new point is found inside the hypersphere (at $i = 1$) the radius is updated with the new minimum Euclidean distance and the algorithm continues the search with the new SC. This process can be seen as a tree search through M levels where each node on each level contains P branches. If $T_i \leq 0$, in any level i, the squared Euclidean distance from the root to that node has exceeded the SC and the entire branch plus all its descendants can be discarded, yielding a speed increase compared to an exhaustive search. The search finishes when the radius has been reduced so that no more points are found that satisfy the SC: the last point found satisfying the SC is the ML solution $\hat{\mathbf{s}}_{\mathbf{ml}}$.

In order to further reduce the complexity of the SD, the points that satisfy (4) are searched according to increasing distance to z_i, following the Schnorr-Euchner (SE) enumeration [11]. The use of this enumeration has two effects:

- On a particular node, The SE enumeration follows the branches with lowest distance increment $|s_i - z_i|^2$ first in any level i. Thus, the first points searched are more likely to be the ML solution, reducing the overall complexity of the search.
- Although the initial radius R is normally set according to the noise variance per antenna σ^2, the use of the SE enumeration reduces the effect the initial radius has on the complexity of the SD. From a simulation point of view, the initial radius still has a marginal effect on the complexity of the SD [6]. However, in a parallel implementation of the algorithm, the initial value can be set to the end of the scale so that no estimate of the noise level is required at the receiver [8].

3. MIMO PROTOTYPING PLATFORM AND TOOLS

The MIMO system and algorithms described in this paper have been implemented on a rapid prototyping platform based at the University of Mondragon. This platform, whose main features and operating modes have been previously presented in [9], consists of the following three elements: HERON rapid prototyping boards from Hunt Engineering Ltd. [12], RF transceivers and software tools.

3.1 Rapid Prototyping Boards

The platform is based on modular rapid prototyping HERON HEPC9 boards. The main advantage of those peripheral component interconnect (PCI)-based carrier cards consists of its very flexible architecture, based on an internal bus which allows communication of up to 400 mega bytes per second (MBps) between the modules. The following modules have been chosen for the implementation described in this work:

- Two HERON-IO2V2 modules with 4 analog inputs and 4 analog outputs of up to 125 mega samples per second (MSPS) with 12 and 14 bits of resolution, respectively. These modules include a 1-million (M)-gate Xilinx VirtexII FPGA and allow real-time in-system debugging with Xilinx Chipscope [13]. In addition, it is possible to perform co-simulation in a MATLAB/Simulink environment for Xilinx System Generator-based designs [14].
- One HERON-IO5 module with 2 analog inputs and 2 analog outputs of up to 210 MSPS with 12 and 16 bits of resolution, respectively. This module includes a 3M-gate VirtexII FPGA, which also contains a JTAG debugging interface.
- One HERON-FPGA3 module with a 1M-gate VirtexII FPGA.

3.2 RF Transceivers

The platform is equipped with Maxim's MAX2827EVKit boards, which can transmit or receive radio frequency (RF) signals in the 2.4 and 5 GHz bands. These transceivers can modulate and demodulate baseband IQ signals of a bandwidth of up to 20 MHz. This solution avoids the need for an implementation of algorithms such as modulators, digital up converters, etc., in order to generate the analog signals required by a transceiver. The combination of the analog ports of the aforementioned prototyping boards and these transceivers allow the implementation of systems with up to three transmit and receive antennas. Figure 2 shows two of these RF transceivers with the HEPC9-based rapid prototyping platform.

3.3 Software Design and Simulation Tools

A combination of MATLAB/Simulink and Xilinx System Generator has been selected as the main design tool to allow co-simulation of MATLAB algorithms, simulated VHDL implementations and FPGA-running blocks. This solution offers a simple and intuitive GUI-based hardware design and simulation tool for DSP algorithm engineers, achieving a balance between hardware abstraction level and real-time performance.

All the algorithms mentioned in this paper have been first tested in MATLAB and then translated to hardware blocks using Xilinx System Generator. Once the design has

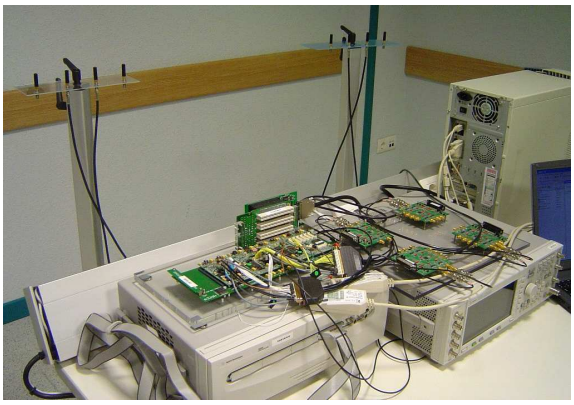

Figure 2: Main elements of the HEPC9-based MIMO signal processing prototyping platform.

been completed, Xilinx synthesis tools have been used to generate the bitstreams required for the hardware-based co-simulation, as well as the VHDL netlists for the final implementation. Xilinx Chiscope has been selected as the real-time on-hardware debugger.

4. REAL-TIME MIMO IMPLEMENTATION

4.1 MIMO System Model and Algorithms

4.1.1 System Model

Figure 3 shows the basic 2×2 MIMO spatial multiplexing model that has been implemented. The data bits are split into two 16-QAM streams which are transmitted independently and received synchronously at the two receive antennas.

A complete MATLAB-based model has been created and adapted to Simulink. A burst frame-based transmission system has been assumed with 128 data symbols transmitted per antenna. In addition, a 32-symbol preamble is transmitted per antenna to allow for effective synchronization and channel estimation to be performed at the receiver. The analog to digital converters (ADCs)' 12-bit resolution has been chosen for the precision of the input signals.

4.1.2 Algorithms

The following algorithms have been implemented:

- *Frame synchronization*: a multi-antenna extension of the double-sliding window technique has been applied [15].
- *Sample-time synchronization*: an ML approach has been chosen according to [16].
- *Frequency Offset Estimation*: a reduced complexity iterative offset estimation technique has been used as in [17].
- *Channel Estimation*: a basic training-based LS (Least-Squares) MIMO channel estimator has been implemented.
- *Inverse calculation and normalized Cholesky decomposition*: required by the SD for the initial zero forcing (ZF) equalization and the tree search.
- *MIMO detection*: The SD algorithm described in section 2 has been implemented with System Generator and included in the MIMO design. Details of the implementation can be found in [7] for a 4×4 system.
- *Inline MIMO channel emulator*: A flat Rayleigh channel emulator has been created to allow hardware co-simulation of the full system. This channel emulator is based on Gaussian noise generators and channel coefficients stored in a large RAM block. This allows to test the hardware implementation at its maximum rates without breaking the flat-fading channel assumption.

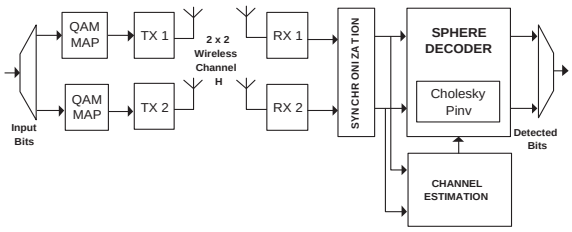

Figure 3: Structure of a basic 2×2 MIMO spatial multiplexing system.

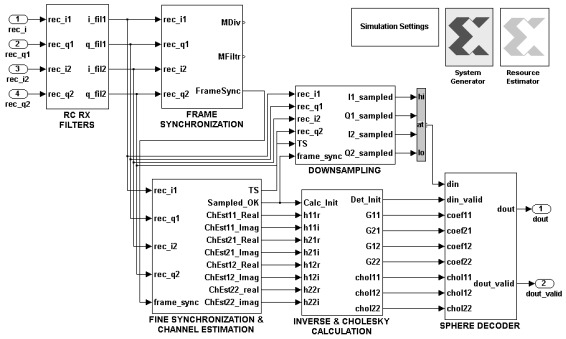

Figure 4: Top-level block diagram of the implemented MIMO receiver

4.2 High-Level Design and Hardware Co-Simulation

A fully flexible hardware co-simulation system has been implemented, allowing the progressive testing of the SD algorithm. The following implementation steps have been executed in order to evaluate the effect of real-communication impairments and quantization on the performance of the SD:

- *Ideal simulation*: The first simulation system, with perfect synchronization, known channel and no filters has been implemented initially to validate the integration of the SD and the 12-bit quantization error floor.
- *Estimated channel, real-time calculated inverse and Cholesky*: This version has been implemented to evaluate the effects of imperfect channel estimation and fixed-point calculations when obtaining the Cholesky decomposition and the inverse of the channel.
- *Complete System*: A final system has been implemented with all the algorithms required to interface with the real RF transceiver signals or the hardware-emulated channel.

Figure 4 shows the top-level block diagram of the MIMO receiver implemented with System Generator.

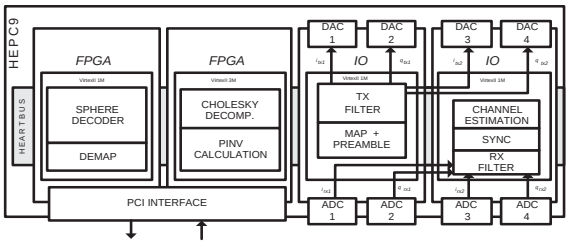

Figure 5: Structure of a 2×2 real-time MIMO implementation on the HERON modules of the HEPC9 board.

4.3 Final Real-Time Implementation

Figure 5 shows a diagram of the HEPC9 implementation of the 2×2 MIMO system with the distribution of the signal processing algorithms through the Heron modules available. The resource use has been distributed among four FPGA modules, which are connected through HEPC9's data bus. All the data flow of the real-time system is controlled through the PCI bus by a C++ application running on a host PC. Although the system can run at a higher symbol rate, we have reduced it to 100 kilo symbols per second (ksps) to allow for the flat-fading channel assumption of (1) to be valid with real transmission. Higher symbol rates can still be tested on the platform with the inline channel emulator.

5. RESULTS

Table 1 shows the FPGA resources of the complete MIMO system using 16-QAM modulation. For clarity purposes, only the number of multipliers and slices are shown. They are compared against the total number of multipliers and slices available on the HEPC9 boards. The three main blocks of the receiver are also shown to indicate the distribution of the resources. The calculation of the inverse of the channel matrix and the Cholesky decomposition of the Gram matrix are the most computationally intensive tasks. It should be noted that those two operations have not been optimized from an implementation point of view given that the focus of this work was on the integration of the SD in a MIMO system. The implementation of the SD requires a relatively small FPGA area, indicating that several SDs could be implemented in parallel on the same prototyping platform. The algorithm named 'Comm. & Control' corresponds to the logic required for the inter-module data communication and the PCI-based control of the real-time execution flow.

The bit error ratio (BER) performance as a function of the signal to noise ratio (SNR) per bit of the different versions of the system is shown in Figure 6. The results have been measured using the FPGA-based channel emulator, averaging over 5,000 channel realizations. Five curves, representing the different implementation stages are shown, together with the floating-point MATLAB version of the SD. It can be seen how the quantization process causes an error floor to appear at high SNR, which is larger when 12 bits are used for the input data instead of the initial 16 bits (considering ideal channel estimation and floating-point matrix calculations in both cases). The BER performance additionally degrades when the channel estimation block is added and fixed-point inverse and Cholesky calculations are performed.

Algorithm	Mults	Slices	% Slices
Transmitter	0	1,320	5.3%
Receiver	74	11,923	48.3%
Sync & Ch. Est.	*18*	*2,693*	*10.9%*
Inv. & Chol.	*33*	*4,608*	*18.6%*
SD	*23*	*3,370*	*13.7%*
Ch. Emulator	20	1,771	7.2%
Comm. & Control	0	1,542	6.2%
Total Used	96	16,556	67.0%
Total Available	216	24,696	

Table 1: FPGA Resources used by the final real-time implementation.

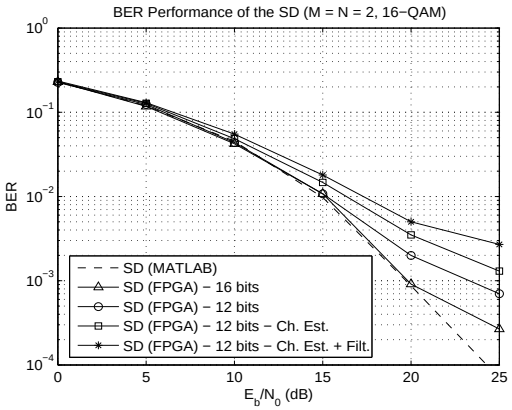

Figure 6: BER of the SD at different implementation stages

Finally, the last curve represents the BER performance of the complete system when transmit and receive filters are added. It can be seen how the quantization process and the effect it has on the channel estimation and the matrix calculations are the main factors determining the BER performance degradation compared to an ideal system.

Figure 7 shows the throughput of the SD for the aforementioned implementation levels. The throughput in mega bits per second (Mbps) is calculated according to

$$Q_{avg} = M \cdot \log_2 P \cdot f_{clock} \,/\, C_{avg} \;\; \text{(Mbps)} \qquad (7)$$

where f_{clock} is the clock frequency of the system in MHz and C_{avg} is the average number of clock cycles required to detect a MIMO symbol. The maximum clock frequency of the SD, $f_{clock} = 50\,\text{MHz}$, has been considered for the calculations although real transmission has been performed at a lower frequency. The minimum number of cycles is $C_{min} = 13$ resulting in a maximum throughput $Q_{max} = 30.77\,\text{Mbps}$. It can be seen how the 16-bit implementation of the SD approximates Q_{max} at high SNR per bit. A lower throughput is achieved by the other systems due to the effect the quantization has on the tree search of the SD. It causes some additional paths of the tree to be searched, *slowing down* the detection of the symbols. The degradation in performance is larger at high

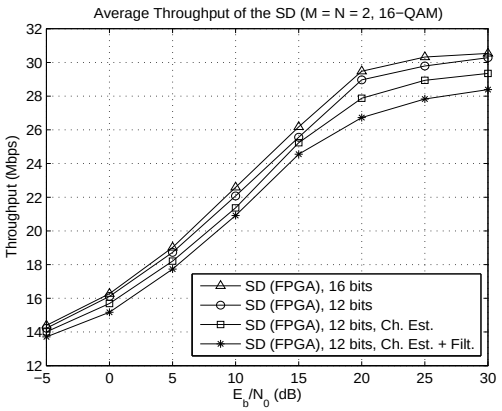

Figure 7: Throughput of the SD at different implementation stages

SNR per bit where the quantization noise is larger than the Gaussian noise. Finally, more SDs could be implemented in parallel to increase the average throughput like in [7],[8].

6. CONCLUSION AND FUTURE WORK

This paper has analyzed the integration of the SD in a real-time MIMO system where actual impairments, such as imperfect channel estimation, quantization and synchronization effects are considered. A 2×2 low-rate system has been developed using Xilinx System Generator in order to obtain BER and throughput results, evaluating the performance of the SD at several implementation steps. The main conclusions from this work can be summarized as:

- The BER performance of the SD on the FPGA approximately matches that of MATLAB, except at high SNR. The difference appears due to the fixed-point precision used for the input data and for the operations performed to obtain the input matrices (channel inverse and Cholesky decomposition).
- The throughput of the SD decreases as the system approaches a realistic transmission and reception case. A throughput loss of approximately 6% has been observed at high SNR.
- The MIMO platform and tools have been proved to be very practical in order to test the validity of the SD implementation in a real MIMO system. The homogeneity of the design flow has favoured the integration of the work of the two research groups involved.

As future work lines, the results of this paper can be extended to larger MIMO systems where additional resources would be required. In addition, a more detailed analysis of the fixed-point precision blocks could help identifying what the main causes of the quantization errors are. Finally, the inclusion of a robust channel equalizer and adaptive channel estimation could help evaluating the SD in higher rate transmissions with larger data bursts.

Acknowledgements

The first and third authors' work is supported by the Department of Education, Universities and Research of the Basque Government through Researcher Training Grants BFI03.378 and BFI05.428.

The second author's work is partially sponsored by Alpha Data Ltd.

REFERENCES

[1] G. J. Foschini, "Layered space-time architecture for wireless communication in a fading environment when using multi-element antennas," *Bell Labs Technical Journal*, pp. 41–59, Oct. 1996.

[2] C. Kose and B. Edwards, "WWiSE proposal: High throughput extension to the 802.11 standard," 11-05-0149-00-000n. [Online]. Available: http://www.wwise.org/technicalproposal.htm

[3] M. Rupp, A. Burg, and E. Beck, "Rapid prototyping for wireless designs: the five-ones approach," *Signal Processing*, vol. 83, pp. 1427–1444, 2003.

[4] T. Kaiser, A. Wilzeck, M. Berentsen, and M. Rupp, "Prototyping for MIMO systems: An overview," in *Proc. 12th European Signal Processing Conference (EUSIPCO '04)*, Vienna, Austria, Sept. 2004.

[5] E. Viterbo and J. Boutros, "A universal lattice code decoder for fading channels," *IEEE Trans. Inform. Theory*, vol. 45, no. 5, pp. 1639–1642, July 1999.

[6] M. O. Damen, H. E. Gamal, and G. Caire, "On maximum-likelihood detection and the search for the closest lattice point," *IEEE Trans. Inform. Theory*, vol. 49, no. 10, pp. 2389–2402, Oct. 2003.

[7] L. G. Barbero and J. S. Thompson, "Rapid prototyping of the sphere decoder for MIMO systems," in *Proc. IEE/EURASIP Conference on DSP Enabled Radio (DSPeR '05)*, vol. 1, Southampton, UK, Sept. 2005, pp. 41–47.

[8] A. Burg, M. Borgmann, M. Wenk, M. Zellweger, W. Fichtner, and H. Bölcskei, "VLSI implementation of MIMO detection using the sphere decoding algorithm," *IEEE J. Solid-State Circuits*, vol. 40, no. 7, pp. 1566–1577, July 2005.

[9] M. Mendicute, J. Altuna, G. Landaburu, and V. Atxa, "Platform for joint evaluation of FPGA-implemented and MATLAB algorithms in real MIMO transmissions," in *Proc. IEE/EURASIP Conference on DSP Enabled Radio (DSPeR '05)*, vol. 1, Southampton, UK, Sept. 2005, pp. 31–34.

[10] B. M. Hochwald and S. ten Brink, "Achieving near-capacity on a multiple-antenna channel," *IEEE Trans. Commun.*, vol. 51, no. 3, pp. 389–399, Mar. 2003.

[11] C. P. Schnorr and M. Euchner, "Lattice basis reduction: Improved practical algorithms and solving subset sum problems," *Mathematical Programming*, vol. 66, pp. 181–199, 1994.

[12] Hunt Engineering Ltd., "http://www.hunteng.co.uk."

[13] Xilinx, Inc., "http://www.xilinx.com."

[14] The MathWorks, Inc., "http://www.mathworks.com."

[15] J. Heiskala and J. Terry, *OFDM Wireless LANs: A Theoretical and Practical Guide*. Indiana, USA: Sams Publishing, 2002.

[16] A. F. Naguib, V. Tarokh, N. Seshadri, and A. R. Calderbank, "A space-time coding modem for high-data-rate wireless communications," *IEEE J. Solid-State Circuits*, vol. 16, no. 8, pp. 1459–1478, Oct. 1998.

[17] F. Simoens and M. Moeneclaey, "A reduced complexity frequency offset estimation technique for flat fading mimo channels," in *Proc. IEEE CAS Symposium on Emerging Technologies*, vol. 2, Shanghai, China, June 2004, pp. 705–708.

ANALYTICAL EXIT FUNCTIONS FOR THE PERFORMANCE EVALUATION OF ITERATIVE MIMO RECEIVERS WITH CHANNEL ESTIMATION ERROR

M. Mendicute, J. Altuna, and V. Atxa

Communications and Digital Signal Processing Area, Department of Electronics
University of Mondragon
Loramendi, 4 20500, Mondragon, Spain
phone: + (34) 943739412, fax: + (34) 943 791536, email: mmendikute@eps.mondragon.edu
http://www.eps.mondragon.edu

ABSTRACT

Analytical extrinsic information transfer (EXIT) functions provide an accurate and flexible method to analyze and calculate the performance of iterative linear multiple input-multiple output (MIMO) receivers through their decomposition into independent elementary blocks, such as the linear combiner or the demapper. These analytical functions have been shown to be very accurate to evaluate the performance of linear MIMO receivers with perfect channel knowledge in Rayleigh-fading channels.

This contribution extends this analysis to MIMO receivers with channel estimation, deriving new analytical transfer functions and adapting the performance evaluation algorithm. Bit error rate (BER) results are provided for training-based and soft decision directed expectation-maximization (EM) channel estimation techniques, showing the validity and accuracy of this analysis method.

1. INTRODUCTION

Multiple input-multiple output (MIMO) techniques enable high-rate data transfers and improved link quality through the use of multiple antennas at both transmitter and receiver [1]. When the number of transmit antennas grows or a forward error correcting (FEC) coding scheme is used, the optimal detection of the transmitted information bits becomes prohibitively complex. Iterative receivers, based on the turbo principle, can approach the optimal performance limits of these coded MIMO systems with reduced complexity, by transferring extrinsic soft information between the outer soft-input soft-output (SISO) decoder and the inner SISO MIMO detector [2].

The performance of MIMO receivers depends on the accuracy of the channel matrix estimate, which can be obtained using training-based or semi-blind techniques. Several analysis of channel estimation effects and iterative estimator algorithms have been conducted for turbo MIMO receivers, mainly based on adaptive filter theory and the EM algorithm [3, 4].

EXIT charts have been shown to be powerful semi-analytical tools for analyzing and calculating the performance of iterative MIMO receivers [5, 6]. Nevertheless, the EXIT transfer chart of each MIMO detector depends on the channel state, leading to lower accuracy when Rayleigh-fading channels are used and the mean of output mutual information values is used to calculate an unique EXIT chart for each signal to noise ratio (SNR) [5]. This limitation may be overcome if the MIMO detector is decomposed into elementary blocks, such as the linear combiner (LC) or the non-linear soft symbol demapper, and analytical EXIT transfer functions are used to describe their behavior [7]. This method provides a more flexible and accurate tool for the analysis and BER performance evaluation of turbo MIMO receivers. Its validity has been shown in [7] for quasi-static Rayleigh-fading MIMO channels, where only the EXIT function of the MIMO detector needs to be calculated online for each channel state, which is perfectly known at the receiver.

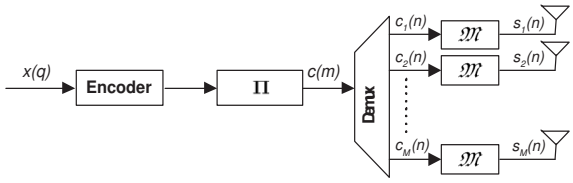

Figure 1: Diagram of a MIMO transmitter with coding and interleaving.

This contribution extends these analytical EXIT functions to channel estimation-based MIMO receivers. A new transfer function is derived for minimum mean square error-parallel interference cancellation (MMSE-PIC) receivers with channel estimation error and the performance evaluation algorithm of [7] is adapted. The accuracy and validity of these functions are shown for classical training-only based and soft decision-directed EM channel estimation algorithms. The results shown here can be extended to other iterative linear receivers, such as turbo-equalizers or multiuser detectors.

2. SYSTEM MODEL

The considered theoretical system model has, in the general case, M transmit and N receive antennas, with $N \geq M$, denoted as $M \times N$. Figure 1 shows the structure of the transmitter. The information symbol bits $x(q)$ are encoded, interleaved and demultiplexed. The resulting bits $c_k(n)$ are independently mapped onto a generic constellation of B points, modulated and transmitted simultaneously by M antennas.

Assuming symbol-synchronous receiver sampling and ideal timing, the received N-vector, using matrix notation, is given by

$$\mathbf{r}(n) = \mathbf{H}\mathbf{s}(n) + \boldsymbol{\eta}(n), \tag{1}$$

where $\mathbf{s}(n) = [s_1(n), s_2(n), ..., s_M(n)]^T$ denotes the vector of transmitted symbols with $\mathrm{E}[|s_i(n)|^2] = 1$, $\boldsymbol{\eta}(n) =$

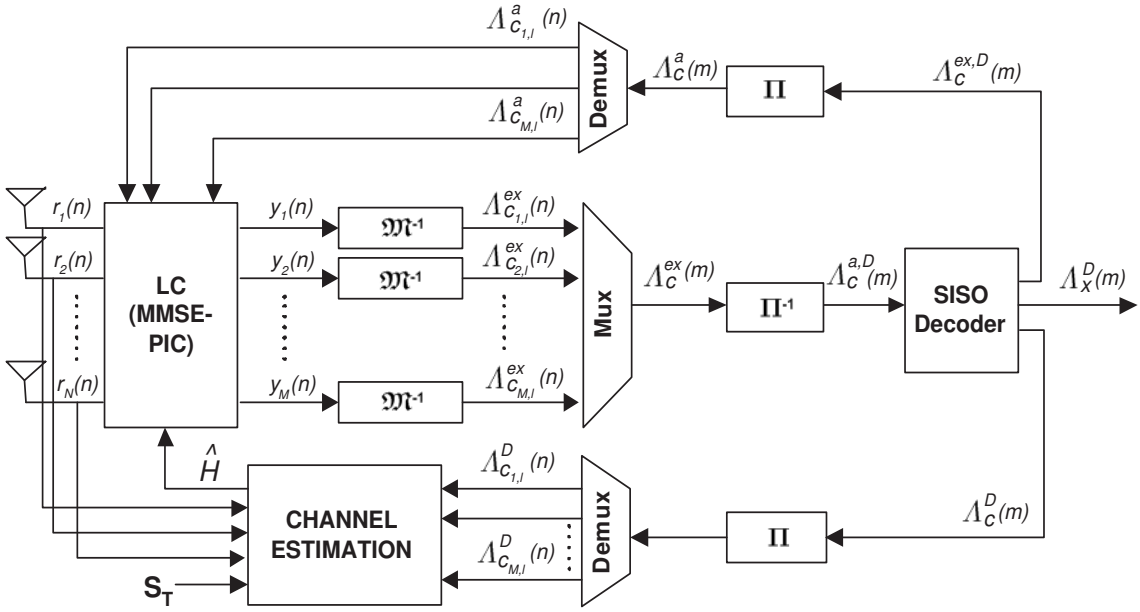

Figure 2: Diagram of a generic interference cancellation-based iterative MIMO receiver with channel estimation.

$[\eta_1(n),\eta_2(n),...,\eta_N(n)]^T$ is the vector of independent and identically distributed (i.i.d.) complex Gaussian noise samples with covariance matrix $E\{\eta(n)\eta^H(n)\}=\mathbf{I}_N N_0$, $\mathbf{r}(n)=[r_1(n),r_2(n),...,r_N(n)]^T$ is the vector of received symbols and $n=1,...,L$, where L represents the number of symbols in a frame. $\mathbf{H}$ denotes the $N\times M$ channel matrix, which is assumed constant for a frame.

Figure 2 shows the structure of the iterative receiver. The received symbols $\mathbf{r}(n)$ are processed by the SISO MIMO detector, whose outputs are the soft symbol estimates $\mathbf{y}(n)=[y_1(n),y_2(n),...,y_M(n)]^T$. A MIMO detector that carries out parallel interference cancellation (PIC) and minimum mean squared error (MMSE) combining operations will be assumed for the rest of this paper, which can be summarized as:

$$\mathbf{r}'_k(n)=\mathbf{r}(n)-\sum_{\substack{m=1\\m\neq k}}^{M}\hat{\mathbf{h}}_m\tilde{s}_m=\mathbf{r}(n)-[\hat{\mathbf{H}}\tilde{\mathbf{s}}(n)-\hat{\mathbf{h}}_k\tilde{s}_k(n)] \quad (2)$$

and

$$y_k(n)=\mathbf{w}_k^H\mathbf{r}'_k(n), \quad (3)$$

where k denotes the detected branch, $\hat{\mathbf{h}}_k$ is the kth column of channel matrix estimate $\hat{\mathbf{H}}$ and $\tilde{\mathbf{s}}(n)$ is an $M\times 1$ vector of soft symbols $\tilde{s}_k(n)$, which are derived from a priori log-likelihood ratio (LLR) metrics $\Lambda^a_{c_{k,l}}(n)$ fed back from the decoder [8].

The spatial combining matrix $\mathbf{w}_k$ is calculated from the estimated channel matrix $\hat{\mathbf{H}}$ as follows:

$$\mathbf{w}_k=(\hat{\mathbf{H}}\bar{\mathbf{V}}\hat{\mathbf{H}}^H+(1-\bar{v}_k)\hat{\mathbf{h}}_k\hat{\mathbf{h}}_k^H+\mathbf{I}N_0)^{-1}\hat{\mathbf{h}}_k, \quad (4)$$

where matrix $\bar{\mathbf{V}}=diag(\bar{v}_1,...,\bar{v}_M)$ represents the mean of symbol variance matrices $\mathbf{V}(n)=diag(v_1(n),...,v_M(n))$ with [6, 7]:

$$v_k(n)=E\{|s_k(n)-\tilde{s}_k(n)|^2\}=E\{|s_k(n)|^2\}-|\tilde{s}_k(n)|^2.$$

As can be seen in the figure, a channel estimate $\hat{\mathbf{H}}$ is provided to the MIMO detector by a channel estimation block, whose inputs are the received symbols, the training symbol matrix $\mathbf{S}_T$ and soft information from decoded information bits. For the sake of simplicity, only the a posteriori probability (APP) LLR metrics $\Lambda^D_c(m)$ will be considered for iterative channel estimation, as in [3, 4].

The symbol estimates $\mathbf{y}(n)$ are soft-demapped [8], providing the extrinsic LLRs of the coded bits $\Lambda^{ex}_{c_{k,l}}$, which become the input of the SISO decoder, after multiplexing and de-interleaving operations. The soft decoder delivers the following metrics:

- APP LLRs of the uncoded bits $\Lambda^D_x(m)$, whose signs define the finally detected bit values.
- Extrinsic LLRs of coded bits $\Lambda^{ex,D}_c(n)$, which are fed back to the MMSE-PIC for interference cancellation
- APP LLRs of the coded bits $\Lambda^D_c(m)$ for channel re-estimation.

3. ANALYTICAL EXIT FUNCTIONS FOR BER PERFORMANCE EVALUATION

The EXIT transfer function-based performance evaluation method of [7] divides a generic front-end (FE) into two elementary blocks, a LC and a non-linear demapper. In this paper the FE is the MIMO detector, which will be decomposed into three elementary devices: the MMSE-PIC linear combiner, the non-linear demapper and the channel estimation block. In [7], where the channel is perfectly known at the receiver, the FE is represented by the following parametric transfer functions:

$$\Gamma_k=F_k(I^R_{in};\mathbf{H},N_0),$$

$$I^R_{out,k}=G(\Gamma_k,I^R_{in}) \quad (5)$$

and

$$I_{out}^{R} = \frac{1}{M}\sum_{k=1}^{M} I_{out,k}^{R}\,. \tag{6}$$

Function F_k describes the LC behaviour for a certain channel state and SNR, giving an effective signal to interference and noise ratio (SINR) value Γ_k for each branch depending on the input mutual information (MI) I_{in}^{R}. Function G characterizes the soft demapper, as described in [7], and its output is the MI at each demapped branch $I_{out,k}^{R}$. Parting from these analytical functions and the EXIT transfer function of the SISO decoder, which does not depend on any system parameter, the authors in [7] introduced a performance evaluation algorithm that reduces drastically the simulation time and shows good accuracy in quasi-static Rayleigh-fading MIMO channels. Only F_k must be calculated online for each channel realization, while the rest of the functions are generated off-line.

4. ANALYTICAL EXIT FUNCTIONS WITH CHANNEL ESTIMATION ERRORS

Only one of the aforementioned EXIT transfer functions, F_k, needs to be changed if channel estimation error is included in the analysis method. Function F_k will now be defined by a new parameter, the estimated channel error matrix $\tilde{\mathbf{H}}$:

$$\Gamma_k = F_k(I_{in}^{R}; \mathbf{H}, N_0, \tilde{\mathbf{H}}), \tag{7}$$

where $\tilde{\mathbf{H}} = \mathbf{H} - \hat{\mathbf{H}}$ is the channel estimation error. These variables will be generated for each channel realization by the channel estimation block, whose generation function H_{est} can be represented for the jth iteration as:

$$\hat{\mathbf{H}}^{(j)} = H_{est}(\mathbf{H}, No, \mathbf{S}_T, I_{in}^{R,(j)}), \tag{8}$$

where $I_{in}^{R,(j)}$ is the input MI at the jth iteration. Therefore, the randomly generated channel estimate depends on the channel state, the noise, the transmitted training sequence and the mutual information statistics fed back from the decoder, if iterative channel estimation is used.

4.1 Analytical transfer function of MMSE-PIC with channel estimation error

The output SINR Γ_k at the kth branch of a generic MMSE receiver can be defined as [9]:

$$\Gamma_k = \frac{E\{s_k s_k^H\}}{tr(E\{e_k e_k^H\})} - 1 = \frac{1}{E\{e_k e_k^H\}} - 1, \tag{9}$$

where $e_k = s_k - y_k$. Parting from Equations (1-3) and omitting the symbol index n, e_k can be written as:

$$e_k = s_k - \mathbf{w}_k^H \left(\mathbf{h}_k s_k + \sum_{\substack{m=1 \\ m\neq k}}^{M} \mathbf{h}_m s_m - \sum_{\substack{m=1 \\ m\neq k}}^{M} \hat{\mathbf{h}}_m \tilde{s}_m + \eta \right)$$

$$= s_k - \mathbf{w}_k^H \left(\mathbf{h}_k s_k + \sum_{\substack{m=1 \\ m\neq k}}^{M} \mathbf{h}_m (s_m - \tilde{s}_m) + \sum_{\substack{m=1 \\ m\neq k}}^{M} \tilde{\mathbf{h}}_m \tilde{s}_m + \eta \right),$$

where $\tilde{\mathbf{h}}_m$ is the mth column of the channel estimation error matrix $\tilde{\mathbf{H}}$.

Assuming $E\{s_k s_k^H\} = 1$, $E\{(s_k - \tilde{s}_k)(s_k - \tilde{s}_k)^H\} = v_k$ and $E\{(\tilde{s}_k \tilde{s}_k^H)\} = E\{(s_k \tilde{s}_k^H)\} = 1 - v_k$, the error variance can be expressed as

$$E\{e_k e_k^H\} = 1 - \mathbf{w}_k^H \mathbf{h}_k - \mathbf{h}_k^H \mathbf{w}_k + \mathbf{w}_k^H \mathbf{R}_{rr} \mathbf{w}_k,$$

where

$$\mathbf{R}_{rr} = \mathbf{h}_k \mathbf{h}_k^H + N_0 \mathbf{I}_M + \sum_{\substack{m=1 \\ m\neq k}}^{M} \mathbf{h}_m v_m \mathbf{h}_m^H + \underbrace{\sum_{\substack{m=1 \\ m\neq k}}^{M} \tilde{\mathbf{h}}_m (1 - v_m) \tilde{\mathbf{h}}_m^H}_{\mathbf{T}}. \tag{10}$$

As can be seen, the effect of wrong channel estimate is twofold: the combining vector $\mathbf{w}_k^H$ is not matched to the actual channel $\mathbf{H}$ and a new error term $\mathbf{T}$ appears in Equation (10) due to the wrong cancellation of detected symbols.

4.2 Adaptation of the performance evaluation algorithm

The performance evaluation algorithm of [7] can be extended to Rayleigh-fading iterative receivers with channel estimation, independently of the estimation technique:

Performance Evaluation Algorithm

(0) Generate $\tilde{\mathbf{H}}$.
(1) Initialization: $j = 1$; $I_{out}^{D,(0)} = 0$.
(2) Get FE input MI. $I_{in}^{R,(j)} = I_{out}^{D,(j-1)}$.
(3) Generate estimate $\hat{\mathbf{H}}^{(j)} = H_{est}(\mathbf{H}, No, \mathbf{S}_T, I_{in}^{R,(j)})$.
(4) Compute $\bar{\mathbf{V}}$ from $I_{in}^{R,(j)}$, as in [7].
(5) Calculate $\mathbf{w}_k$ vectors from (4) and Γ_k values from (9).
(6) Compute $I_{out,k}^{R,(j)}$ and $I_{out}^{R,(j)}$ via (5) and (6).
(7) Obtain the decoder's output $I_{out}^{D,(j)} = f^D(I_{out}^{R,(j)})$.
(8) Calculate $BER^{(j)} = f_{BER}(I_{out}^{D,(j)})$.
(9) Return to step (2) with $j = j + 1$.

Algorithm 1: BER performance evaluation algorithm for each channel realization of an iterative MIMO receiver with channel estimation.

As can be seen in Algorithm 1, a new step has been included, numbered as (3), where a new channel estimate is generated for each channel realization and turbo iteration. The rest of the algorithm works as detailed in [7], transfering MI values between the MIMO detector and the outer soft decoder. Functions f^D and f_{BER} represent the EXIT transfer function and the BER estimation function of the decoder, respectively. $I_{out}^{D,(j)}$ is the output MI of the decoder and j represents the iteration index.

5. APPLICATION EXAMPLES

Function $H_{est}(\mathbf{H}, No, \mathbf{S}_T, I_{in}^{R})$ calculates a channel estimate for each channel realization based on the information fed back from the decoder as APP LLRs and the statistics of the training process. Two classical channel estimation techniques will be considered: training-based least squares (LS) and soft decision-directed EM.

5.1 Training-based LS channel estimation

If a training symbol matrix $\mathbf{S}_T$ of dimensions $M \times L_T$ is sent before data transmission and LS channel estimation is applied, the estimated channel is:

$$\hat{\mathbf{H}} = \mathbf{R}\mathbf{S}_T^H \left(\mathbf{S}_T \mathbf{S}_T^H\right)^{-1},$$

where $\mathbf{R}$ is an $N \times L_T$ matrix with the received training signal. $\hat{\mathbf{H}}$ is an unbiased estimate of $\mathbf{H}$, the estimation error is uncorrelated among the N receivers and the covariance matrix for each row is [10]:

$$E\{\tilde{\mathbf{h}}_n^H \tilde{\mathbf{h}}_n\} = N_0 \left(\mathbf{S}_T \mathbf{S}_T^H\right)^{-1}.$$

If $\mathbf{S}_T$ is formed by orthogonal training sequences, i.e, $\mathbf{S}_T \mathbf{S}_T^H = L_T \mathbf{I}_M$, the elements of the error matrix $\tilde{\mathbf{H}}$ become i.i.d. complex random variables with mean zero and variance N_0/L_T.

The estimate generation function $H_{est}^{(1)}(\mathbf{H}, No, \mathbf{S}_T)$, which does not depend on I_{in}^R if only training symbols are used for channel estimation, must then create an estimate $\hat{\mathbf{H}}$ according to the aforementioned statistics for each channel realization of the performance evaluation method described in Algorithm 1.

5.2 EM channel estimation

Training-only based channel estimation techniques do not profit from the iterative nature of turbo receivers. Many algorithms have been developed to re-estimate the channel from hard and soft decision statistics fed back from the SISO decoder. The classical EM channel estimation technique [3, 4] has been chosen here to show how iterative estimation can be included in the analytical EXIT function-based performance evaluation method. Based on [3, 4], the EM channel estimate obtained as

$$\hat{\mathbf{H}}^{(j+1)} = \bar{\mathbf{R}}_{rs}^{(j)} \left[\bar{\mathbf{R}}_s^{(j)}\right]^{-1}.$$

If the iteration index j is omitted, the correlation matrices $\bar{\mathbf{R}}_{rs}^{(j)}$ and $\bar{\mathbf{R}}_s^{(j)}$ become:

$$\bar{\mathbf{R}}_{rs} = \sum_{n=1}^{N_s} \mathbf{r}(n)\bar{\mathbf{s}}^H(n) = \mathbf{H}\mathbf{R}_s' + \theta,$$

$$\bar{\mathbf{R}}_s(i,k) = \begin{cases} N_s & ;\ i = k \\ \sum_{n=1}^{N_s} \bar{\mathbf{s}}_i(n)\bar{\mathbf{s}}_k^*(n) & ;\ i \neq k \end{cases} \tag{11}$$

and

$$\mathbf{R}_s' = \sum_{n=1}^{N_s} \mathbf{s}(n)\bar{\mathbf{s}}^H(n)\ ,\ \theta = \sum_{n=1}^{N_s} \eta(n)\bar{\mathbf{s}}^H(n), \tag{12}$$

where $\bar{\mathbf{s}}(n)$ are the soft symbol estimates obtained from the APP LLRs fed back to the channel estimation block [8], while θ is the matrix of weighted noise samples with autocovariance $N_0\mathbf{R}_s''$, where

$$\mathbf{R}_s'' = \sum_{n=1}^{N_s} \bar{\mathbf{s}}(n)\bar{\mathbf{s}}^H(n). \tag{13}$$

The estimated channel $\hat{\mathbf{H}}$ is a biased estimate of $\mathbf{H}$ and can be written as:

$$\hat{\mathbf{H}} = \mathbf{H}\mathbf{R}_s'\bar{\mathbf{R}}_s^{-1} + \theta\bar{\mathbf{R}}_s^{-1}. \tag{14}$$

The estimation function $H_{est}(\mathbf{H}, No, \mathbf{S}_T, I_{in}^{(j,R)})$ must generate an estimate $H^{(j)}$ for all the iterations $j > 1$ following Equation (14), while the training-based function $H_{est}(\mathbf{H}, No, \mathbf{S}_T)$ is used at the first iteration. Thus, matrices of Equations (11-13) must be calculated from the output statistics of the decoder. A very simple approach has been followed which calculates the aforementioned matrices according to the following approximations:

$$\hat{\bar{\mathbf{R}}}_s(i,k) = \begin{cases} N_s & ;\ i = k \\ N_s(1-\sigma_p)\mathbf{w}_i^H \mathbf{h}_k \mathbf{h}_k^H \mathbf{w}_i & ;\ i \neq k \end{cases} \tag{15}$$

$$\hat{\mathbf{R}}_s'(i,k) = \begin{cases} N_s\sigma_p & ;\ i = k \\ N_s(1-\sigma_p)\mathbf{h}_k^H \mathbf{w}_i & ;\ i \neq k \end{cases} \tag{16}$$

$$\hat{\mathbf{R}}_s''(i,k) = \begin{cases} N_s\sigma_p & ;\ i = k \\ N_s(1-\sigma_p)\mathbf{w}_i^H \mathbf{h}_k \mathbf{h}_k^H \mathbf{w}_i & ;\ i \neq k\ . \end{cases} \tag{17}$$

The value of $\sigma_p = E\{\bar{\mathbf{s}}_k \bar{\mathbf{s}}_k^H\}$ has been calculated off-line for each constellation alphabet when generating the EXIT transfer function of the decoder. The approximations of Equations (15-17) have been tested for quaternary phase shift keying (QPSK) modulation with several different channel realizations.

6. RESULTS

A system with $M = 4$ transmit and $N = 4$ receive antennas has been chosen to validate the performance evaluation method. Simulations with QPSK modulation have been conducted to compare the classical Monte-Carlo (MC) simulation and the EXIT-based analytical performance evaluation method with channel estimation error. Up to 10000 data blocks of 2048 coded bits have been simulated with a quasi-static Rayleigh-fading MIMO channel. Walsh codes of 4×8 and 4×16 symbols have been sent as training symbols and perfect timing and demodulation have been assumed at the receiver. A non-recursive non-systematic convolutional code with generator polynomials $\{5, 7\}_8$ and the common log-map BCJR algorithm have been selected for FEC encoding and decoding, respectively, with a random interleaver.

Figure 3 shows the BER comparison of EXIT and MC techniques for the iterative MMSE-PIC receiver with LS channel estimation and a 4×8 training matrix. As can be seen, the EXIT-based analysis gives slightly optimistic and quite accurate results for training-based channel estimation. MC simulation with perfect channel estimation has been included in the figures as reference. Figure 4 shows the same comparison for a training matrix of dimensions 4×16 symbols with similar results.

Figure 5 extends the comparison to EM-based channel estimation with the techniques and simplifications of section 4.3. The BER estimation accuracy is shown for a system with iterative channel estimation and initial training matrix of dimensions 4×8. These results show that this method and the simplifications assumed can be used to estimate or predict the BER performance of iterative channel estimation-based MIMO receivers. For the case of EM channel estimation, further analysis is required to extend the aforementioned assumptions to other modulations and MIMO detectors.

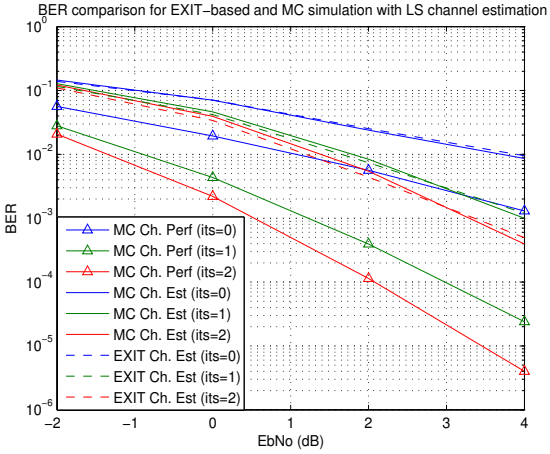

Figure 3: Comparison of EXIT fuction-based and MC simulation with LS channel estimation and a 4×8 training matrix.

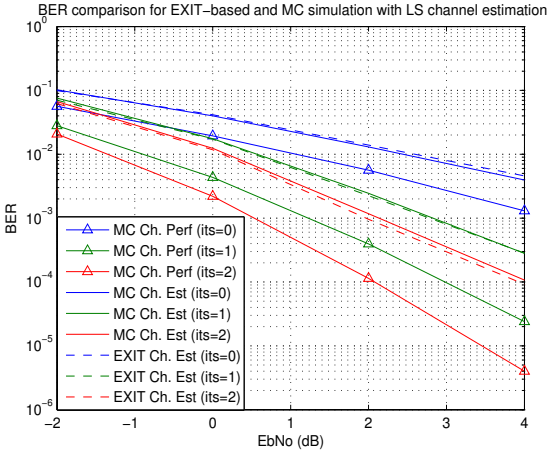

Figure 4: Comparison of EXIT fuction-based and MC simulation with LS channel estimation and a 4×16 training matrix.

7. CONCLUSION AND FURTHER RESEARCH

This paper has shown an effective and complexity-reduced method to include channel estimation errors on analytical EXIT function-based performance evaluation methods. An analytical transfer function has been derived for an MMSE-PIC receiver with channel estimation error. An algorithm has been shown which allows to evaluate the performance of different channel estimation techniques in iterative linear turbo receivers and comparative results have been provided for QPSK transmission with trained LS and soft decision-directed EM channel estimation.

As future work lines, these results can be extended to other modulations or different turbo-based applications, such as multiuser detection or turbo-equalization. Other interesting work lines include the analysis of other channel estimation techniques, based on soft or hard decisions, and the use of the different LLR metrics available at the decoder.

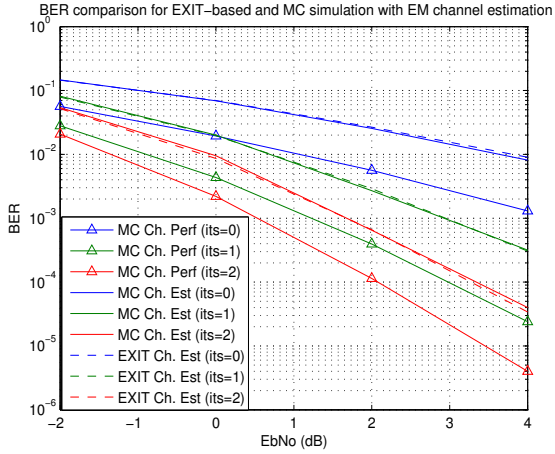

Figure 5: Comparison of EXIT fuction-based and MC simulation with soft decision-directed EM channel estimation and an initial 4×8 training matrix.

REFERENCES

[1] G. J. Foschini, "Layered space-time architecture for wireless communication in a fading environment when using multi-element antennas," *Bell Labs Technical Journal*, pp. 41–59, Oct. 1996.

[2] M. Sellathurai and S. Haykin, "Turbo-BLAST for wireless communications: theory and experiments," *IEEE Transactions on Signal Processing*, vol. 50, no. 10, pp. 2538–2546, 2002.

[3] J. Boutros, F. Boixadera, and C. Lamy, "Bit-interleaved coded modulations for multiple-input multiple-output channels," in *IEEE International Symposium on Spread Spectrum Techniques and Applications*, New Jersey, USA, Sept. 2000, vol. 1, pp. 123–126.

[4] M. A. Khalighi, and J. Boutros, "Channel estimation in turbo-BLAST detectors using EM algorithm," in *IEEE International Conference on Acoustics, Speech, and Signal Processing (ICASSP'05)*, Philadelphia, USA, Mar. 2005, vol. 3, pp. 1037–1040.

[5] C. Hermosilla, and L. Szczeciński, "EXIT charts for turbo receivers in MIMO systems," in *7th International Symposium on Signal Processing and Its Applications (ISSPA'03)*, Paris, France, July 2003, vol.1, pp. 209–212.

[6] E. Biglieri, A. Nordio and G. Taricco, " Iterative receivers for coded MIMO signalling," *Wireless Communications and Mobile Computing*, no. 4, pp. 697–710, 2004.

[7] C. Hermosilla, and L. Szczeciński, " Performance evaluation of linear turbo receivers using analytical extrinsic information transfer functions," *EURASIP Journal On Applied Signal Processing, special issue on turbo processing*, no. 6, pp. 892–905, Oct. 2005.

[8] M. Tüchler, R. Koetter and A. C. Singer, " Minimum mean squared error using a piori information," *IEEE Transactions on Signal Processing*, vol. 50, no. 3, pp. 673–683, Mar. 2002.

[9] A. Paulraj, R. Nabar, and D. Gore, *Introduction to Space-Time Wireless Communications*, Cambridge University Press, 2003.

[10] T. L. Marzetta, "BLAST training: Estimating channel characteristics for high capacity spacetime wireless," in *Proc. 37th Anual Allerton Conference on Communication, Control, and Computing*, Monticello, IL, Sept. 1999, pp. 958–9662.

Plataforma para la evaluación de algoritmos Matlab y hardware VHDL en transmisiones reales MIMO

Mikel Mendicute y Jon Altuna
Área de Tratamiento Digital de la Señal y Comunicaciones, Departamento de Electrónica
Escuela Politécnica Superior de Mondragón
e-mail: {mmendikute, jaltuna}@eps.mondragon.edu

***Abstract*— This contribution describes a MIMO simulation and hardware validation platform suitable for a progressive implementation of a real-time MIMO wireless system. We describe a platform which allows to share Matlab, simulated VHDL and real hardware designs while transmitting through a real MIMO channel. The applicability and first results of this platform are shown for a narrowband 2x2 spatial multiplexing system operating in the 2.4 GHz band.**

I. Introducción

Las técnicas de transmisión MIMO (Multiple-Input Multiple-Output), cuyas elevadas capacidades teóricas comenzaron a vislumbrase una década atrás, se han convertido en el principal recurso para alcanzar los límites que los nuevos estándares de comunicaciones inalámbricas exigen. A modo de ejemplo, las propuestas para las futuras redes WLAN 802.11n pretenden alcanzar tasas de bits de entre 100 y 300 Mbps empleando técnicas MIMO, tales como la codificación espacio-temporal o la multiplexación espacial [1].

Las principales desventajas de la transmisión multiantena consisten en la multiplicación del hardware requerido, debido al incremento del número de cadenas de transmisión y recepción, y en un incremento notable en la complejidad del tratamiento de señal, que puede llegar a crecer exponencialmente con el número de antenas de transmisión y recepción.

Esta elevada complejidad es la que provoca que la mayoría de prototipos MIMO sean de los denominados ”off line”, es decir, con señales reales transmitidas y almacenadas, procesadas posteriormente empleando tiempo y recursos excesivos, como por ejemplo, una aplicación matlab sobre un PC. Debido a la inminente inclusión de MIMO en los estándares de transmisión inalámbrica, se está generando un gran interés entorno a la implementación en tiempo real de estos sistemas, como muestran los recientes productos y prototipos presentados [2][3].

Esta contribución presenta una plataforma que permite pasar paulatinamente de la simulación Matlab de un sistema de transmisión inalámbrica MIMO a sistemas de transmisión de tiempo real implementados empleando dispositivos DSP o FPGA.

Como se puede observar en la figura 1, se ha tomado como punto de partida un modelo basado en simulaciones Matlab y VHDL . El objetivo final, en cambio, consiste en un sistema de transmisión en tiempo real implementado íntegramente en dispositivos FPGA. Se han destacado dos entre los varios

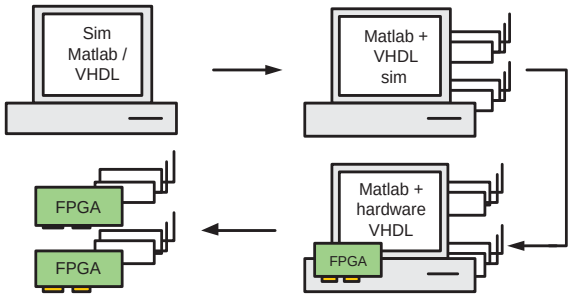

Fig. 1. Diferentes estadios para la simulación/validación progresiva de sistemas de transmisión MIMO de tiempo real.

estadios que pueden darse: el de la transmisión real ”off line” empleando únicamente código ejecutado en el PC (Matlab y VHDL simulado) y aquél en el que parte de los algoritmos son ejecutados en las FPGA. Este último es el que posibilita el paso progresivo desde el entorno de simulación a la ejecución en tiempo real.

La estructura de este artículo es la siguiente: en la segunda sección se resume el modelo básico MIMO considerado, así como los algoritmos que se requieren para su funcionamiento en una transmisión real. En el tercer apartado se describen los elementos de que consta la plataforma y su especificación técnica. En la cuarta sección se muestran las diferentes posibilidades que ofrece la plataforma. En el último apartado se resumen los principales resultados obtenidos, así como las conclusiones que se derivan del trabajo presentado en este documento.

II. Modelo y algoritmos MIMO

A. Modelo del sistema MIMO escogido

Se ha decidido escoger un sistema MIMO sencillo, consistente en una transmisión de multiplexación espacial de portadora única y banda estrecha. A modo de ejemplo, se ha empleado una tasa de 50 Ksps en la banda de 2’4 GHz. La modulación puede variar desde BPSK hasta 16QAM. Se han empleado dos antenas en cada extremo de la transmisión. Como ya se explicará más adelante, la plataforma resulta absolutamente flexible de cara a una futura ampliación u optimización.

La figura 2 muestra los principales bloques que forman un sistema multiantena de multiplexación espacial con M antenas

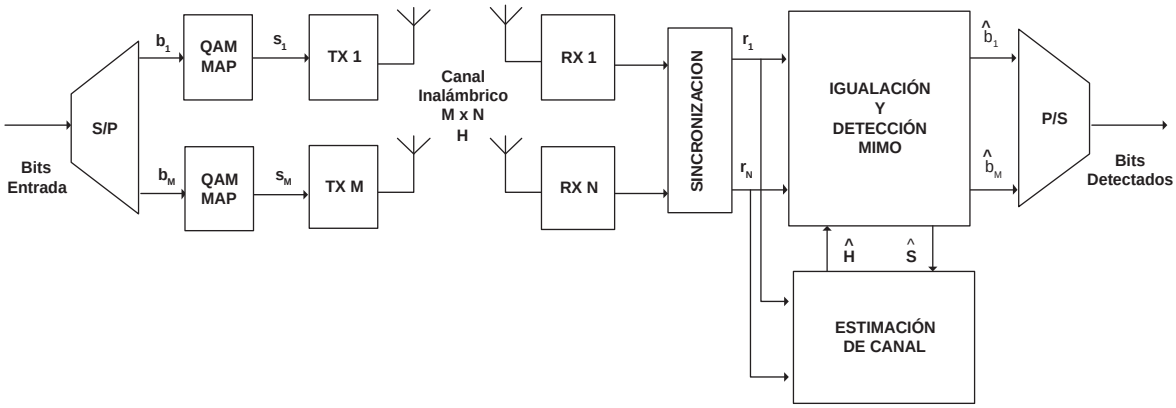

Fig. 2. Bloques de un sistema MIMO de multiplexación espacial.

de transmisión y N de recepción. Los secuencia de bits de información a transmitir se divide en M subcadenas, cada una de las cuales es transmitida simultáneamente por una antena de transmisión. La señal transmitida es recibida simultáneamente en N antenas de recepción.

Para el caso más simple, con un canal no dispersivo o de desvanecimiento plano, el sistema puede modelarse de la siguiente manera si se supone una perfecta sincronización:

$$\mathbf{r} = \sqrt{\frac{E_s}{M}}\mathbf{H}\mathbf{s} + \mathbf{n} \tag{1}$$

donde **H**, **r** y **s** representan la matriz del canal MIMO, el vector de símbolos recibidos y el vector de símbolos transmitidos, respectivamente. E_s y **n** representan la energía transmitida por cada período de muestreo y el vector de ruido en las antenas de recepción, respectivamente.

Se ha realizado un modelo Matlab completo del sistema que ha sido utilizado para testar la plataforma de simulación y validación. Para el caso del canal simulado, se ha empleado un modelo Rayleigh con un grado de correlación variable, de tal forma que pueda representar diferentes ubicaciones y separaciones de las antenas [4]. Se ha asumido un modelo de transmisión por tramas cortas que incluyen un preámbulo para las tareas de sincronización y estimación del canal, por lo que éste puede considerarse prácticamente constante durante una trama.

B. Algoritmos seleccionados para la plataforma

Se han implementado todos los algoritmos necesarios para la aplicación del modelo Matlab a la transmisión y recepción de señales MIMO reales. A continuación se enumeran brevemente los algoritmos escogidos para el receptor:

- *Sincronización de trama*: se ha empleado una extensión multiantena del algoritmo de doble ventana deslizante [5].
- *Selección del instante de muestreo*: se ha escogido un algoritmo ML (Maximum Likelihood) similar al descrito en [6].
- *Estimación del offset entre frecuencias*: se ha elegido un algoritmo iterativo de reducida complejidad, presentado en [7].
- *Estimación de canal*: se han implementado los algoritmos supervisados MIMO básicos LS (Least-Squares) y LMMSE (Least Minimum Mean Squared Error).
- *Detección MIMO*: se utilizan los algoritmos lineales fundamentales ZF (Zero-Forcing) y MMSE (Minimum Mean Squared Error), así como los no lineales ML y V-BLAST [8].

III. Descripción de la plataforma

La plataforma MIMO que se describe en este documento está compuesto básicamente por un PC dotado de los siguientes elementos:

- Transceptores RF bibanda a 2'4 y 5 GHz.
- Tarjetas PCI de adquisición y generación de señales analógicas.
- Tarjetas modulares de desarrollo rápido DSP y FPGA Heron HEPC9 de Hunt Engineering.
- Software de simulación: Matlab, ModelSim.
- Software de síntesis y programación FPGAs: Xilinx ISE y herramientas Heron.

En los siguientes apartados se expondrán las especificaciones técnicas de cada uno de estos elementos y su aplicación dentro de la plataforma que se describe en este documento.

A. Frontales y Generadores RF

La plataforma dispone de varias tarjetas MAX2827EVKit de la casa Maxim para la transmisión y recepción de señales en las bandas de 2'4 y 5 GHz. Estas tarjetas permiten modular y demodular señales IQ de hasta 20 MHz de ancho de banda. Emplean una referencia externa de 40 MHz que debe estar sincronizada para todos los transceptores de un extremo de la comunicación. Al trabajar con las señales IQ en banda base, estos transceptores permiten omitir la implementación del modulador, pero requieren la utilización de dos señales (I y Q) por cada antena.

Para el caso en el que se quiera aprovechar al máximo las salidas disponibles, éstas pueden generarse moduladas a una frecuencia intermedia y ser desplazadas por un generador RF hasta la frecuencia deseada. De esta manera sólo se requiere una salida analógica por cada antena de transmisión. Como ejemplo, esta solución ha permitido emplear sistemas de prueba de hasta 2x3 empleando dos generadores RF en la transmisión y los transceptores RF en la recepción.

B. Tarjetas de generación y adquisición

La plataforma dispone de una tarjeta CH-3150 de la casa Acquitek que permite generar dos señales analógicas con una precisión de hasta 12 bits y 20 MSps. La tarjeta incluye otras prestaciones, entre las que destacan dos entradas analógicas de características similares. Posee una memoria de hasta 16 MB y ofrece varias interfaces para su control, destacándose la posibilidad de emplear funciones directas desde Matlab.

Junto con esta tarjeta se ha incluido una tarjeta PCI-9812A de la casa Adlink que permite muestrear cuatro señales simultáneamente con una precisión de 12 bits a 20 MSps. Si se sincroniza esta tarjeta de adquisición con la mencionada anteriormente, se puede llegar a construir un sistema dotado de 2 salidas y 6 entradas analógicas de 12 bits de resolución. Al igual que la anterior, esta tarjeta puede ser controlada completamente desde una aplicación Matlab.

Estas tarjetas de adquisición y generación permiten un testado completo de los algoritmos seleccionados en transmisiones ”off-line” gobernadas por una aplicación Matlab.

C. Tarjetas de desarrollo rápido HEPC9

De cara a la implementación real de los algoritmos VHDL, se han incluido dos tarjetas de desarrollo rápido HEPC9 de la casa Hunt Engineering. Estas tarjetas, de interfaz PCI, poseen un bus de comunicación interna que llega hasta los 400 MBps y una estructura completamente flexible, gracias a su modularidad. Los módulos de que dispone las tarjetas incluidas en la plataforma son las siguientes:

- Dos módulos HERON-IO2V2 que posibilitan hasta 4 entradas y 4 salidas analógicas de hasta 125 MSps de 12 y 14 bits de resolución. Incluyen una FPGA VirtexII de 1M puertas y múltiples entradas y salidas digitales. Estos módulos pueden ser utilizados para la adquisición de señales recibidas para el caso en que se requiere una tasa de muestreo superior a los 20 MHz de las tarjetas de adquisición.
- Dos módulos HERON-FPGA3 provistos de una FPGA VirtexII de 1M puertas. Estos módulos, así como los anteriores, permiten su depurado in-system y en tiempo real empleando la herramienta ChipScope de Xilinx.
- Dos módulos HERON4-C6701 provistos de DSPs TMS320C6701, de coma flotante y 16 bits a 167 MHz, de la casa Texas Instruments.

Las tarjetas HEPC9 poseen una API en C que permite configurar y comunicarse con cualquiera de sus módulos a través del bus PCI. Se ha desarrollado una aplicación que gestiona la transmisión de secuencias de información hacia o desde la tarjeta, de tal forma que ésta pueda ser introducida en el flujo de una aplicación simulada en Matlab. Este montaje está orientado a la transmisión de señales generadas y procesadas en Matlab a las FPGAs de cara al testado de éstas.

D. Software de simulación y síntesis

La plataforma descrita ha sido combinada con las aplicaciones de simulación Matlab y ModelSim. El primero permite implementar con sencillez todos los modelos y algoritmos requeridos, siendo el primer paso para la implementación del sistema. Una vez que los algoritmos sean testados, pueden ser sustituidos por diseños VHDL empleando la herramienta ”Link for Modelsim” de Matlab. Esto permite el testado de un diseño dentro de la simulación completa Matlab e incluso empleando, como ya se expondrá posteriormente, señales reales de una transmisión ”off-line”.

De cara a la síntesis e implementación real de los diseños VHDL, se ha utilizado la herramienta de síntesis habitual de Xilinx junto a las librerías y plantillas ofrecidas por la plataforma Heron para la programación individual de los módulos del HEPC9 y la transmisión de información a través del bus PCI.

IV. Ejemplos de aplicación: Modos de funcionamiento de la plataforma

Este apartado pretende mostrar los diferentes modos en los que puede operar la plataforma y las posibilidades que ofrece de cara a la progresiva implementación de algoritmos MIMO de tiempo real.

A. Sistema Matlab de transmisión real MIMO off-line

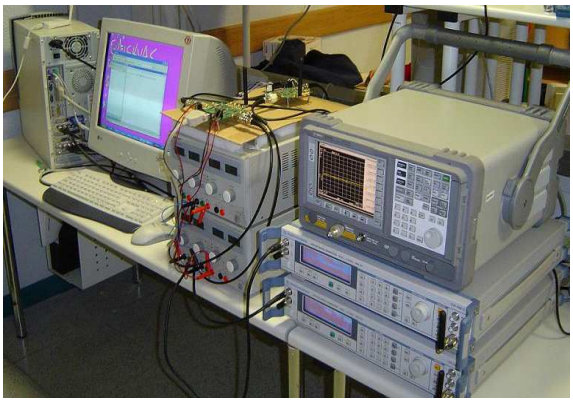

Fig. 3. Plataforma de laboratorio para transmisiones MIMO off-line procesadas en Matlab.

Se ha realizado el montaje 2x2 que se resume en la fotografía de la figura 3. Las señales a transmitir son generadas y moduladas a una frecuencia intermedia de 100 KHz dentro de la aplicación Matlab. Estas señales son transmitidas empleando las salidas analógicas a dos generadores RF que desplazan la señal a la frecuencia de 2’437 GHz.

Las señales transmitidas son recibidas en dos frontales, cuyas salidas IQ son leídas por Matlab empleando cuatro de

las entradas analógicas de que dispone el PC. Este montaje ha servido para testar la validez de los algoritmos Matlab y es el punto de partida para la validación de los diseños VHDL en transmisiones reales.

B. Transmisión off-line con implementación VHDL parcial

El montaje citado en el apartado anterior puede combinarse con la utilización de la plataforma Heron, de tal forma que se pueda realizar parte del procesamiento de la señal empleando implementaciones reales VHDL. El diagrama de la figura 4 muestra la estructura y el flujo de las señales en este modo de operación.

A modo de ejemplo, si se quiere analizar el rendimiento y la complejidad de la implementación de determinadas técnicas de detección MIMO, éstas pueden ser comparadas empleando señales transmitidas reales, mientras que el resto del procesado de señal se sigue realizando en Matlab. En el diagrama de la figura 4 es la propia aplicación Matlab la que genera y recibe los datos, pero parte de esta tarea puede ser implementada en la plataforma Heron si se desea, por ejemplo, analizar un sistema en el que todo el receptor está implementado en la FPGA.

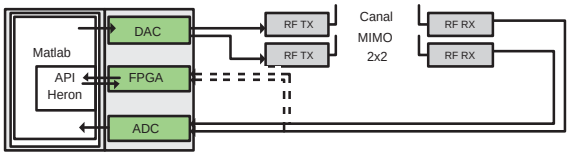

Fig. 4. Esquema de un modelo que permite combinar procesado de señal implementado en Matlab con implementaciones VHDL reales.

C. Implementación completa real-time

Tal y como se ha expuesto anteriormente, esta plataforma ofrece un camino relativamente sencillo de cara a la implementación VHDL de sistemas de comunicación MIMO de tiempo real. Como ya se ha apuntado, la plataforma Heron HEPC9 y los módulos de que dispone la plataforma permiten implementar un sistema 2x2 o incluso 4x4 si se generan y reciben señales moduladas, en lugar de en banda base. La figura 5 muestra un diagrama de la plataforma Heron con sus diferentes módulos y los algoritmos que se implementarán en cada uno de ellos. La capacidad de esta plataforma ya está siendo demostrada en [3], donde se está empleando para la implementación de un sistema MIMO-OFDM 4x4.

V. Conclusiones y líneas futuras

Este artículo describe una plataforma desarrollada para la validación de algoritmos y diseños VHDL reales orientados a sistemas de comunicaciones inalámbricas multiantena. El objetivo del sistema presentado es el de facilitar el tránsito desde simulaciones Matlab a diseños VHDL implementados en una plataforma de desarrollo.

Combinando tarjetas de adquisición y generación de señales analógicas, frontales RF de 2.4-5 GHz y tarjetas Heron HEPC9 de prototipado rápido para sistemas basados en FPGA/DSP,

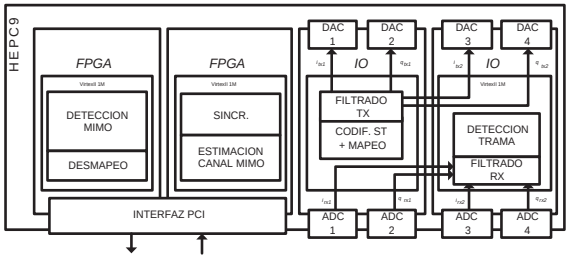

Fig. 5. Posible estructura del sistema MIMO de tiempo real.

esta plataforma permite realizar de manera sencilla la tarea de simulación y validación conjunta de aplicaciones Matlab, diseños VHDL implementados en FPGAs y la utilización de señales reales transmitidas y procesadas "off-line".

Esta plataforma está siendo utilizada de cara a la implementación de un sistema MIMO de tiempo real básico, consistente en un esquema 2x2 de multiplexación espacial y banda estrecha a 2.4 GHz. Este sistema será el punto de partida para el análisis de la implementación en tiempo real de sistemas más realistas y de mayor capacidad.

Agradecimientos

Los autores agradecen la financiación recibida del Departamento de Educación, Universidades e Investigación del Gobierno Vasco a través de una Beca para Formación de Investigadores.

Referencias

[1] C. Kose, B. Edwards, et al., IEEE 802.11/05-0149-01-000n, "WiSE group PHY and MAC specification,"

[2] A. Van Zelst, T.C.W. Schenk, "Implementation of a MIMO OFDM based Wireless LAN system," *IEEE Transactions on Signal Processing*, vol. 52, no. 2, pp. 483-494, Feb. 2004.

[3] S. Häne, D. Perels et al., "Implemetation Aspects of a Real-Time Multi-Terminal MIMO-OFDM Testbed" *IEEE Radio and Wireless Conference (RAWCON)*, Atlanta, GA, Sept. 2004.

[4] K.I. Pedersen, J.B. Andersen, J.P. Kermoal, P.E. Mogensen, "A stochastic Multiple-Input Multiple-Output radio channel model for evaluation of space-time codes" *Proc IEEE VTC 2000 Fall*, Boston, 2000

[5] J. Heiskala, J. Terry, *OFDM Wireless LANs: A Theoretical and Practical Guide*, Indiana, U.S.A.: Sams Publishing, 2002. ISBN:0-672-32157-2

[6] A.F. Naguib, V. Tarokh et al., "A Space-Time Coding Modem for High-Data-Rate Wireless Communications", *IEEE Journal on Selected Areas in Communications*, vol. 16, no. 8, Oct. 1998.

[7] F. Simoens, M. Moeneclaey, "A Reduced Complexity Frequency Offset Estimation Technique for Flat Fading MIMO Channels", *IEEE CAS Workshop/Symposium on Emerging Technologies, MWC*, Shanghai, China, Jun. 2004.

[8] G. D. Golden, G. J. Foschini, R. A. Valenzuela, P. W. Wolniansky, "Detection Algorithm and Initial Laboratory Results using the V-BLAST Space-Time Communication Architecture " *Electronics Letters, Vol. 35, No. 1, Jan. 7, 1999, pp. 14-15, 1999*

Sistema “Hardware in the Loop” para el prototipado rápido de algoritmos MIMO de tiempo real

Mikel Mendicute, Gorka Landaburu, Jon Altuna, Vicente Atxa e Iraitz Zuazabeitia
E-mail {mmendikute, glandaburu}@eps.mondragon.edu
Área de Tratamiento Digital de la Señal y Comunicaciones, Departamento de Electrónica
Universidad de Mondragón
Loramendi, 4, 20500 Mondragón, España

***Abstract*- Multiple-Input Multiple-Output (MIMO) techniques have become the main solution to reach the data rates expected for new wireless communications standards. The implementation of these multi-antenna systems has become specially important to validate the enhancements advanced by analytical results, requiring the development of specific testbeds and rapid prototyping platforms.**

This contribution shows a real-time “Hardware in the Loop” (HaLo) approach which eases the rapid prototyping of wireless MIMO communication systems. A Matlab/Simulink-based HaLo system is shown for a modular rapid prototyping Heron platform, whose features allow the implementation of real-time MIMO wireless algorithms at different design levels. The coexistence of offline Matlab/Simulink code and real-time hardware running on various FPGA devices is specially considered. The structure of the HaLo approach and main implementation issues are shown with several specific application examples, such as a complete 2x2 spatial multiplexing system.

I. Introducción

Las técnicas MIMO (Multiple input-multiple output) posibilitan comunicaciones de elevadas tasas de bits y calidad de enlace superior incluyendo varias antenas, tanto en transmisión como en recepción [1]. Son una de las tecnologías clave escogidas para los nuevos y futuros estándares de comunicaciones inalámbricas [2].

Las principales desventajas de MIMO son la multiplicación del hardware, debida al mayor número de cadenas de transmisión y recepción, y la complejidad inherente a los algoritmos multi-antena de tratamiento digital de la señal. Esta complejidad ha ocasionado la aparición de numerosas plataformas “offline”, en las cuales el procesamiento es realizado en Matlab [3], a pesar de la importancia que tiene la validación realista de los algoritmos de tiempo real en el prototipado de los sistemas inalámbricos MIMO [4].

Matlab representa la herramienta perfecta para el análisis, tanto teórico como simulado, de algoritmos MIMO, gracias a sus numerosas librerías y su entorno matricial de coma flotante. Sin embargo, las simulaciones basadas en Matlab están lejos de la evaluación realista de los algoritmos, debido a las múltiples simplificaciones que implican. Por lo tanto, el prototipado de sistemas MIMO se ha convertido en un campo de creciente importancia, permitiendo evaluar aspectos relativos a la implementación y su complejidad desde los primeros estadios del proceso de diseño, acelerándolo y volviéndolo más seguro.

El paso del análisis teórico a la implementación real exige el desarrollo de plataformas de prototipado rápido y herramientas

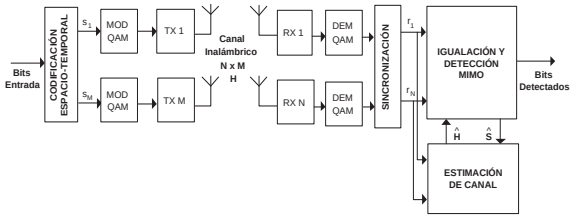

Fig. 1. Modelo básico de un sistema inalámbrico MIMO.

que permitan la co-simulación de diseños implementados en hardware y código Matlab. Además de la co-simulación, estos sistemas deben proporcionar medios para la ejecución en tiempo real de los algoritmos y la realización de transmisiones inalámbricas a través un canal MIMO real. Es aquí donde interviene el concepto de “Hardware in the Loop” (HaLo), el cual fue aplicado a sistemas MIMO en [5] y presentado como producto en [6].

No obstante, la implementación HaLo de un sistema de prototipado MIMO es factible empleando herramientas comunes y plataformas modulares de desarrollo rápido. Esta contribución muestra la implementación HaLo de un sistema de desarrollo para comunicaciones MIMO, combinando herramientas de alto nivel (Matlab/Simulink, Xilinx System Generator) y de bajo nivel (herramientas de diseño y síntesis de Xilinx), ampliando las prestaciones de tiempo real y co-simulación de la plataforma MIMO presentada en [7].

II. Modelo MIMO básico

La Fig. 1 muestra un sistema inalámbrico MIMO con M antenas de transmisión y N de recepción, en el que los bits de datos son codificados espacial y temporalmente en M cadenas de símbolos, los cuales son modulados y transmitidos simultáneamente por M antenas. Estas señales son recibidas en N antenas de recepción y demoduladas síncronamente. Tras la demodulación, la sincronización y la estimación de canal, los bits de datos son recuperados por el algoritmo de detección MIMO.

Un sistema MIMO de desvanecimiento plano puede representarse en banda base de la siguiente forma:

$$\mathbf{r} = \sqrt{\frac{E_s}{M}}\mathbf{H}\mathbf{s} + \mathbf{n}$$

donde $\mathbf{r}$ es un vector de $N \times 1$ con las señales recibidas, $\mathbf{s}$ es un vector de $M \times 1$ con las señales transmitidas y $\mathbf{n}$ es

un vector de $N \times 1$ con el ruido aditivo gaussiano blanco. E_s representa la potencia de la señal transmitida y **H** la matriz del canal, de dimensiones $M \times N$, definida como:

$$\mathbf{H} = \begin{pmatrix} h_{11} & h_{12} & ... & h_{1M} \\ h_{21} & h_{22} & ... & h_{2M} \\ : & : & : & : \\ h_{N1} & h_{N2} & ... & h_{NM} \end{pmatrix}$$

donde h_{nm} representa la ganancia compleja del canal entre la antena de tranmisión m y la de recepción n.

La utilización de MIMO multiplica el límite de capacidad de canal establecido por Shannon. A modo de ejemplo, si las ganancias de los subcanales MIMO están decorreladas y son desconocidas en recepción, dicho límite de capacidad de canal crece linealmente con el mínimo de los números de antenas de transmisión y recepción [1].

A pesar del gran incremento de capacidad que las técnicas MIMO permiten, su implementación conlleva varias dificultades de coste y complejidad:

- Se requieren $M \times N$ antenas y cadenas de radiofrecuencia (RF), incrementando el coste y el tamaño de un equipo inalámbrico.
- La complejidad de la mayoría de algoritmos de procesado de la señal crece linealmente con el número de antenas, e incluso exponencialmente para determinados algoritmos, tales como la detección MIMO óptima.
- En sistemas en los que la implementación de los algoritmos se encuentre distribuida entre varios módulos, el ancho de banda requerido para el intercambio de información puede crecer dramáticamente.
- La distribución de los relojes y retardos debe ser controlada, para garantizar la transmisión y recepción simultánea de las diferentes cadenas RF.

III. Descripción de la plataforma

La Fig. 2 muestra los principales elementos de la plataforma MIMO de prototipado rápido basada en HaLo, que pueden resumirse de la siguiente manera:

1) Tarjeta modular de prototipado rápido.
2) Transceptores RF Maxim MAX2827EVKit.
3) Mástiles con las antenas de transmisión y recepción.
4) Ordenadores personales para diseño, depuración y monitorización.

A. Tarjeta y módulos de prototipado rápido

La plataforma esta basada en una tarjeta de prototipado rápido Heron HEPC9 de Hunt Engineering [8]. Esta tarjeta modular tiene una arquitectura absolutamente flexible, basada en un bus interno que permite comunicaciones de hasta 400 MBps entre los módulos. Los siguientes cuatro módulos han sido escogidos e instalados en la tarjeta para la aplicación que se detalla en este artículo:

- 2 módulos HERON-IO2V2 con 1 FPGA Virtex2 de 1 millón (M) de puertas lógicas, con 2 entradas y 2 salidas analógicas de hasta 125 MSPS, de 12 y 14 bits de resolución, respectivamente.
- 1 módulo HERON-IO5 con 1 FPGA Virtex2 de 3M de puertas, con 2 entradas y 2 salidas analógicas de hasta 160 MSPS, de 12 y 16 bits de resolución, respectivamente.

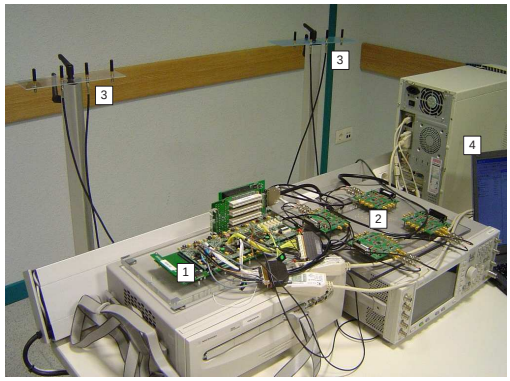

Fig. 2. Principales elementos de la plataforma MIMO HaLo.

Este módulo, al igual que el citado IO2V2, permite la depuración en tiempo real a través de una interfaz JTAG, utilizando la herramienta Chipscope de Xilinx [9]. Esta interfaz también posibilita la co-simulación de Simulink, System Generator y hardware Xilinx, por lo que será utilizado para controlar la ejecución HaLo.

- 1 módulo HERON-C6701, con un microprocesador DSP Texas Instruments TMS320C6701, de coma flotante de 16 bits y un reloj de hasta 167 MHz.

Esta tarjeta HEPC9 es controlada desde un ordenador personal a través del interfaz PCI, permitiendo su configuración, la programación de los dispositivos FPGA y la transferencia de datos.

B. Transceptores RF

La plataforma está equipada con cuatro tarjetas MAX2827EVKit de la casa Maxim, las cuales pueden transmitir o recibir señales RF en las bandas de 2,4 y 5 GHz. Estas tarjetas son capaces de modular y demodular señales IQ de hasta 20 MHz de ancho de banda. Esta solución evita la implementación de los moduladores y demoduladores, pero obliga a emplear dos señales de transmisión y recepción por cada transceptor.

IV. Prototipado rápido basado en el sistema "Hardware in the Loop"

Orientado al prototipado rápido de sistemas de comunicación MIMO, se ha adoptado una metodología de diseño que posibilita:

- La coexistencia de algoritmos distribuidos en varias FPGAs, procesando los algoritmos en tiempo real, y de código Matlab ejecutando offline determinados algoritmos del sistema de comunicaciones MIMO.
- El traslado progresivo del código elaborado en Matlab a una arquitectura eficiente de tiempo real, haciendo posible su validación en entornos y condiciones reales en cualquier etapa del diseño.
- Un completo diseño gráfico de todo el sistema desde Simulink, incluyendo la distribución de recursos específicos de la plataforma, el establecimiento de las conexiones entre módulos y la generación de todos los

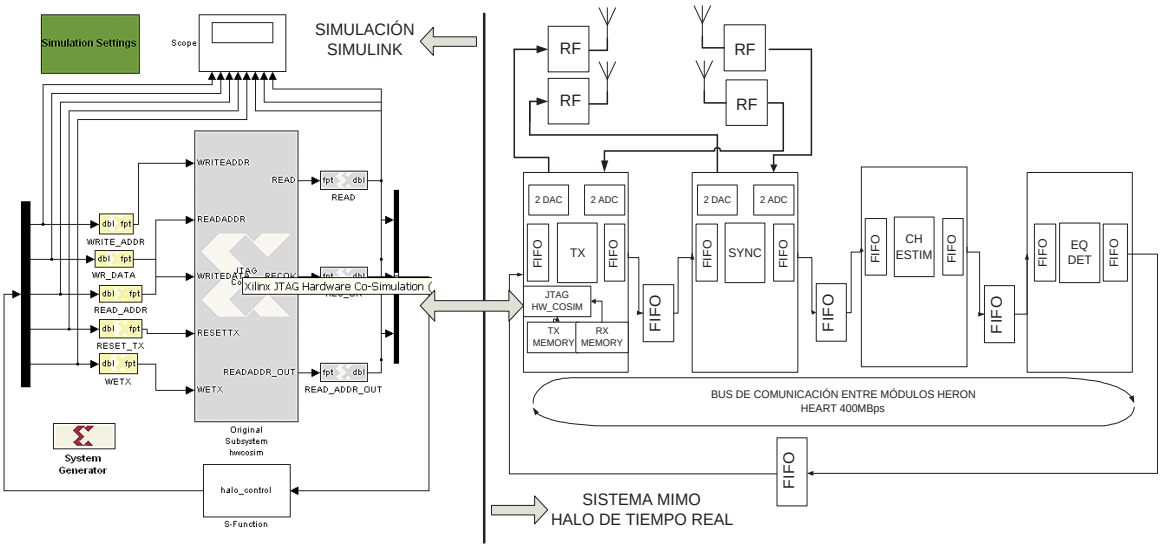

Fig. 3. Esquema de un sistema fundamental HaLo MIMO 2x2 controlado desde Simulink.

bitstreams de las FPGAs que conforman la plataforma de la Fig. 2.

A. *Metodología y herramientas empleadas*

La metodología que se ha establecido está basada en la herramienta Matlab/Simulink de Mathworks [10] en combinación con System Generator for DSP e ISE Project Navigator de Xilinx [9]. Estas herramientas proporcionan un equilibro entre la abstracción del hardware y un diseño eficiente, de una manera gráfica e intuitiva.

La metodología de prototipado rápido adoptada para la implementación de un nuevo algoritmo MIMO puede resumirse en las siguientes etapas:

1) El primer diseño y la validación del algoritmo se realizan en Matlab. Tal y como se expondrá posteriormente, el código Matlab se ejecuta dentro del sistema HaLo mediante bloques S-Function de Simulink.
2) El código Matlab es trasladado a bloques de Simulink.
3) Los bloques de Simulink son reemplazados gradualmente por bloques de System Generator, de modo que pueden ser mapeados directamente en la FPGA. En esta etapa, la resolución de los datos es modificada selectivamente, pasando progresivamente del tipo doble de Matlab a cualquier precisión de coma fija. Por otro lado, los bloques de System Generator pueden ser verificados de dos formas diferentes:
   - Co-Simulación Hardware: El algoritmo se ejecuta en hardware con el reloj marcado por Simulink, no en tiempo real.
   - HaLo: El algoritmo se ejecuta en hardware y en tiempo real.
4) Como último paso, las herramientas de bajo nivel pueden ser empleadas si se requiere mayor eficiencia en el hardware.

Esta metodología permite, independientemente de la etapa de diseño en la que se encuentre el nuevo algoritmo, la posibilidad de testarlo y verificarlo en condiciones finales, es decir, reales. Asimismo, el código puede ser fácilmente depurado de una etapa a otra instanciando ambas en paralelo y comparando sus salidas.

B. *"Hardware in the Loop"*

Existen dos modos en los que un bloque de co-simulación de System Generator puede ser sincronizado con su hardware en la FPGA: la opción "single-stepped", donde Simulink gestiona el pulso de reloj de la FPGA, y el modo "free-running", donde el código de la FPGA se ejecuta en tiempo real con un reloj externo. Este último ha sido escogido para la implementación HaLo, ya que el hardware en la FPGA debe ejecutarse en tiempo real. De esta manera se establecen dos dominios de reloj: el dominio de Simulink, en el que se ejecuta el código offline, y el de tiempo real, en el que se sitúan las FPGAs.

La Fig. 3 muestra el modelo fundamental de un esquema HaLo MIMO 2x2 que posibilita la transmisión y la recepción de datos generados desde Matlab, aplicando algoritmos de procesado de la señal en tiempo real sobre un canal MIMO. La interfaz de ambos dominios de reloj se lleva a cabo mediante memorias asíncronas situadas dentro de la FPGA, conectadas a Simulink mediante el puerto JTAG. La Fig. 3 muestra, en su lado izquierdo, los bloques Simulink encargados del control HaLo, donde un bloque S-Function con código Matlab gestiona el envío y recepción de los datos, mientras que en el lado derecho se muestra el esquema básico de los algoritmos que se ejecutan en tiempo real.

Tal y como se puede observar en la Fig. 3, la unión entre Simulink y la plataforma se ha establecido en el primer módulo. Una vez todos los datos han sido cargados en la memoria de transmisión de la FPGA de dicho módulo, da comienzo el procesado de la señal en tiempo real:

- En el primer módulo se han implementado los algoritmos de códificación espacio-temporal, el mapeo QAM y la etapa de filtrado de transmisión.

- Los datos son transmitidos y recibidos mediante los transceptores de RF sobre un canal MIMO real.
- Tal y como se observa en la Fig. 3, los datos recibidos son filtrados y sincronizados en el segundo módulo, mientras que la estimación de canal, la igualación y los algoritmos de detección son aplicados en los módulos posteriores.
- La trama detectada vuelve al primer módulo, cerrando el lazo, y se almacena en la memoria de recepción.
- Finalmente, la trama es recibida en Simulink, donde el completo funcionamiento de todo el sistema de comunicaciones MIMO puede ser evaluado.

C. Distribución de los recursos

Las plataformas modulares no suelen proporcionar librerías especificas para habilitar sistemas HaLo y requieren que el código de usuario sea introducido en una estructura fija, necesaria para asegurar el correcto uso de los recursos de la plataforma y las conexiones entre módulos. A su vez, System Generator proporciona librerías específicas sólo para un número limitado de plataformas comerciales. Por lo tanto, la estructura y los mecanismos de conexión entre módulos deben ser incluidos en el flujo de diseño.

Por otro lado, la mayoría de algoritmos MIMO se basan en la razonable asunción de que las cadenas de transmisión y recepción están perfectamente sincronizadas. A medida que crece el número de antenas de recepción y de transmisión, es muy probable que un único módulo no pueda albergar todas las cadenas de transmisión o de recepción, dificultando su sincronización. Por ello, tal y como se aprecia en Fig. 3, las cadenas de transmisión y de recepción deben ser distribuidas en la plataforma empleando retardos deterministas basados en las conexiones inter-modulares que se hallan establecido.

El equipo de diseño ha desarrollado librerías específicas en System Generator para el control de la comunicación entre módulos, el manejo de recursos y la sincronización de las cadenas RF. Al mismo tiempo, la modificación del flujo de síntesis permite crear todos los ficheros de carga de las FPGAs de la plataforma. Por lo tanto, se ha conseguido que todo el diseño pueda ser simulado, generado y testado a tiempo real desde Simulink.

V. Aplicaciones

A. Sistema completo MIMO 2x2

El sistema HaLo ha sido empleado para implementar un completo sistema MIMO 2x2 que incluye los siguientes algoritmos: detección de trama, sincronización de periodo de símbolo, corrección de offset en frecuencia, estimación de canal LS y detección MIMO empleando la pseudoinversa o un decodificador esférico [11].

B. Emulador de canal

Los canales reales son imprevisibles y no resultan adecuados para las primeras pruebas de un nuevo algoritmo. Por lo tanto, se ha desarrollado e implementado en FPGA un emulador de canal Rayleigh de banda base, que permite depurar los algoritmos de tiempo real. No obstante, para ciertos tests y algoritmos, dicho canal Rayleigh puede ser excesivamente ideal, requiriendo canales más complejos. El sistema HaLo posibilita la utilización de cualquier canal modelado en Matlab, empleando una configuración como la de la Fig. 4.

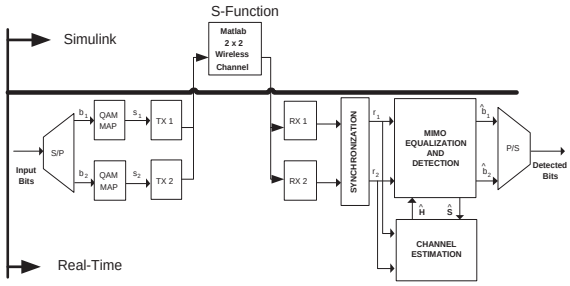

Fig. 4. Ejecución en tiempo real con canal emulado en Matlab

VI. Conclusiones y líneas futuras

Esta contribución ha presentado un sistema "Hardware in the Loop", desarrollado sobre una plataforma modular y con un completo diseño basado en Simulink, que posibilita la integración rápida de nuevos algoritmos MIMO. El sistema posibilita la validación de un nuevo algoritmo con señales y requisitos reales, independientemente de la etapa de diseño en la que se encuentre. Se ha detallado la estructura de la plataforma y se han mostrado varios ejemplos de aplicación, entre los que destaca un sistema completo MIMO 2x2.

De cara a la ampliación del trabajo descrito en este artículo, la plataforma será extendida a un modelo MIMO 3x3 y se realizará una completa revisión de las librerías que permita su utilización con la versión 8.1 del System Generator. Asimismo, se pretende incluir la simulación y la generación del código de los DSPs en el flujo de diseño automatizado basado en Simulink.

Agradecimientos

Los dos primeros autores están financiados por el Departamento de Educación, Universidades e Investigación del Gobierno Vasco a través de las Becas de Formación de Investigadores BFI03.378 y BFI05.428.

Referencias

[1] G. J. Foschini, "Layered space-time architecture for wireless communication in a fading environment when using mulpiple elements antennas," *Bell Labs Technical Journal*, vol. 12, no. 2, pp. 41–59, Oct. 1996.

[2] "High-throughput phisical layer specification v. 1.27," Enhanced Wireless Consortium, Dec. 2005. Available online: http://www.enhancedwirelessconsortium.org.

[3] C. Mehlfuhrer, S. Geirhofer, S. Caban, and M. Rupp, "A flexible MIMO testbed with remote access," in *Proc. 13th European Signal Processing Conference (EUSIPCO)*, vol. 1, Antalya, Turkey, Sept. 2005.

[4] T. Kaiser, A. Wilzeck, M. Berentsen, and M. Rupp, "Prototyping for MIMO systems: An overview," in *Proc. 12th European Signal Processing Conference (EUSIPCO)*, Vienna, Sept. 2004.

[5] M. Stege, F. Schäfer, M. Henker, and G. Fettweis, "Hardware in a Loop - A system prototyping platform for MIMO approaches," in *Proc. ITG Workshop on Smart Antennas*, Munich, Germany, Mar. 2004.

[6] Signalion GmbH: "http://www.signalion.com".

[7] M. Mendicute, J. Altuna, G. Landaburu, and V. Atxa, "Platform for joint evaluation of FPGA-implemented and MATLAB algorithms in real MIMO transmissions," in *Proc. IEE/EURASIP Conference on DSP Enabled Radio (DSPeR)*, vol. 1, Southampton, UK, Sept. 2005, pp. 31–34.

[8] Hunt Engineering: "http://www.hunteng.co.uk/".

[9] Xilinx: "http://www.xilinx.com".

[10] Mathworks: "http://www.mathworks.com".

[11] M. Mendicute, L. G. Barbero, G. Landaburu, J. S. Thompson, J. Altuna, and V. Atxa, "Real-time implementation of a sphere decoder-based MIMO wireless system," Submited as Invited Paper to the 14th European Signal Processing Conference (EUSIPCO), Florence, Italy, Sept. 2006.

References

[Acquitek] Acquitek, Inc., http://www.acquitek.com.

[Adjoudani03] A. Adjoudani, E. C. Beck, A. P. Burg, G. M. Djuknic, T. G. Gvoth, D. Haessig, S. Manji, M. A. Milbrodt, M. Rupp, D. Samardzija, A. B. Siegel, T. Sizer, C. Tran, S. Walker, S. A. Wilkus, and P. W. Wolniansky, "Prototype experience for MIMO BLAST over third-generation wireless systems", *IEEE Journal on Selected Areas on Communications*, vol. 21, no. 3, 440–451, Apr. 2003.

[Adlink] Adlink Technology, Inc., http://www.adlinktech.com.

[Alamouti98] S. Alamouti, "A simple transmit diversity technique for wireless applications", *IEEE Journal on Selected Areas on Communications*, vol. 16, no. 8, 1451–1458, 1998.

[Bahl74] L. R. Bahl, J. Cocke, F. Jelinek, and J. Raviv, "Optimal decoding of linear codes for minimizing symbol error rate", *IEEE Transactions on Information Theory*, vol. 20, no. 2, 284–287, Mar. 1974.

[Barbero05a] L. G. Barbero and J. S. Thompson, "Rapid prototyping of the sphere decoder for MIMO Systems", in *Proc. IEE/EURASIP Conference on DSP Enabled Radio (DSPeR '05)*, vol. 1, pp. 41–47, Southampton, UK, Sep. 2005.

[Barbero05b] L. G. Barbero and J. S. Thompson, "Rapid prototyping system for the evaluation of MIMO receive algorithms", in *Proc. IEEE International Conference on Computer as a Tool (EUROCON '05)*, vol. 2, pp. 1779–1782, Belgrade, Serbia and Montenegro, Nov. 2005.

[Barhumi03] I. Barhumi, G. Leus, and M. Moonen, "Optimal training design for MIMO OFDM systems in mobile wireless channels", *IEEE Transactions on Signal Processing*, vol. 51, no. 6, 1615–1624, 2003.

[Berrou93] C. Berrou, A. Glavieux, and P. Thitimajshima, "Near Shannon limit error-correction coding and decoding: Turbo-codes (1)", in *Proc. IEEE International Conference on Communications (ICC '93)*, vol. 2, pp. 1064–1070, Geneva, Ch, May 1993.

[Biglieri98] E. Biglieri, J. Proakis, and S. Shamai, "Fading channels: Information-theoretic and communications aspects", *IEEE Transactions on Information Theory*, vol. 44, no. 6, 2619–2692, Oct. 1998.

[Biglieri04] E. Biglieri, A. Nordio, and G. Taricco, "Iterative receivers for coded MIMO signalling", *Wireless Communications and Mobile Computing (WCMC '04)*, , no. 4, 697–710, 2004.

[Biguesh04] M. Biguesh and A. B. Gershman, ""MIMO channel estimation: optimal training and tradeoffs between estimation techniques", in *Proc. IEEE International Conference on Communications (ICC '04)*, vol. 5, pp. 2658–2662, Jun. 2004.

[Biguesh06] M. Biguesh and A. B. Gershman, "Training-based MIMO channel estimation: A study of estimator tradeoffs and optimal training signals", *IEEE Transactions on Signal Processing*, vol. 54, no. 3, 884–893j, Mar. 2006.

[Bingham90] J. A. C. Bingham, "Multicarrier modulation for data transmission: an idea whose time has come", *IEEE Communications Magazine*, vol. 28, no. 5, 5–14, 1990.

[Bölckskei02] H. Bölckskei, R. W. J. Heath, and A. Paulraj, "Blind channel identification and equalization in OFDM-based multiantenna systems", *IEEE Transaction on Signal Processing*, vol. 50, no. 1, 96–109, 2002.

[Böhnke03] R. Böhnke, D. Wübben, and V. Kühn, "Reduced complexity MMSE detection for BLAST architectures", in *Proc. IEEE Global Telecommunications Conference (GLOBECOM '03)*, San Francisco, California, USA, Dec. 2003.

[Boutros00] J. J. Boutros, F. Boixadera, and C. Lamy, "Bit-interleaved coded modulations for multiple-input multiple-output channels", *IEEE International Symposium on Spread Spectrum Techniques and Applications (ISSSTA '00)*, vol. 1, 123 – 126, 2000.

[Brink01] S. T. Brink, "Convergence behaviour of iteratively decoded parallel concatenated codes", *IEEE Transactions on Communications*, vol. 49, no. 10, 1727–1737, Oct. 2001.

[Burg05] A. Burg, M. Borgmann, M. Wenk, M. Zellweger, W. Fichtner, and H. Bolcskei, "VLSI Implementation of MIMO detection using the sphere decoding algorithm", *IEEE Journal of Solid-State Circuits*, vol. 40, no. 7, 1566 – 1576, 2005.

[Burg06] A. Burg, *VLSI Circuits for MIMO Wireless Communication Systems*, vol. 169 of *Microelectronics*, Hartung-Gorre, 2006.

[Buzzi04] S. Buzzi, M. Lops, and S. Sardellitti, "Performance of iterative data detection and channel estimation for single-antenna and multiple-antennas wireless communications", *IEEE Transactions on Vehicular Technology*, vol. 53, no. 4, 1085 – 1104, 2004.

[Caban06] S. Caban, C. Mehlführer, R. Langwieser, A. Scholtz, and M. Rupp, "Vienna MIMO testbed", *EURASIP Journal on Applied Signal Processing*, vol. 2006, 1–13, 2006.

[Cardoso93] J. F. Cardoso and A. Souloumiac, "Blind beamforming for non-Gaussian signals", *IEEE Proc. Radar and Signal Processing*, vol. 140, no. 6, 362–370, Dec. 1993.

[Chung06] J. Chung, S. Park, and S. Lee, "Effect of channel estimation errors on the performance of MIMO-OFDM systems in correlated fading channels", in *Proc. Canadian Conference on Electrical and Computer Engineering*, pp. 478–481, May 2006.

[Coldrey07] M. Coldrey and P. Bohlin, "Training-based MIMO systems - Part I: performance comparison", *IEEE Transactions on Signal Processing*, vol. 55, no. 11, 5464–5476, 2007.

[Colieri02] S. Colieri, M. Ergen, A. Puri, and A. Bahai, "A study of channel estimation in OFDM systems", in *Proc. IEEE Vehicular Technology Conference (VTC '02)*, vol. 2, pp. 894–898, 2002.

[Coon03] J. Coon, J. Siew, M. Beach, A. Nix, S. Armour, and J. McGeehan., "A comparison of MIMO-OFDM and MIMO-SCFDE in WLAN environments", in *Proc. Global Telecommunications Conference (GLOBECOM '03)*, vol. 6, pp. 3296 – 3301, Dec. 2003.

[Cosovic07] I. Cosovic and G. Auer, "Capacity of MIMO-OFDM with pilot-aided channel estimation", *EURASIP Journal onWireless Communications and Networking*, vol. 7, no. 5, Jan. 2007.

[Damen00] O. Damen, A. Chkeif, and J.-C. Belfiore, "Sphere decoding of space-time codes", in *Proc. IEEE International Symposium on Information Theory (ISIT '00)*, p. 362, Sorrento, Italy, Jun. 2000.

[Damen03] M. O. Damen, H. E. Gamal, and G. Caire, "On maximum-likelihood detection and the search for the closest lattice point", *IEEE Transactions on Information Theory*, vol. 49, no. 10, 2389–2402, Oct. 2003.

[Dardari00] D. Dardari, V. Tralli, and A. Vaccari, "A theoretical characterization of nonlinear distortion effect on OFDM systems", *IEEE Transactions on Communications*, vol. 48, no. 10, 1755–1764, Oct. 2000.

[Deng03] X. Deng, A. Haimovich, and J. Garcia-Frias, "Decision directed iterative channel estimation for MIMO systems", in *Proc. IEEE International Conference on Communications (ICC '03)*, vol. 4, pp. 2326–2329, May 2003.

[Edward08] K. Edward, J. Shi, M. Mckay, M. Ho, and G. Xiqi, "Analytical performance of MIMO-SVD systems in ricean fading channels with channel estimation error and feedback delay", *IEEE Transactions on Wireless Communications*, vol. 7, no. 4, 1315–1325, 2008.

[EWC05] EWC, "EWC Enhanced Wireless Consortium publication: HT PHY Specification V1.27", Dec. 2005.

[Falconer02] D. Falconer, S. Ariyavisitakul, A. Benyamin-Seeyar, and B. Eidson, "Frequency-domain equalization for single-carrier broadband wireless systems", *IEEE Communications Magazine*, vol. 40, no. 4, 58–66, 1-4-2002.

[Farhang-Boroujeny95] B. Farhang-Boroujeny, "Pilot-based channel identification: Proposal for semi-blind identification of fading channels", *Electronic Letters*, vol. 31, no. 13, 1044–1046, Jun. 1995.

[Foschini96] G. Foschini, "Layered space-time architecture for wireless communications in a fading environment when using multi-element antennas", *Bell Labs Technical Journal*, vol. 1, no. 2, 41–59, 1996.

[Foschini98] G. Foschini and M. Gans, "On limits of wireless communications in a fading environment when using multiple antennas", *Wireless Personal Communications Magazine - Kluwer Academic*, vol. 6, no. 3, 311 – 335, 1998.

[Furrer07] S. Furrer and D. Dahlhaus, "Multiple-antenna signaling over fading channels with estimated channel state information: Performance analysis", *IEEE Transactions on Information Theory*, vol. 53, no. 6, 2010–2027, Jun. 2007.

[Golden99] G. D. Golden, G. J. Foschini, R. A. Valenzuela, and P. W. Wolniansky, "Detection algorithm and initial laboratory results using V-BLAST space-time communication architecture", *Electronics Letters*, vol. 35, no. 1, 14–16, Jan. 1999.

[Grant00a] A. Grant, "Joint decoding and channel estimation for linear MIMO channels", *2000 IEEE Wireless Communications and Networking Conference (WCNC '00)*, pp. 1009 – 1012, 2000.

[Grant00b] A. Grant, "Joint decoding and channel estimation for space-time codes", *IEEE Vehicular Technology Conference (VTC '00)*, vol. 1, no. 52D, 416 – 420, 2000.

[Hassibi00] B. Hassibi and B. M. Hochwald, "How much training is needed in multiple-antenna wireless links?", *Bell Labs Technical Journal*, 2000.

[Hassibi01] B. Hassibi and H. Vikalo, "On the expected complexity of sphere decoding", in *Proc. 35th Asilomar Conference on Signals, Systems and Computers*, vol. 2, pp. 1051–1055, Monterey, CA, Nov. 2001.

[Heiskala02] J. Heiskala and J. Terry, *OFDM Wireless LANs: A Theoretical and Practical Guide*, Sams Publishing, Indiana, USA, 2002.

[Hermosilla03] C. Hermosilla and L. Szczeciński, "EXIT charts for turbo receivers in MIMO systems", in *Proc. International Symposium on Signal Processing and its Applications (ISSPA '03)*, vol. 1, pp. 209–212, Paris, France, Jul. 2003.

[Hermosilla05] C. Hermosilla and C. Szczeciński, "Performance evaluation of linear Turbo receivers using analytical extrinsic information transfer functions", *EURASIP Journal on Applied Signal Processing*, , no. 6, 892–895, Oct. 2005.

[Hochwald03] B. M. Hochwald and S. ten Brink, "Achieving Near-Capacity on a Multiple-Antenna Channel", *IEEE Trans. Commun.*, vol. 51, no. 3, 389–399, Mar. 2003.

[Horseman03] T. Horseman, J. Webber, M. Abdul-Aziz, R. Piechocki, M. Beach, A. Nix, and P. Fletcher, "A software and hardware evaluation of revolutionary Turbo MIMO OFDM schemes for 5GHz WLANs", in *Proc. 57th IEEE Vehicular Technology Conference (VTC '03-Spring)*, vol. 4, pp. 2788–2792, Seoul, Korea, Apr. 2003.

[Huang08] X. Huang, C. Liang, and J. Ma, "System Architecture and Implementation of MIMO Sphere Decoders on FPGA", *IEEE Transacations on VLSI Systems*, vol. 16, no. 2, 188–197, Feb. 2008.

[Hunt] Hunt Engineering, Inc., http://www.hunt.com.

[IEEE99] IEEE, "IEEE Std 802.11a-1999 part 11: Wireless LAN medium access control (MAC) and physical layer (PHY) specifications: High-speed physical layer in the 5 GHz band", Sep. 1999.

[IEEE03a] IEEE, "IEEE Std 802.11g-2003 part 11: Wireless LAN medium access control (MAC) and physical layer (PHY) specifications: Amendment 4: Further higher data rate extension in the 2.4 GHz band", 2003.

[IEEE03b] IEEE, "Part 16: Air interface for fixed broadband wireless access systems Ű Amendment 2: Medium access control modifications and additional physical layer specifications for 2-11 GHz, 802.16a IEEE standard for local and metropolitan Area Networks", Jun. 2003.

[IEEE07] IEEE, "IEEE Std 802.11n-2007 part 11: Wireless LAN medium access control (MAC) and physical layer (PHY) specifications", Jun. 2007.

[Jagannatham06] A. K. Jagannatham and B. D. Rao, "Whitening-rotation-based semi-blind MIMO channel estimation", *IEEE Transactions on Signal Processing*, vol. 54, no. 3, 861 – 869, 2006.

[Kaiser04] T. Kaiser, A. Wilzeck, M. Berentsen, and M. Rupp, "Prototyping for MIMO systems: An overview", in *Proc. 12th European Signal Processing Conference (EUSIPCO '04)*, Vienna, Austria, Sep. 2004.

[Khalighi05] M. A. Khalighi and J. Boutros, "Channel estimation in turbo-BLAST detectors using EM algorithm", in *IEEE International Conference on Acoustics, Speech, and Signal Processing (ICASSP '05)*, vol. 3, pp. 1037–1040, Mar. 2005.

[Kim05] J. Kim, J. Park, and D. Hong, "Performance analysis of channel estimation in OFDM systems", *IEEE Signal Processing Letters*, vol. 12, Jan. 2005.

[Krondorf06] M. Krondorf, T. J. Liang, R. Irmer, and G. Fettweis, "Improved channel estimation for complexity-reduced MIMO-OFDM receiver by estimation of channel impulse response length.", in *Proc. 12th European Wireless Conference (EW '06)*, Athens, Greece, Apr. 2006.

[Lang04] T. Lang, B. M. Sadler, and D. Min, "Pilot-assisted wireless transmissions: general model, design criteria, and signal processing", *IEEE Signal Processing Magazine*, vol. 21, 12–25, Nov. 2004.

[Larsson03] E. G. Larsson, P. Stoica, and J. Li, "Orthogonal space-time block codes: Maximum likelihood detection for unknown channels and unstructured interferences", *IEEE Transactions on Signal Processing*, vol. 51, no. 2, 362–372, 2003.

[Li99] Y. Li, N. Seshadri, and S. Ariyavisitakul, "Channel estimation for OFDM systems with transmitter diversity in mobile wireless channels", *IEEE Journal on Selected Areas in Communications*, vol. 17, no. 3, 461–471, 1999.

[Li00] X. Li, H. Huang, G. Foschini, and R. Valenzuela, "Effects of iterative detection and decoding on the performance of BLAST", in *Proc. IEEE Global Communications Conference (GLOBECOM '00)*, vol. 2, pp. 1061–1066, 2000.

[Li03] Y. Li and H. J. Wang, "Channel estimation for MIMO-OFDM wireless communications", in *Proc. IEEE Conference on Personal Indoor and Mobile Communications (PIMRC '03)*, vol. 3, pp. 2891–2895, IEEE, Sep. 2003.

[Marzetta99a] T. Marzetta, "BLAST training: estimating channel characteristics for high-capacity space-time wireless", in *Proc. Allerton Conference on Communication, Control and Computing*, Monticello, IL, 1999.

[Marzetta99b] T. Marzetta and B. Hochwald, "Capacity of a mobile multiple-antenna communication link in Rayleigh flat fading", *IEEE Transactions on Information Theory*, vol. 45, no. 1, 139–157, Jan. 1999.

[Mathworks] The Mathworks, Inc., http://www.mathworks.com.

[Maxim] Maxim Integrated Products, http://www.maxim-ic.com.

[Medbo98] J. Medbo and P. Schramm, "Channel models for HIPERLAN/2 in different indoor scenariosm, EP BRAN 3ERI085B, ETSI", 1998.

[Medles03] A. Medles and D. T. M. Slock, "Augmenting the training sequence part in semiblind estimation for MIMO channels", in *Proc. of The 37th Asilomar Conference on Signals, Systems and Computers*, vol. 2, pp. 1825–1829, Nov. 2003.

[Mehlführer05] C. Mehlführer, F. Kaltenberger, M. Rupp, and G. Humer, "A scalable rapid prototyping system for real-time MIMO OFDM transmissions", in *Proc. 2nd IEE/EURASIP Conference on DSP Enable Radio (DSPeR '05)*, Southampton, UK, Sep. 2005.

[Mendicute04a] M. Mendicute, J. Altuna, V. Atxa, and J. M. Zabalegui, "Performance comparison of OFDM and FDE single-carrier modulation for spatial multiplexing MIMO systems", in *Proc. IEEE Workshop on Signal Processing Advances in Wireless Communications (SPAWC '04)*, pp. 532 – 535, Lisbon, Portugal, Sep. 2004.

[Mendicute04b] M. Mendicute, J. Altuna, J. S. Thompson, and V. Atxa, "Performance of frequency-domain MIMO equalization for cyclic-prefixed single-carrier spatial multiplexing", in *Proc. EURASIP European Signal Processing Conference (EUSIPCO '04)*, pp. 1849–1952, Vienna, Austria, Sep. 2004.

[Mendicute05] M. Mendicute, J. Altuna, G. Landaburu, and V. Atxa, "Platform for joint evaluation of FPGA-implemented and MATLAB algorithms in real MIMO transmissions", in *Proc. IEE/EURASIP Conference on DSP Enabled Radio (DSPeR '05)*, vol. 1, pp. 31–34, Southampton, UK, Sep. 2005.

[Mendicute06a] M. Mendicute, L. G. Barbero, G. Landaburu, J. S. Thompson, J. Altuna, and V. Atxa, "Real-time implementation of a sphere decoder-based MIMO wireless system", in *Proc. EURASIP European Signal Processing Conference (EUSIPCO '06)*, Florence, Italy, Sep. 2006.

[Mendicute06b] M. Mendicute, G. Landaburu, J. Altuna, V. Atxa, and I. Zuazabeitia, "Sistema "Hardware in the Loop" para el prototipado de algoritmos MIMO de tiempo real", in *XXI National Assembly of the International Union of Radio Science (URSI '06)*, Oviedo, Spain, Sep. 2006.

[Mendicute07] M. Mendicute, J. Altuna, and V. Atxa, "Analytical EXIT functions for the performance evaluation of iterative MIMO receivers with channel estimation error", in *Proc. EURASIP European Signal Processing Conference (EUSIPCO '07)*, Florence, Italy, Sep. 2007.

[Mentor] Methor Graphics, Coorp., http://www.mentor.com.

[Míguez02] J. Míguez and L. Castedo, "Semiblind space-time decoding in wireless communications: a maximum likelihood approach", *Signal Processing*, vol. 82, no. 1, 1–18, Jan. 2002.

[Minn06] H. Minn, N. Al-Dhahir, and Y. Li, "Optimal training signals for MIMO OFDM channel estimation in the presence of frequency offset and phase noise", *IEEE Transactions on Communications*, vol. 54, no. 10, 1754–1759, Oct. 2006.

[Muquet99] B. Muquet, M. Courville, P. Duhamel, and V. Buzenac, "A subspace based blind and semi-blind channel identification method for OFDM systems", in *Proc. IEEE Workshop Signal Processing Advances in Wireless Commications (SPAWC '99)*, pp. 170–173, 1999.

[Mysore05] N. Mysore and J. Bajcsy, "The impact of channel estimation errors and co-antenna interference on the performance of a coded MIMO system", *EURASIP Journal on Applied Signal Processing*, , no. 11, 1680–1697, 2005.

[Naguib98] A. F. Naguib, V. Tarokh, N. Seshadri, and A. R. Calderbank, "A space-time coding modem for high-data-rate wireless communications", *IEEE Journal on Solid-State Circuits*, vol. 16, no. 8, 1459–1478, Oct. 1998.

[Paulraj97] A. J. Paulraj and C. B. Papadias, "Space-time processing for wireless communications", *IEEE Signal Processing Magazine*, vol. 14, no. 6, 49–83, Nov. 1997.

[Paulraj03] A. Paulraj, R. Nabar, and D. Gore, *Introduction to Space-Time Wireless Communications*, Cambridge University Press, Cambridge, UK, 2003.

[Ranheim05] A. Ranheim, "A decoupled approach to adaptive signal separation using an antenna array", *IEEE Transactions on Vehicular Technology*, vol. 48, 2005.

[Rupp03] M. Rupp, A. Burg, and E. Beck, "Rapid prototyping for wireless designs: the five-ones approach", *Signal Processing*, vol. 83, 1427–1444, 2003.

[Sabri08] K. Sabri, M. E. Badaoui, F. Guillet, A. Adib, and D. Aboutajdine, "On blind MIMO system identification based on second-order cyclic statistics", *Hindawi Research Letters in Signal Processing*, vol. 2008, 2008.

[Schnorr94] C. P. Schnorr and M. Euchner, "Lattice basis reduction: Improved practical algorithms and solving subset sum problems", *Mathematical Programming*, vol. 66, 181–199, 1994.

[Schumacher04] L. Schumacher and B. Dijkstra, "Description of a MATLAB implementation of the indoor MIMO WLAN channel model proposed by the IEEE 802.11 TGn channel model special committee", Jan. 2004.

[Sellathurai02] M. Sellathurai and S. Haykin, "Turbo-BLAST for wireless communications: Theory and experiments", *IEEE Transactions on Signal Processing*, vol. 50, no. 10, 2538 – 2546, 2002.

[Shannon48] C. Shannon, "A mathematical theory of communication", *Bell Labs Technical Journal*, vol. 27, 379–423, 1948.

[Signalion] Signalion, http://www.signalion.com.

[Simoens04] F. Simoens and M. Moeneclaey, "A reduced complexity frequency offset estimation technique for flat fading MIMO channels", in *Proc. IEEE CAS Symposium on Emerging Technologies*, vol. 2, pp. 705–708, Shanghai, China, Jun. 2004.

[Sinplicity] Sinplicity, Inc., http://www.sinplicity.com.

[Stege04] M. Stege, F. Schfer, M. Henker, and G. Fettweis, "Hardware in a loop - A system prototyping platform for MIMO approaches", in *Proc. ITG Workshop on Smart Antennas (WSA '04)*, Mar. 2004.

[Struhsaker01] P. Struhsaker and K. Griffin, "Analysis of PHY waveform peak to mean ratio and impact on RF amplification", *contribution to IEEE 802.16.3c-01/46*, Mar. 2001.

[Sun02] Q. Sun, D. C. Cox, H. C. Huang, and A. Lozano, "Estimation of continuous flat fading MIMO channels", *IEEE Transactions On Wireless Communications*, vol. 1, 549–553, Oct. 2002.

[Swindlehurst02] A. L. Swindlehurst, "Blind separation of space-time block coded signals via the analytic constant modulus algorithm", in *Proc. of Sensor Array and Multichannel Signal Processing Workshop (SAM '02)*, pp. 447–451, 2002.

[SystemC] Open SystemC Iniative,http://www.systemc.org

[Talwar96] S. Talwar, M. Viberg, and A. Paulraj, "Blind separation of synchronous co-channel digital signals using an antenna array - Part I: algorithms", *IEEE Transactions on Signal Processing*, vol. 44, no. 5, 1996.

[Tarokh99] V. Tarokh, H. Jafarkhani, and A. R. Calderbank, "Space-time block codes from orthogonal designs", *IEEE Transactions on Information Theory*, vol. 45, no. 5, 1456–1467, 1-7-1999.

[Telatar99] I. E. Telatar, "Capacity of multi-antenna gaussian channels", *European Transactions on Telecommunications*, vol. 10, no. 6, 585–595, Nov. 1999.

[Tong94] L. Tong, G. Xu, and T. Kailath, "Blind identification and equalization based on second-order statistics", *IEEE Transactions on Information Theory*, vol. 40, no. 2, 1994.

[Tong98] L. Tong and S. Perreau, "Multichannel blind identification: from subspace to maximum likelihood methods", *Proceedings of the IEEE*, vol. 86, no. 10, 1998.

[Tüchler02] M. Tüchler, R. Koetter, and A. Singer, "Turbo equalization: principles and new results", *IEEE Transactions on Communications*, vol. 50, no. 5, May 2002.

[Veen96] A. J. V. Veen and A. Paulraj, "An analytical constant modulus algorithm", *IEEE Transactions on Signal Processing*, vol. 44, 1136–1155, May 1996.

[Via07] J. Via, I. Santamaria, A. Sezgin, and A. Paulraj, "SOS-based blind channel estimation under space-time block coded transmissions", in *Proc. IEEE Signal Processing Advances in Wireless Communications (SPAWC '07)*, pp. 1–5, Jun. 2007.

[Wang03] J. Wang and C. Zhao, "A semi-blind detection algorithm for V-BLAST systems", in *Proc. IEEE Global Communications Conference (GLOBECOM '03)*, vol. 2, pp. 808–813, Jun. 2003.

[Xilinx] Xilinx, Inc., http://www.xilinx.com .

[Xilinx08] Xilinx, Inc., "System Generator for DSP User Guide", http://www.xilinx.com/support/sw_manuals/sysgen_user.pdf.

[Yong04] T. Yong and A. Goldsmith, "Capacity of fading MIMO channels with channel estimation error", in *Proc. IEEE International Conference on Communications (ICC '04)*, vol. 2, pp. 808–813, Jun. 2004.

[Zelst01] A. V. Zelst, R. V. Nee, and G. Atwater, "Turbo BLAST and its performance", in *Proc. IEEE VehicularTechnology Conference (VTC '01-Spring)*, pp. 1283–1286, 2001.

[Zelst04] A. V. Zelst and T. C. W. Schenk, "Implementation of a MIMO OFDM-based wireless LAN system", *IEEE Transactions on Signal Processing*, vol. 52, no. 2, 483–494, 2004.

[Zhu03a] H. Zhu, B. Farhang-Boroujeny, and C. Schlegel, "Pilot embedding for joint channel estimation and data detection in MIMO communication systems", *IEEE Communications Letters*, vol. 7, no. 1, 30–32, Jan. 2003.

[Zhu03b] X. Zhu and R. Murch, "Layered space-time equalization for wireless MIMO systems", *IEEE Transactions on Wireless Communications*, vol. 2, no. 6, 1189–1203, Nov. 2003.